SEDIMENT INFILLING RATE OF LOWERMOST MISSISSIPPI RIVER BORROW PITS AND IMPACTS ON DOWNSTREAM DREDGING

IOANNIS Y. GEORGIOU[1], MARTIJN BREGMAN[1], FRANCESCA MESSINA[1], DIANA DI LEONARDO[1], YUSHI WANG[2], SHAN ZOU[2], JOHN SWARTZ[1], MIKE MINER[1], SYED KHALIL[3], RICK RAYNIE[3]

[1]The Water Institute [2]ARCADIS [3]Coastal Protection and Restoration Authority

Produced for and funded by the Coastal Protection and Restoration Authority under Task Order 72 – Subtask 2

March 2023

Report #P-00392-1

ABOUT THE WATER INSTITUTE

The Water Institute is an independent, non-profit, applied research institution advancing science and developing integrated methods to solve complex environmental and societal challenges. We believe in and strive for more resilient and equitable communities, sustainable environments, and thriving economies. For more information, visit www.thewaterinstitute.org.

SUGGESTED CITATION

Ioannis Y. Georgiou, Martijn Bregman, Francesca Messina, Diana Di Leonardo, Yushi Wang, Shan Zou, John Swartz, Mike Miner, Syed Khalil, Rick Raynie (2023). Numerical Modeling to Estimate Sediment Infilling Rate of Lowermost Mississippi River Borrow Pits and Impacts on Downstream Dredging. The Water Institute. Prepared for and/or funded by the Coastal Protection and Restoration Authority. Baton Rouge, LA.

ACKNOWLEDGEMENTS

This project was supported by the Coastal Protection and Restoration Authority (CPRA) under Task Order 72 Louisiana Sediment Management Plan (LASMP), Subtask 2: Numerical Modeling to Estimate Sediment Infilling Rate of Lowermost Mississippi River Borrow Pits on Lateral Bars and Impact on Downstream Dredging with funding from RESTORE for CPRA's Regional Geology and Sediment Management Program (RGSM). Syed Khalil (CPRA), Principal Investigator (for all the Sub-Tasks and Activities under TO72) provided technical/scientific guidance, insight, and support throughout the project. We are thankful to Rick Raynie for his insights in completion of the project.

The authors thank Benjamin Hartman with Baird & Associates for close coordination on data requests for projects BA-0191/BA-0203, and Weeks Marine for sharing the monthly monitoring surveys which greatly contributed to the infilling analysis. Nicholas Cox from Moffatt and Nichol Engineers for coordinating and sharing pre-construction surveys from the Alliance borrow area with permission from the National Oceanic and Atmospheric Administration. Authors also want to thank the U.S. Army Corps of Engineers, New Orleans District, and specifically Dave Ramirez, for sharing synoptic flow measurements along the Olga Revetment which were used to calibrate the Lowermost Mississippi River Model. Alex Kolker (LUMCON) and Dallon Weathers (Delta Marine Geo) shared recent synoptic flow measurements for Neptune Pass, and Brendan Yuill (U.S. Army Corps of Engineers) for his contribution to the early stages of model improvements and model sensitivity analysis.

Brad Miller and Rudy Simoneaux of the Coastal Protection and Restoration Authority (CPRA) provided guidance on the scope of work. Geologists, geomorphologists, scientists, and engineers from the Institute and CPRA contributed to this work and to the development of this report and are acknowledged with thanks.

This report was reviewed, edited, and formatted by Charley Cameron of the Institute.

PREFACE

This report was developed by The Water Institute (the Institute) for the Coastal Protection and Restoration Authority under Task Order 72 Louisiana Sediment Management Plan (LASMP), Subtask 2: Numerical Modeling to Estimate Sediment Infilling Rate of Lowermost Mississippi River Borrow Pits on Lateral Bars and Impact on Downstream Dredging. The report builds on previous work performed by the Institute and recommendations made under Task Order 17 (Yuill, Allison, & Meselhe, 2013; Yuill, Gaweesh, Allison, & Meselhe, 2015).

The report summarizes the analyses conducted on pre-dredging surveys, post-dredging surveys, and repeat bathymetry surveys collected by dredging companies and engineering firms working with CPRA on existing restoration projects.

This study quantifies infilling rates for borrow pits in the Lowermost Mississippi River and provides insight into relative importance of processes and parameters that control infilling rates. From these results, relationships have been developed—such as how infill rates vary with the flood hydrograph—that can be used to estimate availability (recharge rate) of this renewable sand resource over the long term to inform the Louisiana Coastal Master Plan and Barrier Island System Management Program and ultimately the design of the projects contained within those programs.

EXECUTIVE SUMMARY

The work presented in this report uses numerical models and field observations to investigate the governing processes that control borrow pit infilling in the Mississippi River to promote sustainable sand extraction. The analysis focuses on borrow pit infilling rates, and on the local and regional effects induced by the presence of borrow pits. This study aims to help planners, project managers, engineers, and scientists make informed decisions about restoration projects using renewable river sand/sediment by providing insights into the rate at which sand can be sustainably extracted from river bars. The study utilized and leveraged existing borrow pit bathymetry surveys and sediment observations to improve the scientific understanding of borrow area morphologic response and dynamics, calibrate and validate numerical models, and compare survey results with model predictions.

Two areas of the Mississippi River investigated were, the Alliance Anchorage Bar (River Mile 65) and the Venice Anchorage Bar (River Mile 8). Two existing borrow pits were analyzed by using both surveys and numerical models: the Alliance Anchorage Borrow Pit (AABP) and the Venice Anchorage Borrow Pit (VABP). Two sets of simulations were performed using the two models to test various environmental scenarios: different river hydrographs (including raising and falling limbs), different upstream sediment supplies, different bar stratigraphy (i.e., bed composition and properties) and different borrow pit volumes.

Repeated surveys were a crucial element in this research and provided important information on borrow pit infilling and the timing and spatial variability of that infilling. This improved the understanding of inter-annual dynamics and controls on sediment infilling, enhanced model morphodynamic validation, and broadened model applications. The observed infilling rates for three portions of the VABP exhibit non-uniform spatial infilling trends. All three areas experienced the highest infilling rates during the rising limb of the hydrographs, during which all three sites showed an average vertical accretion rate of ~ 0.15–0.17 m/week, corresponding to volumetric infilling of 93,000 to 225,000 m^3/month. During lower flows (~15,000 m^3/s) all three areas experienced reduced infilling rates (from 8,000–12,000 m^3/month), and for flows lower than 15,000 m^3/s, infilling was negligible.

For observed infilling rates, modeling results show that the hydrograph shape, and in particular the rate at which the river discharge increases during the rising limb, strongly influences infilling trends. Three trends and corresponding infilling rates were identified for VABP:

- No infilling rates for river discharge below 10,000 m^3/s (i.e., 353,000 cfs)
- 0–100,000 m^3/week for river discharge between 10,000 and 20,000 m^3/s (i.e., 353,000–706,000 cfs)
- 100,000 to 300,000 m^3/week for river discharge above 20,000 m^3/s (i.e., 706,000 cfs)

Similarly, three trends and corresponding infilling rates were identified for AABP

- No infilling rates for river discharge below 15,000 m^3/s (i.e., 530,000 cfs)
- 0–100,000 m^3/week for river discharge between 15,000 and 22,000 m^3/s (i.e., 530,000 – 777,000 cfs)

- 100,000–300,000 m^3/week for river discharge above 22,000 m^3/s (i.e., 777,000 cfs)

The simulations showed an average annual infilling of approximately 50% (± 3%) for AABP and 28 % (± 10%) for VABP, depending on the hydrograph shape. The borrow pit depth also strongly influenced infilling rates: shallower pits infill slower and can reduce infill rates by approximately 36% for AABP and up to 48% for VABP.

The strong correlation between infilling rates and the hydrograph shape suggests a secondary control on infilling rates, proportional to residual flow and corresponding streamwise slope in the river, indicating that the location of the pit along the river (i.e., river mile and sand bar where the pit is located) controls sediment trapping efficiency.

Modeling results highlighted that borrow pits promote annual bed aggradation in channels next to the pits, but at rates that are one order of magnitude lower than deposition within the pit. Bed elevation in the main river channel remains well below the authorized navigation depth; therefore, deposition in the channel does not represent a threat for navigation. Numerical model simulations also show that borrow pits do not affect sedimentation and erosion patterns at bars upstream of the pits, but they do reduce aggradation at the sand bars where they are located as well as sand bars downstream.

The presence of the VABP reduced maintenance dredging between Venice and the Head of Passes by 3–9 %, depending on the hydrograph, and showed no influence on maintenance dredging below Head of Passes.

The simulations performed to test the effect of different sediment class distributions did not show a significant impact on borrow pit infilling rates; however, sediment class distributions did influence sand bar aggradation and degradation dynamics. When bed composition coarsens, and there is more available coarse sediment in suspension from upriver sources, upriver sand bars will aggrade and in turn, starve the sand bars downriver. The coarser riverbed supplies less sediment, and thus cannot make up the difference of the volume lost to upriver sand bar aggradation during these conditions. A sensitivity analysis to test the role of upstream sediment supply on local and regional bar dynamics indicated negligible influence on sand bar dynamics for bars located at both the Alliance Reach and the Venice Reach. When coarser sediment is more available as suspended load—as well as when the riverbed composition coarsens—at the Alliance Reach, the Alliance Anchorage Bar and the Belair Revetment Bar sequester more sand (5–35%), thus starving the downstream sand bars of sediment and reducing aggradation (15–38%). When finer sediment is more available as suspended load, both the Venice Anchorage Bar and the Pilottown Anchorage Bar exhibit increased aggradation of approximately 9 and 12%, respectively.

The information presented in this report provides valuable insights for planners to inform the borrow pit dredging activity timeline. The work highlighted the importance of repeated bathymetry surveys during and after borrow pit construction to help quantity long-term pit evolution and pit infilling, as well as documenting additional local processes that influence pit wall evolution and pit morphology. Future additional modeling analysis would help estimate infilling rates along the Mississippi River. Infilling rate estimates for other sand bars along the river, and potentially from multiple dredging sites, would be beneficial to develop an empirical correlation to forecast infilling rates as a function of stream power and

could represent a powerful tool for engineers and planners to estimate first order infilling rates and time which will be key to plan dredging activities.

TABLE OF CONTENTS

LIST OF FIGURES

LIST OF TABLES

LIST OF ACRONYMS

Acronym	Term
AABP	Alliance Anchorage Borrow Pit
BAMM	Borrow Area Monitoring and Management
BP	Borrow Pit
Breton SD	Mid Breton Sediment Diversion
BHP	Below Head of Passes
CPRA	Coastal Protection and Restoration Authority
CRMS	Coastwide Reference Monitoring System
HDDA	Hopper Dredge Disposal Area
MBSD	Mid Barataria Sediment Diversion
MRSC	Mississippi River Ship Channel
NOAA	National Oceanic and Atmospheric Administration
RM	River Mile
SD	Sediment Diversion
USACE	U.S. Army Corps of Engineers
USGS	United States Geological Survey
VABP	Venice Anchorage Borrow Pit

UNIT TABLE

Abbreviation	Term
cm	Centimeter
cfs	Cubic feet per second
ft	Feet
km	Kilometers
m	Meters
m^3	Cubic meter
m^2	Square meter
MCY	Million cubic yards
s	second

1.0 INTRODUCTION

Much of the world's population lives close to coastlines, and this proximity is of increasing concern due to the threat posed by sea-level rise (SLR). Barrier islands and backbarrier marshes, which comprise 10% of coastal landscapes globally, are particularly susceptible to erosion during rising sea levels and require nourishment or restoration using sand resources (Ranasinghe, Duong, Uhlenbrook, Roelvink, & Stive, 2013). The ongoing transgression of the Mississippi River Delta Plain (MRDP) and the limited sand availability throughout the MRDP makes coastal Louisiana particularly vulnerable and in urgent need of new, and preferably renewable, sand resources (CB&I, 2015; Flocks, Miner, Twichell, Lavoie, & Kindinger, 2009; Miner, Kulp, FitzGerald, Flocks, & Weathers, 2009). To implement the state's 2023 Coastal Master Plan, Louisiana needs approximately 700–800 million cubic meters to build marsh creation and land bridge restoration projects (CPRA, 2023;).whereas 5 to 11 billion cubic meters of sediment is needed to offset future land losses (Blum & Roberts, 2009; Khalil et al., 2018). Suitable and renewable sediment resources for marsh construction and high-quality sand for barrier island restoration are relatively scarce in the MRDP. Transporting sediment from outside of the system (e.g., from offshore and riverine sources) is optimal, and contributes to a net increase in sediment availability within the coastal system.

While this transport of sediment can present an attractive option, it is not always cost effective to use sand from outside the system for coastal nourishment and restoration projects. To inform long-term restoration planning and management of valuable sediment resources, the Louisiana Sediment Management Plan (LASMP) was developed, and a component of that plan (Borrow Area Monitoring and Management [BAMM]) seeks to develop better understanding of the dynamics of sand mining of lateral bars in the Mississippi River. It was previously hypothesized that mining sand bars in the Lower Mississippi River is an opportunity to explore renewable sand in the river that can be more routinely used for coastal restoration projects (Finkl, Khalil, Andrews, Keehn, & Benedet, 2006; Yuill et al., 2013). As such, this study aims to increase understanding of sediment infill rates for in-river borrow areas through empirical analysis and multi-dimensional numerical modeling. The project addresses two key questions: (1) what is the recharge or infilling rate of in-river borrow pits, and how does that affect local sediment transport regimes, and (2) do in-river borrow pits affect downstream sediment transport and can they potentially reduce navigation maintenance dredging requirements downstream?

This study builds on previous research conducted by The Water Institute (the Institute) under Task Order 17 from the Coastal Protection and Restoration Authority (CPRA; Yuill et al., 2013, 2015), which included a synthesis of field observations and analysis of three Lower Mississippi River borrow areas, namely the Bayou Dupont, Hermitage, and MR-E Scofield Island project borrow areas. Previous efforts (Yuill et al., 2013) provided recommendations on monitoring and numerical modeling strategies for future borrow areas to promote sustainable sand extraction. This and other recent research, including research conducted in support of the Mississippi River Hydrodynamics and Delta Management Study (MRHDMS) and the Lowermost Mississippi River Management Program (LMRMP; Allison et al., 2012; Allison & Pratt, 2017; Harmar et al., 2005; Moffatt & Nichol, 2012; Moffatt and Nichol, 2011; Mossa, 1996; Nittrouer et al., 2011a; Ramirez & Allison, 2013a; Wang, 2019; Yuill et al., 2013, 2015), have improved the understanding of sand fluxes at several locations in the Lower Mississippi River channel.

However, gaps remain in quantifying infilling rates for in-river borrow pits, and in understanding the governing processes that control those infilling rates.

Sand dynamics are essential to understanding the geomorphology of the Lower Mississippi River because sand comprises the majority of the channel bed sediment, as well as a significant portion of the river's annual sediment load (M. A. Allison et al., 2012). Knowledge about how sand transport rates increase and how they fluctuate seasonally with flow discharge has increased over the last decade (M. Allison, Di Leonardo, Eckland, Ramatchandirane, & Weathers, 2018a, 2018b). However, uncertainty in estimating rates and patterns of scour and shoaling regionally (~10s of river miles) and over time at annual to decadal intervals continues to hinder operational-use predictions of riverbed morphology. The high uncertainty in riverbed predictions poses significant challenges to river managers as shoaling presents a costly problem for navigation and commerce, and scour may undermine river training and flood control structures with potentially global economic consequences.

Furthermore, uncertainty in how sand bars evolve throughout an annual hydrograph hampers the ability to accurately predict sand infilling rates in borrow pits located on sand bars, as regional-to-local sediment transport processes and attendant geomorphic feedbacks are poorly understood (Moffatt & Nichol, 2012; Yuill et al., 2013). For example, Yuill et al. (2015) found that the rising limb of the 2011 river flood eroded approximately 4 feet of sediment from a riverine borrow near Alliance, Louisiana (Figure 1), while sedimentation during the falling limb of the hydrograph equaled approximately the same magnitude (i.e., + 4 feet). A modeling study by Moffatt and Nichol (2011), using a simulation matrix of several steady state conditions and look up tables showed that infilling rates depend on the river hydrograph. Experiments conducted by Moffatt and Nichol in the Alliance Anchorage Borrow Pit (AABP) show that following dredging of a pit that is 6.57 MCY, infilling will reach 67% of the dredged volume within the first year and can vary from 46% to 86%. Additional experiments by Moffat and Nichol showed that infilling of borrow pits dredged to -90 ft NAVD88 can fill by 50% within 0.61 years and to 75% within 1.37 years, and when dredged to -70 ft NAVD88, they can fill by 50% in 0.65 years, and to 75% by 1.56 years (Moffatt and Nichol, 2011).

From a process standpoint, there is limited understanding of the timescales in which sand moves within and through reaches, how sand is trapped and/or released in large bars, and how disruptions to the sediment transport regime, such as those posed by riverine sand mining to support restoration projects, may influence navigation channel maintenance dredging requirements downstream.

This study uses both numerical models and field observations. The modeling approach is partially informed by a modeling strategy previously outlined by Yuill et al. (2013). Yuill et al. (2013) highlighted the importance of allocating sufficient resources to gather adequate field observations to (1) improve scientific understanding of the physical processes governing the infilling of borrow sites and (2) adequately calibrate and validate numerical models that could be used to provide quantitative information of borrow site infilling rates. Existing modeling work (Moffatt and Nichol, 2011; Yuill et al., 2013) identified that borrow pit infilling rates vary between sites along the length of the Mississippi River. Moreover, they showed that the initial cut volume, most notably pit depth, poses a first order control on the infilling rate. However, the modeling approach utilized by Moffatt & Nichol (2011) included the use of steady state models and look up tables, rather than evaluating sediment transport and resulting infilling for the full hydrograph, and lacked the adequate field observations to fully calibrate and validate their

model. The work presented in this report extended previous work (Moffatt and Nichol, 2011; Yuill et al., 2013), confirmed their results, overcame some limitations, and provided a more comprehensive understanding of drivers of borrow pit infilling to help inform and promote sustainable sand extraction.

The study also leveraged new bathymetry and sediment observations for model calibration and validation, and new, robust, and frequent borrow pit surveys to (1) better understand borrow area morphologic response and (2) compare survey results with model predictions. The objective of this study is to help planners, project managers, and engineers and scientists at CPRA make informed decisions about restoration projects using river sand by providing insights on the rate at which this sand can be sustainably extracted from river bars.

Key research questions that were investigated in this study include:

1. What are the underlying infilling governing processes?
2. What are the infilling rates of LMR borrow pits?
3. How do pits affect local and regional sediment transport?
4. What are the impacts to downstream dredging?

2.0 METHODS AND DATA ANALYSIS

To accomplish the research objectives, both field observations and numerical models were used in this study. This section provides an overview of the field datasets, analysis, observation methods, and numerical models and the methodologies employed to investigate the borrow areas. This section is a summary of those methods. More details on methods and analysis, model development, improvements, and calibration are available in Appendix A, Appendix B, and Appendix C of this report.

2.1 FIELD OBSERVATIONS

The project team, after conducting a literature review during the synthesis period of the project, engaged with CPRA project managers and engineering firms who were, at the time of writing, working on existing restoration projects during the early phase of this study. Through this engagement, the project team was able to identify opportunities to obtain useable field data. These data included pre-dredging surveys, post-dredging surveys, and—where available—repeat bathymetry surveys for use in the infilling analysis and for sediment transport and morphology model calibration. The Mississippi River bathymetric surveys conducted by the National Oceanic and Atmospheric Administration (NOAA) in 2018 were used as initial bathymetry for all models in this study (Dasler, 2019a). Digital Elevation Models (DEMs) were converted to spatial point clouds, which were then interpolated onto the model computational domains at their respective resolution using the triangulation method. Historic bathymetry previously compiled by Yuill et al. (2013) was used to reference historic infilling rates and borrow pit bed level changes at the AABP for comparative analysis, and were supplemented with 2018 and 2020 surveys. Analysis for the Venice Anchorage Borrow Pit (VABP), shown in Figure A-1, used pre-dredged NOAA 2018 multibeam surveys (Dasler, 2019a). Monthly single beam surveys conducted by Weeks Marine were used to determine infilling rates. The VABP was incrementally surveyed coincident with dredging operations. The first of these surveys was conducted on October 25, 2021, and the most recent survey used in the analysis was taken on January 23, 2023. The first infilling rates were calculated based on the December 20, 2021 survey, which represented the end of dredging in the southernmost part of the borrow area (Area 1, described in Appendix A). Rasters with a resolution of 5 m were created for each of the survey periods. The infilling analysis for each area was performed with surveys conducted after dredging was complete in that specific area of the borrow pit and before dredging started in another location of the borrow pit. This was identified using the dredge cut sequence, also obtained from Weeks Marine. The monthly surveys were used to generate infilling volumes along with statistics for each of the cut-fill analysis. More details on the methods, analysis, and results can be found in Appendix A.

2.2 NUMERICAL MODELING

Three different numerical models were used in this study; two 3-dimensional Delft3D-4 models (Deltares, 2014) and a FLOW-3D computational fluid dynamic (CFD) model (Flow Science, Inc., 2023). A fourth Delft3D-4 model (Reins, 2018) was used to inform some of the sensitivity tests and experiments, and to generate boundary conditions for sediment routing.

Delft3D-4 is a physics-based model that simulates shallow water (hydrostatic) hydrodynamics and sediment transport on a structured curvilinear grid. Hydrodynamics are simulated by solving the depth-integrated, Reynolds-averaged Navier-Stokes equations for incompressible and free surface flow

(Deltares, 2014; Lesser, Roelvink, van Kester, & Stelling, 2004). Delft3D-4 is widely applied to simulate hydrodynamics, sediment transport, and morphology in rivers and coastal areas around the world (Caldwell & Edmonds, 2014; Hajek & Wolinsky, 2012; Leonardi, Canestrelli, Sun, & Fagherazzi, 2013; Lesser et al., 2004; Marciano, Wang, Hibma, de Vriend, & Defina, 2005; Nardin, Mariotti, Edmonds, Guercio, & Fagherazzi, 2013; Van Der Wegen, Jaffe, & Roelvink, 2011; Yuill et al., 2015).

FLOW-3D is a three-dimensional commercial CFD model in which fluid motion is described with non-linear transient, second-order differential Navier-Stokes equations. The numerical algorithm used in FLOW-3D is based on both finite difference and finite volume methods applied to a structured computational grid for computational efficiency, allowing for higher order solvers and robust conservation properties, and for simulation of complex geometries such as in-river bottom bathymetry including sand bars and irregular bank boundaries, as well as the need to include the geometry of the borrow pit (Flow Science, Inc., 2023). FLOW-3D uses the FAVOR™ algorithm to define complex geometries (Hirt & Nichols, 1981; Hirt & Sicilian, 1985), the Volume of Fluid (TrueVOF™ ; Barkhudarov, 2023) method to capture free-surface variations (Hirt & Nichols, 1981), and offers several options to represent turbulence closure including the Renormalization Group analysis (RNG) approach (Yakhot & Orszag, 1986; Yakhot & Smith, 1992) .

The first Delft3D-4 model used in this study, named the “Alliance Model” covers the Mississippi River channel from River Mile (RM) 55 to RM 75 (Figure 1). This model is a variant of the model developed for previous studies (Yuill et al., 2015). It was adopted and updated for use in this study. Updates performed by the project team included adjustments to the computational domain and model grid, refinement and de-refinement to optimize computational efficiency, updates to the bathymetry and boundary conditions, model re-calibration using recent suspended sediment observations as well as recent and historic bedform flux and morphology observations (M. Allison et al., 2018b, 2018a). The resolution of the model varied from approximately 12×20 m in the vicinity of the borrow pit to approximately 12×100 m upstream and downstream, and used 10 vertical layers throughout the water column in sigma coordinates. The sediment transport model used both cohesive and non-cohesive sediment classes; cohesive silt, and three sand classes with a median grain diameter of 92, 183, and 367 microns, and initial stratigraphy informed by surface grab samples and borings (M. Allison et al., 2018b, 2018a). More details on the model updates are provided in Appendix B.

The second Delft3D-4 model is named the “Lowermost Mississippi River (LMR) Model” (Figure 1). The model domain includes the Mississippi River downstream of the Bohemia Spillway near Bayou Lamoque and includes the Mississippi River main distributaries. This model was adopted from previous studies (Reins, 2018), and received various updates including (1) adjustments to the computational domain to better encompass all Mississippi River distributaries, (2) better integration and inclusion of east bank outflows including Neptune Pass and Fort St. Philip, (3) re-calibrated flow distribution with historic synoptic flows, (4) re-calibration of the sediment flux with more recent observations, and (5) morphology calibration using field observations and infilling analysis from monthly surveys. The resolution of this model is 25 m in transverse direction and 50 m in streamwise direction between Neptune Pass and Head of Passes and used 10 vertical layers throughout the water column in sigma coordinates. The sediment transport model used both cohesive and non-cohesive sediment classes; cohesive mud, cohesive silt, and three sand classes with a median grain diameter of 92, 183, and 367 microns, and initial stratigraphy

informed by surface grab samples and borings obtained from the engineer on record for the Upper Barataria Marsh Creation Project (Baird and Associates; Allison et al., 2018a, 2018b). More details on the model updates are provided in Appendix C.

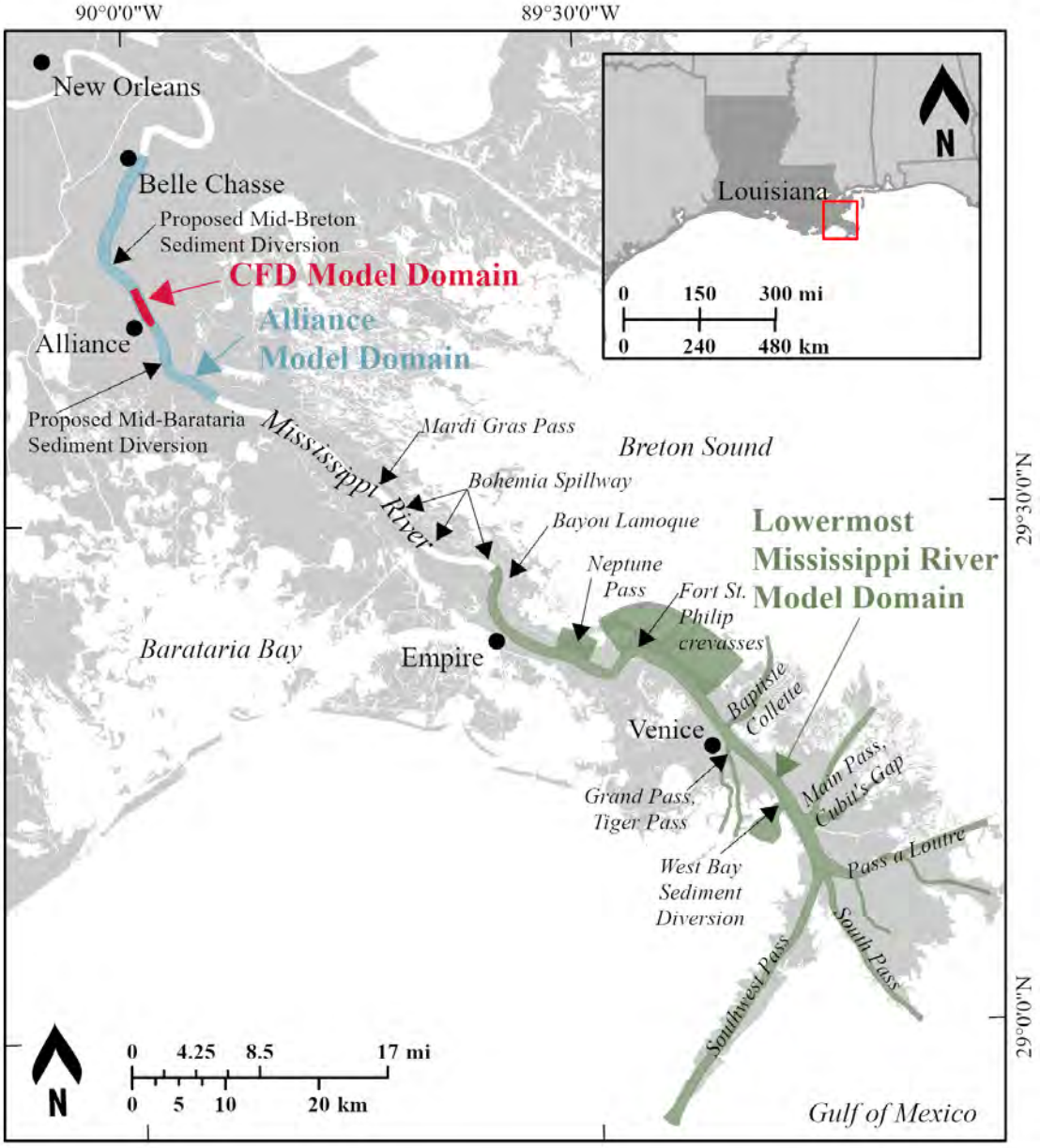

Figure 1. Study area map of the Lower Mississippi River, location, and spatial extent of the numerical models used in this work.

The Alliance Model (see Figure 2) covers a segment of the river within the "Transfer Reach", a stretch of ~190 km that does not require dredging to maintain authorized navigation depths (Espostio, Courtois, Swartz, & Miner, 2021). There are multiple sand bars along this river segment, some of which have been the site of dedicated dredging for use in coastal restoration projects (Moffat and Nichol, 2012; Moffatt & Nichol, 2012; Poff, Bass, Sweeney, Bahlinger, & Chatellier, 2011; T. Baker Smith, Inc., 2011; Thomson et al., 2019). This study focused on the AABP partly because of historical observations of infilling rates (Yuill et al., 2013) and partly because of the ongoing Upper Barataria Marsh Creation Project (NMFS,

2023). The AABP was manually implemented into the model around RM 65 using the dredge cut footprint proposed and shared with the Institute by Moffatt and Nichol, the engineer of record for the project. The pit has a surface area of 580,000 m^2, a bottom elevation of -27.4 m NAVD88 for a total volume of 5.3 million m^3 (Figure 2). The model used recent bathymetry and was calibrated with newer suspended and bedform flux measurements (M. Allison et al., 2018b, 2018a). For testing purposes, one additional simulation was also performed using the same pit geometry but reducing the pit bottom elevation to -22.9 m NAVD88 (i.e., approximately half of the depth of the original pit) resulting in a total volume of 3.4 million m^3, a reduction of 36% compared to the original volume.

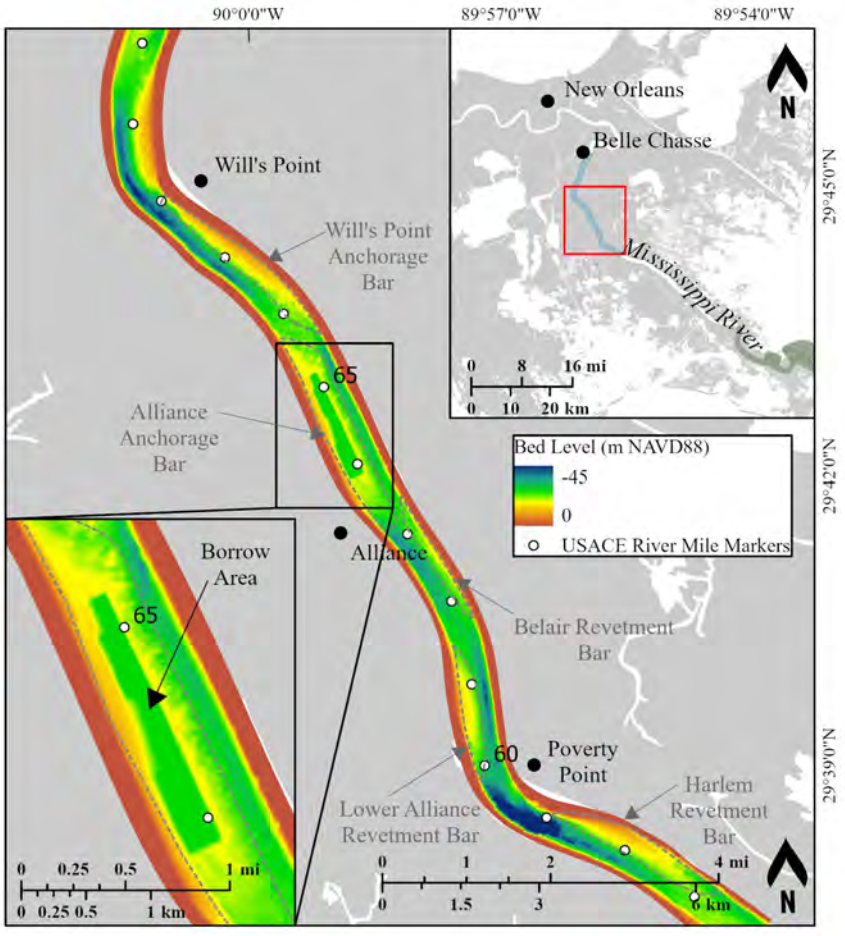

Figure 2. Model domain and bathymetry of the Delft3D-4 Alliance Model. The studied hypothetical borrow area had a surface area of 580,000 m^2 and volume of 5.3 million m^3. Gray dashed lines show polygons identifying the river sand bars used for volumetric calculations.

The LMR Model covers the lowermost part of the river (Figure 3), from the end of the Bohemia Spillway near Bayou Lamoque to the Gulf of Mexico with the addition of all major distributaries including Southwest Pass, an area that requires frequent maintenance dredging. The model domain was selected to span this reach for the following reasons. First, because the reach below Venice is frequently dredged, and this serves as an analog for study of the impacts of borrow infilling to downstream maintenance dredging, and second, because of the ongoing dredging as part of the Barataria Basin Ridge and Marsh

Creation Project – Spanish Pass Increment (BA-0203), and the availability of frequent (i.e., monthly) surveys for comparison between model results and infilling rates derived from surveys. The borrow pit area was located near Lower Venice Anchorage and was implemented in the LMR Model as shown in Figure 3. This borrow pit is referred to as VABP in this study and is located around RM 8. It has a surface area of 620,000 m^2 and a bottom elevation of -18.5 m NAVD88, resulting in a volume of 4.5 million m^3. For testing purposes, one simulation was also performed using the same pit geometry but with the pit bottom reduced to an elevation of -14.8 m NAVD88 (i.e., approximately half of the depth of the original pit) for a total volume of 2.3 million m^3.

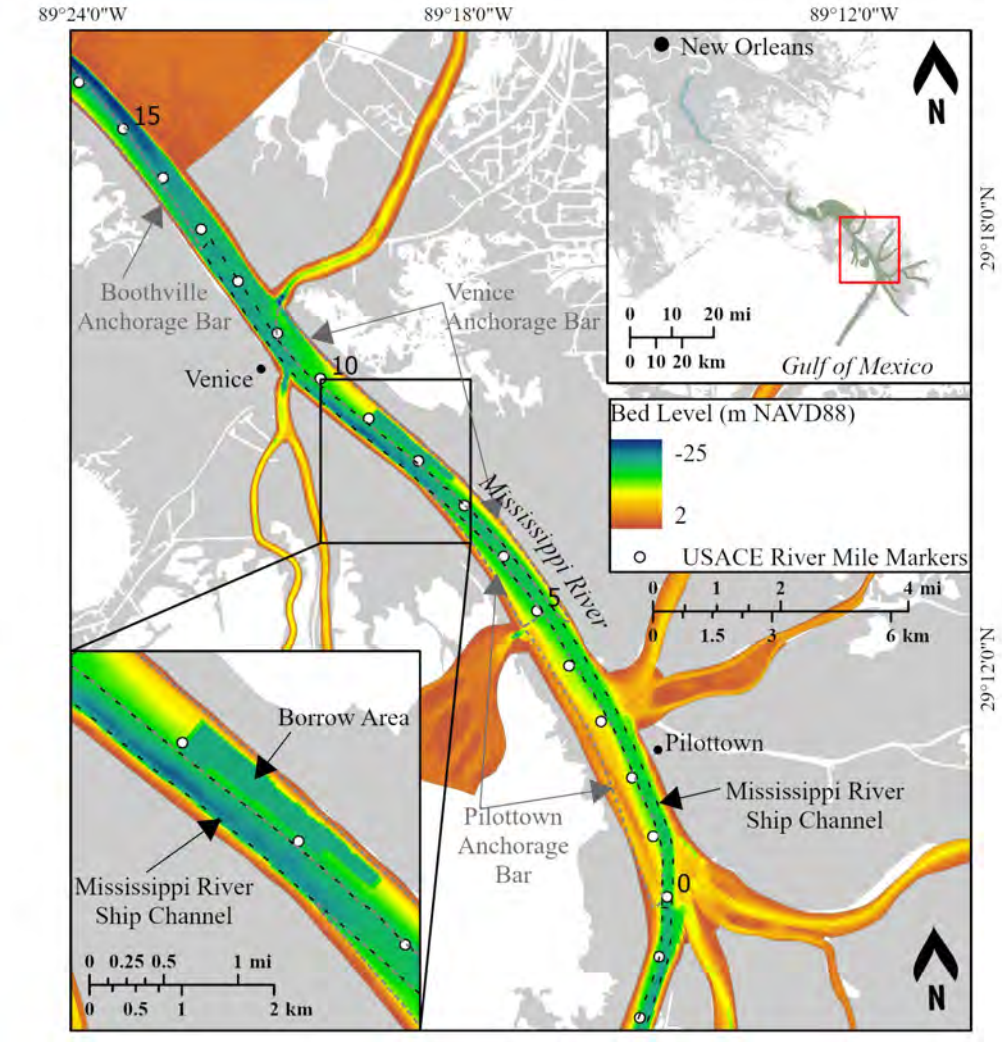

Figure 3. Model domain and bathymetry of the Delft3D-4 LMR Model. The studied hypothetical borrow area had a surface area of 620,000 m^2 and volume of 4.5 million m^3. Gray dashed lines show polygons identifying the river sand bars used for volumetric calculations. Black dashed line shows the Mississippi River Ship Channel where a navigable depth of 45 feet is maintained.

The two Delft3D-4 models were used to perform a matrix of simulations testing a wide variety of environmental scenarios to investigate the influence of different factors on borrow pit infilling. This includes evaluating the role of transient conditions by performing simulations for an entire year, capturing

the rise and fall of the river flow and stage, and evaluating the various controls on hydrograph seasonality. The role of upstream sediment supply on local sediment transport and on pit infilling was also investigated, together with the role of bar stratigraphy in influencing infilling rates. The latter was assessed by changing the bed composition and corresponding bed properties. The effect of different pit geometry and locations was also analyzed. Finally, the relative changes in infilling rates due to the presence of anthropogenic factors, such as implementation of sediment diversions, and the impacts of borrow pits on downstream maintenance dredging were quantified.

Four different hydrographs were investigated with the Alliance Model:

- 2010: An intermediate flow year with several peaks that do not exceed one million cfs.
- 2011: An intermediate flow year with one big single flood peak in spring
- 2016 (i.e., October 2015 to September 2016): An intermediate flow year with two early peaks.
- 2019 (i.e., September 2018 to August 2019): A high flow year with one prolonged peak

Additional information on how these four hydrographs were selected is provided in Appendix D. Two other hydrographs, 2015 and 2021, were used for the LMR Model. These two hydrographs were selected because of the availability of observational data for model validation (see Appendix C), and because they represent a low flow year (i.e., 2021) and an intermediate flow year (2015). Additionally, the area around Neptune Pass (Figure 1) experienced considerable changes over the past decade, where 10 years ago the outlet was small and carried much lower flow compared to present conditions in which the outlet carries a significant flow connecting the Mississippi River with Quarantine Bay (Alex S. Kolker, Weathers, Swann, Cloutier, & Renfro, 2022). For instance, in 2015 the outflow through the Ostrica reach which includes Neptune Pass was approximately 900 m^3/s (32,000 cfs; The Water Institute, 2015), and during a survey in 2022, the outflow was 3,681 m^3/s (130,000 cfs) for a similar discharge in the river (Alex S. Kolker et al., 2022). Similarly, measured outflows along the Fort St. Philip crevasses obtained by the U.S. Army Corps of Engineers, New Orleans District show that before 2015 outflows were of the order of 850–1,132 m^3/s (30,000–40,000 cfs) along this reach, reached 1,330 – 2,265 m^3/s (47,000–80,000 cfs) in 2016, and exceeded 2,830 m^3/s (100,000 cfs) since, reaching 3,737 m^3/s (132,000 cfs) in 2018 and 4,105 m^3/s (145,000 cfs) in 2019 (USACE, 2022b). As such, hydrographs 2015 and 2021 represent, respectively, the pre- and post-Neptune Pass change conditions. Details on hydrograph selections and their shape are presented in Appendix D.

Additional simulations evaluating the role of upstream sediment supply included testing higher and lower concentrations of sediment, of the order of 20%, while maintaining the same sediment rating curve. Testing also included the effect of bed sediment supply, accomplished by changing the bed composition both in terms of sediment grain size distribution and sorting. The influence of other anthropogenic impacts such as sediment diversions were evaluated by quantifying infilling rates with the presence of the Mid Barataria and the Mid Breton sediment diversions (MBSD and Breton SD, respectively), and the influence of borrow pit depth on infilling rates were evaluated by additional simulations with different initial bottom elevation (and therefore volume excavated) of the borrow pits. It should be noted that the influence of borrow pits on diversion efficiency was not evaluated in this study.

Full matrixes summarizing all the simulations that were performed are available in Appendix B and Appendix C.

3.0 RESULTS

3.1 INFILLING RATES

3.1.1 Field Observation Analysis

Infilling rates and volumes calculated from the monthly time-series single-beam surveys provided an opportunity to relate observed pit sediment dynamics to the Mississippi River hydrograph and also provided data for model calibration. The VABP was divided into three sub-areas (Figure 4) utilizing the dredge cut sequence to establish when each of the sub-areas was fully dredged to specifications. Figure 4 shows the infilling measured for the first and last time periods in each area, and Appendix A provides maps that show infilling through all time periods.

Infilling throughout the borrow pit and for each of the sub-areas was nonuniform and did not exhibit a spatial trend. In Area 1, the downstream parts of the pit experience more infilling, but in Area 2 the upstream part exhibits more infilling (Figure 4). Despite Area 3 being the most recently dredged and experiencing the least infilling during the analysis periods, it appears to be infilling more evenly compared to Area 1 and Area 2, at least initially (Figure 4). The total sediment captured by the borrow pit increased in all the areas over time as expected, however, the sediment infilling rate decreased over time (Table A-1; Figure 4). Bedforms also exist in the borrow pits. Movement of these bedforms contributed to some of the negative infilling values (seen in the darker blue colors in Figure 4) because migration of dune and ripple crests and troughs caused the bed elevation to change, but bedform migration does not necessarily mean there is a change in volume (this can be seen particularly well in Area 3). Despite bedform movement resulting in parts of the bed appearing lower locally, the infilling volume within the borrow pit did not change solely because of bedform migration, because the sums of all raster cells are taken over the whole area of analysis, capturing net change within the pit regardless of bedform migration. Note that because the bathymetry data was collected using single beam sonar, bedform-scale dynamics are not fully captured.

The Area 1 mean bed level change from infilling was more than 0.15 m/week (vertical aggregation) during the first two months following completion of dredging, which coincided with the rising limb of the Mississippi River hydrograph (Figure 5). Bed aggradation rate within the borrow pit declined to approximately 0.05 m/week by February of 2022 and when flow in the river dropped below ~20,000 m^3/s (i.e., 700,000 cfs) in April the infilling stopped. Similarly, between March and April of 2022, Area 2 experienced similar bed level response post dredging of more than 0.15 m/week, when the flow in the river was rising again and reached ~28,000 m^3/s (i.e., 980,000 cfs), and fell to approximately 0.1 m/week from April through June of 2022, during which time the flow varied from ~22,500 to ~15,500 m^3/s (i.e., 800,000 cfs to 550,000 cfs). Bed level change when flows in the river declined further to less than ~14,000 m^3/s (i.e., 500,000 cfs) were much less than 0.05 m/week. In Area 3, dredging was completed after Areas 1 and 2, and hence during lower and declining flows in the river (declining from ~22,000 to ~15,500 m^3/s [i.e., 780,000 to 550,000 cfs]) and bed elevation change was of the order of 0.03 m/week and remained through December, 2022 (Figure 5).

Area 1 is approximately 313,225 m^2, and dredging was completed on December 20, 2021. Initial infilling rates within a month of dredging were approximately 225,000 m^3/month, declining rapidly to

approximately 74,000 m^3/month in February 2022, and declining further to 40,000 m^3/month through March 24, 2022. By May 23, 2022, the decline in flow in the river reduced infilling rates to nearly zero, fluctuating from 18,000 to 60,000 m^3/month through December 27, 2022, before increasing to 230,000 m^3/month for the month of January 2023. Area 2 is approximately 173,775 m^2, and dredging was complete by February 23, 2022. Initial infilling rates within the first month were approximately 125,000 m^3/month, declining rapidly to approximately 75,000 m^3/month through May 23, 2022, and fluctuated between 1,000 to 10,000 m^3/month through December 27, 2022, before increasing to 110,000 m^3/month for the month of January 2023. Area 3 is approximately 145,325 m^2, and dredging was completed by May 23, 2022. Infilling rates for this area were low initially because the flow in the river was low upon completion of the dredging. The infilling rates remained low fluctuating from 2,000 to 20,000 m^3/month through the end of the year (December 27, 2022), and in the month of January 2023, infilling rates increased to approximately 95,000 m^3/month (Table A-1; Figure 5).

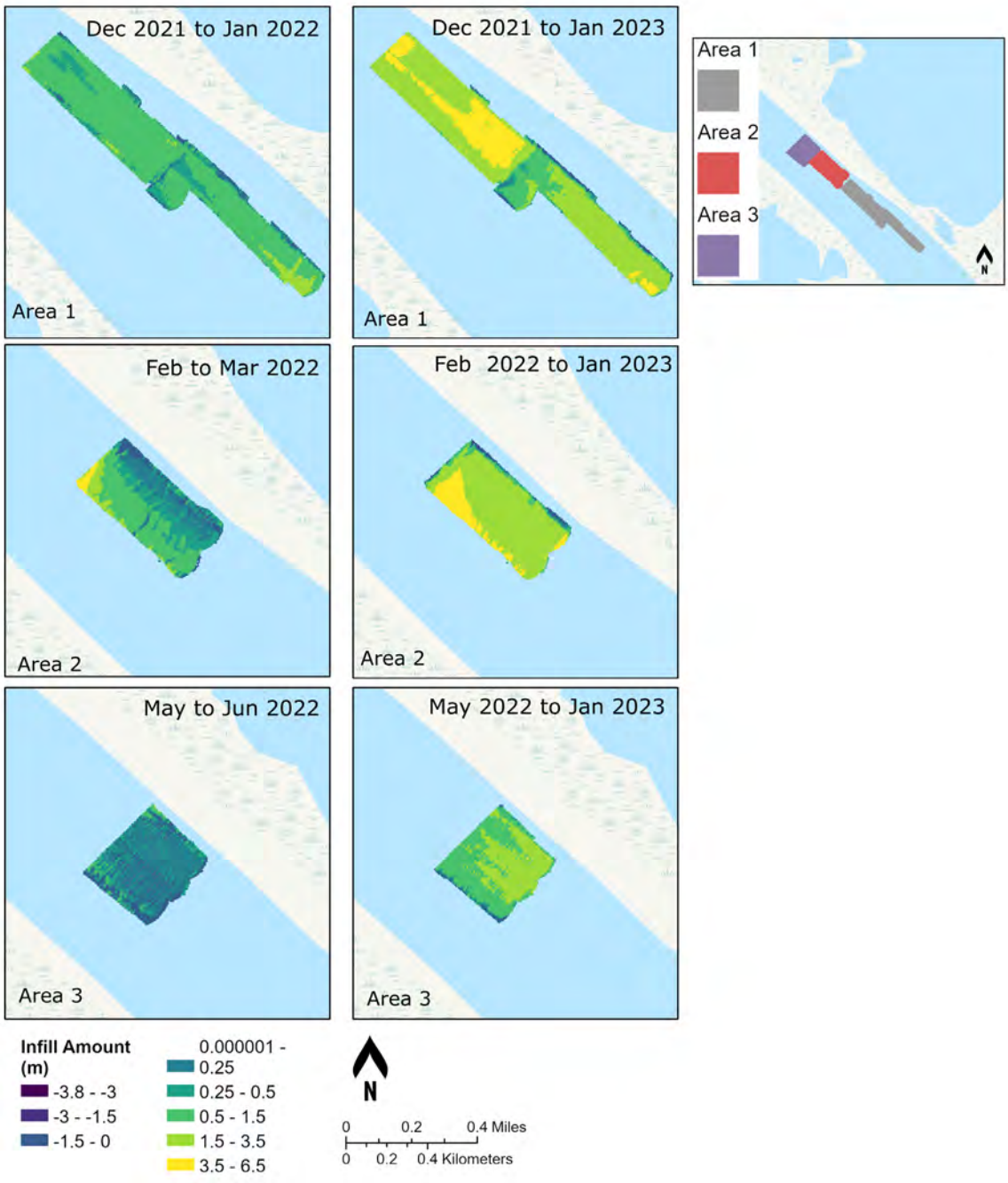

Figure 4. Summary of vertical aggradation showing infilling amounts (in meters), with the first infilling period for each sub-area of the VABP on the left and the last infilling period on the right. A map of these three areas is shown on the right and in Figure A-6.

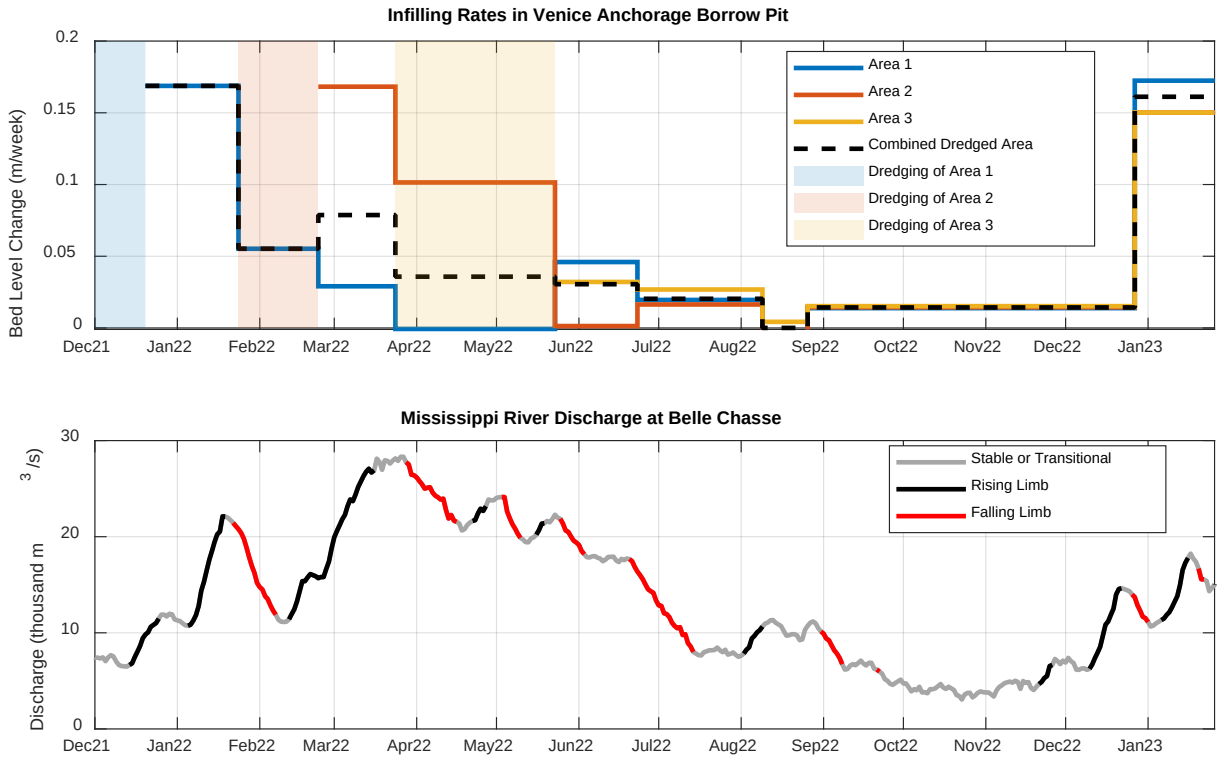

Figure 5. Measured infilling rates of the VABP during and after completion of dredging for the Spanish Pass Ridge Creation Project, which took place in December 2021 (Area 1, 313,000 m^2), February 2022 (Area 2, 174,000 m^2), and April-May 2022 (Area 3, 145,000 m^2) (upper panel). The Mississippi River Discharge at Belle Chasse plot indicates periods which had rising and falling limbs (lower panel). Rising and falling limbs were calculated using a two-week window. Relatively high infilling rates were found for Area 1 directly after dredging finished in December 2021, which coincides with a rising limb in the Mississippi River hydrograph. Similar infilling rates were found for Area 2 directly after dredging finished in February 2022, which also coincides with a rising limb. Area 1 is located downstream of Area 2 and infilled at a much lower rate after dredging of Area 2. Infilling rates were relatively low for all sub-areas between June and December but strongly increased again in January 2023.The lines indicating infilling rates for Areas 2 and 3 overlaped during this timeframe. This figure only contains vertical infilling rates (instead of volumes) because the borrow pit footprint expanded over time due to ongoing dredging.

3.1.2 Numerical Modeling Results

Simulated infilling patterns indicate that annual bed level change in both the AABP and VABP borrow pits locally exceeded 8 m (Figure 6). Greater infilling rates are predicted for the AABP (Figure 6A and C) in comparison with the VABP (Figure 6B and D). The AABP initially shows the largest magnitude bed level changes at the upstream end of the borrow pit (Figure 6C, day 99) however this pattern is reversed from day 199 onward as evidenced by relatively larger deposition near the downstream end of the pit and erosion of previously deposited material at the upstream end of the pit. By contrast, infilling patterns in the VABP did not show the same reversal, and instead consistently experiences the largest bed level changes at the upstream side of the pit during the first-year post-dredging.

Simulated bed level changes are not only limited to deposition within the borrow pit but also entail erosion at the upstream and downstream channel-pit transitions. For instance, model results show that for the AABP, the observed headcutting (~4 m vertical erosion) at the upstream part of the pit appeared to be an extension of an erosional zone on the upstream portion of the Alliance Bar (~2 m vertical erosion) trending toward the pit (Figure 6A and C) which also showed erosion of the east pit wall that separates the borrow pit from the channel thalweg. Erosion of the downstream terminus of the borrow pit (~2 m) and downstream bar migration are likely responsible for the deposition (~2–4 m) seen at the downstream end of the Alliance Bar, approximately one kilometer from the downstream pit terminus (Figure 6A and C). Similarly, for the VABP, erosion of the bar upstream appeared widespread but low in magnitude (~1 m) which promoted deposition that infills the upstream part of the pit to near pre-dredge bed elevation (Figure 6B and D). Deposition and bed level change along the pit diminished downstream, until the downstream pit terminus, where the model predicted erosion of the pit wall. Erosion was greatest at the end of the pit but diminished within 1 km of the pit in the downstream direction (Figure 6B and D).

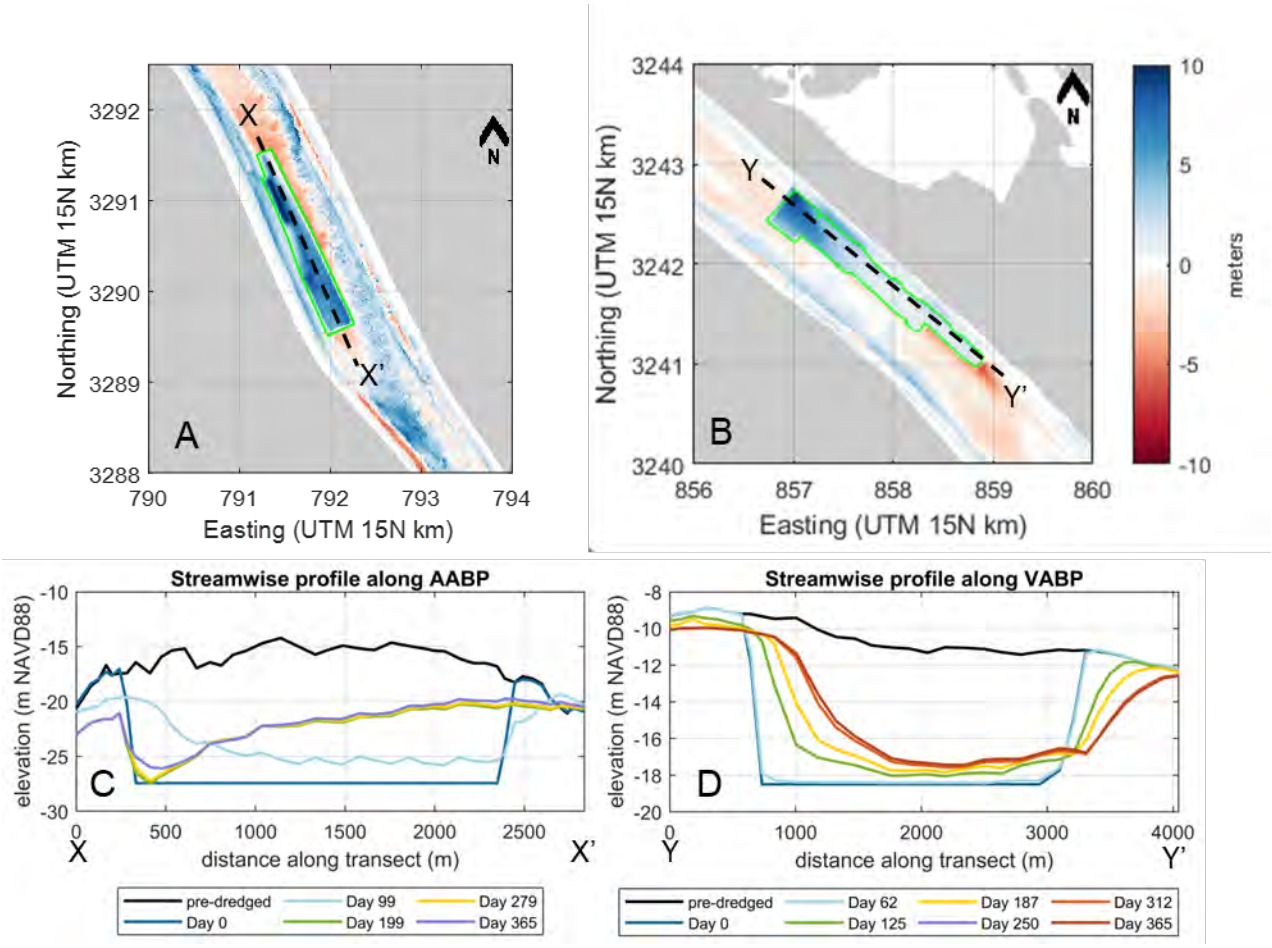

Figure 6. Modeled annual bed level change difference between scenarios with and without borrow pit for (A) the AABP (RM 65) with the 2011 hydrograph and (B) the VABP (RM 8) with the 2015 hydrograph. Borrow pit footprints are indicated by the green polygons. Streamwise bed level profile X-X' (see panel A for location) along the AABR for pre-dredged scenario (C), when the pit was dredged and for several subsequent timestep using 2011 hydrograph; streamwise bed level profile Y-Y' (see panel B for location) along the VABR for pre-dredged scenario (D), when the pit was dredged and for several subsequent timestep using 2015 hydrograph.

The model-simulated infilling rates for both borrow pits are on the order of 1–3 million m^3 per year (Table 1 and Table 2). The infilled volumes correspond to approximately 22% to 54% of the original borrow pit volumes depending on the hydrograph and translate to average bed level changes within the pits that vary between 1.6 and 4.7 m. Higher infilling rates were found for the AABP despite similar surface areas between AABP (580,000 m^2) and VABP (620,000 m^2). The AABP shows similar infilling volumes for all four hydrographs examined, whereas the VABP experiences nearly twice as much infilling for hydrograph 2015 compared with 2021. Approximately 65% of the infilled sediment in the VABP consists of fine sand (median diameter 92 microns), while about 15% is very fine (median diameter 183 microns) and/or medium sand (median diameter 367 microns),, and approximately 20% of the infilled material is silt. The AABP is primarily filled with fine sand (~55%, median diameter 183 microns) and medium sand (~30%, median diameter 367 microns), and the remaining 15% of infilled material is very fine sand (median diameter 92 microns), or silt. These estimates are general and represent averages, as the exact composition of the infilled material depends on the hydrograph and varies spatially throughout the borrow pit.

Model simulations testing the influence of the initial pit depth on infilling rates for AABP and VABP, while maintaining the same pit footprints, indicate a similar reduction in infilling volume. For the AABP infilling volume decreased from 2.65 to 1.69 million m^3 (-36%) for the 2011 hydrograph, whereas the VABP infilling decreased from 1.98 to 1.03 million m^3 (-48%) for the 2015 hydrograph. Relative infilling rates of the two shallower pits remained similar to the original pits: 49% for the AABP and 44% for the VABP (Table 1; Table 2).

Table 1. Infilling volumes, infilling rates, and average bed level change for the AABP over a 7-month period of various hydrographs that includes the flood peaks. Cumulative water volumes are shown as a reference in the rightmost column. The results are presented for a 7-month period because one of the annual simulations performed started presenting unstable behaviour after that. All simulation reched the maximum infilling volumes after 7 months.

Hydrograph	Infilling Volume (million m^3)	Infilling Rate (% of Borrow Pit Volume)	Average Bed Level Change in Pit (m)	Water Volume (million m^3)
2010	2.53	48%	4.36	368,339
2011	2.65	50%	4.56	361,770
2016	2.64	50%	4.54	373,078
2019	2.73	51%	4.71	431,781
2011 with 36% smaller pit volume	1.69	49%	2.92	361,770

Table 2. Infilling volumes, infilling rates, and average bed level change for the VABP over a 12-month period for the 2015 and 2021 hydrographs. Cumulative water volumes are shown as a reference in the rightmost column.

Hydrograph	Infilling Volume (million m^3)	Infilling Rate (% of Borrow Pit Volume)	Average Bed Level Change in Pit (m)	Water Volume (million m^3)
2015	1.98	43%	3.16	533,087
2021	1.00	22%	1.61	459,827
2015 with 50% smaller pit volume	1.03	44%	1.65	533,087

Borrow pit infilling rates correlate strongly with discharge and sand transport rates in the Mississippi River (Figure 7 and Figure 8). Models indicate higher infilling rates during periods of relatively high sand transport, which overlap with periods of high river discharge (i.e., above 20,000 m^3/s or 706,000 cfs). As expected, the decline of sand transport to negligible magnitudes for discharges lower than 15,000 m^3/s (530,000 cfs) corresponds to negligible borrow pit infilling during these periods. The largest sand transport rates, in contrast, are found during high discharges (i.e., above 30,000 m^3/s or 1.06 million cfs). Most of the infilling for a given hydrograph typically occurs during a relatively brief period of time (2–4 weeks), when the river is rising. Model results show that the rate of rise in river discharge (Figure 7B) is proportional to the increase in suspended and bedload sand transport (Figure 7C), with a corresponding increase in the cumulative borrow pit infilling predicted (Figure 7A). This can be observed for the AABP during the first and second months following the start of the hydrograph 2010 and during the fourth month since the start of hydrograph 2016 (Figure 7A), and for the VABP by the months of March and April for hydrograph 2021 (Figure 8A).

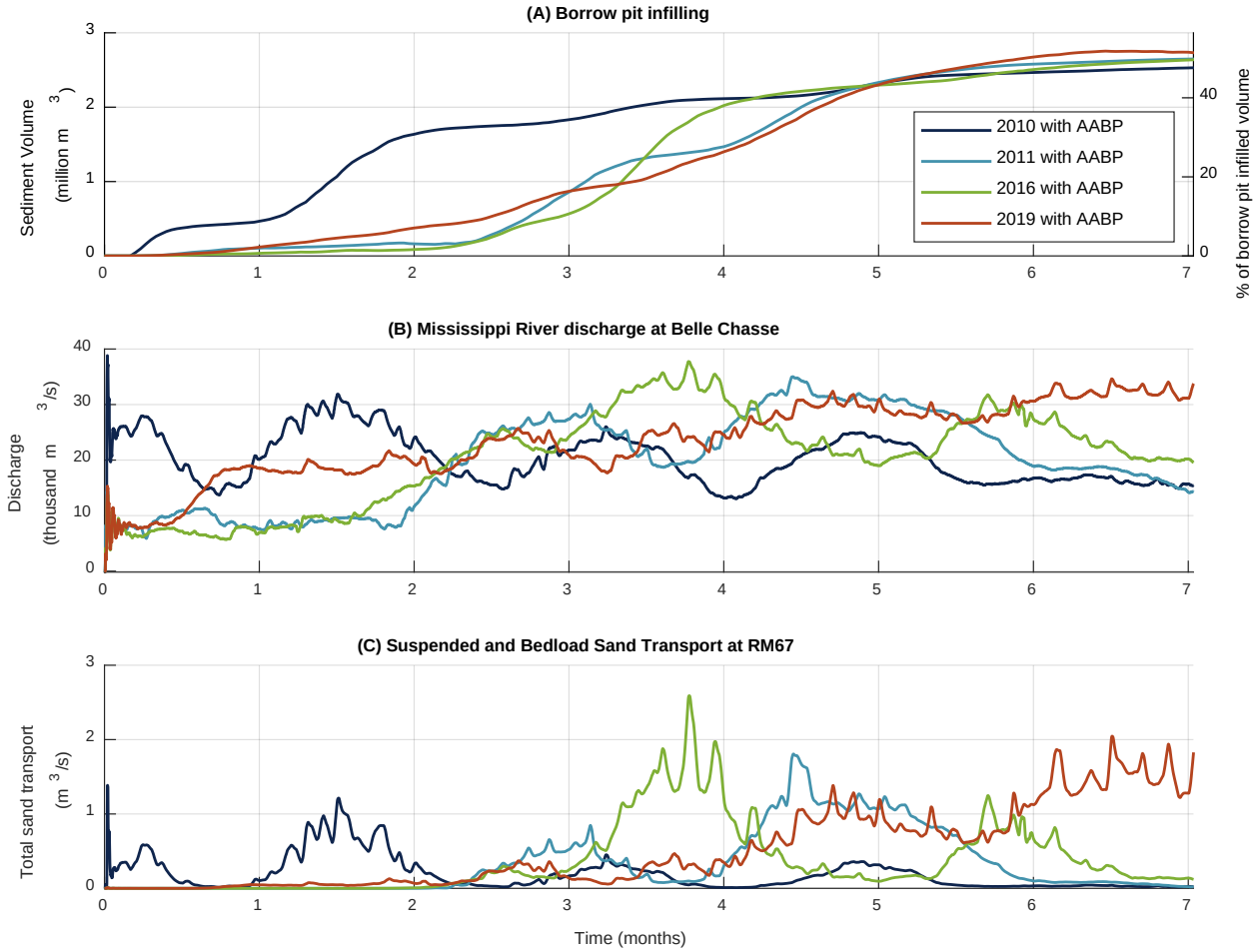

Figure 7. AABP infilled volume of sediment and infilled percentage volume relative to the original pit volume (A), Mississippi River discharge at Belle Chasse (B), and total sand transport at RM 67 (i.e., just upstream of the pit) (C) modeled for the Alliance Model with four different hydrographs.

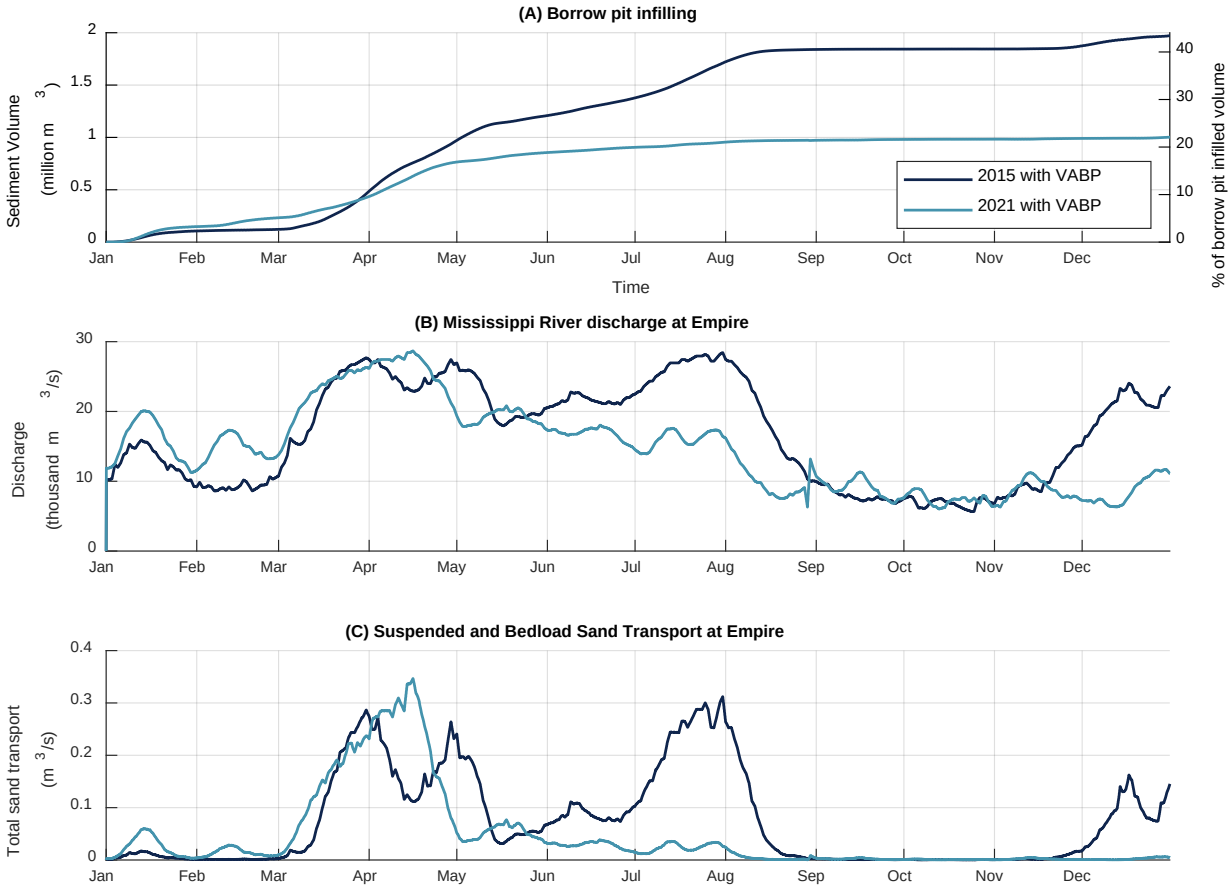

Figure 8. VABP infilled volume of sediment and infilled percentage volume relative to the original pit volume (A), Mississippi River discharge at Empire (B), and total sand transport at Empire (C) modeled for the Lowermost Mississippi River with two different hydrographs.

The operation of upstream sediment diversions has a noticeable influence on borrow pit infilling volumes (Table 3). Model results indicate that annual borrow pit infilling volumes reduce by 19% when the MBSD is operated in accordance with current plans (Messina, Bregman, Jung, Yuill, & Roberts, 2019; USACE, 2022a), and infilling volumes are reduced by as much as 30% when both the MBSD and Breton SD are operating simultaneously (Messina et al., 2021). These reductions in borrow pit infilling volumes are the result of a reduction of the residual flow in the river at the VABP, following upstream flow extraction by the sediment diversion projects, because both diversions operate during periods with high river discharges, such as March and April 2021 (see Figure C-17 in Appendix C) when most infilling takes place. Reducing the residual river flow downstream during those periods attenuates the hydrograph peak and reduces borrow pit infilling. Furthermore, the combination of diversion operations and resulting flow extraction, and the increased outflows in the LMR Model due to present day crevassing along the east bank (as evident by contrasting the 2015 to the 2021 hydrograph, Table 3), further underscore the influence of the hydrograph on borrow pit infilling rates.

Adjustments in upstream sediment supply, tested by increasing and reducing the upstream sediment concentration by 20%, showed no changes in infilling rates for both AABP (Figure B-13A) and VABP (Figure C-15A). Experiments with modified sediment characteristics (i.e., larger grain diameters for the very fine and fine sand fractions, see details in Table C-2) performed with the Alliance Model showed that while the total sand transport decreased by up to 25% (Figure B-14C), it resulted in a 5% increase in the infilling rates at AABP (Figure B-14A). Sensitivity tests performed to evaluate the influence of bed composition on sediment entrainment and infilling rates showed slightly different results for the two borrow pits. At the AABP, when the fine sand composition in the bed decreases (i.e., from 43% to 25% in the top layer, and from 71% to 50% in the bottom layer following increasing of the corresponding medium sand percentages; see details in Table B-3), total sand transport rates are reduced by 10% when discharge exceeds 20,000 m^3/s (Figure B-12B and C). Cumulative infilling is most noticeably influenced when flows are above 30,000 m^3/s, resulting in an increase in sediment infilling volumes of 8% (or 230,000 m^3) by the end of the year for hydrograph 2011 (Figure B-12A). At the VABP, when the fine sand bed composition increases, total sand transport remains unchanged regardless of flow (Figure C-14B and C) and the cumulative infilling shows a small increase (+ 2-3%; Figure C-14A).

For additional details the reader is directed to Sections B.7 and C.7 in Appendix B and Appendix C, respectively.

Table 3. Infilling volumes, infilling rates, and average bed level change for the VABP over a 12-month period for scenarios with and without MBSD and Breton SD for the 2015 and 2021 hydrographs.

Hydrograph and Scenario	Infilling Volume (million m^3) [difference relative to no-diversion scenario]	Infilling Rate (% of Borrow Pit Volume)	Average Bed Level Change in Pit (m)	Water Volume (million m^3) [difference relative to no-diversion scenario]
2021	1.00	22%	1.61	459,827
2021 with MBSD	0.81 [-19%]	18%	1.30	430,217 [-6%]
2021 with MBSD and Breton SD	0.71 [-30%]	16%	1.13	412,761 [-10%]
2015	1.98	43%	3.14	533,087
2015 with MBSD	1.64 [-17%]	36%	2.63	496,156 [-7%]
2015 with MBSD and Breton SD	1.44 [-27%]	32%	2.30	473,642 [-11%]

The correlation between borrow pit infilling (i.e., presented as bed level change over time) and the Mississippi River discharge volumes and trends (Figure 9) resulting from model results confirm that little to no infilling occurs when river discharges remain below 10,000 m^3/s for VABP and 15,000 m^3/s for AABP which corresponds to the average flow when sand is entrained from the river bed into suspension (Ramirez & Allison, 2013b; Yuill et al., 2015). Results from both borrow pits show that infilling rates increase linearly with discharge when flow exceeds 10,000–15,000 m^3/s and reach an inflection point around 20,000 m^3/s for AABP and 22,000 m^3/s for VABP where discharges continue to increase linearly, but at a higher rate. Infilling rates are typically highest during the rising limb of the river hydrograph (Figure 9A and C), with infilling volumes reaching 500,000 m^3/week for AABP and 100,000 m^3/week for VABP. Infilling rates during the falling limb of the hydrograph (Figure 9B and D) are typically lower and the higher degree of scatter demonstrates a weaker correlation between infilling and discharge particularly for the AABP.

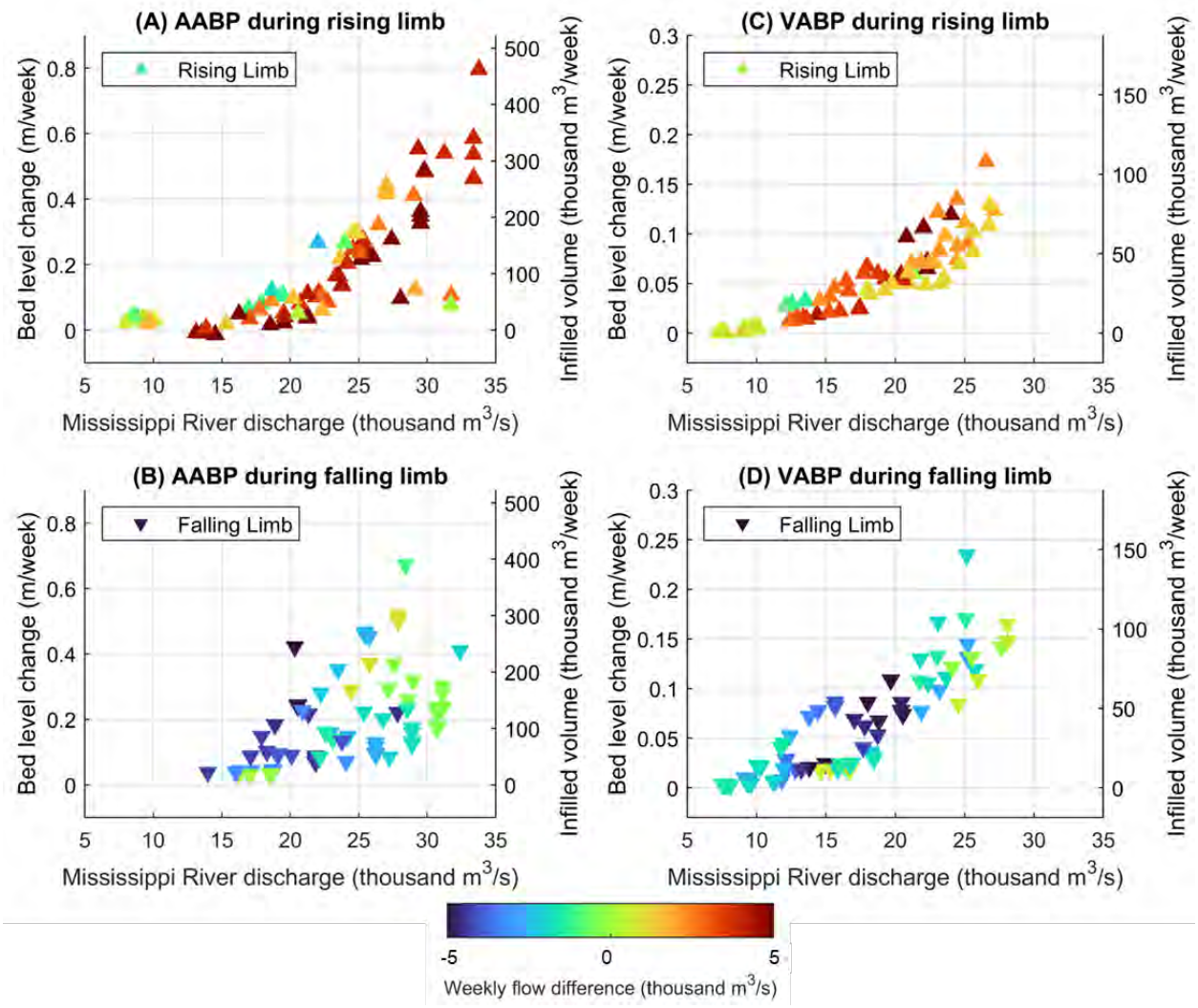

Figure 9. Modeled infilling rates (as weekly bed level change) of the AABP as a function of weekly averaged water discharge in the Mississippi River during rising limb (A) and falling limb (B). Modeled infilling rates (as weekly bed level change) of the VABP as a function of weekly averaged water discharge in the Mississippi River during rising limb (C) and falling limb (D). A two-week window was used to determine if it was a raising or a falling limb. The color of the data points indicates the slope of weekly discharge in the Mississippi River (i.e., difference with the discharge the previous week).

A comparison between model results and measured infilling rates and their correlation with the Mississippi River discharge (Figure 10) suggest that the Alliance Model tends to overestimate infilling rates in the AABP (Figure 10A) while model results are in closer agreement with measurements for the VABP (Figure 10B). The measured weekly infilling rates for the AABP (Figure 9A) are based on bathymetric surveys that were obtained relatively infrequently (i.e., 2–6 months; (Yuill et al., 2013, 2015) whereas daily model data were available for the Alliance Model and were averaged on a weekly basis. The low frequency of these surveys for AABP hinders the analysis of the short-term infilling variations that might be related to flood peaks and corresponding sand entrainment.

More frequent bathymetric surveys (i.e., monthly or every two months) were available for the VABP between December 2021 and January 2023, a period with larger fluctuations in river discharge. Surveys

focused on three sub-areas of the pit (Figure 10B). Measured infilling rates are slightly larger for discharges below 10,000 m^3/s (353,000 cfs) but in close agreement with model results for discharges above 15,000 m^3/s (530,000 cfs). Some of the outliers in measured infilling rates are possibly a result of the ongoing dredging activity while the bathymetric surveys were obtained. The infilling rates averaged across the entire area that was dredged at a given point in time (Figure 10B) show less scatter and a close agreement with model results.

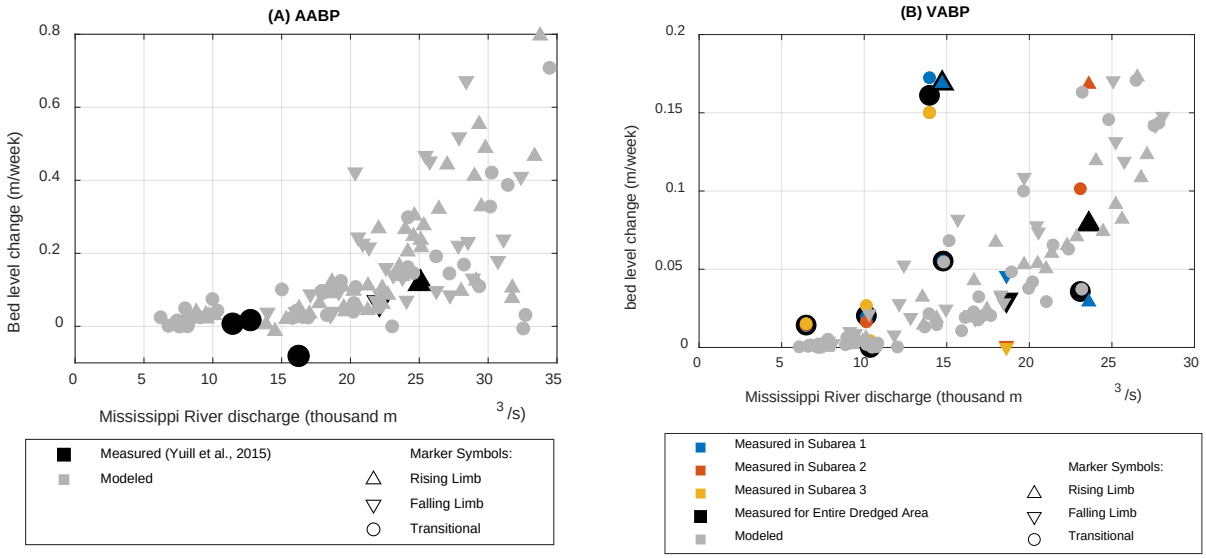

Figure 10. Comparison between modeled and measured infilling rates in (A) the AABP and (B) the VABP. Panel A shows in gray modeled infilling rates for the AABP (580,000 m^2) using results from all tested hydrographs (i.e., 2010, 201, 2016 and 2019) and, in black, measured infilling rates of the borrow area (280,000 m^2) that was dredged in 2010 for the Bayou Dupont marsh creation project (also see section B.8 in Appendix B) (Yuill et al., 2015). Both modeled and measured borrow areas are situated at the same channel bar near the Alliance Anchorage, however, measured infilling rates are on the lower end of modeled infilling rates. Panel B shows modeled infilling rates for the VABP (620,000 m^2) and measured infilling rates of the borrow areas 1, 2 and 3 (combined area of 632,000 m^2) dredged between December 2021 and May 2022 for the Spanish Pass Ridge Creation Project (see Appendix A). Infilling rates measured for each sub-area are represented by colored markers, infilling rates averaged for the entire dredged area (which expands over time) are represented by the black markers. A two-week window was used to determine if it was a rising or a falling limb. The high infilling (~0.15–0.17 m/week) observed for VABP, can be explained by the early onset of the 2022 and the 2023 flood. During the early onset of the flood infilling rates in the field appear to be three times higher. Models did not resolve this process well, as they did not predict that abrupt a transition during the flood onset, but show very good agreement for the rest of the year. This high infilling is short-lived, and after approximately two weeks, as in the next monthly surveys, rates in the field were similar to those predicted by the model.

3.2 SIMULATED LOCAL AND REGIONAL SEDIMENT TRANSPORT TRENDS

Numerical models offer a unique framework to study and analyze the local and regional effects of borrow pits. Proximal and distal changes induced by the borrow pit (Figure 11; Figure 12) showed little influence in suspended sand concentrations or bed levels greater than 1 km upstream of the pit footprints. The most significant reductions of suspended sand concentrations were found within the borrow pits (Figure 11), where the highest rate of bed aggradation also occurs (Figure 12) and in the channel located adjacent to the pits, which also experienced bed aggradation. These reductions locally exceeded 10 mg/L which is equivalent to a 30% reduction of the absolute sediment concentrations (Figure 11). Similar results were found by Brown and Bell in their analysis of a conceptual Spanish Pass Restoration borrow pit (Figure 14 and 15 in Brown & Bell, 2019).

The upstream and downstream channel-pit transitions experienced increased sediment concentrations and some degree of bed level degradation, most noticeably in the first kilometer downstream of the pit (Figure 11; Figure 12). Further downstream of the borrow pits, a more extensive but smaller-magnitude reduction of suspended sand concentrations was observed, which diminished in magnitude with distance from the pit. Suspended sand concentrations were reduced by up to 5 mg/L which equates to up to 10% of the absolute sand concentrations. This reduction was mostly diminished at the downstream end of the Alliance Model (~12 km downstream of the AABP) and was fully diminished near Head of Passes in the LMR Model (~12 km downstream of the VABP). Bed level degradation is of the order of decimeters in the first kilometers downstream of both borrow pits, and also diminished in magnitude with distance from the borrow pits.

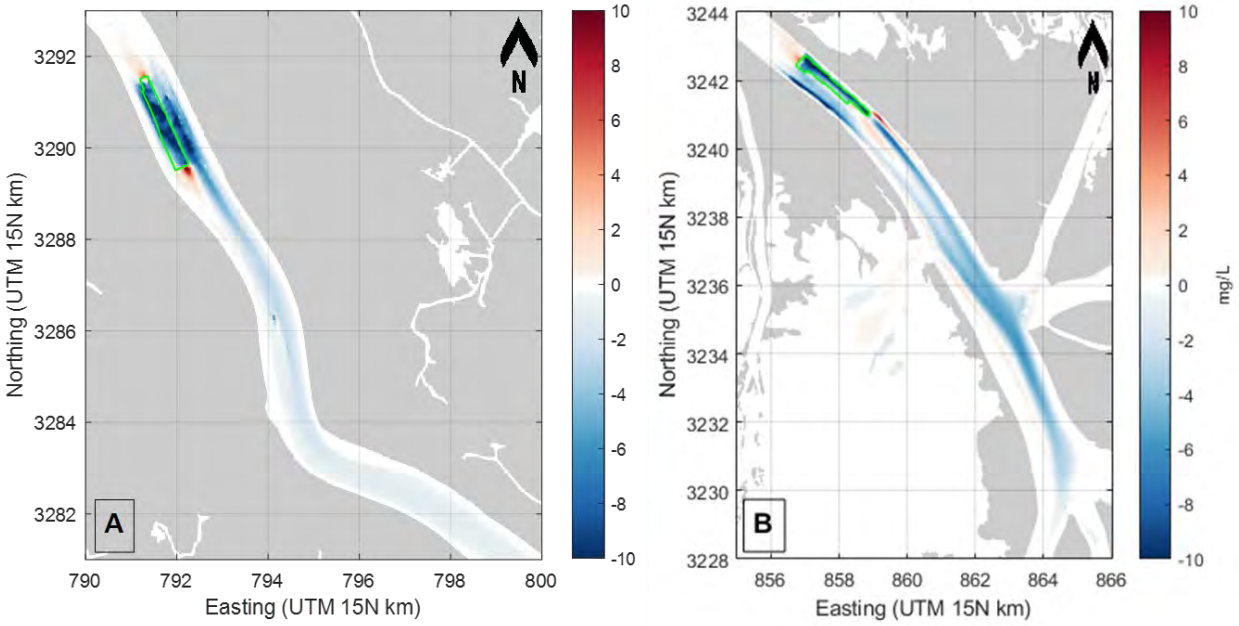

Figure 11. Difference in depth-averaged suspended sand concentrations (mg/L) between with-pit and without-pit scenarios for (A) the AABP (RM 65) during the rising limb of the 2011 hydrograph (March 15) and (B) the VABP (RM 8) during the rising limb of the 2015 hydrograph (March 15). Absolute suspended sand concentrations at both borrow pits ranged between 20 to 40 mg/L during this time. Borrow pit footprints are indicated by the green polygons.

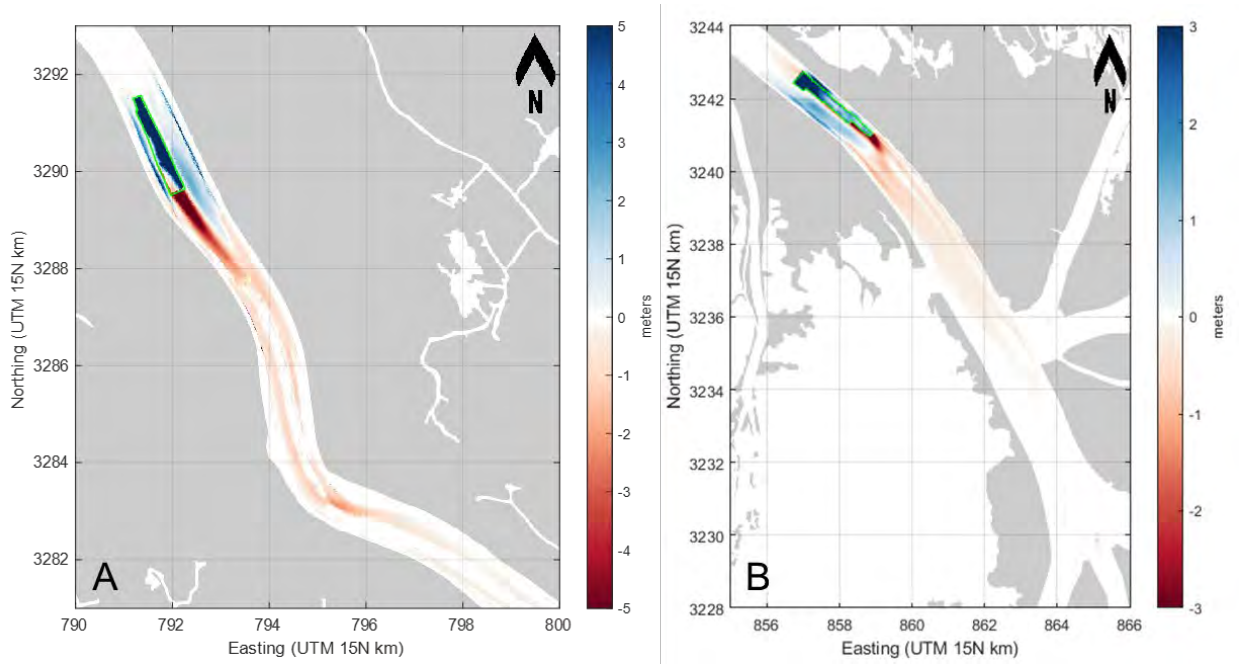

Figure 12. Annual bed level change difference (meters) between scenarios with and without borrow pit for (A) the AABP (RM 65) with the 2011 hydrograph and (B) the VABP (RM 8) with the 2015 hydrograph. Borrow pit footprints are indicated by the green polygons.

A quantitative assessment of volumetric evolution of sand bars and dredging volumes comparing simulations with and without pit scenarios confirmed the influence of borrow pits to downstream geomorphology (Figure 13, Figure 14, Figure 15, and Figure 16). Specific polygons (outlined with gray dashed lines in Figure 2 and Figure 3), were used to calculate volumetric changes over time for selected river bars upstream and downstream of the pits. No noticeable impacts are found for sand bars upstream of the AABP (i.e., Wills Point Anchorage Bar presented in Figure 13) and VABP (i.e., Boothville Anchorage Bar presented in Figure 15 and Figure 16). The sand bars that contain the borrow pits, i.e., the Alliance Anchorage Bar for the AABP (Figure 13 and Figure 14) and the Venice Anchorage Bar for the VABP (Figure 15 and Figure 16), captured noticeably larger sediment volumes in the with-pit scenarios due to infilling of the borrow pits.

Borrow pits have the opposite effect on downstream sand bars where reduced aggradation or increased degradation can be observed. However, for the AABP (Figure 13 and Figure 14), the combined reduction of channel bar volume downstream of the pit (Belair, Lower Alliance, and Harlem revetment bars) was approximately 870,000 m^3, which is equal to 48% of the 1.79 million m^3 of volume gained at the Alliance Anchorage Bar that contains the AABP. The reduction of volume in the Pilottown Anchorage bar downstream of the VABP was approximately 710,000 m^3 for the 2015 hydrograph, a reduction of 26% compared to the without-pit scenario. This reduction is equal to 60% of the 1,200,000 m^3 of volume gained at the Venice Anchorage Bar where the VABP is located (Figure 15 and Figure 16).

Experiments with finer bed composition performed with the LMR Model showed less aggradation (~3%) of the Boothville Anchorage Bar, which is located upstream, more aggradation of the Venice Anchorage Bar (~9%) and the Pilottown Anchorage Bar (~12%). Experiments with changes in upstream sediment

supply via changes in sediment concentration did not show significant deviations in bar dynamics. Model results varied for the Alliance reach. Experiments with a reduced upstream sediment concentration (~20%) showed less aggradation of the Wills Point Bar (~2%) and the Alliance Anchorage Bar (~2%). However, the three smaller sand bars located downstream of Alliance Anchorage Bar (i.e., Belair Revetment Bar, Lower Alliance and Harlem Revetment Bar), showed a combination of aggradation and degradation patterns (volumetric change from +2% and -7%). Moreover, experiments with coarser bed composition and coarser sediment composition supplied upstream, showed less aggradation at the Will Point Bar (~8-9%), more aggradation of the Alliance Anchorage Bar (~5-11%), more aggradation of the Belair Revetment Bar (~33-35%) and finally, less aggradation on the two sand bars downriver (~15-38%). It is noted that the three sand bars located downstream of the Alliance Anchorage are approximately half to one-quarter the size of the Alliance Anchorage bar itself.

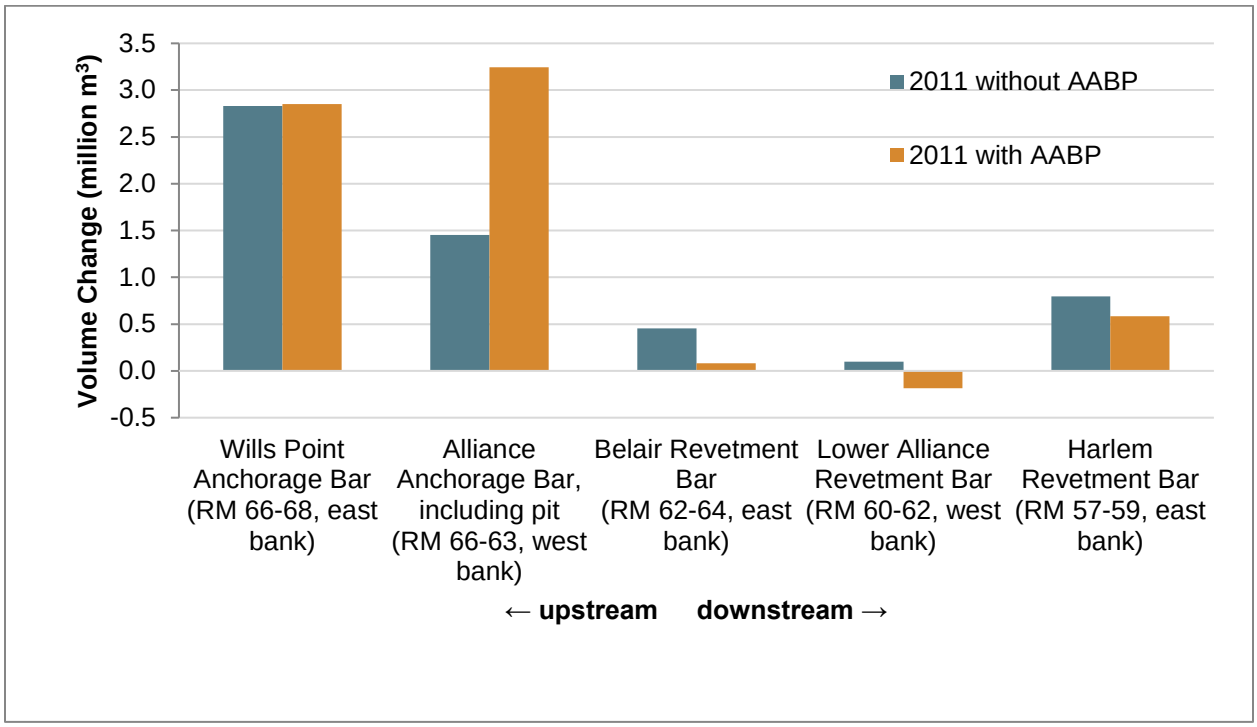

Figure 13. Volume changes at sand bars between Wills Point (RM 66) and Myrtle Grove (RM 58) for scenarios without and with the Alliance Anchorage Borrow Pit (AABP, RM 65) after the first 7 months of hydrograph 2011. See Figure 2 for locations of polygons used to define bars for these calculations.

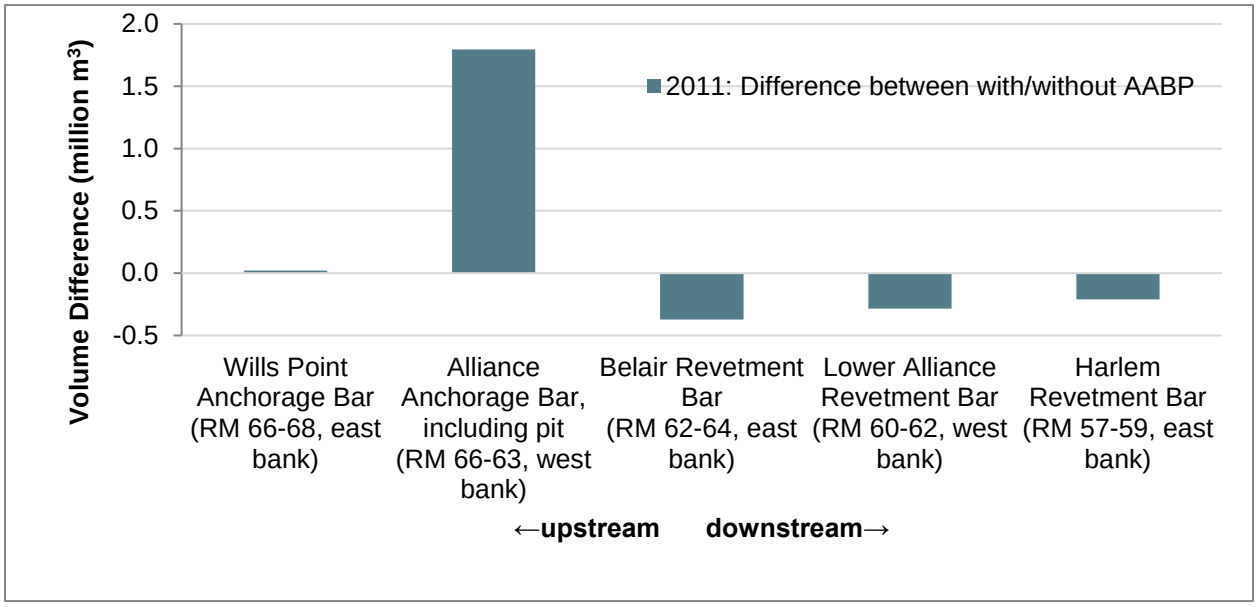

Figure 14. Volume differences between with-pit and without-pit scenarios showing the modeled impact of the Alliance Anchorage Borrow Pit (AABP, RM 65) on proximal sand bars after the first 7 months of the 2011 hydrograph. Positive volume change indicates an increase of aggradation (or decrease of degradation) due to the presence of a borrow pit.

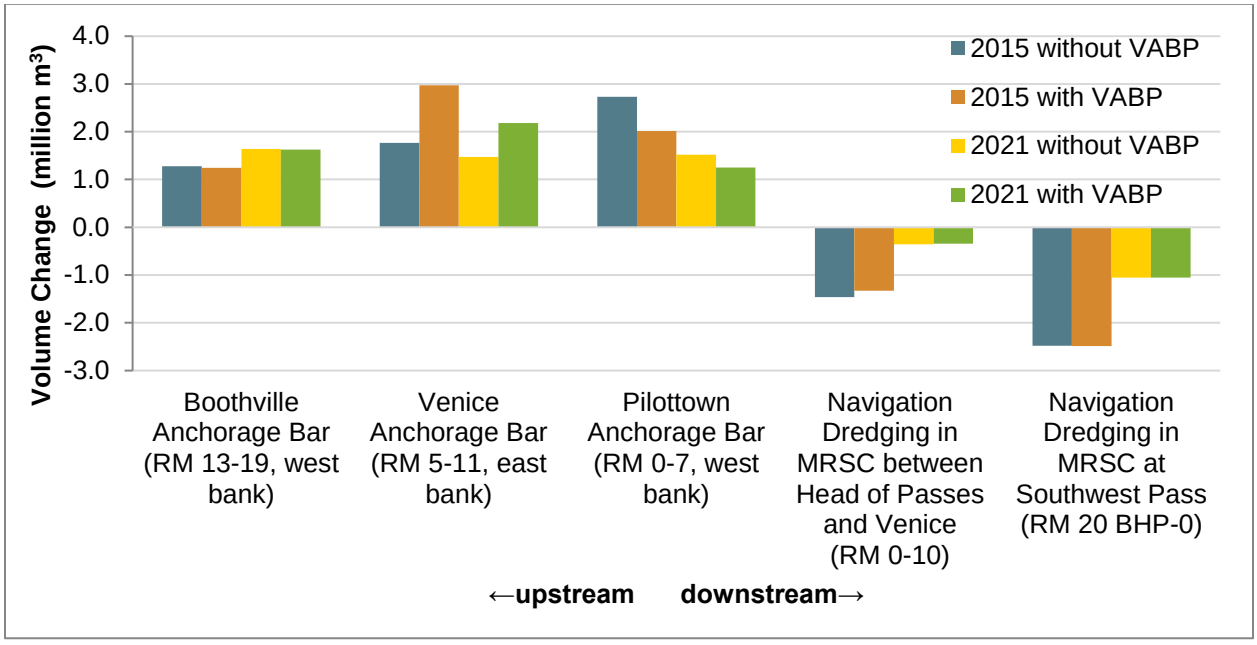

Figure 15. Volume changes at sand bars and dredged volumes from the MRSC between Venice (RM 13) and Southwest Pass (RM 20 Below Head of Passes [BHP]) for scenarios without and with the Venice Anchorage Borrow Pit (VABP, RM 8) for hydrographs 2015 and 2021. See Figure 3 for locations of polygons used to define bars for these calculations.

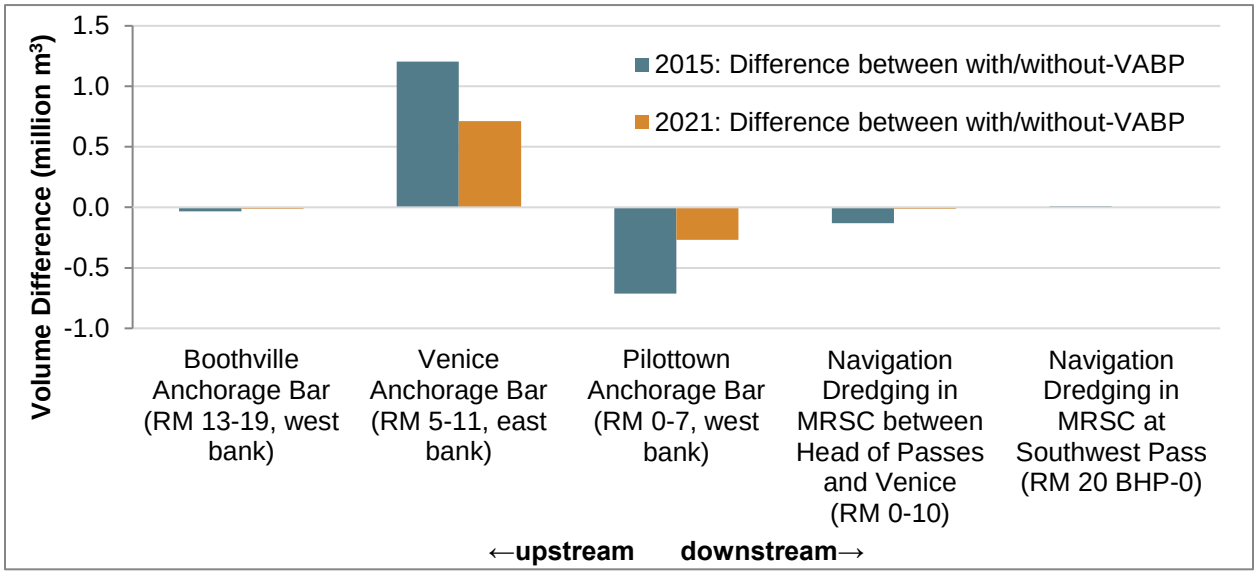

Figure 16. Volume differences between with-pit and without-pit scenarios showing the modeled impact of the Venice Anchorage Borrow Pit (VABP, RM 8) on proximal sand bars and navigation dredging in the MRSC. Results are shown for the 2015 and 2021 hydrographs. See Figure 3 for locations of polygons used to define bars for these calculations. Positive volume change indicates an increase of aggradation (or decrease of degradation) due to the presence of a borrow pit, or an increase in navigation dredging.

3.3 IMPACT ON NAVIGATION DREDGING

Downstream impacts of the VABP are not only limited to channel bar volumes but also influence navigation dredging in the Mississippi River Ship Channel (MRSC) between Venice and Head of Passes (Table 4). Model results suggest that the presence of the VABP reduces dredging volumes in the MRSC between Venice and Head of Passes by 9% and 3% for the 2015 and 2021 hydrographs, respectively. There are no noticeable changes in dredging volumes in the MRSC downstream of Head of Passes, which is in line with results of suspended sand concentration (Figure 11) which demonstrate that borrow pit impacts are mostly diminished in the vicinity of Head of Passes.

Table 4. Navigation dredging volumes for scenarios with and without the Venice Anchorage Borrow Pit (VABP). Cumulative water volumes are shown as a reference in the rightmost column.

Hydrograph	Volume dredged in MRSC between Venice and Head of Passes (million m^3) [difference relative to without-pit scenario]	Volume dredged in MRSC at Southwest Pass (million m^3) [difference relative to without-pit scenario]	Water Volume (million m^3)
2015 without VABP	-1.46	-2.48	533,087
2015 with VABP	-1.33 [-9%]	-2.49 [0%]	533,087
2021 without VABP	-0.35	-1.06	459,827
2021 with VABP	-0.34 [-3%]	-1.06 [0%]	459,827

Flow and sediment load reductions in the Mississippi River associated with upstream sediment diversions can influence navigation dredging requirements. The presence of MBSD resulted in a 29% reduction of

dredged volumes in the MRSC between Venice and Head of Passes and in a 18% reduction along Southwest Pass. The presence of both MBSD and Breton SD resulted in a 44% reduction of dredged volumes in the MRSC between Venice and Head of Passes and in a 26% reduction along Southwest Pass (Figure C-18).

4.0 DISCUSSION

4.1 THE LOWER MISSISSIPPI RIVER AS A RENEWABLE SAND RESOURCE

Analysis of the infilling rates predicted by the model show higher infilling rates for the AABP than the VABP. The predicted vertical aggradation for the AABP is two to three times higher than the aggradation predicted at VABP. Simulations showed that the highest vertical aggradation (infilling) occurs during the rising limb of a hydrograph, and specifically the early rise of the hydrograph, where most of the change in discharge and stage takes place. The simulations showed that the most influential parameter controlling infilling is the shape of the hydrograph, and specifically how fast the discharge is changing, or the stage is rising. This response dominates infilling rates compared to all other parameters examined in this study (e.g., changes in upstream suspended sediment concentration, bed stratigraphy, and sediment distribution within the bed).

Results from ensemble simulations show an average annual infilling of approximately 50% (± 3%) for AABP and of 28% (± 10%) for VABP, depending on the hydrograph shape. Results showed that shallower pits infill slower and can reduce infill rates by approximately 36% for AABP and up to 48% for VABP. These results suggest that borrow pits near the Alliance Reach will infill within 5–6 years to nearly 98 to 99% of the initial cut/volume. For borrow pits near the Venice reach, infilling for the same 5 – 6-year period is lower, 70% to 94%, depending on the hydrograph. Infilling rates in the Venice Reach show a higher variance than the results in the Alliance Reach, suggesting that despite having less constrained infilling rates along the Alliance Reach, the model show more convergence, compared to the Venice Reach where infill rates are more constrained from the field, but models show divergence and variance, suggesting similar confidence in the predictions. The borrow pits at either location, especially along the Alliance Reach, can infill to 100 % sooner than 5–6 years if conditions in the river differ from the conditions simulated in this study since there is a strong dependency on the inter-annual shape of the hydrograph. Moreover, when borrow pits become nearly full, infilling rates toward the end of the infilling cycle can be higher in the field than those predicted by models. For example, dynamics and associated migration of large bedforms during floods likely contribute significantly to infilling, a process that numerical models do not fully resolve. Lastly, hydrographs that exhibit multiple peaks throughout the year have more inter-annual variation and more likely to contribute to increased infilling. Previous studies show slightly higher infilling rates (Moffatt & Nichol (2011), and reported 90% infilling within 1.24 to 2.68 years for deeper pit cuts (about -90 ft NAVD88), and 90% infilling within 1.64 to 3.65 years for shallower pit cut (about -70 ft NAVD88). It should be noted that the infilling rates reported by Moffatt & Nichol (2011) were calculated using steady state models and look up tables and did not account for hydrographs shapes, rising limbs, and falling limbs. These differences in the methodology could explain the differences in infilling rates reported, as corroborated by the observations of infilling at the Venice Anchorage, which show a large variation in interannual infilling strongly influenced by the hydrograph (Figure 5, Figure 10).

In addition to a strong correlation of infilling rates to the shape and duration of the hydrograph, field observations (Yuill et al., 2013 and this study), and model results suggest a secondary control on infilling rates induced by residual flow, which in turn controls the streamwise slope in the river, signifying that

location along the river matters on sediment trapping efficiency. On the one hand, along the Alliance reach, future flow extractions will be managed (e.g., sediment diversions), and to a greater extent, their impacts on infilling are predictable. On the other hand, in the lower river, flow loss through over-banking and crevassing, can more significantly influence stream power, river transport capacity and thus infilling rates. Therefore, in the lowermost river where over-banking and crevassing prevail, accurate predictions of infilling are less dependent on hydrograph shape, and more dependent on residual flow and loss of stream power.

4.2 MAIN PARAMETERS AND DYNAMICS CONTROLLING INFILLING

Model results for the AABP showed very similar infilling volumes (~50%) within the first 7 months of all four analyzed hydrographs (i.e., 2010, 2011, 2016, 2019) suggesting that conditions in all four years were equally efficient in borrow pit infilling within the considered period. Despite the cumulative Mississippi River discharge being 16% lower during the first seven months of 2011 than during the first seven months of 2019, model results show infilling volumes that are only 1% (Table 1). However, when looking at the infilled volume over time (Figure 7) it appears that the hydrograph shape, which correlates with the total sand transport flux, plays an important role in borrow pit infilling. More specifically, the rate at which discharge increases (i.e., how steep the rising limb is) strongly influences infilling rates (Figure 9).

Different trends are found for the VABP where model results suggest a stronger dependency of infilling on the river hydrograph. A reduction of cumulative discharge of 14% between 2015 and 2021 results in almost half the infilling rates. This can be attributed to a double flood peak in the 2015 hydrograph (i.e., March, July) compared to a single flood peak (i.e., March) for the 2021 hydrograph (Figure 8).

Correlations between bed level change in the borrow pits and the Mississippi River discharge (Figure 9) for the AABP and VABP show similar trends, but different absolute infilling rates. In both cases, three trends can be observed:

- The first trend for below 15,000 m^3/s for AABP and 10,000 m^3/s for VABP, where no infilling can be observed.
- The second trend between 15,000 and 22,000 m^3/s for AABP and between 10,000 m^3/s and 20,000 m^3/s for VABP, with a linear relationship between infilling and discharge
- The third trend above 20,000–22,000 m^3/s with a steeper linear relationship between infilling and discharge

The absence of infilling in the first trend is in line with other studies (Yuill et al., 2015) and corresponds to the average flow below which sand is not in suspension (Ramirez & Allison, 2013b; Yuill et al., 2015). Borrow pit infilling follows a linear relationship in the second trend with a weekly infilling of ~3,000 m^3 for every 1,000 m^3/s increase of river discharge in the AABP, and a weekly infilling of ~2,700 m^3 for every 1,000 m^3/s increase of river discharge in VABP. In the third trend, infilling rate continues to be linear, but is approximately seven times higher for AABP with an increase in weekly infilling of ~22,000 m^3 for every 1,000 m^3/s increase in river discharge, and is almost twice for VABP with an increase in weekly infilling of ~5,500 m^3 for every 1,000 m^3/s increase in river discharge. Correlation between bed level change and the Mississippi River discharge during the falling limb (Figure 9), exhibit more scatter compared to the rising limb, and a clear trend isn't obvious. This response suggests that the governing

dynamics during the falling limb are not unique, and they might depend on the shape of the hydrograph, how peaky the hydrograph is, or how long those peaks persist.

When comparing modeled infilling rates with observations (Figure 10), both models show a close agreement with observations, particularly for the VABP. However, it appears that the Alliance Model tends to overestimate the infilling in the AABP. Nevertheless, due to the scarcity and low frequency of available survey data, it is not possible to determine this with certainty.

Both models demonstrate reasonable skill when comparing modeled and measured sediment concentrations and transport rates. Specifically, there is a close agreement with observational values when comparing bed load transport (Figure B-11) and total sediment flux (Figure B-6, Figure B-10, upper panels of Figure C-12, and Figure C-13). However, larger differences are found when comparing sand concentrations and fluxes (Figure B-5, Figure B-8, lower panels of Figure C-12, and Figure C-13). The Alliance Model tends to underestimate sand concentrations when compared to the available data (Section B.5.3). However, there are no available measurements for sediment concentrations during the rising limb or absolute peak discharges (>30,000 m^3/s [1,060,000 cfs], Figure B-5 to Figure B-10). On the other hand, the LMR Model, which utilizes the same model settings and calibration factors, overestimates sand concentrations when compared to USACE measurements (Sharp et al., 2013) during peak discharges (lower panels of Figure C-12 and Figure C-13). This is most noticeable for discharges locally exceeding 15,000 m^3/s (530,000 cfs), which correspond to a discharge at Belle Chasse of approximately 25,000 m^3/s (900,000 cfs). The LMR Model tends to simulate a somewhat exponential increase in sediment concentrations as river discharge increases, whereas the measured data shows a weaker, more linear increase. This observation may suggest the shortcomings of current (generalized) transport formulations (e.g., the Van Rijn sediment transport formulae) in fully capturing suspended sand transport dynamics in the Mississippi River across the entire range of discharges. However, it is important to note the limited availability of measurement data. The available field data is limited to a small number of deployments over relatively short periods of time, ranging from months to years. For example, data collected in 2010 and 2011 by (Ramirez & Allison, 2013b) shows that sand concentrations are higher during the first flood peak (e.g. March 2011) in comparison to subsequent peaks (e.g. May 2011). For the LMR Model, no sediment transport data were available for the years that were used for model calibration (i.e., 2015 and 2020), and the only available data (i.e., 2009, 2010, and 2011) were used to calibrate sediment transport fluxes (see Section C.5.3).

Measured concentrations and transport rates show a high variability and are influenced by the dynamic flow regime of the river, which can rapidly change due to variability in turbulence or tidal effect.. (Ramirez & Allison, 2013b). The infilling rates, derived from bed level change observed over longer time periods, are less vulnerable to the spatiotemporal variability of river conditions compared to instantaneous measurements of suspended sand transport. Moreover, sand transport rate is not the only factor that influences infilling. Various other factors, such as local bathymetry and flow patterns also play a significant role in the infilling process. For these reasons, even if the LMR Model appears to over predict sand in suspension, the infilling rates are fairly well calibrated as shown in Figure 10B. Moreover, more field data were available to calibrate infilling rates, and only few suspended sediment observations were available, Since the main objective of this work was to evaluate borrow pit morphology evolution and infilling rate, it was decided to prioritize infilling rate calibration instead of over-calibrating the model to

match a few suspended sand transport observations that were specific to a specific year and river discharge. Given these considerations, the model's skill was deemed acceptable for the purpose of this study, primarily due to the good agreement found when comparing infilling rates.

The effect of hydrograph shape and peak slopes on borrow pit infilling is also supported by the results of the simulations performed including the presence of sediment diversions. Results show that a 6–11% reduction of water volume in the Mississippi River translates into a 17–30% reduction (i.e., three times larger) of infilled borrow pit volumes (Table 3), noting that sediment diversions are expected to start operating when the Mississippi River discharge exceeds 12,742 m^3/s (i.e., 450,000 cfs), and their discharge will gradually increase until reaching maximum capacity when the river reaches 28,316 m^3/s (i.e., 1,000,000 cfs). This suggests that diversions will extract water and sediment from the Mississippi River during the hydrograph peaks, including the rising limb phases when suspended sediment concentrations are higher, influencing the suspended sediment concentrations in the residual flow reaching the borrow pits and, therefore, influencing borrow pit infilling rates.

Model results also show that borrow pit geometry, and more specifically borrow pit depth, affects the pit efficiency in capturing sediment: the deeper the pit, the faster it infills. The channel cross-sectional area in the vicinity of the pit increases when the borrow pit is deeper, causing water velocity to decrease and, therefore, sediment to deposit more readily.

Change in sediment concentration upstream did not affect borrow pit infilling rates found for the 1-year simulations performed in this study. When imposing higher or lower sediment concentrations, both Alliance and LMR models tend to find a dynamic equilibrium in sediment concentrations by depositing or eroding bed sediments just downstream of the upstream boundary. These adjustments take place within the first one or two sand bars and generally occur upstream of the area of interest in which the borrow pits are located. While longer term simulations may produce results that would eventually influence the area proximal to the borrow pit, the existing results suggest that the role of the hydrograph, its steepness, and the stream power play a chief role at influencing infilling rates and dominate over the role of the upstream change in the suspended sediment concentration. Similarly, changes in the bed composition, and those changes made to test the supply of sediment from the bed produced small changes in borrow pit infilling, of the order of 5–10% annual change for the AABP and the VABP. More detailed results are presented in Appendix B and Appendix C.

The type of sediment captured by the borrow pits varies dependent on location. Both the AABP and the VABP sequester predominantly fine sand. However, in addition to fine sand, the AABP tends to capture also medium sand, while the VABP tends to capture more very fine sand and silt. These are general estimates and vary throughout the hydrograph and the degree of infilling.

4.3 LOCAL IMPACTS OF BORROW PITS ON SEDIMENT TRANSPORT AND MORPHOLOGY

The most significant morphological impacts of borrow pits occur within the sand bar where the borrow pit is located. Flow velocities decrease along the borrow pit because the pit locally enlarges the river cross section, resulting in sediment deposition and bar aggradation (both inside and outside of the pit). This process primarily contributes to infilling of the borrow pits with rates up to 5 m per year, with

simultaneous deposition within the channel thalweg adjacent to the borrow pit, albeit lower and up to 1 m per year. Despite deposition and resulting local aggradation of the MRSC located next to the VABP, the channel remains well below authorized dredging depths (~5 m), a result that is corroborated by previous studies (Brown & Bell, 2019). The sand bars where the borrow pits are located, when the pits are present, sequester more sand, with 46% to 82% of this change by volume happening within the pits. Model projected volumetric changes shows that the sediment intercepted by the pit does not only originate from material transported downstream by the Mississippi River, but 23% (for AABP) to 40% (for VABP) is supplied from erosion of the proximal portion of the bar along the channel-pit transition, suggesting that the pits do influence bar dynamics of the bar they occupy. The differences between AABP and VABP show that infilling dynamics and the capacity of the pit to capture sediment transported in the river also depend on the borrow pit location in a streamwise sense (i.e., infill rate decreases downstream for this study area because of reduced stream power associated with flow loss to crevasses and passes along the Mississippi River between AABP and VABP).

The origin of sediment deposited within the borrow pits is partly sourced from suspended and bedload sediment flux transported by the Mississippi River, and partly sourced from local sand bar erosion near the bar-pit transitions from slope failure and headcutting. Volumetric analysis (Figure 13; Figure 14; Figure 15; Figure 16; Table 1;Table 2), suggests that approximately 68% of the AABP sediment infilling originates from sources upstream of the Alliance Anchorage Bar and about 32% is due to bar dynamics (e.g. bar inflation and migration) of the Alliance Anchorage Bar itself. For the VABP, 60–70% of the sediment infilling is sourced from areas upstream of the Venice Anchorage Bar, and about 30–40% is due to bar dynamics of the Venice Anchorage Bar. Furthermore, the AABP appears to be capturing sediment at twice the rate of VABP (see Figure 9), suggesting that the location of the borrow pit—both along the Mississippi River in a streamwise sense as well as the pit location on the bar itself—plays an essential role in pit sediment trapping efficiency, regardless of the strong dependency on hydrograph shape and flood duration.

4.4 REGIONAL IMPACTS OF BORROW PITS ON SEDIMENT TRANSPORT AND MORPHOLOGY

Borrow pits have little to no impacts on sand bars located upstream of the borrow pits (Figure 13, Figure 14, Figure 15 and Figure 16), however, borrow pits do influence the sand bar where the pits are located as well as sand bars located downstream. Locally, the sand bars where the borrow pits are located experience less bar inflation (except for the pit itself), and the sand bars located downstream experience reduced aggradation. For both AABP and VABP, the reduction in downstream aggradation (i.e., lower volume of sediment deposition) is less than half of the sediment volume sequestered by the borrow pit, suggesting that the remaining sediment volume captured by the pit was sediment moving downriver that was intercepted (52% for AABP and 30% for VABP). As a result, the reduction of sediment flux downstream of the VABP causes less shoaling (up to 26% less aggradation) at the Pilottown Anchorage Bar (an area sufficient draft clearance is critical as the lowermost anchorage along the MRSC) for the selected hydrographs examined.

The presence of sediment diversions reduces aggradation at the Venice Anchorage sand bar (a reduction of 9% if MBSD is in operation and 14% if both diversions are in operation), and at the Pilottown Anchorage Bar downstream (i.e., a reduction of 15% if MBSD is in operation and 24% if both diversions

are in operation, see Figure C-18). The reduction predicted by the models is proportional to the number of diversions in operation, or more specifically the percentage flow each of the diversions extracts from the river. A similar reduction in aggradation occurs upstream of the VABP at the Boothville Anchorage Bar, where when both diversions are operating the reduction is approximately 24%, and the reduction in aggradation is larger when only the MBSD is in operation (-31%; Figure C-18).

Sensitivity analysis, testing the role of upstream sediment supply on local and regional bar dynamics indicated negligible influence on sand bar dynamics for bars located at either the Alliance reach or the Venice reach. When coarser sediment is more available as suspended load, as well as when the riverbed composition coarsens, at the Alliance reach, the Alliance Anchorage Bar and the Belair Revetment Bar sequester more sand (5-35%), thus starving the downstream sand bars of sediment reducing aggradation of the order of 15 to 38%. When finer sediment is more available as suspended load, both the Venice Anchorage Bar and the Pilottown Anchorage Bar exhibit increased inflation of approximately 9 and 12% respectively.

4.5 IMPACT OF BORROW PITS ON DOWNSTREAM SEDIMENTATION AND MAINTENANCE DREDGING FOR NAVIGATION

The presence of the VABP does not influence the maintenance dredging volumes in Southwest Pass downstream of Head of Passes. However, depending on the hydrograph, model results show a reduction in annual maintenance dredging volumes between Venice and Head of Passes of approximately 3 to 9% (Table 4 and Figure 15 and Figure 16). The simulation with the 2015 hydrograph shows a 3 % reduction in maintenance dredging and the 2021 hydrograph simulation predicts a reduction of approximately 9%. The 3-fold increase between the two simulations is likely due to the lower discharge and a reduction in transport capacity associated with the 2015 hydrograph compared to the 2021 hydrograph, due to outflows associated with enlargement of Neptune Pass in 2021, which withdraws significant flow and sediment from the river.

The corresponding reduction in shoaling (18 to 26% less aggradation) that was predicted at Pilottown Anchorage Bar will be critical in the context of maritime safety in the vicinity of SWP.

Overall, the sediment volume captured by the VABP is significantly higher than the reduction in dredging volumes, suggesting that: (1) the presence of the VABP reduces the need for downstream maintenance dredging (~3-9%), and (2) the VABP is efficient in capturing sediment that would otherwise deposit on the Pilotttown Anchorage bar or continue further downstream and deposit in other distributaries (e.g., West Bay, Cubit’s gap, South Pass, Pass A Loutre).

5.0 CONCLUSION

5.1 THE IMPORTANCE OF SURVEYS

The analysis presented in this report could not have been performed without frequent repeat borrow pit monitoring surveys. The results demonstrate how sequential single and multi-beam surveys collected at borrow pits during dredging provide valuable insights on borrow pit infilling and the timing and spatial variability of infilling.

Observed infilling rates for three portions of the VABP exhibit non-uniform spatial infilling trends. All three areas experienced the highest infilling rates during the rising limb of the hydrographs, during which all three areas showed an average vertical accretion rate of ~ 0.15–0.17 m/week, corresponding to volumetric infilling of 93,000 to 225,000 m^3/month. During lower flows (~15,000 m^3/s) all three areas experienced reduced infilling rates (from 8,000–12,000 m^3/month), and for flows lower than 15,000 m^3/s, infilling was negligible.

These surveys improved the understanding of inter-annual dynamics and controls on sediment infilling, enhanced model validation related to infilling predictions, and broadened model applications to investigate infilling rates for a wide variety of factors such as different hydrographs, different sediment concentrations, and the presence of sediment diversions. Continuation of repeat surveys during and post construction of projects would be beneficial for future analysis and can help to better quantify post construction long-term pit evolution, pit infilling, and help document additional local processes on evolution of pit walls and other related local processes affecting pit morphology. While monthly surveys are ideal and have proven incredibly useful for this project, when not available, quarterly or semi-annual surveys can still be useful if planned around the river hydrograph.

5.2 INFILLING RATES AND VARIABILITY ALONG THE RIVER

Like observations, modeling results show that the hydrograph shape, which is proportional to the total sand transport, plays a significant role in borrow pit infilling. Specifically, the rate at which discharge increases (i.e., how steep the hydrograph rising limb is) strongly influences infilling rate. Three trends and corresponding infilling rates were identified (Table 5 and Table 6)

Table 5. Three infilling rate trends for AABP

Mississippi River Discharge		AABP infilling rates
[m^3/s]	[cfs]	[m^3/week]
<15,000	530,000	No infilling
15,000 - 22,000	777,000	0 - 100,000
>22,000	>777,000	100,000 - 300,000

Table 6. Three infilling rate trends for VABP

Mississippi River Discharge		VABP infilling rates
[m^3/s]	[cfs]	[m^3/week]
<10,000	353,000	No infilling
10,000 - 20,000	353,000 - 706,000	0 - 100,000
>20,000	>706,000	100,000 - 300,000

No clear trends were found during the falling limb, suggesting that the dynamics during the falling limb are more complex and that more analysis is needed to identify and constrain the environmental factors that control infilling during those conditions, since discharge doesn't play a chief role during the falling limb as much as it does for the rising limb.

Ensemble simulations show an average annual infilling of approximately 50% (± 3%) for AABP and of 28 % (± 10%) for VABP, depending on the hydrograph shape, and that shallower pits infill slower and can reduce infill rates by approximately 36% for AABP and up to 48% for VABP. These results suggest that borrow pits near the Alliance reach will infill within 5–6 years to nearly 98–99% of the initial cut volume, while near the Venice reach, infilling for the same period of 5–6 years will be lower from 70% to 94%, depending on the hydrograph. The modeling results show more convergence at Alliance which increases confidence regardless of having fewer field observations to ground truth predictions, and more variance in the modeling predictions along the Venice Reach, but with more constrained field observations. Thus, the overall confidence in the predictions is similar between the two sites.

The simulated influence of sediment diversions operating upstream showed that diversions reduce infilling rates proportional to the flow extracted by the diversion. For each percentile reduction of discharge there is a three-fold reduction in volumetric infilling rate.

The borrow pit depth strongly influences infilling rates; deeper borrow pits infill faster than their shallower counterparts. In the lower river near Venice, a pit that is half as deep than the original pit at the same location infills 50% slower than the deeper pit, and at Alliance, a pit that is half as deep infills approximately 38% slower compared to their deeper counterparts.

In addition to a strong correlation of infilling rates to the shape and duration of the hydrograph, model results suggest a secondary control on infilling rates, proportional to residual flow and corresponding streamwise slope in the river, indicating that location of the pit along the river (i.e., RM and sand bar where the pit is located) controls sediment trapping efficiency. This is particularly important in the lower river, where flow loss through crevassing can influence stream power, river transport capacity and thus, infilling rates. Hence, in the lower river, accurate predictions of infilling are less dependent on hydrograph shape, and more dependent on residual flow and loss of stream power.

The information above highlights important insights for planners to inform the timeline for dredging activities, as well as consider the environmental and physical variables used to estimate infilling rates.

5.3 LOCAL AND REGIONAL IMPACTS ON SEDIMENT TRANSPORT AND MORPHOLOGY

Borrow pits promote annual bed aggradation in channels next to the pits, but generally at rates that are an order of magnitude lower than deposition within the pit. Regardless, the deposition in the channel does not affect navigation because bed elevation there remains well below the authorized navigation depth.

Borrow pits do not affect sedimentation and erosion trends on upstream sand bars, however, the sand bars that the borrow pits are located on as well as the sand bars located downstream experience reduced aggradation.

The presence of the VABP reduced maintenance dredging by 3–9 %, depending on the hydrograph, between Venice and Head of Passes, and showed no influence in maintenance dredging below Head of Passes. The reduction in maintenance dredging volume was 15–100 times smaller than sediment volume captured by VABP, suggesting it captures sediment that would otherwise deposit on the Pilottown Anchorage Bar or further downstream in other distributaries (e.g., West Bay, Cubit's gap, South Pass, Pass A Loutre).

Experiments performed to test the effect of coarser or finer sediments in suspension did not significantly affect borrow pit infilling rates, but influence sand bar aggradation and degradation dynamics. For instance, when bed composition coarsens and there is more available coarse sediment in suspension from upriver sources, upriver sand bars aggrade, and starve sand bars downriver. The coarser riverbed supplies less sediment, and thus cannot make up the difference of the sediment deficit created by sediment volume captured by upriver sand bar aggradation during these conditions.

The sensitivity analysis performed to test the role of upstream sediment supply on local and regional bar dynamics indicated negligible influence on sand bar dynamics for bars located at either the Alliance reach or the Venice reach. When coarser sediment is more available as suspended load, as well as when the riverbed composition coarsens, at the Alliance reach, the Alliance Anchorage Bar and the Belair Revetment Bar sequester more sand (5-35%), thus starving the downstream sand bars of sediment reducing aggradation (15 to 38%). When finer sediment is more available as suspended load, both the Venice Anchorage Bar and the Pilottown Anchorage Bar exhibit increased aggradation of approximately 9 and 12% respectively.

5.4 RECOMMENDATIONS FOR FUTURE WORK

The work presented here addressed several of the research questions identified by Yuill et at., (2013), and successfully provided more accurate information on the infilling rates for borrow sites, on recovery time of borrow pits, and on the impact on dredging. Moreover, the larger geographic extent of the models used in this study, as compared to that used by Moffatt and Nichol, (2011), allowed for the investigation of spatially distributed impacts as well.

There are additional questions which were not addressed in this work but would be beneficial to investigate in the future. These include questions related to estimates of cumulative impacts of multiple dredging sites and long term (e.g., multiyear–decadal) impacts. Having infilling rate estimates from other sand bars along the river, and potentially from multiple dredging sites, would be beneficial to develop an

empirical function to forecast infilling rates as a function of stream power. The work presented in this report shows how the borrow pit location along the river controls sediment trapping efficiency. However, having only two locations (i.e., Alliance Anchorage bar and Venice Anchorage bar) where model predictions were verified with observations, it is challenging to develop a meaningful relationship between location of the borrow pit along the river and infilling rates. Additional studies could provide the framework to develop such a correlation and allow engineers and planners to have an easy-to-use tool to estimate first order infilling rates and time which will be key to plan dredging activities. One of the models (the Alliance Model) overestimated transport rates when the Mississippi River discharge locally exceeds 15,000 m^3/s. Additional observations and more specific modeling analysis is recommended to investigate if the current transport formulations (e.g., the Van Rijn sediment transport formulae) tend to overestimate suspended sand transport in the Mississippi River during periods of high discharges. These modeling experiments, tuned to local conditions, can focus in areas where sediment transport observations exist presently, to determine model sensitivity to those formulas, at different locations and at different flows.

Additional observations and analysis of suspended and bedform sediment flux can also be beneficial if focused on acquiring sand transport rates over the duration of a spring flood peak to elucidate on the internal dynamics and correlation between sand transport rate and borrow pit infilling. Sediment tracer studies can be leveraged or also be considered and would present research opportunities to understand the origin of infilling sediments and better correlate high-energy conditions with high infilling rates.

Finally, the types of sediment (i.e., sand or fines) that contributed to borrow pit infilling was not specifically investigated in this study. However, future projects can consider collecting sediment samples over time as a function of infilling or consider collecting cores post infilling to determine the type of sediment captured by the borrow pits to better constrain model skill and predict sediment quality available for restoration. This could also provide important insights to help design pits that are most efficient in trapping sand.

REFERENCES

ALDEN Research Laboratory, Inc. (2020). *Exploratory Evaluation of CFD based Sediment Transport Modeling as a Tool for Sediment Diversion Structure Design*. Holden, Massachusetts: Alden.

Allison, M. A., Demas, C. R., Ebersole, B. A., Kleiss, B. A., Little, C. D., Meselhe, E. A., … Vosburg, B. M. (2012). A water and sediment budget for the lower Mississippi–Atchafalaya River in flood years 2008–2010: Implications for sediment discharge to the oceans and coastal restoration in Louisiana. *Journal of Hydrology*, *432–433*, 84–97. https://doi.org/10.1016/j.jhydrol.2012.02.020

Allison, M. A., & Pratt, T. C. (2017). Discharge controls on the sediment and dissolved nutrient transport flux of the lowermost Mississippi River: Implications for export to the ocean and for delta restoration. *Journal of Hydrology*, *555*, 1–14. https://doi.org/10.1016/j.jhydrol.2017.10.002

Allison, M., Di Leonardo, D. R., Eckland, A. C., Ramatchandirane, C., & Weathers, D. (2018a). *Mid-Barataria Diversion Technical Team Field Data Support*. The Water Institute of the Gulf, Prepared for the Coastal Protection and Restoration Authority (CPRA) under task order 59.

Allison, M., Di Leonardo, D. R., Eckland, A. C., Ramatchandirane, C., & Weathers, D. (2018b). *Mid-Breton Diversion Technical Team Field Data Support*. The Water Institute of the Gulf, Prepared for the Coastal Protection and Restoration Authority (CPRA) under task order 59.

Barkhudarov, M. (2023). *Lagrangian VOF advection Method for FLOW3D.*

Blum, M. D., & Roberts, H. H. (2009). Drowning of the Mississippi Delta due to insufficient sediment supply and global sea-level rise. *Nature Geoscience*, *2*(7), 488–491. https://doi.org/10.1038/ngeo553

Bregman, M., Messina, F., Jung, H., Yuill, B. T., Baustian, M. M., & Georgiou, I. Y. (2020). *Basin Wide model Version 4: Basin Wide model for Mid-Breton Sediment Diversion modeling* (p. 137 + Appendices) [Task Order 51.3. Final Report]. Baton Rouge, LA: The Water Institute of the Gulf. Funded by the Coastal Protection and Restoration Authority.

Brown, G. L., & Bell, G. L. (2019). *Two-Dimensional Numerical Model Analysis of Proposed Borrow Pits on Sedimentation in the Mississippi River*. 36.

Caldwell, R. L., & Edmonds, D. A. (2014). The effects of sediment properties on deltaic processes and morphologies: A numerical modeling study. *Journal of Geophysical Research: Earth Surface*, *119*(5), 961–982. https://doi.org/10.1002/2013JF002965

CB&I. (2015). *Louisiana Borrow Area Management and Monitoring (BAMM) Program* (p. 30). Boca Raton, Florida: CB&I Government Solutions.

CPRA. (2023). *Louisiana's Comprehensive Master Plan for a Sustainable Coast* (p. 100) [4th Edition, Draft Plan Release]. Baton Rouge, LA: Louisiana Coastal Protection and Restoration Authority, the State of Louisiana.

Dasler, J. (2019a). *Descriptive report to accompany Survey H13194*. NOAA National Centers for Environmental Information, Office of Coast Survey. Retrieved from NOAA National Centers for Environmental Information, Office of Coast Survey website: https://www.ngdc.noaa.gov/nos/H12001-H14000/H13194.html

Dasler, J. (2019b). *Descriptive Report to Accompany Survey H13194*. Retrieved from https://www.ngdc.noaa.gov/nos/H12001-H14000/H13194.html

Deltares. (2014). *Delft3D-FLOW: Simulation of multidimensional hydrodynamic flows and transport phenomena, including sediments* (User Manual No. Version 3.15.32158). Delft, The Netherlands: Deltares. Retrieved from Deltares website: http://oss.deltares.nl/documents/183920/eeb97903-151a-49bf-a13a-54b616da47a9

Esposito, C. R., Georgiou, I. Y., & Kolker, A. S. (2013). Hydrodynamic and geomorphic controls on mouth bar evolution. *Geophysical Research Letters*, *40*(8), 1540–1545. https://doi.org/10.1002/grl.50333

Esposito, C. R., Georgiou, I. Y., & Straub, K. M. (2020). Flow loss in deltaic distributaries: Impacts on channel hydraulics, morphology, and stability. *Water Resources Research*, *56*(5), e2019WR026463. https://doi.org/10.1029/2019WR026463

Espostio, C., Courtois, A., Swartz, J., & Miner, M. D. (2021). *Lowermost Mississippi River Management Program: Synthesis and analysis of LMR deep draft navigation dredging activities* (p. 61). Baton Rouge, LA: The Water Institute of the Gulf. Produced for and funded by the Coastal Protection and Restoration Authority under Task Order 69. Retrieved from The Water Institute of the Gulf. Produced for and funded by the Coastal Protection and Restoration Authority under Task Order 69 website: https://thewaterinstitute.org/assets/docs/projects/LMRMP_Synthesis-and-Analysis-of-LMR-Deep-Draft-Navigation-Dredging-Activities.pdf

Eustis Engennering Company, Inc. (2006). *Geotechnical investigation, State of Louisiana, department of natural resources, Coastal Restoration and Management, Mississippi river sediment delivery system Bayou dupont, Louisiana. DNR contract no. 2503-05-46, State/federal project no. BA-39, Eustis engineering project no. 19183* (p. 32) [Technical Report]. Metaire, Louisiana: Eustis Engennering Company, Inc.

Finkl, C. W., Khalil, S. M., Andrews, J., Keehn, S., & Benedet, L. (2006). Fluvial sand sources for barrier island restoration in Louisiana: Geotechnical investigations in the Mississippi River. *Journal of Coastal Research*, *224*, 773–787. https://doi.org/10.2112/06A-0011.1

Flocks, J. G., Miner, M. D., Twichell, D. C., Lavoie, D. L., & Kindinger, J. L. (2009). Evolution and preservation potential of fluvial and transgressive deposits on the Louisiana inner shelf: Understanding depositional processes to support coastal management. *Geo-Marine Letters*, *29*(6), 359–378. https://doi.org/10.1007/s00367-009-0164-4

Flow Science, Inc. (2023). *FLOW-3D Version 12.0 User Manual*. Santa Fe, NM.

Fugro Consultant, Inc. (2012). *Geotechnical Data Report, Mississippi River Long Distance Sediment Pipeline, Project (BA-39), Geotechnical characterization of Wills Point, Alliance Anchorage, and*

Alliance South, LDRN RSIQ no. 2503-10-12, Task 5, Plaquemines Parish, Louisiana (Technical Report No. 04.55124014; p. 61). Baton Rouge LA: Fugro Consultant, Inc.

Georgiou, I. Y., & Trosclair, K. J. (2013). *Measurements of lateral flow from the Mississippi River at Mardi Gras cut using synoptic ADCP near the Bohemia Spillway* (pp. 1–4) [Preliminary field report]. The Lake Pontchartrain Basin Foundation. Retrieved from The Lake Pontchartrain Basin Foundation website: https://saveourlake.org/wp-content/uploads/PDF-Documents/our-coast/Mardi%20Gras%20Pass/MGP-Summary%20Discharge-June2013.pdf

Hajek, E. A., & Wolinsky, M. A. (2012). Simplified process modeling of river avulsion and alluvial architecture: Connecting models and field data. *Sedimentary Geology*, *257–260*, 1–30. https://doi.org/10.1016/j.sedgeo.2011.09.005

Harmar, O. P., Clifford, N. J., Thorne, C. R., & Biedenharn, D. S. (2005). Morphological changes of the Lower Mississippi River: Geomorphological response to engineering intervention. *River Research and Applications*, *21*(10), 1107–1131. https://doi.org/10.1002/rra.887

Hirt, C. W., & Nichols, B. D. (1981). Volume of fluid (VOF) method for the dynamics of free boundaries. *Journal of Computational Physics*, *39*(1), 201–225. https://doi.org/10.1016/0021-9991(81)90145-5

Hirt, C. W., & Sicilian, J. M. (1985). *A porosity technique for the definition of obstacles in rectangular cell meshes*. Presented at the International Conference on Numerical Ship Hydrodynamics, 4th. Retrieved from https://trid.trb.org/view/394627

Khalil, S. M. (2019). *General guidelines: Exploration for sediment resources for coastal restoration* (No. Version_VIII). Baton Rouge, LA: Coastal Protection and Restoration Authority.

Kolker, Alex S., Weathers, H. D., Swann, C., Cloutier, T., & Renfro, A. A. (2022). *Neptune Pass: The Mississippi River's largest new distributary*. Presented at the American Geophysical Union 2022 Fall Meeting, Chicago, IL. Retrieved from https://alexkolker.com/2023/02/13/neptune-pass-the-mississippi-rivers-largest-new-distributary/

Kolker, Alexander S., & Weathers, H. D. (2022). *Technical Report: Discharge Study At Bayou Tortillon*. Retrieved from https://alexkolker.files.wordpress.com/2022/11/33f1e-tech_report_may_2022_may_31_crevasse_bayou_tortillon.pdf

Leonardi, N., Canestrelli, A., Sun, T., & Fagherazzi, S. (2013). Effect of tides on mouth bar morphology and hydrodynamics: Effect of Tides on Mouth Bar. *Journal of Geophysical Research: Oceans, 118*(9), 4169–4183. https://doi.org/10.1002/jgrc.20302

Lesser, G. R., Roelvink, J. A., van Kester, J. A. T. M., & Stelling, G. S. (2004). Development and validation of a three-dimensional morphological model. *Coastal Engineering, 51*(8–9), 883–915. https://doi.org/10.1016/j.coastaleng.2004.07.014

Liang, M., Meselhe, E., Messina, F., & Ortals, C. (2016). *Sediment Diversions: Optimization of the Operation Plans* (No. Task Order 41). Baton Rouge, LA: The Water Institute of the Gulf.

Marciano, R., Wang, Z. B., Hibma, A., de Vriend, H. J., & Defina, A. (2005). Modeling of channel patterns in short tidal basins. *Journal of Geophysical Research: Earth Surface, 110*(F1). https://doi.org/10.1029/2003JF000092

McCorquodale, J. A., Amini, S., Teran, G., Gurung, T., Kenny, S., Gaweesh, A., … Pereira, J. (2017). *Development and application of a regional 3-D model for the lower Mississippi River* (Final Report No. Task Order 36; p. 340). Baton Rouge, LA: Prepared for and funded by the Coastal Protection and Restoration Authority.

Messina, F., Bregman, M., Jung, H., Yuill, B., & Roberts, H. (2019). *Mid-Barataria Sediment Diversion Engineering Modeling Support: Production Runs with the Basin Wide model Version 3* (p. 43) [Technical Memorandum]. Baton Rouge, LA: The Water Institute of the Gulf. Prepared for and funded by the Coastal Protection and Restoration Authority.

Messina, F., Georgiou, I. Y., Bregman, M., Jung, H., Yuill, B. T., Liu, B., … Baustian, M. M. (2021). *Mid-Breton Sediment Diversion Engineering Modeling Support: Production Runs with the Basin*

Wide model Version 4 [Revised March 2022]. Baton Rouge, LA: The Water Institute of the Gulf. Funded by the Coastal Protection and Restoration Authority under Task Order 77.

Miner, M. D., Kulp, M. A., FitzGerald, D. M., Flocks, J. G., & Weathers, H. D. (2009). Delta lobe degradation and hurricane impacts governing large-scale coastal behavior, South-central Louisiana, USA. *Geo-Marine Letters*, *29*(6), 441–453. https://doi.org/10.1007/s00367-009-0156-4

Moffat and Nichol. (2012). *Mississippi River Long Distance Sediment Pipeline, Final (95%) Design Report.* Baton Rouge, LA.

Moffatt & Nichol. (2012). *Investigations of Potential Mississippi River Borrow Areas. Final Report*. Baton Rouge, LA. Retrieved from http://lacoast.gov/reports/ project/4940405~1.pdf

Moffatt and Nichol. (2011). *Appendix H – Delft3D borrow area modeling. Long distance sediment pipeline (LSSP)* (30% Design Report. No. December 16th, 2011 Draft; p. 28).

Mossa, J. (1996). Sediment dynamics in the lowermost Mississippi River. *Engineering Geology*, *45*(1–4), 457–479. https://doi.org/10.1016/S0013-7952(96)00026-9

Nardin, W., Mariotti, G., Edmonds, D. A., Guercio, R., & Fagherazzi, S. (2013). Growth of river mouth bars in sheltered bays in the presence of frontal waves. *Journal of Geophysical Research: Earth Surface*, *118*(2), 872–886. https://doi.org/10.1002/jgrf.20057

Nittrouer, J. A., Allison, M. A., & Campanella, R. (2008). Bedform transport rates for the lowermost Mississippi River. *Journal of Geophysical Research: Earth Surface*, *113*(F3). https://doi.org/10.1029/2007JF000795

Nittrouer, J. A., Mohrig, D., & Allison, M. (2011). Punctuated sand transport in the lowermost Mississippi River. *Journal of Geophysical Research*, *116*(F4), F04025. https://doi.org/10.1029/2011JF002026

Nittrouer, J. A., Mohrig, D., Allison, M. A., & Peyret, A.-P. B. (2011). The lowermost Mississippi River: A mixed bedrock-alluvial channel. *Sedimentology*, *58*(7), 1914–1934. https://doi.org/10.1111/j.1365-3091.2011.01245.x

NMFS. (2023, February 15). Upper Barataria Marsh Creation Project | NOAA Fisheries. Retrieved March 2, 2023, from NOAA website: https://www.fisheries.noaa.gov/southeast/habitat-conservation/upper-barataria-marsh-creation-project

Ocean Survey, Inc. (2011). *Geophysical and Gotechnical Investigation, Long Distance Sediment Pipeline Project—Bayou Dupont Borrow Area, Mississippi River, Louisiana* (No. OSi Report #11ES002; p. 144). Metaire, Louisiana: Ocean Survey, Inc.

OCM Partners. (2022). *2022 USGS CoNED Topobathymetric Model (1885—2021): Northern Gulf of Mexico*. Retrieved from https://www.fisheries.noaa.gov/inport/item/67613

Poff, M., Bass, A., Sweeney, R., Bahlinger, K., & Chatellier, M. (2011). Feasibility study analysis for riverine sand mining/Scofield Island restoration. *Journal of Coastal Research*, *Special Issue*(59), 235–245. https://doi.org/10.2112/SI59-025.1

Ramirez, M. T., & Allison, M. A. (2013a). Suspension of bed material over sand bars in the Lower Mississippi River and its implications for Mississippi Delta environmental restoration. *Journal of Geophysical Research: Earth Surface*, *118*(2), 1085–1104. https://doi.org/10.1002/jgrf.20075

Ramirez, M. T., & Allison, M. A. (2013b). Suspension of bed material over sand bars in the Lower Mississippi River delta environmental restoration. *Journal of Geophysical Research: Earth Surface*, *118*, 1085–1104. https://doi.org/doi:10.1002/jgrf.20075

Ranasinghe, R., Duong, T. M., Uhlenbrook, S., Roelvink, D., & Stive, M. (2013). Climate-change impact assessment for inlet-interrupted coastlines. *Nature Climate Change*, *3*(1), 83–87. https://doi.org/10.1038/nclimate1664

Reins, N. J. (2018). *Long Term Bathymetry Changes in the Lower Mississippi River due to Variability in Hydrograph and Variable Diversion Schemes* (Dissertation, University of New Orleans). University of New Orleans. Retrieved from https://scholarworks.uno.edu/td/2490/

Sharp, J. A., Little, C., Brown, G., Pratt, T., Heath, R. E., Hubbard, L., … Ganesh, N. (2013). *West Bay Sediment Diversion Effects*. 274.

T. Baker Smith, Inc. (2011). *Mississippi River long distance sediment pipeline project* (Data Collection Report No. BA-43 EB). Baton Rouge, LA: Coastal Protection and Restoration Authority,.

The Water Institute. (2015). *Patterns of water discharge and sediment flux at the Ostrica-Ft. St. Philip Channel Complex during high flow*. The Water Institute of the Gulf, Baton Rouge, LA.

Thomson, G., Hartman, B., Miller, B., Gillen, D., Clark, M., Batiza, R., … Sellers, A. (2019). Development of borrow areas along the lower Mississippi River. *Coastal Sediments 2019*, 870–879. Tampa/St. Petersburg, Florida, USA: WORLD SCIENTIFIC. https://doi.org/10.1142/9789811204487_0076

USACE. (2022a). *Environmental Impact Statement for the Proposed Mid-Barataria Sediment Diversion project Plaquemines Parish, LA*. New Orleans, LA: Prepared by GEC. Retrieved from Prepared by GEC website: https://www.mvn.usace.army.mil/Missions/Regulatory/Permits/Mid-Barataria-Sediment-Diversion-EIS/

USACE. (2022b). *Olga revetment discharge data*. U.S. Army Corps of Engineers.

Van Der Wegen, M., Jaffe, B. E., & Roelvink, D. (2011). Process-based morphodynamic modeling: Hindcast of decadal erosion and deposition patterns in San Pablo Bay, California, USA. *The Proceedings of the Coastal Sediments 2011*, 1841–1852. Miami, Florida, USA: World Scientific Publishing Company. https://doi.org/10.1142/9789814355537_0139

Van Rijn, L. C. (1993). *Principles of sediment transport in rivers, estuaries and coastal seas*. Amsterdam: Aqua Publications.

Viparelli, E., Nittrouer, J. A., & Parker, G. (2015). Modeling flow and sediment transport dynamics in the lowermost Mississippi River, Louisiana, USA, with an upstream alluvial-bedrock transition and a downstream bedrock-alluvial transition: Implications for land building using engineered diversions. *Journal of Geophysical Research: Earth Surface*, *120*(3), 534–563. https://doi.org/10.1002/2014JF003257

Wang, B. (2019). *Sediment transport and channel morphology of a natural and a leveed alluvial river* (Master of Science). Louisiana State University, Baton Rouge, LA.

Weathers, H. D., Allison, M., Ramatchandirane, C., & Yuill, B. (2016). *Water and Sediment Dynamics in the Fort St. Philip Crevasse During the 2016 Highwater Event*. Presented at the State of the Coast 2016.

Yakhot, V., & Orszag, S. A. (1986). Renormalization group analysis of turbulence. I. Basic theory. *Journal of Scientific Computing*, *1*(1), 3–51. https://doi.org/10.1007/BF01061452

Yakhot, V., & Smith, L. M. (1992). The renormalization group, the ε-expansion and derivation of turbulence models. *Journal of Scientific Computing*, *7*(1), 35–61. https://doi.org/10.1007/BF01060210

Yuill, B. T., Allison, M. A., & Meselhe, E. A. (2013). *Sediment Infilling of Channel Bars in the Lowermost Mississippi: Observations and Recommendations for Monitoring and Modeling* (p. 59) [Technical Report]. Baton Rouge, LA.: The Water Institute of the Gulf. Funded by the Coastal Protection and Restoration Authority under Task Order 17.

Yuill, B. T., Gaweesh, A., Allison, M. A., & Meselhe, E. A. (2015). Morphodynamic evolution of a lower Mississippi River channel bar after sand mining: In-channel borrow pit infilling. *Earth Surface Processes and Landforms*, *41*(4), 526–542. https://doi.org/10.1002/esp.3846

APPENDICES

APPENDIX A. FIELD OBSERVATIONS

Sediment infilling rates and volumes of Mississippi River borrow areas are essential for understanding sediment availability for coastal restoration projects such as marsh creation, ridge restoration, and barrier island nourishment. The Mississippi River is assumed to be Louisiana's largest renewable sediment source. Thus, understanding infilling rates using field observations is critical to elucidate the controls on infilling and provide additional datasets to calibrate deterministic models. This study leveraged field observations from the Spanish Pass Ridge and Marsh Restoration Project (BA-0191) and the more recent construction of the Barataria Basin Ridge and Marsh Creation Project – Spanish Pass Increment (BA-0203). The BA-0203 commonly referred to as the Spanish Pass Project (SPP) and is the first increment under construction. The project will build 1538 acres of marsh and 132 acres of a ridge, creating a total of 1670 acres of habitat extending approximately 7.5 miles to the west of Venice, LA. The material to build this increment originates from the dredging of sand bars in the Mississippi River just east of Venice and extending downriver by approximately 2.5 miles. The dredging company that submitted the winning bid and was selected for the project is Weeks Marine. The total project cost is $86.6 million. The notice to proceed with the project was issued in February 2021, and sediment pumping began in September 2021. It was initially expected to be completed by December 2022, although dredging continues through February of 2023 while this report is being prepared.

Monthly river surveys conducted by Weeks Marine, the dredging company working on the project, were used to determine the volume of sediment infilling the borrow area over time. The borrow area for the Spanish Pass Project in the Mississippi River south of Venice, Louisiana is shown in Figure A-1.

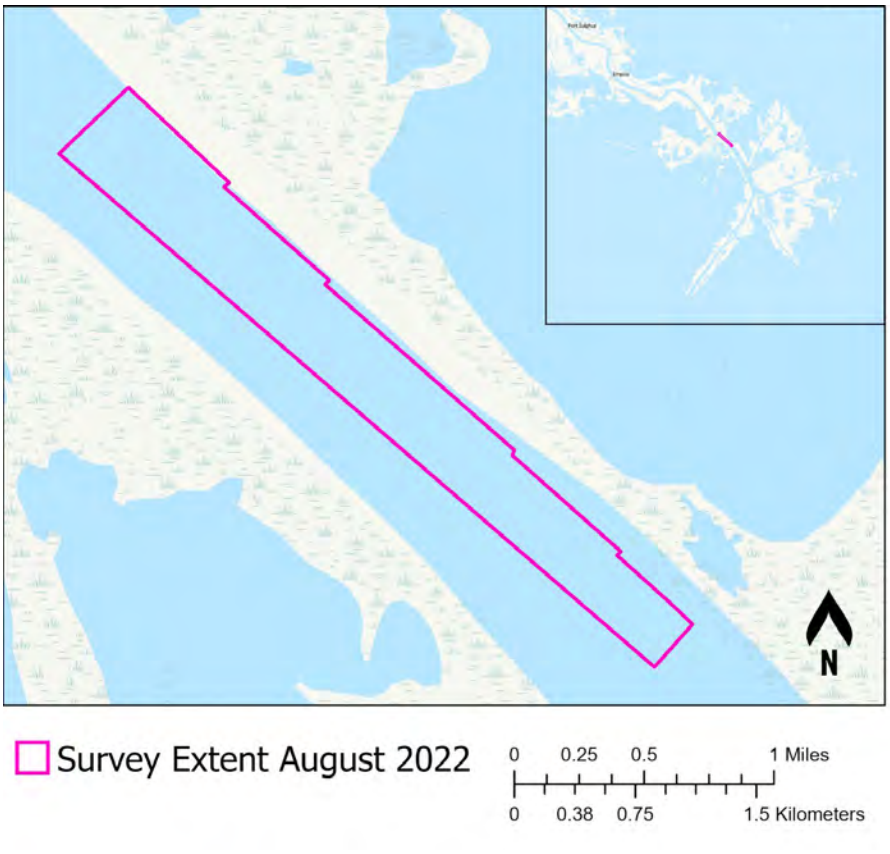

Figure A-1. Study area at the VABP borrow area with inset showing the position of the study area with respect to the Mississippi River Delta Bird's Foot. The survey extent shown is the maximum extent of the surveyed area during the study.

A.1 METHODS

Survey data of the borrow pit during dredging were interpolated to create surfaces used for the infilling analysis.

A.1.1 Available Data

High-density single beam surveys were conducted at approximately monthly intervals beginning at the end of October 2021. Surveys were conducted in UTM 15N and referenced to NAVD88. Both feet and meters were provided; units of meters were used for the analysis. The surveys used for the analysis were conducted at the end of October 2021, November 2021, December 2021, January 2022, February 2022, March 2022, May 2022, June 2022, August 2022, December 2022, and January 2023. Surveying problems experienced during the end of July survey resulted in a replacement survey at the beginning of August; this survey was also used for the analysis. The April survey had irrecoverable errors and was not used for the analysis. The extent of the area covered by the surveys increases as the dredged area increases (Figure A-2). The extents shown delineate the areas of high-density survey data; some survey points exist outside these bounds. In the high-density areas, streamwise survey lines were collected at

approximately 20 m intervals; tie lines were collected in the cross-stream direction approximately every 170 m.

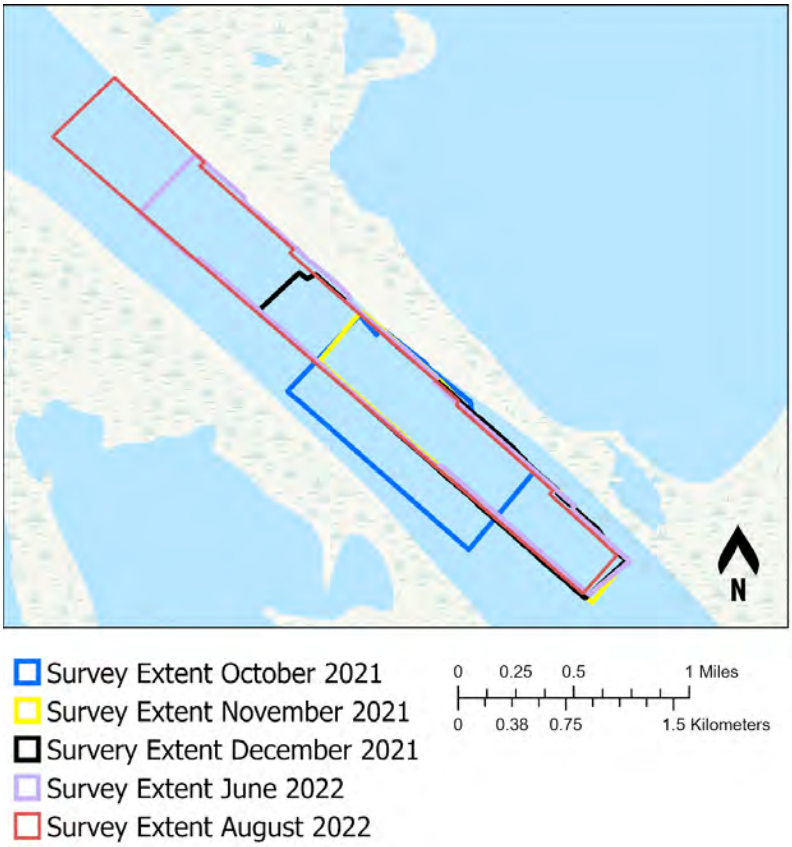

Figure A-2. Survey extents for the VABP borrow area. Survey extents for December and January cover very similar areas; only December is shown for simplicity. Surveys for August, February, March, and May also cover very similar areas; only August is shown for simplicity.

A.1.2 Raster Creation

The tie lines in the survey data often extended well past the high density streamwise survey lines to ensure complete overlap; only the areas containing the high density streamwise lines were used to create bathymetryic surfaces (Figure A-3). Using areas without sufficient survey point density would result in undesirable artefacts in the interpolation. The survey points were first used to create a Triangular Irregular Network (TIN; Figure A-3) using the ESRI Create TIN tool in the 3D Analyst toolbox. Delaunay triangulation was used. Linear interpolation was applied to the TIN to create a 5 m raster using the ESRI TIN to Raster tool from the 3D Analyst toolbox (Figure A-3). A slope raster was also created, using the ESRI Slope tool in the Spatial Analyst toolbox, to check for errors or inconsistencies in the interpolation (not shown). TINs and raster surfaces were created for each survey. When surveys were completed over multiple consective days, points for all the survey days were combined to create a single survey for each month (with the exception of August, which has beginning and end of month surveys).

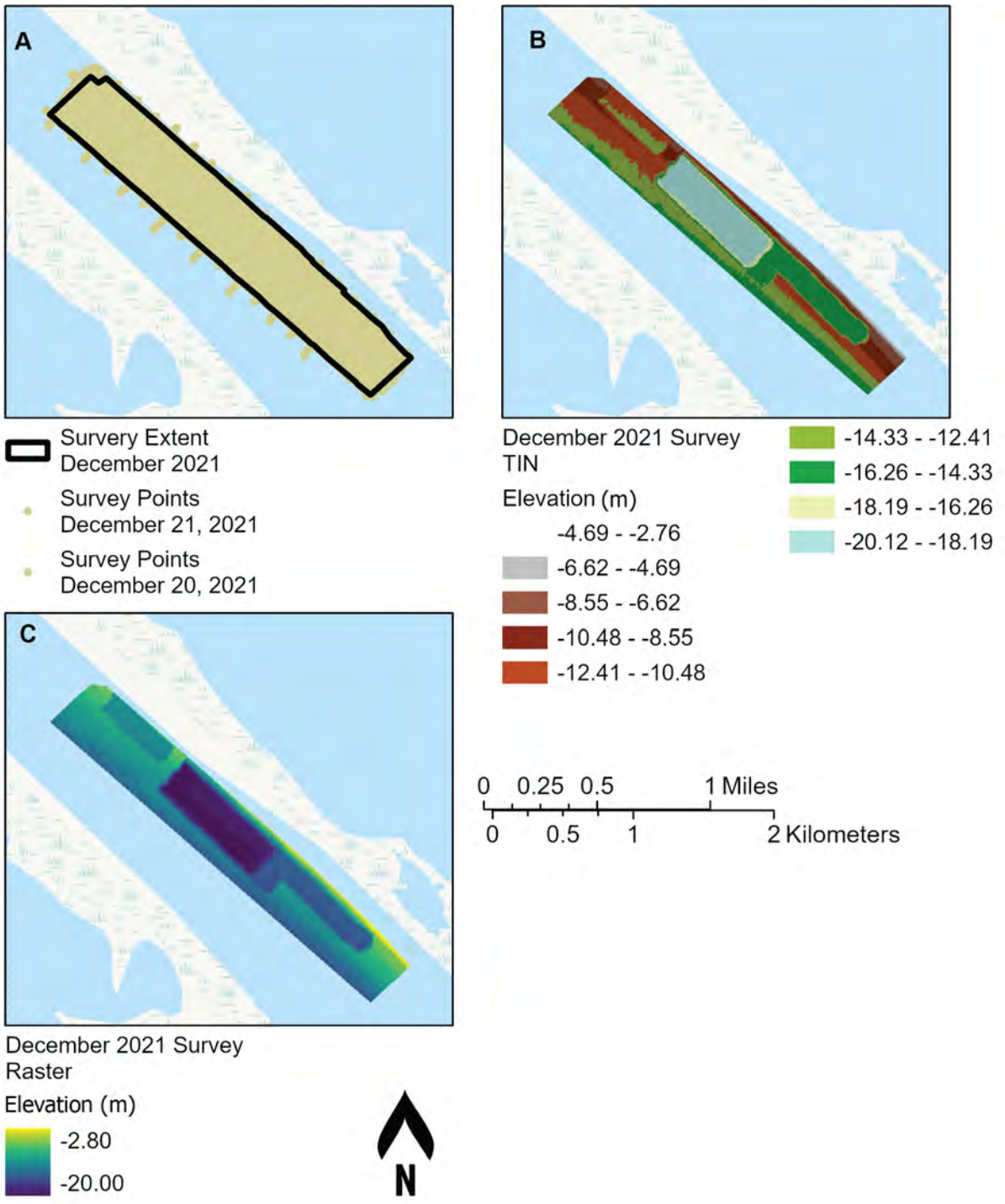

Figure A-3. A: Example survey points that were used to create the TIN and raster surfaces. The survey extent that was used to select the points used to create the surfaces is also shown. B: An example of the TIN created from the December 2021 survey points. C: An example raster surface created from the December 2021 TIN surface.

A.1.3 Infilling Calculations

During active dredging, an area often has material removed (cut) at multiple stages. For these infilling calculations, infill amounts were only calculated once dredging was fully complete across an area. To determine when dredging was finished in an area, the cut sequence obtained from Weeks Marine was used. The cut sequence shows the position of the dredge throughout active dredging (Figure A-4). At the Spanish Pass borrow area, dredging started in the southeast part of the bar and moved to the northwest (Figure A-5). Based on the cut sequences the borrow area was split into three analysis areas for the infill calculations (Figure A-6). Area 1 covers the area that was dredged in October through December. Area 2 covers the area that was dredged from December through February. Area 3 covers the area that was dredged from February to May.

Infilling amounts were calculated by subtracting the bathymetric surface at the end of dredging from each bathymetric surface for the subsequent months. For example, the surface for December was subtracted from the surface for January to obtain the amount of infilling between the end of December to the end of January. All survey elevations are negative meters, referenced to NAVD88. If the result of the subtraction is positive, this indicates that the later survey is shallower, and the difference is the result of infilling (Figure A-7). Negative differences indicate small areas of erosion or sediment redistribution within the dredged area.

Sediment amounts were calculated for each of the three areas starting with the first survey after the end of dredging through the last available survey. There are nine analysis periods for Area 1, seven analysis periods for Area 3, and five analysis periods for Area 3.

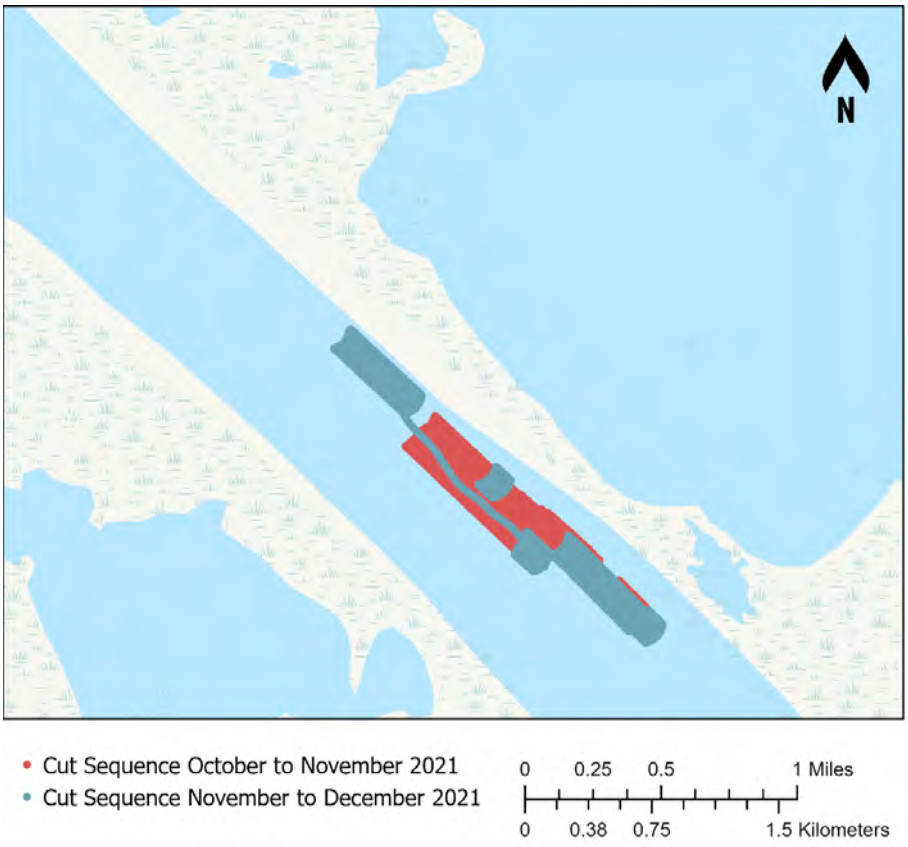

Figure A-4. An example of the cut sequences from October through December 2021. The cut sequences were used to determine where dredging had occurred through time. This information was used to choose the extent of the analysis areas for the infilling analysis.

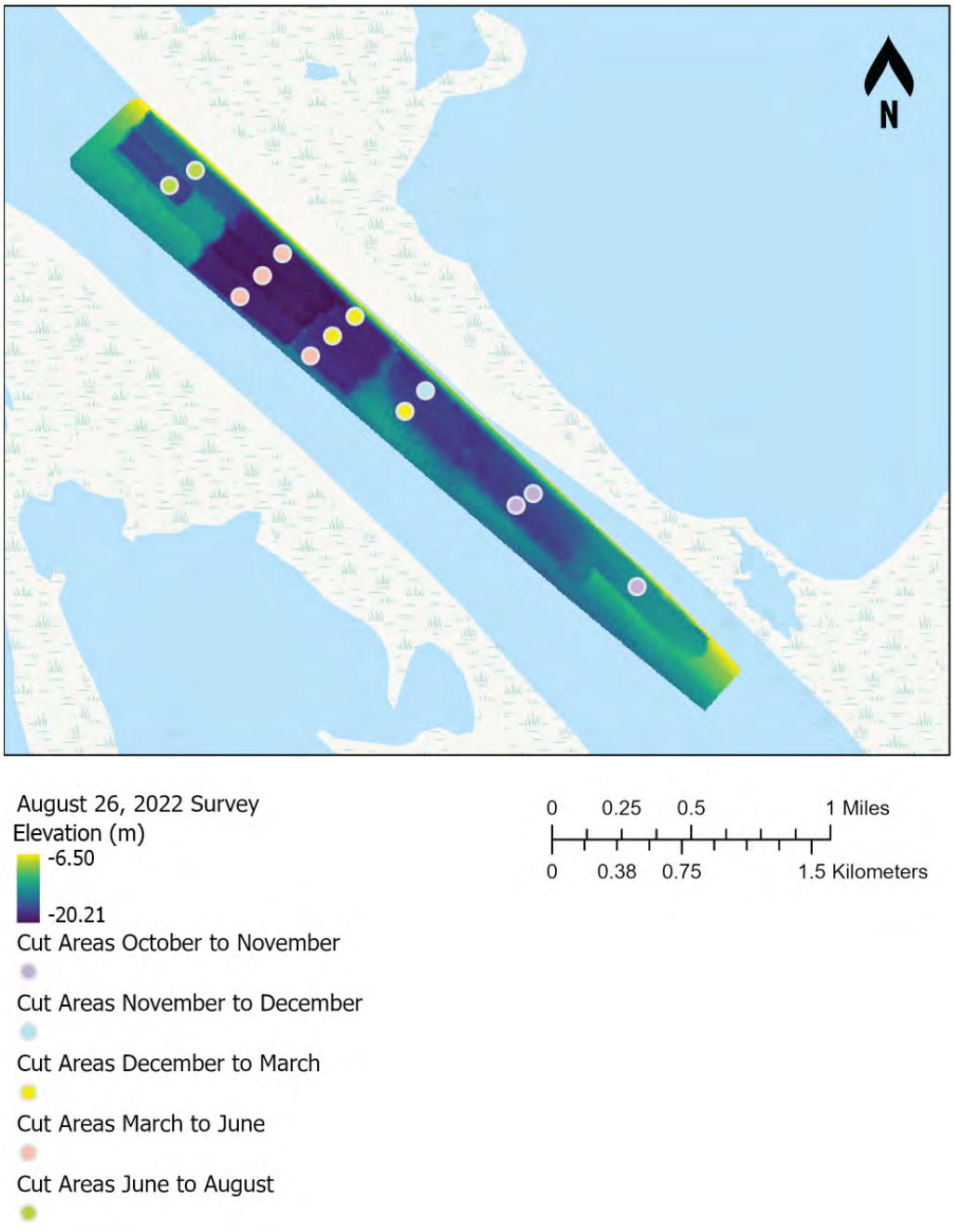

Figure A-5. Approximate centers of the areas dredged from the borrow areas. The movement of the dredge from the southeast part to the northwest part of the borrow area can be seen through time.

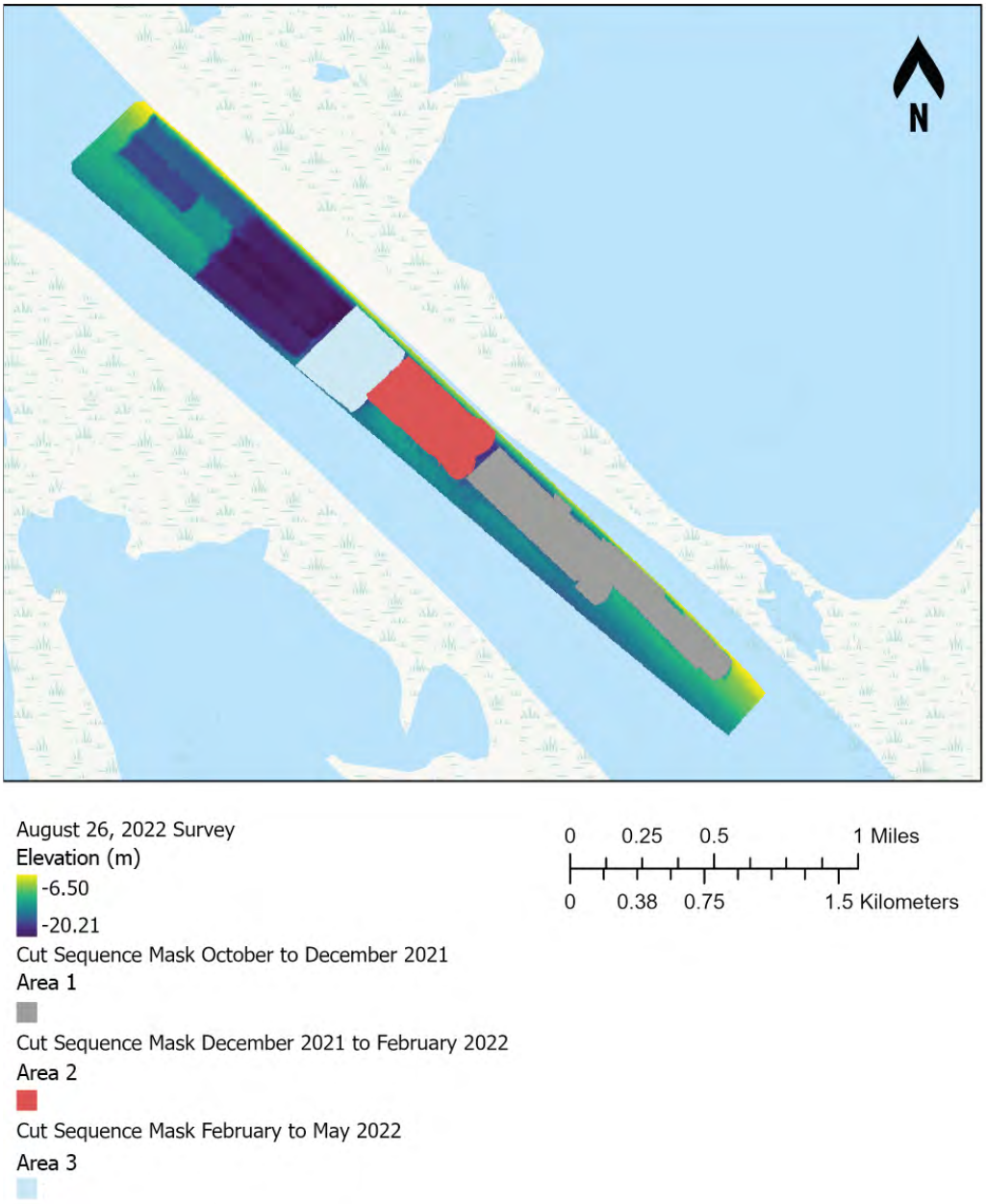

Figure A-6. An example of the masks used to delineate the three analysis areas shown with the August 26 survey for reference. These areas were delineated using the cut sequence. Each analysis area is represented by a constant value raster. Area 1 (furthest downstream, gray) covers the area that was dredged in October through December. Area 2 (middle, red) covers the area that was dredged from December through February. Area 3 (furthest upstream, light blue) covers the area that was dredged from February to May.

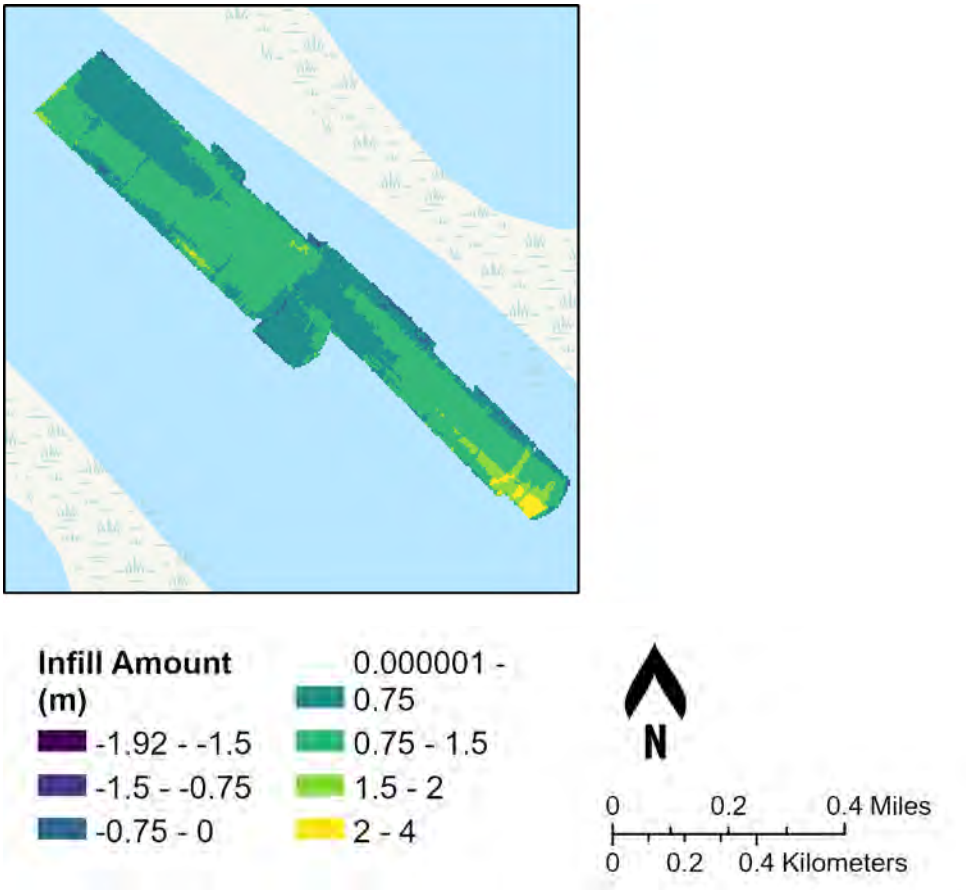

Figure A-7. Example of an infilling raster calculated by subtracting December 2021 elevations from January 2022 elevations. The elevation difference in the borrow area shows the amount of infilling (positive values) between the end of dredging and the January survey. Small areas of negative change around the edges of the dredged areas are potentially the result of sediment slumping.

A.1.4 Statistics

Statistics were calculated for each analysis area using the ESRI Zonal Statistics tool. The zone was defined by the single value raster that defines each analysis area; zone rasters were snapped to the infill rasters for the calculation. All statistics are performed only on non-null values within the zone (Table A-1). The total area of each analysis area is determined by the number of cells, with a non-null value, that are part of the zone. The sum of the raster cell values represents the infill amount, in meters, that each raster represents. The sum is then multiplied by the cell area (25 m^2) to obtain the total infill volume. Volumes per day are also provided by dividing the total volume by the number of days between the first survey after dredging and the survey at the end of the analysis period.

A.2 RESULTS AND DISCUSSION

Sediment infilling amounts (in meters per raster cell) are shown over time for each analysis area (Figure A-8, Figure A-9, Figure A-10, Figure A-11, Table A-1). Infilling is uneven across the borrow pits; no

particular section is infilled first in every area. In Area 1, the downstream parts of the pit experience more infilling, but in Area 2 the upstream end sees more infilling. Although Area 3 is the most recently dredged and experiences the least infilling during the analysis periods, it appears to be infilling more evenly compared to Area 1 and Area 2, at least initially. The total sediment captured by the borrow pit increases in all the areas over time; however, the sediment infilling rate decreases over time (Table A-1).

Bedforms also exist in the borrow pits. Movement of these bedforms contributes to some of the negative infilling values because migration of dune and ripple crests and troughs cause the bed elevation to change without a change in volume. This can be seen especially well in Area 3 (Figure A-12). Although bedform movement results in parts of the bed appearing to lower, the infilling volume within the borrow pit is expected to remain the same because sums are taken over the whole area. It is possible that sediment volume is transferred between analysis areas at the edges (such as movement of a bedform from Area 3 to Area 2), however, this volume is expected to be small and would still be captured in the Area 2 analysis. There is a small *ridge* or *seam* between Area 1 and Area 2 separating pits that were dredged separately; bedforms are not expected to travel past this ridge. There is a similar but much smaller ridge between Area 2 and Area 3, which may prevent bedforms from transferring between the two areas. It should also be noted that the northeast half of Area 1 is significantly deeper than the southwest half (-18 m versus -15 m). These are essentially two separate borrow pits even though it is one analysis area. There is likely not downstream bedform transfer between them. Area 1 experiences much higher infill volumes at the downstream edges of the pits; this may be explained by bedform migration that this then ‘trapped’ at the downstream edge of the borrow pit.

Small areas of bed lowering around the edges of the borrow pits are likely the result of sediment slumping.

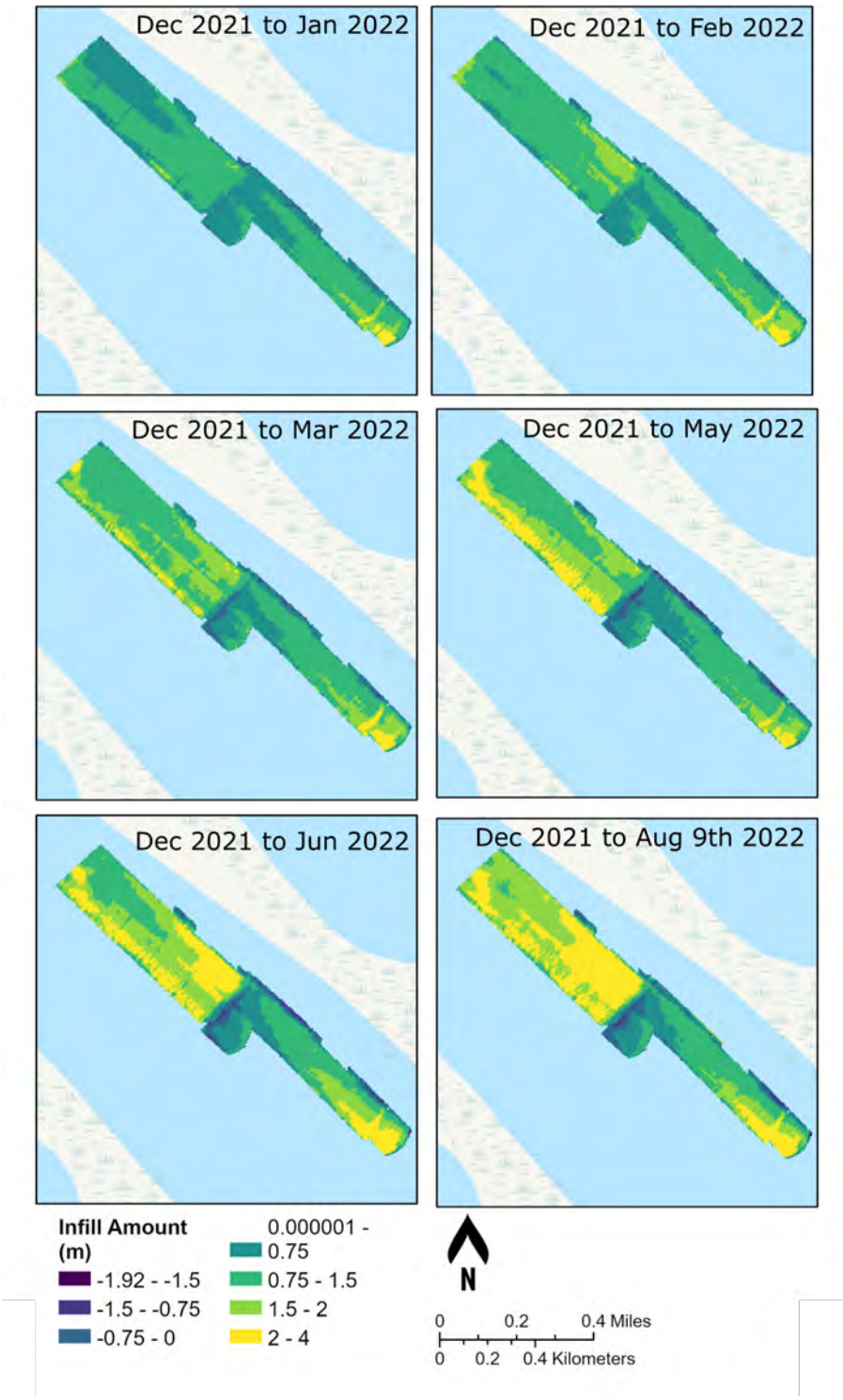

Figure A-8. Raster infill amounts in meters per cell for Area 1 through time. This figure does not include the last three surveys. The last three surveys are included in Figure A-9. The dates are December 2021 through August 2022.

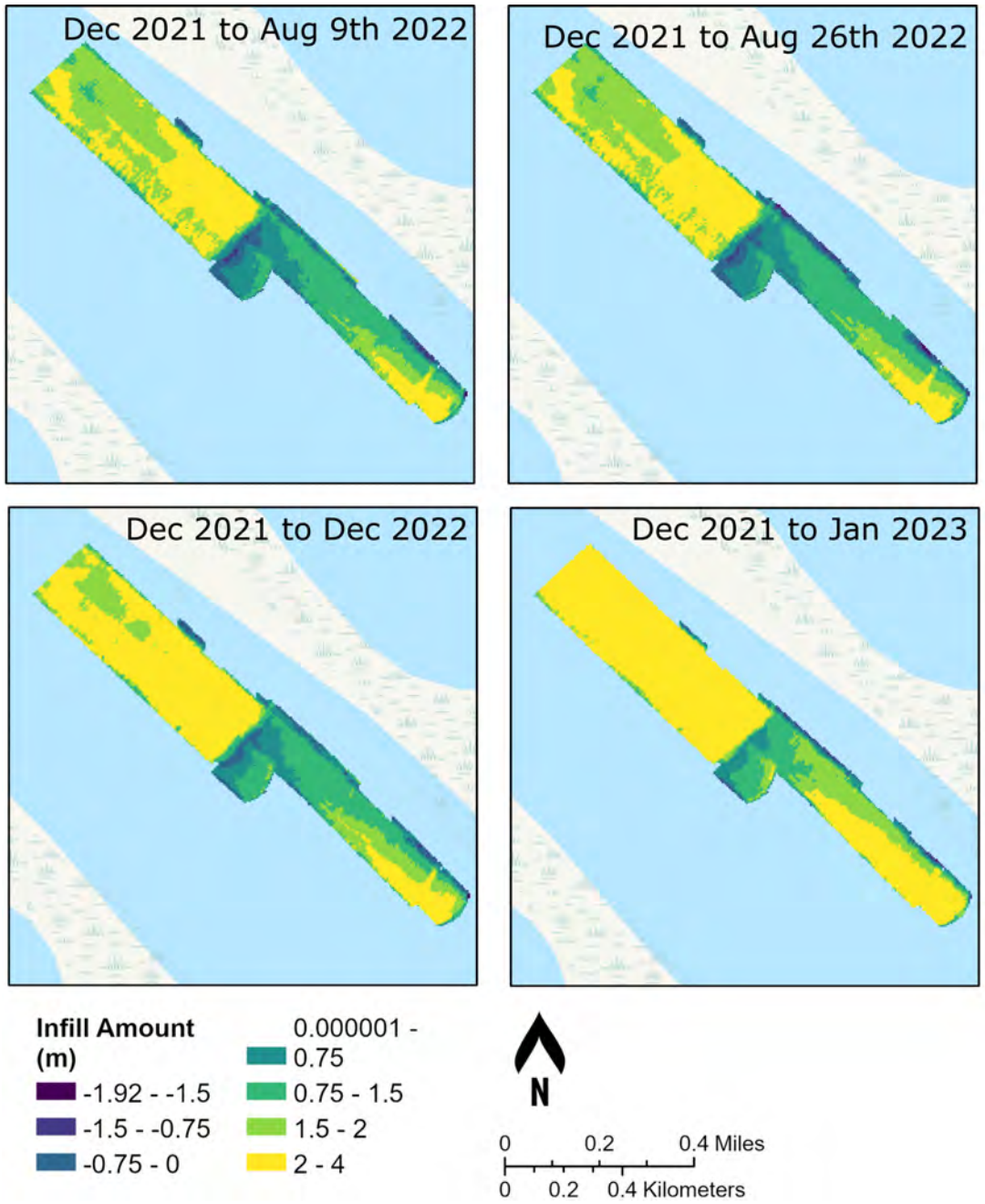

Figure A-9. Raster infill amounts in meters per cell for Area 1 through time, including the final survey at the end of January 2023. The dates are December 2021 through January 2023.

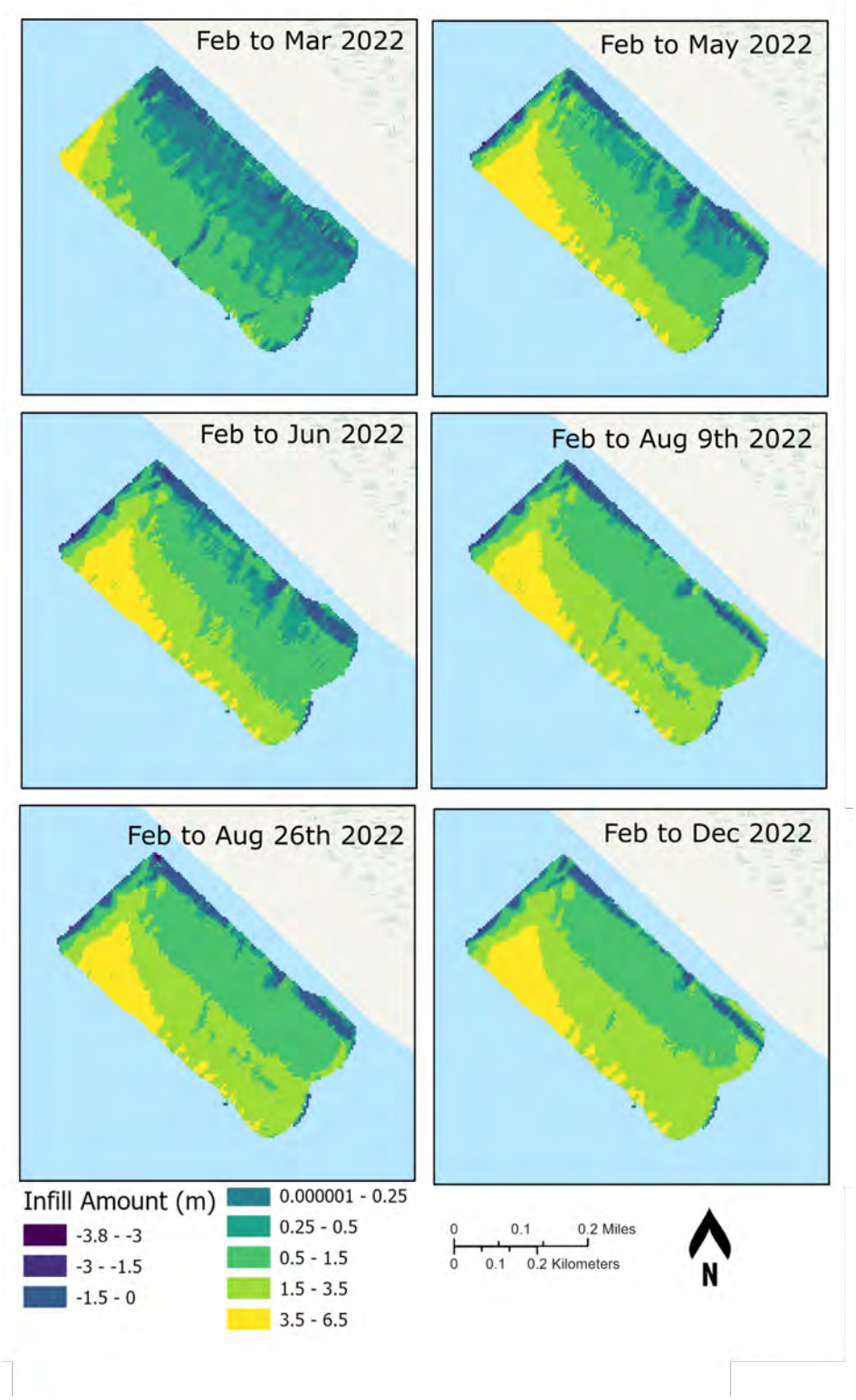

Figure A-10. Raster infill amounts in meters per cell in Area 2 from February to December 2022. The January 2023 survey is included in Figure A-10.

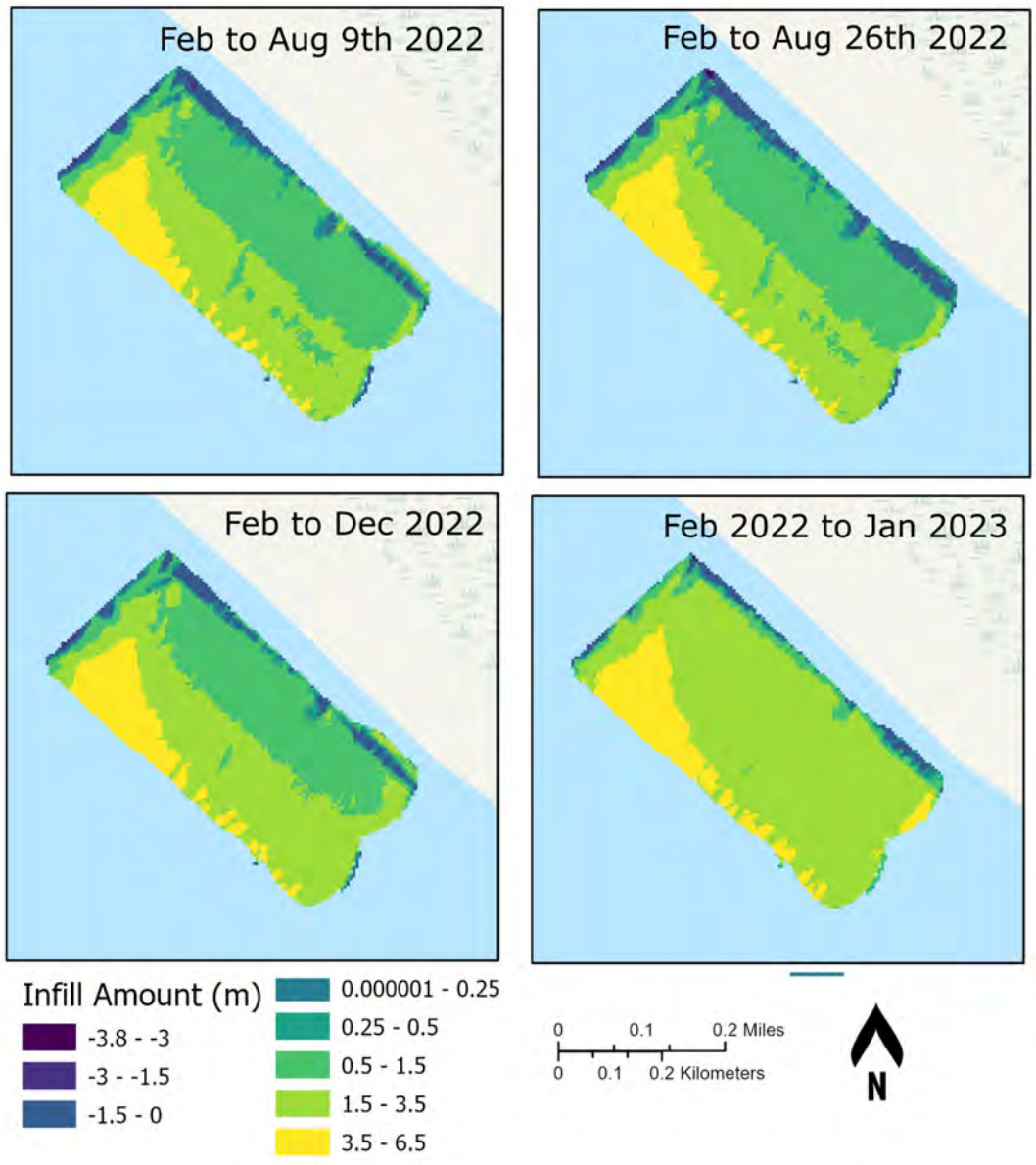

Figure A-11. Raster infill amounts in meters per cell in Area 2 through January 2023.

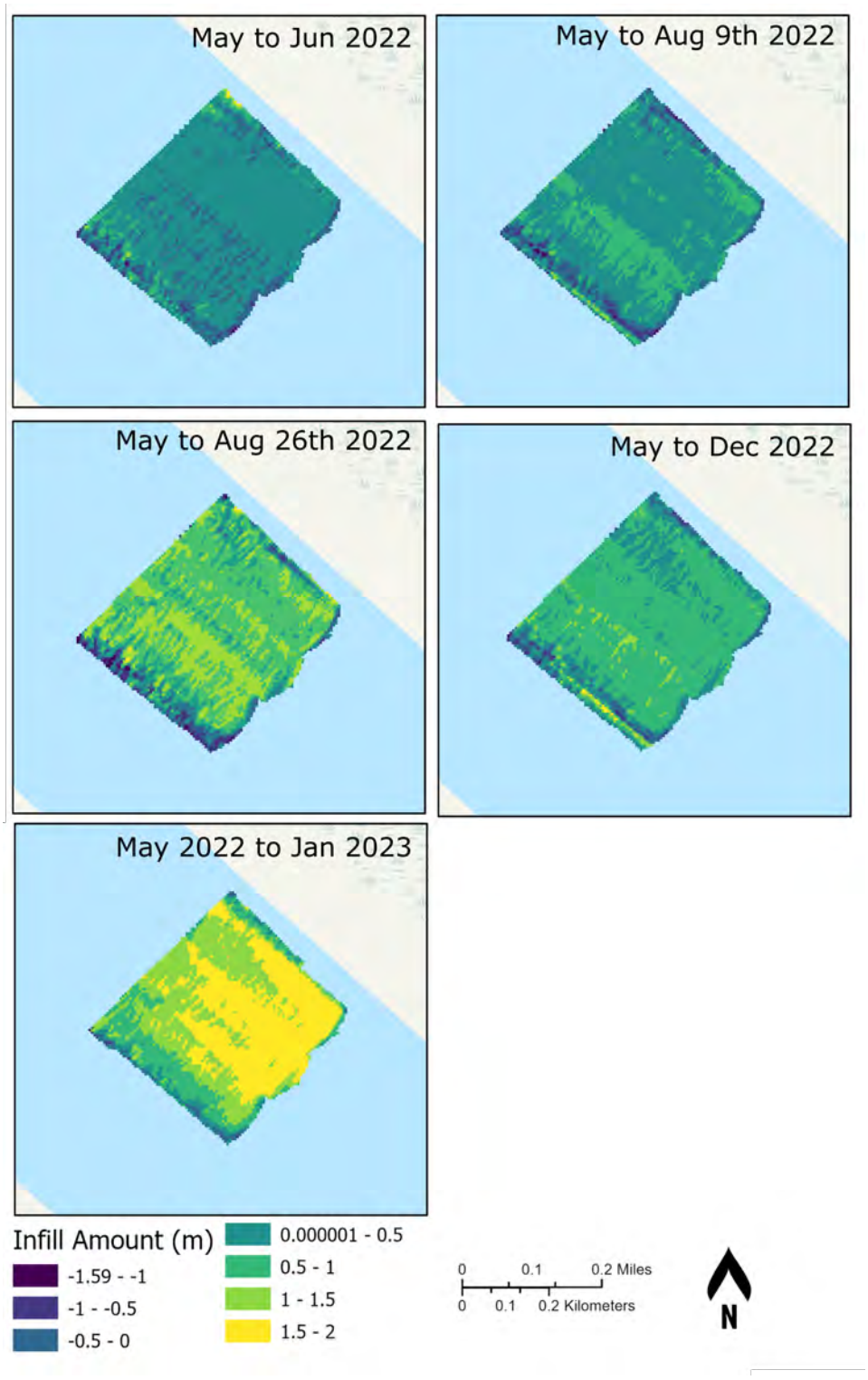

Figure A-12. Raster infill amounts in meters per cell for Area 3 through time.

Table A-1. Infilling statistics for each analysis area. Date start represents the start of the current analysis period, which is a survey date. Date end represents the date of the next survey used to calculate the infill volume. Area represents the total analysis area used for that analysis period; the August 9 and January 27 surveys have slightly smaller footprints that do not fully cover the analysis area. Infill volume is calculated using the elevation change in each raster cell multiplied by the cell area (25 m^2). One month is standardized to 30 days in the m^3/month column. The final analysis period for each analysis area is shown in bold

Area	Date start	Date end	Number of Days	Area (m^2)	Infill Volume (m^3)	Infilling Rate (m^3/day)	Infilling Rate (m^3/month)
1	12/20/2021	1/24/2022	35	313,225	264,299	7,551	226,542
1	1/24/2022	2/23/2022	30	313,225	74,138	2,471	74,138
1	2/23/2022	3/24/2022	29	313,225	37,715	1,301	39,016
1	3/24/2022	5/23/2022	60	313,225	-1,799	-30	-900
1	5/23/2022	6/23/2022	31	313,225	63,771	2,057	61,714
1	6/23/2022	8/9/2022	47	312,675	41,102	875	26,236
1	8/9/2022	8/26/2022	17	313,225	-909	-53	-1,604
1	8/26/2022	12/27/2022	123	313,150	76,102	619	18,561
1	**12/27/2022**	**1/27/2023**	**31**	**310,250**	**239,146**	**7,714**	**231,431**
2	2/23/2022	3/24/2022	29	173,775	121,090	4,176	125,266
2	3/24/2022	5/23/2022	60	173,775	151,113	2,519	75,556
2	5/23/2022	6/23/2022	31	173,775	1,037	33	1,004
2	6/23/2022	8/9/2022	47	173,525	19,119	407	12,204
2	8/9/2022	8/26/2022	17	173,775	-520	-31	-918
2	8/26/2022	12/27/2022	123	173,675	43,983	358	10,728
2	**12/27/2022**	**1/27/2023**	**31**	**172,475**	**115,546**	**3,727**	**111,819**
3	5/23/2022	6/23/2022	31	145,325	20,654	666	19,988
3	6/23/2022	8/9/2022	47	144,925	26,165	557	16,701
3	8/9/2022	8/26/2022	17	145,325	1,515	89	2,674
3	8/26/2022	12/27/2022	123	145,275	38,887	316	9,485
3	**12/27/2022**	**1/27/2023**	**31**	**135,975**	**96,643**	**3,118**	**93,526**

APPENDIX B. ALLIANCE MODEL

The Alliance Model is a further development of an existing Delft3D-4 model developed and described in Yuill et al. (2015). This Appendix provides a detailed description of the model characteristics, improvements, model calibration process, and results from simulation experiments, including sensitivity analysis.

B.1 MODEL IMPROVEMENTS

The original model (Yuill et al., 2015) was improved using new available datasets for initial conditions, model calibration, and newer observations and information to inform model sensitivity analysis. These improvements include:

- Adjustment of horizontal and vertical grid resolutions (this includes refinement and de-refinement balancing resolution where needed and relaxing resolution where reasonable to balance accuracy and computational efficiency).
- Implementation of a spatially varying eddy viscosity informed by experiments conducted with a Regional 3-D Model for the Lower Mississippi River (Reins, 2018).
- Adjusted median grain diameters of the sand fractions and added a silt fraction in the sediment transport model.
- Updated and redefined spatially varying layered bed stratigraphy based on recent field observations (M. Allison et al., 2018b, 2018a)
- Prepared boundary conditions and simulation setups to examine additional river hydrographs (i.e., 2010, 2011, 2016 and 2019).
- Implementation, re-analysis, and validation of an updated morphological scale factor of 10 to allow for morphological simulations of a full river hydrograph to allow examination of full transient conditions.
- Implementation of new monitoring points and cross sections for comparison with measurement data.
- Implantation of polygons to allow for post-processing of regional to local geomorphic change for channel, bar, and borrow pit volumetric analysis and aggradation and degradation patterns.

B.2 MODEL DOMAIN AND GRID

The three-dimensional model represents the Mississippi River between the upstream boundary near Belle Chasse (RM 75) and the downstream boundary located at RM 55 (Figure B-1). The borrow pit is situated in the middle of the domain between RM 64 and 65. The model has a structured curvilinear grid with 457×87 elements. Cell sizes measure between 12 m (laterally) by 20 m (longitudinally) around the borrow pit area. Grid resolution across the rest of the model domains remains similar in lateral direction but is gradually de-refined in longitudinal direction. Most of the grid cells outside of the area of interest therefore gradually increase to around 100 m in streamwise direction. The vertical grid consists of 10

non-equidistant sigma-layers with thinner layers near the bed and thicker layers near the water surface. The layers thicknesses are as follows, expressed as percentage of the water column from top to bottom: 29.2, 22.8, 16.8, 11.8, 7.8, 4.8, 2.8, 1.8, 1.2, and 1.0 %.

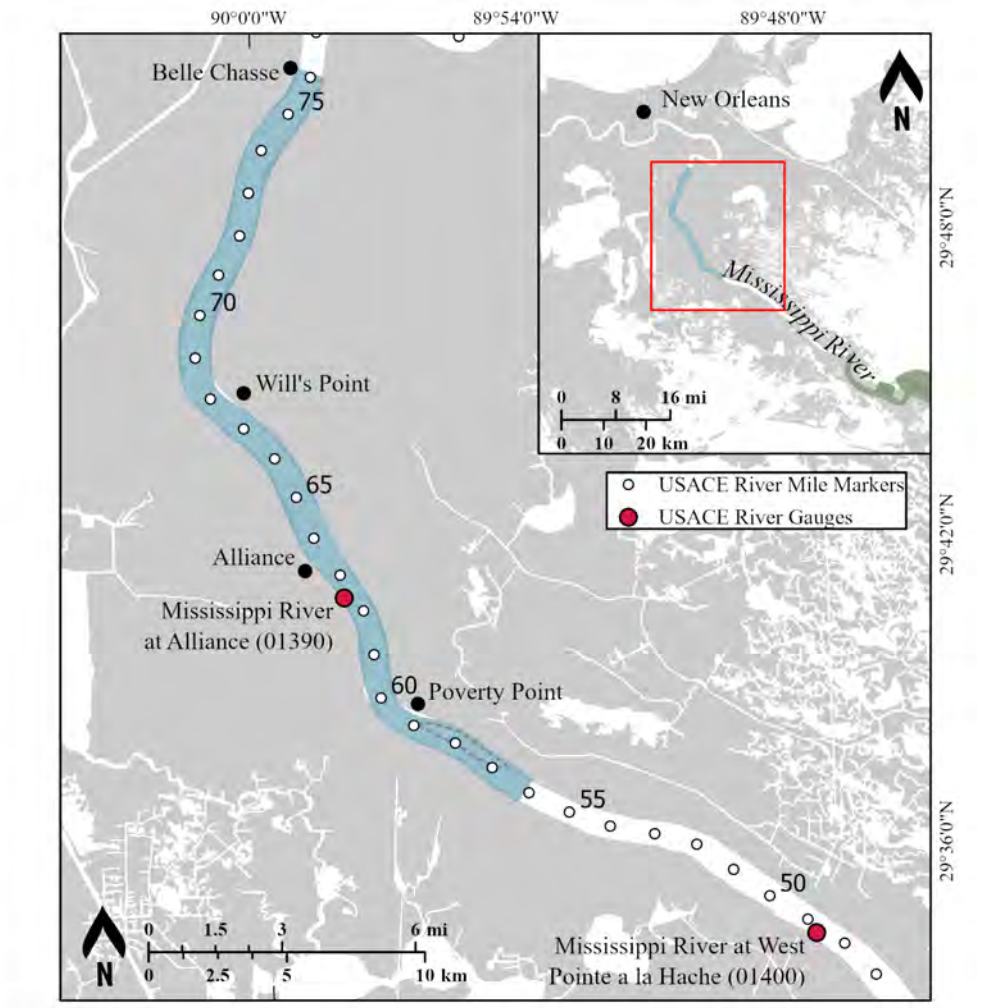

Figure B-1. Model domain of the Alliance Model (in blue) with the USACE river mile markers in white, and the USACE river gauges in red that were used to define the downstream stage boundary condition.

B.3 BATHYMETRY

The model bathymetry is derived from a raster that was collected for the National Oceanic and Atmospheric Administration (NOAA)'s National Ocean Service (NOS) Hydrographic Survey (Dasler, 2019b). The raster (Survey ID H13194) is based on multibeam echo sounder data collected between October 2018 and April 2019. After conversion to a 5-meter raster, the data was interpolated onto the model grid through triangular interpolation. Following model calibration, the AABP was implemented to facilitate experiments and the matrix of simulations presented in Section B.6. The footprint and depth of the borrow pit were informed by pre-dredging surveys conducted by Weeks Marine and the preliminary cut footprint proposed and shared with the Institute by Moffatt and Nichol, who is the engineer of record

for the project. The shared drawings were used to emplace the pit dimensions and used side slopes to determine the shape of the borrow pit and using that information the initially point cloud for the model bathymetry was updated, and the borrow pit shape interpolated onto the model bathymetry.

B.4 HYDRODYNAMICS

B.4.1 Boundary Conditions

The upstream model boundary was set at the United States Geological Survey (USGS) station at Belle Chasse (station number 07374525, Figure B-1) which provides a long-term historical record of Mississippi River discharges and stages. Daily averaged discharge volumes were used as an upstream boundary condition. The downstream model boundary is located at RM 55 where no stage data is available. The nearest stations with stage data are the U.S. Army Corps of Engineers (USACE) gauges at Alliance (013190, at RM 62.5) and West Pointe a la Hache (01400, at RM 48.7) (Figure B-1). These two stages were converted to water levels referenced to NAVD88. Linear interpolation was applied between the water level timeseries at Alliance and West Point a la Hache to obtain the water level timeseries at RM 55, which was used as the downstream boundary condition.

B.4.2 Calibration

The model used a uniform Chézy roughness of 65 $m^{1/2}/s$ which reproduces the most realistic hydrodynamic patterns similar to results reported by Yuill et al. (2015). Despite the fact that the Alliance gauge stage was used to partially inform the downstream boundary conditions, model stage predictions within the model domain near Alliance were compared to that gauge, to ensure reasonable model skill, with results showing a close agreement in Figure B-2. Additional calibration included comparing the model with hydrodynamic observations using vessel based synoptic acoustic doppler current profile (ADCP) data, to ensure predicted velocities agreed with observations. Velocity calibration results (Figure B-3) show that the model reasonably agrees with observations of depth integrated velocity in the transverse direction. The model predicts observed velocity near the west bank (left) very well, slightly underestimates velocity magnitude approximately 50–300 m from the west bank, and slightly overestimates velocity in the main channel and reproduces velocity on the east bank very well (Figure B-3).

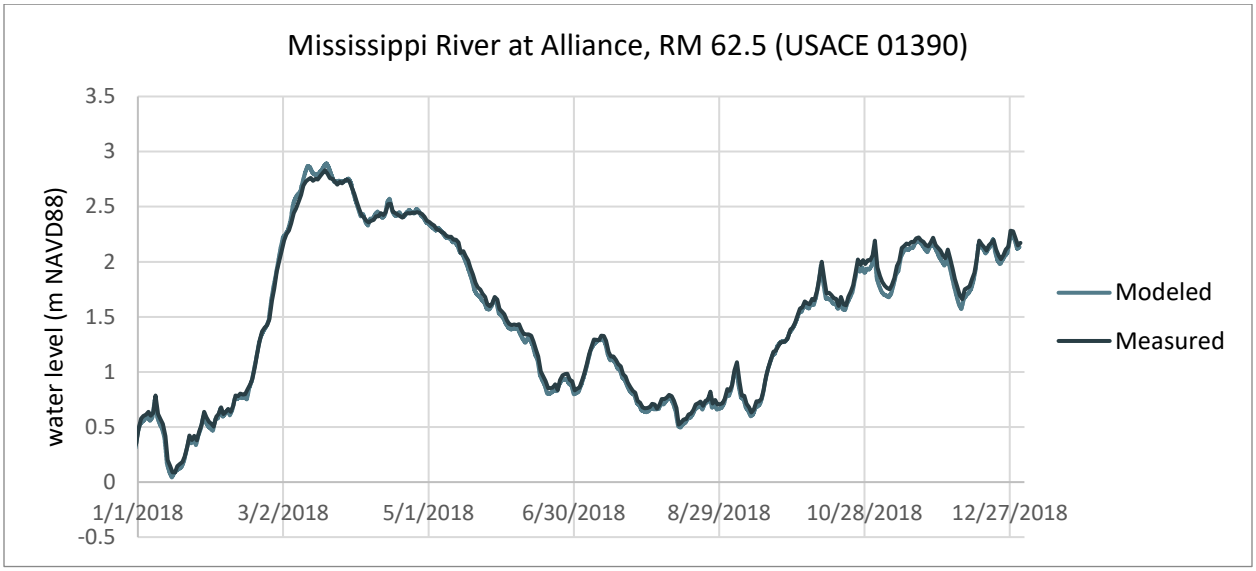

Figure B-2. Comparison of water levels between model and observations at the USACE Mississippi River station at Alliance for year 2018. It should be noted that the Alliance gauge stage was used to partially inform the downstream boundary condition of the model.

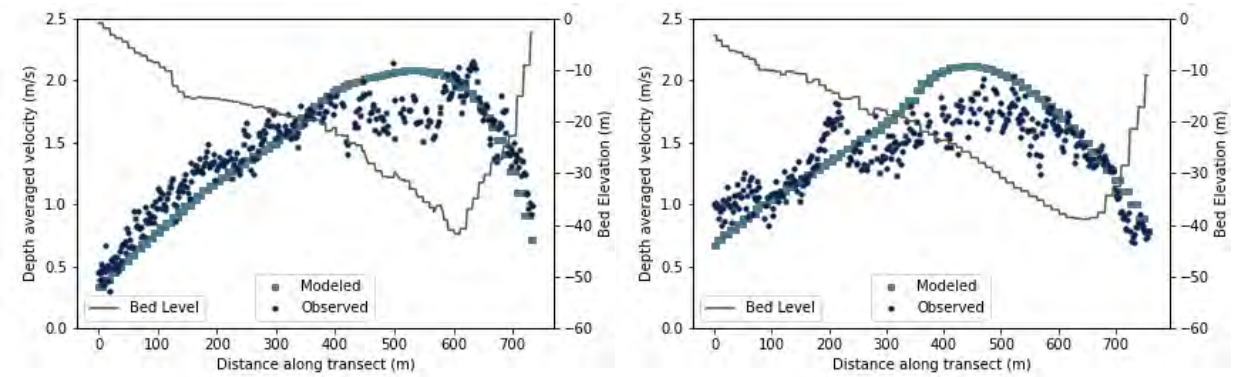

Figure B-3. Comparison of water velocity between model and observations at two transects near Poverty Point for year 2018 (April 24 on the left and April 25 on the right). Observed data from (M. Allison et al., 2018a).The black line shows bed elevation (in m NAVD88) in the model for the same cross sections.

B.5 SEDIMENT TRANSPORT AND MORPHOLOGY

B.5.1 Boundary Conditions

The Van Rijn sediment transport formulae (Van Rijn, 1993) were used to predict a base value for the sand fraction of sediment flux, including suspended sediment and bedload transport, throughout the model domain. Four sediment fractions were included in the model: silt (50 micron) and three classes of sand, consisting of very fine sand (92 micron), fine sand (183 micron), and medium sand (367 micron), based on a previous regional model of the Lower Mississippi River (Reins, 2018). These classes were the same as in Reins, (2018), which follows methodology that was developed and employed previously by McCorquodale et al. (2017). These classes were further confirmed by using bore logs, grab samples and other available geotechnical information conducted by Eustis Engineering Company, Fugro Consultant

Inc., and Ocean Survey Inc. at Bayou Dupont and Wills Point, Alliance Anchorage, and Alliance South (Eustis Engennering Company, Inc., 2006; Fugro Consultant, Inc., 2012; Ocean Survey, Inc., 2011)

The suspended sediment concentration in the Mississippi River imposed at the upstream open boundary was based on observed daily water discharge and though the use of sediment rating curves previously developed by the Institute. In particular:

- A traditional rating curve developed for the Baton Rouge location was used for sand (Bregman et al., 2020; Messina et al., 2021). This curve is a function of water discharge only, it is based on observations spanning 2008–2012, and has the following form:

  Suspended Sand Load (metric tons/day) = $a \times [1 - \exp(-b \times Q_w)] + c \times [1 - \exp(-d \times Q_w)]$

  - $a = -2.145 \times 10^{5}$
  - $b = 2.855 \times 10^{-6}$
  - $c = 3.261 \times 10^{9}$
  - $d = 1.242 \times 10^{-10}$

  where Q_w is the water discharge (cubic meters per second [m^3/s]).

  The sand concentrations at the upstream boundary were assumed to consist of 20% very fine sand, 60% fine sand, and 20% medium sand. Sensitivity simulations were performed with different distributions (see Appendix B.6 Model Simulation Matrix).

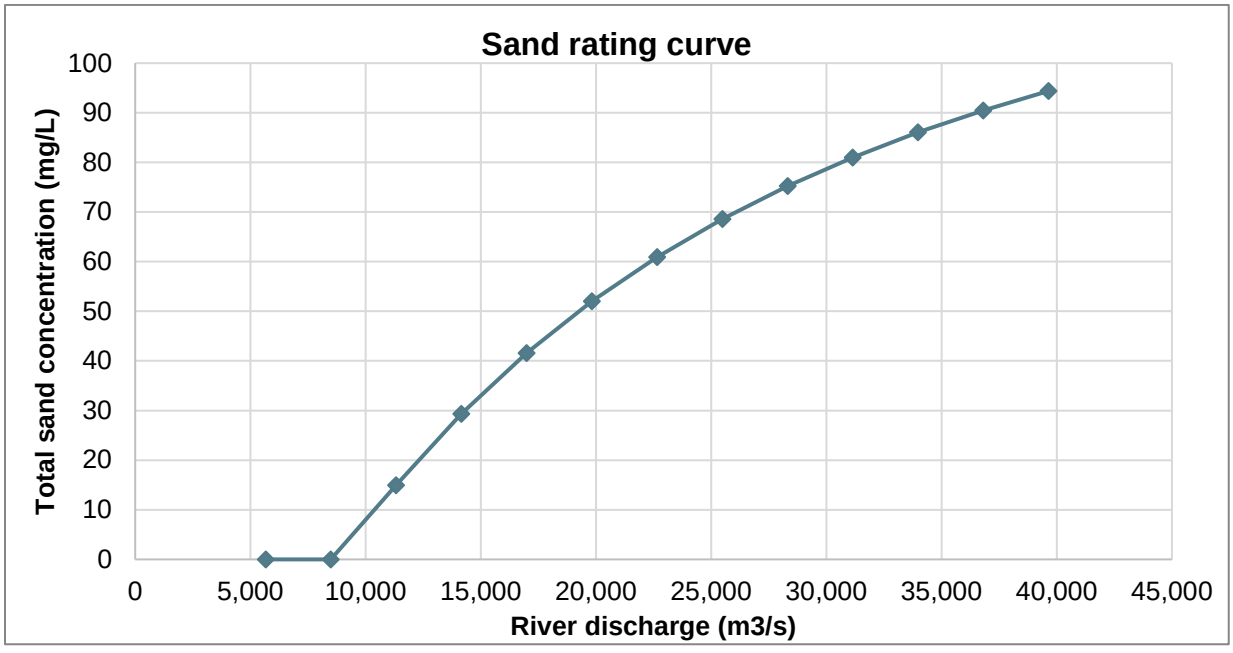

Figure B-4. Sand rating curve used in the model: sand concentration as a function the river discharge.

- A hysteresis rating curve developed for the Belle Chasse location was used for fine sediment. Belle Chasse was selected because this location (USGS gauging station at river kilometer 117.5) has sufficient turbidity data available to develop the hysteresis sediment rating curve for total load (Liang, Meselhe, Messina, & Ortals, 2016). This curve estimates total fine sediment, 75% of it is estimated to be silt based on grain size data available from USGS and this was implemented in the model.

B.5.2 Bed Stratigraphy

The morphology model employs the mobile bed capability of Delft3D-4 by adopting a bed stratigraphy built up of multiple layers that consist of a mixture of different sand fractions (Table B-1). The thickness of the mobile bed was set to 0 in sections deeper than -27.5 m NAVD88 to avoid the presence of erodible bed sediment in section where the riverbed reached the non-erodible substrate, such as in the river's thalweg (Nittrouer, Mohrig, Allison, & Peyret, 2011; Viparelli, Nittrouer, & Parker, 2015). The mobile bed thickness varies between 0 m at a bed elevation of -27.5 m NAVD88 to a maximum of 5 m at or above bed elevations of 15 m NAVD88. Sand bars within the area of interest have bed elevations that fall within this range (Figure 2). The bed composition in the model, which is based on previously collected field data (M. Allison et al., 2018a, 2018b), varies between the five different layers and contains more medium sand in the surface layer and mostly fine sand in the deepest layer, to replicate a graded bed with a coarsening upward sequence (Table B-1). Sensitivity simulations were performed with different bed compositions (see Appendix B.6 Model Simulation Matrix).

Table B-1. Composition (expressed as mass fraction) of sediment layers that form the bed stratigraphy in the morphological model.

Layer number	Very fine sand (%)	Fine sand (%)	Medium sand (%)
1 (surface)	7%	43%	50%
2	7%	58%	35%
3	7%	73%	20%
4	12%	78%	10%
5 (deepest)	22%	71%	7%

B.5.3 Calibration

The model was calibrated by adjusting multiplication factors for suspended sediment reference concentrations to obtain agreement between measured and modeled suspended sediment transport (i.e., sand, silt, and total) at two locations within several kilometers from the borrow pit, at RM 68 and 62 (Figure B-5 through Figure B-10). During the sediment model calibration, suspended sediment data collected by the Institute was used (M. Allison et al., 2018a, 2018b). The final calibration step included ensuring a stable morphology for simulations that lasted for one year, to ensure that the model did not produce morphology runaway behavior. During that process, incremental adjustments were made to the longitudinal and transverse bed gradient factors for bed load transport, to match the overall bar shape and order of bed level change observed in the river from historic and repeat bathymetry (Yuill et al., 2015) and more recent comparisons of bathymetry change such as the 2018 NOAA bathymetry (Dasler, 2019a). An overview of key calibration factors is given in Table B-2.

During the calibration process, additional sensitivity experiments were performed with the model to test variations in parameters such as median grain size, composition and thickness of the bed sediment layer, diffusivity, and viscosity. This interactive process helped develop the final model setup with the default initial conditions finalized for use in the project simulations.

The model reproduced observations of suspended total sediment flux and sand flux in 2018, collected at RM 62 and RM 68, from well to reasonably well. The model reproduced sand transport at RM 68 very well at intermediate flows, and reasonably well at higher flows (Figure B-5), while total transport and silt transport were reproduced by the model very well across all flow regimes (Figure B-6 and Figure B-7). At RM 62, the model reproduced sand transport, silt transport, and finally total transport very well compared to observations for both high and low flow in the river (Figure B-8 to Figure B-10).

Bedform transport rates predicted by this model aligned well with transport rates calculated in previous studies (Figure B-11).

Table B-2. Key model calibration factors for sediment transport and morphology.

Parameter	Value
Multiplication factor for suspended sediment reference concentration	0.5
Multiplication factor for bed-load transport vector magnitude	1
Streamwise bed gradient factor for bed load transport	3
Transverse bed gradient factor for bed load transport	10

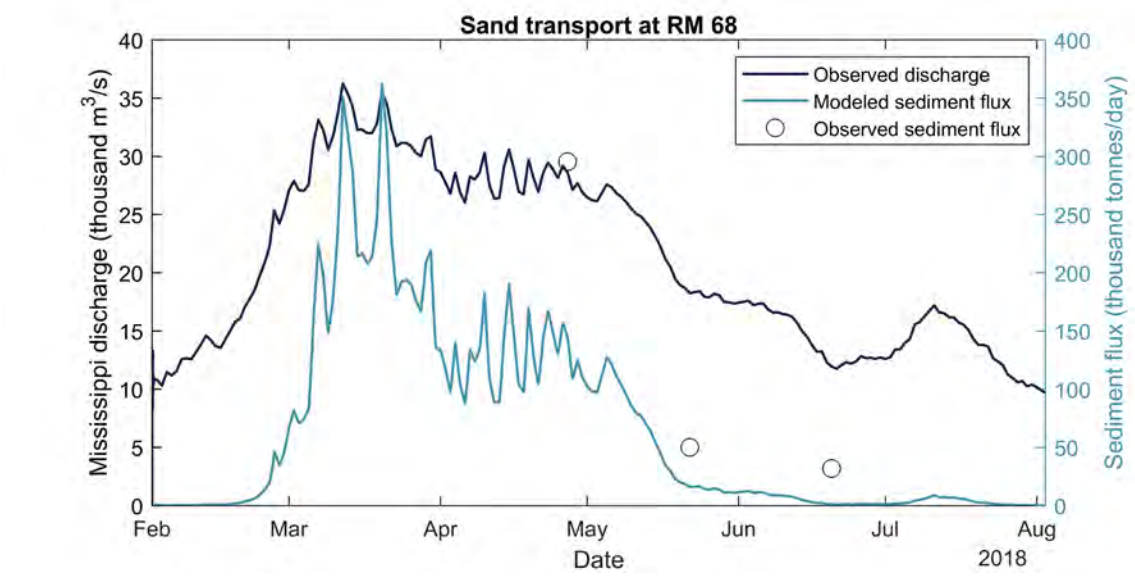

Figure B-5. Observed discharge (blue line), modelled sand transport flux (light blue line) and observed sand fluxes (black circles) at RM 68.

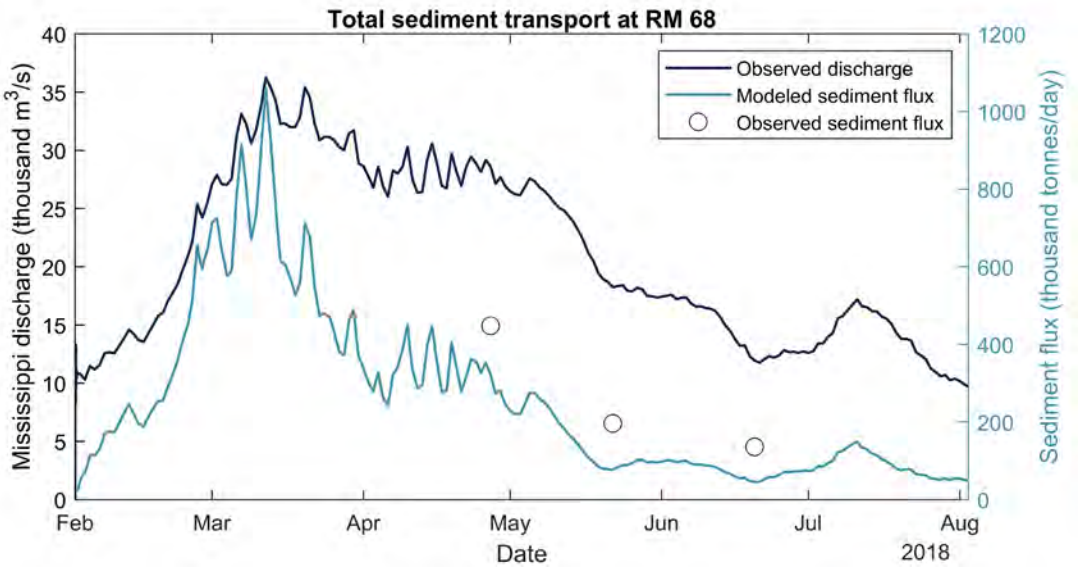

Figure B-6. Observed discharge (blue line), modelled total sediment transport flux (light blue line) and observed total sediment fluxes (black circles) at RM 68.

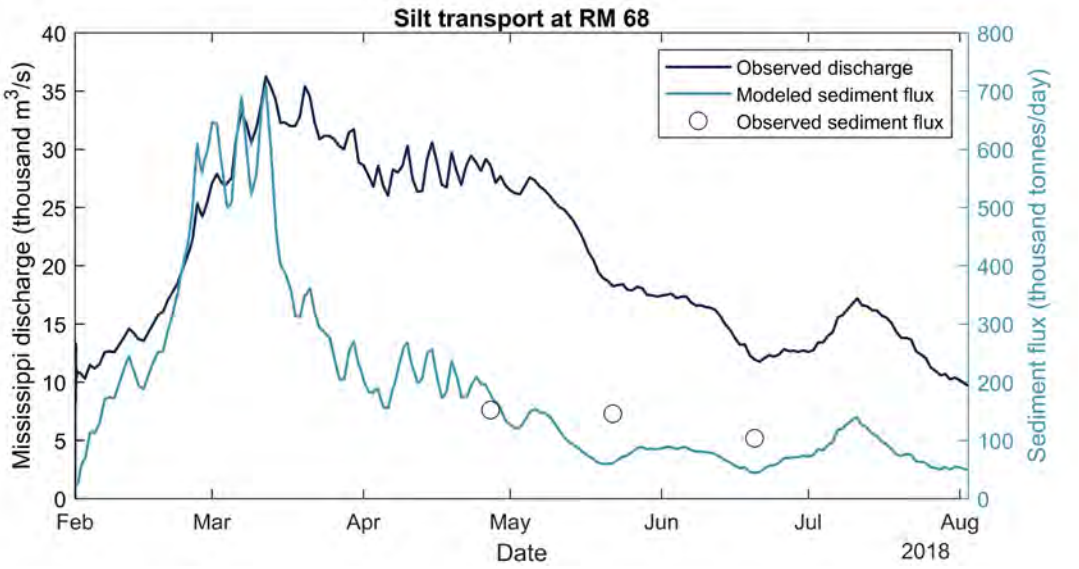

Figure B-7. Observed discharge (blue line), modelled silt transport flux (light blue line) and observed silt fluxes (black circles) at RM 68.

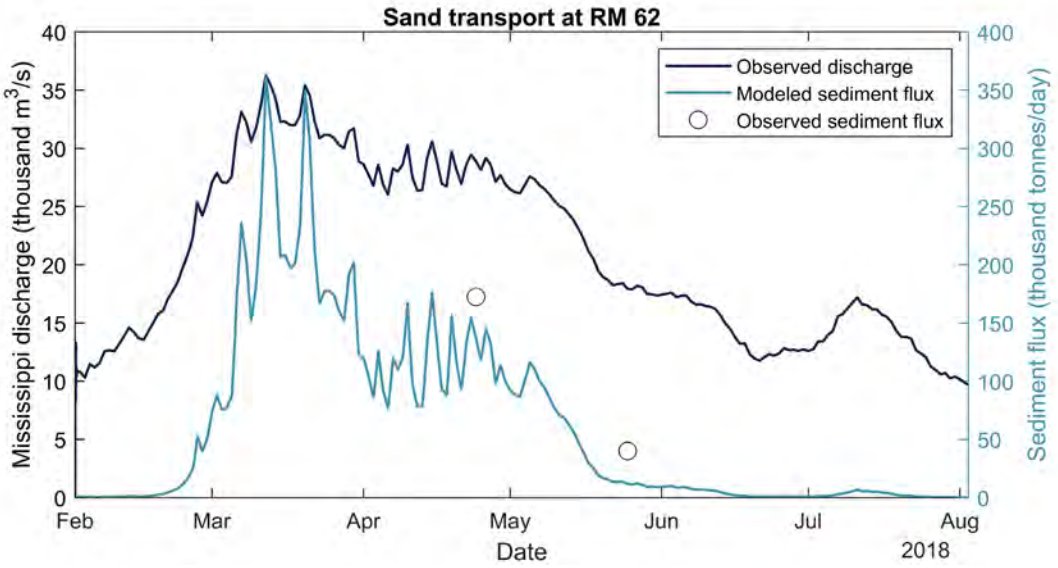

Figure B-8. Observed discharge (blue line), modelled sand transport flux (light blue line) and observed sand fluxes (black circles) at RM 62.

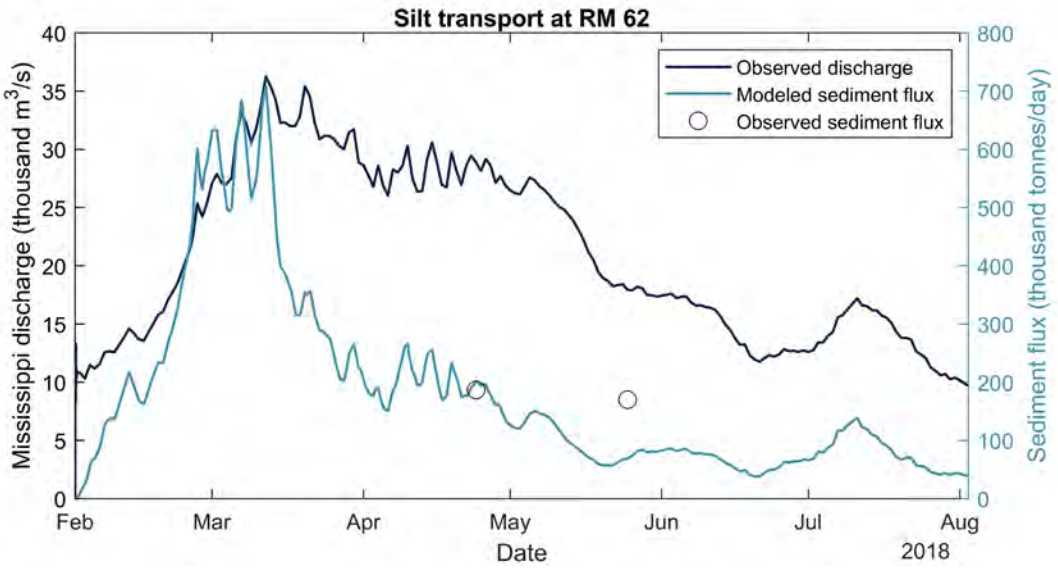

Figure B-9. Observed discharge (blue line), modelled silt transport flux (light blue line) and observed silt fluxes (black circles) at RM 62.

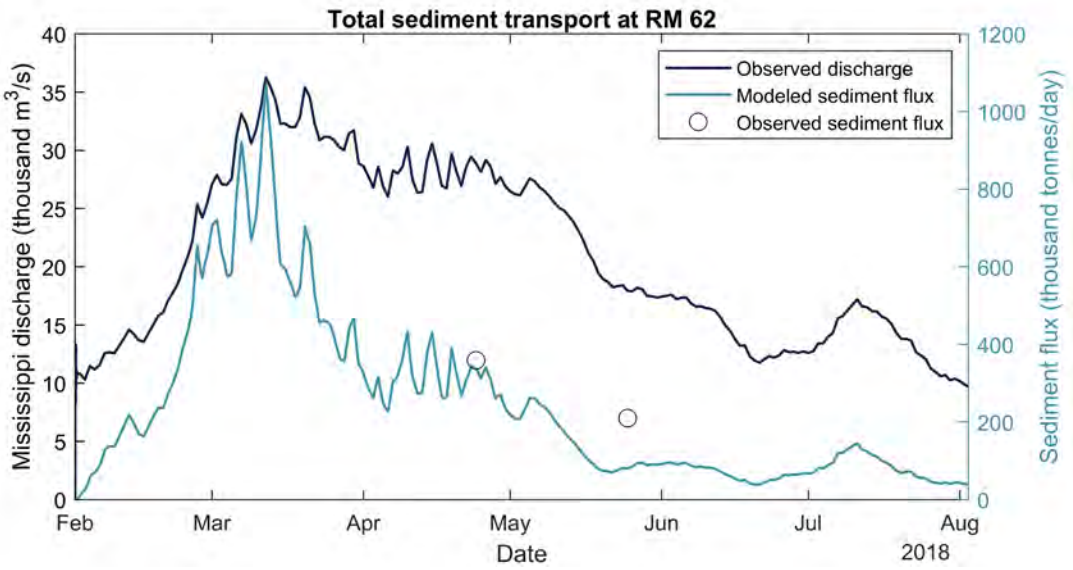

Figure B-10. Observed discharge (blue line), modelled total sediment transport flux (light blue line) and observed total sediment fluxes (black circles) at RM 62.

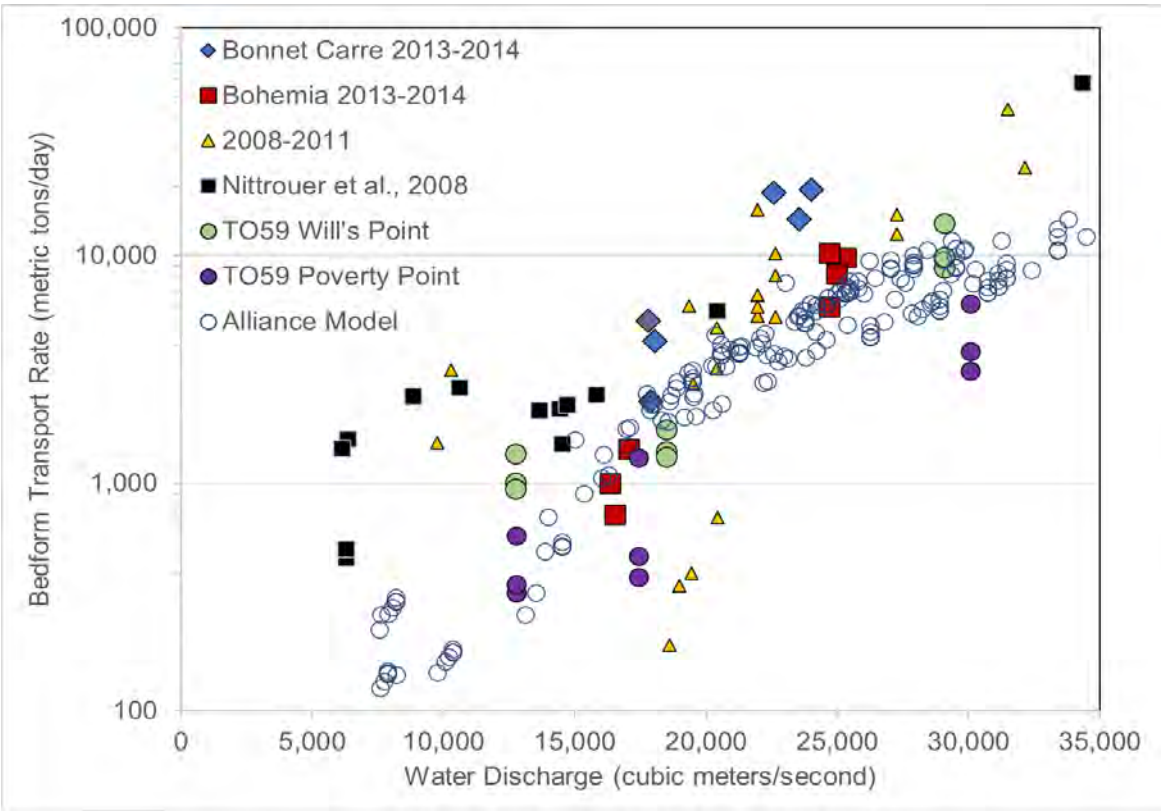

Figure B-11. Bedform transport rates predicted by the Alliance Model in blue circles. Data from previous Mississippi River bedload transport studies at Poverty Point (purple circles), Will's Point (green circles), Bonnet Carré 2018 (orange diamonds), Bonnet Carré 2013–2014, Bohemia 2013–2014 (red squares), Myrtle Grove and other sites further downriver in 2008–2011 (white triangles). Regression published for 2003–2006 in the lower river by (Nittrouer et al., 2008) is included. Figure adapted from (M. Allison et al., 2018a).

B.6 MODEL SIMULATION MATRIX

Baseline simulations with the Alliance Model comprise with-pit and without-pit scenarios for each of the selected river hydrographs (i.e., 2010, 2011, 2016, and 2019). In addition to the baseline simulation for the AABP model which included sediment transport settings and boundary conditions presented in this appendix (i.e. the 2011 hydrograph and the presence of a 5.3 million m^3 borrow pit), additional simulations were performed to test the following: (1) absence of borrow pit, (2) borrow pit with smaller volume, (3) evaluating different hydrographs, (4) assessing the presence of sediment diversion upstream, (5) changes in upstream sediment supply via changes in the upstream sediment concentration, (6) changes in sediment grain size distribution, and (7) changes in sediment grading distribution. Table B-3 presents the matrix of all simulations that were performed and provides detailed information about the changes made to specific parameters or model inputs.

Table B-3. Matrix of all simulations performed with the Alliance Model. VF=very fine, F=fine and M=medium sand. The box highlighted in light blue for each simulation represent the model input that was varied from the baseline simulation.

Simulation Name	Hydrograph	Median sediment diameter (D50)	Upstream sediment supply	Bed sediment grading	Presence of sediment diversions	Variation
2011 with AABP, coarser bed composition	2011	VF sand 92 µm F sand 183 µm M sand 367 µm	20% VF, 60% F and 20% M sand	coarser: 7%/25%/68% VF/F/M in top layer, 22%/50%/28% VF/F/M in bottom layer	None	Bed composition
2010 with AABP	2010	VF sand 92 µm F sand 183 µm M sand 367 µm	20% VF, 60% F and 20% M sand	default: 7%/43%/50% VF/F/M in top layer, 22%/71%/7% VF/F/M in bottom layer	None	Hydrograph
2011 with AABP	2011	VF sand 92 µm F sand 183 µm M sand 367 µm	20% VF, 60% F and 20% M sand	default: 7%/43%/50% VF/F/M in top layer, 22%/71%/7% VF/F/M in bottom layer	None	Baseline
2016 with AABP	2016 (Oct 2015-Sep 2016)	VF sand 92 µm F sand 183 µm M sand 367 µm	20% VF, 60% F and 20% M sand	default: 7%/43%/50% VF/F/M in top layer, 22%/71%/7% VF/F/M in bottom layer	None	Hydrograph

Simulation Name	Hydrograph	Median sediment diameter (D50)	Upstream sediment supply	Bed sediment grading	Presence of sediment diversions	Variation
2019 with AABP	2019 (Sep 2018-Aug 2019)	VF sand 92 µm F sand 183 µm M sand 367 µm	20% VF, 60% F and 20% M sand	default: 7%/43%/50% VF/F/M in top layer, 22%/71%/7% VF/F/M in bottom layer	None	Hydrograph
2011 with AABP, 20% reduced sediment supply	2011	VF sand 92 µm F sand 183 µm M sand 367 µm	20% VF, 60% F and 20% M sand Concentration reduced by 20%	default: 7%/43%/50% VF/F/M in top layer, 22%/71%/7% VF/F/M in bottom layer	None	Sediment concentration
2011 with AABP, larger sand grain diameters	2011	VF sand 150µm F sand 230 µm M sand 340 µm	25% VF, 50% F and 25% M sand	default: 7%/43%/50% VF/F/M in top layer, 22%/71%/7% VF/F/M in bottom layer	None	Sediment Grain Size
2011 with AABP and MBSD	2011	VF sand 92 µm F sand 183 µm M sand 367 µm	20% VF, 60% F and 20% M sand	default: 7%/43%/50% VF/F/M in top layer, 22%/71%/7% VF/F/M in bottom layer	Mid Barataria 75k	Anthropogenic factors

Simulation Name	Hydrograph	Median sediment diameter (D50)	Upstream sediment supply	Bed sediment grading	Presence of sediment diversions	Variation
2011 with AABP MBSD and Breton SD	2011	VF sand 92 µm F sand 183 µm M sand 367 µm	20% VF, 60% F and 20% M sand	default: 7%/43%/50% VF/F/M in top layer, 22%/71%/7% VF/F/M in bottom layer	Mid Barataria 75k + Mid Breton 50k	Anthropogenic factors
2011 without AABP	2011	VF sand 92 µm F sand 183 µm M sand 367 µm	20% VF, 60% F and 20% M sand	default: 7%/43%/50% VF/F/M in top layer, 22%/71%/7% VF/F/M in bottom layer	None	No borrow pit
2011 with AABP, reduced pit volume by 36%	2011	VF sand 92 µm F sand 183 µm M sand 367 µm	20% VF, 60% F and 20% M sand	default: 7%/43%/50% VF/F/M in top layer, 22%/71%/7% VF/F/M in bottom layer	None	Pit Volume Reduction

B.7 MODEL RESULTS

Sensitivity tests evaluating the influence of bed stratigraphy on sediment supply and consequences in infilling rates showed that when the bed composition coarsens from 43% fine sand and 50% medium sand (183 and 367 microns, respectively) to 25% fine sand and 68% medium sand in the upper layer (while maintaining 7% very fine sand of 91 microns), total sand transport rates are reduced (Figure B-12C) increasingly with discharge (Figure B-12) and is ~10% lower when discharge exceeds 20,000 m^3/s (Figure B-12C) for the scenario with a coarser bed composition. Cumulative infilling is most noticeably influenced when flows are above 30,000 cfs, resulting in a reduction in sediment infilling volumes of 8% (or 250,000 m^3) by the end of the year for hydrograph 2011 (Figure B-12A).

Adjustments in upstream sediment supply, tested by reducing the upstream sediment concentration by 20% showed no changes in infilling rates (Figure B-13A). Tests with changed sediment characteristics (i.e., larger grain diameters for the very fine and fine sand fractions) showed that total sand transport decreased appreciably (up to 25%, Figure B-14C) but resulted in a much smaller magnitude change in the infilling rates of the order of 5% (Figure B-14A). Experiments with a reduced pit volume while maintaining the same borrow pit footprint showed little deviation from results with a deeper borrow pit (Figure B-15 A, B, C). Finally, upstream extractions of water and sediment due to the implementation of sediment diversions, showed noticeable change in the results (Figure B-16 A, B, C). The operation of the sediment diversions, removes water and sediment when flow is high in the main stem of the river, thus work to attenuate the hydrograph peak (Figure B-16B). Proportionally, the decline is residual flow resulting from the removal of water due to the diversions diminishes stream power, and thus total sand transport (Figure B-16C). As a result, cumulative infilling rates vary proportional to the flow extraction magnitude, and deviation from the reference case can be as much as 300,000 m^3 of sediment, and by the end of the simulation period total infilling can be more than 10% lower in the scenario where both diversions are operated (Figure B-16A).

Flow seasonality also contributes to the aggradation and degradation of sand bars in the Mississippi River (Nittrouer, Allison, & Campanella, 2008). Model results show that the Wills Point Bar upstream of Alliance Bar exhibits high variance of aggradation trends proportional to the river hydrograph (Figure B-17) with the lower aggradation during 2010 (~1,300,000 m^3) and the highest in 2019 (~4,100,000 m^3), whereas the Alliance Bar exhibits far less variance. Downstream of the Alliance Bar, the Belair Revetment experiences low aggradation, while the Lower Alliance Revetment shows degradation of the same order as Belair (~0.1-300,000 m^3), and lastly Harlem Revetment bar shows aggradation ranging from 200,000–900,000 m^3 (Figure B-17). Changes in the upstream sediment supply, bed composition and size, and distribution of sand between sediment classes has a lesser influence of bar storage, aggradation, and degradation trends compared to the river hydrograph (Figure B-18).

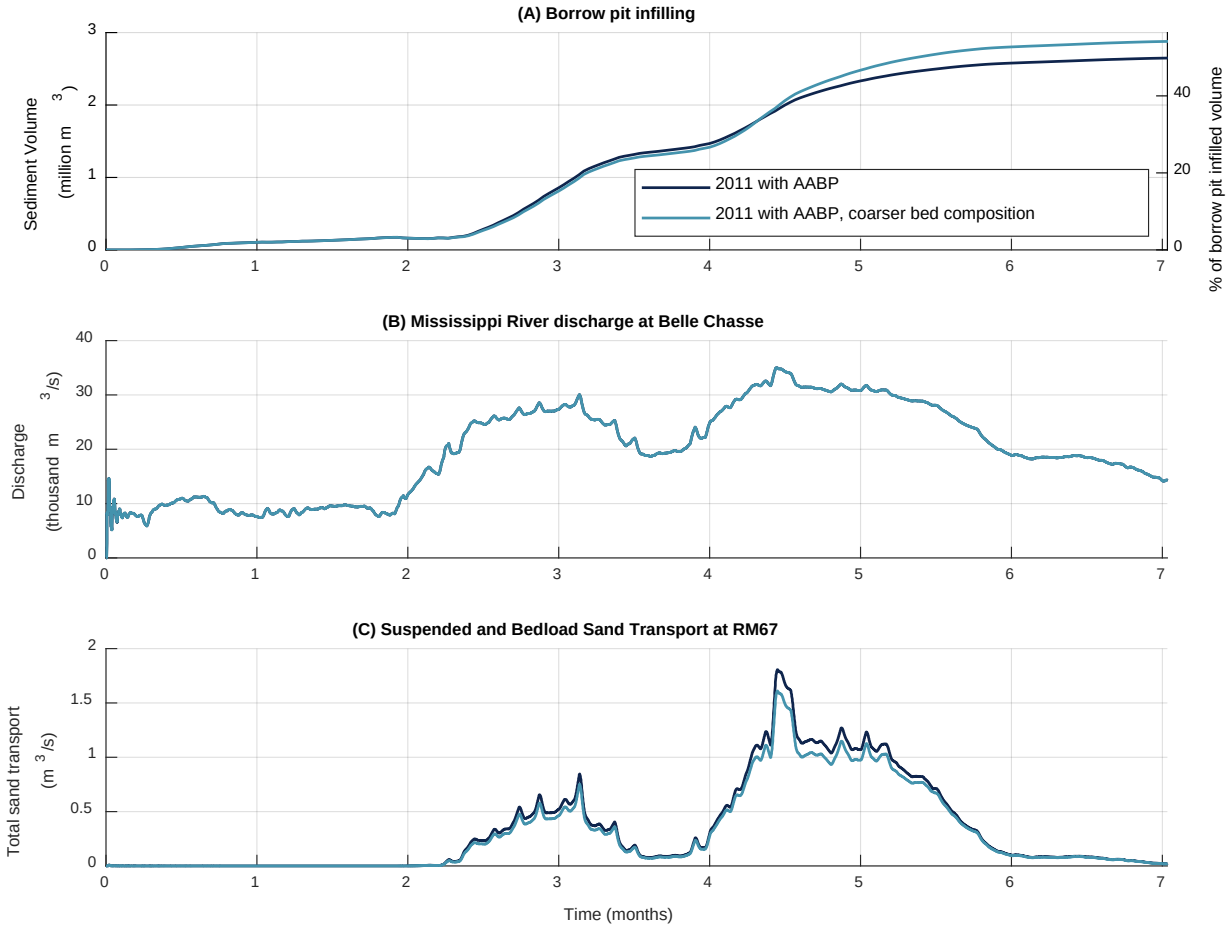

Figure B-12. AABP infilled volume of sediment and infilled percentage volume relative to the original pit volume (A), Mississippi River discharge at Belle Chasse (B), and total sand transport at RM 67 (i.e., just upstream of the pit) (C) modeled for the Alliance Model with the default and a coarser bed composition scenario (Table B-3). The default scenario has 7% very fine sand, 43% fine sand and 50% medium sand in the upper layer. The variation on bed composition has a coarser upper layer consisting of 7% very fine sand 25% fine sand and 68% medium sand. Bed sediments in lower layers become gradually finer for both scenarios.

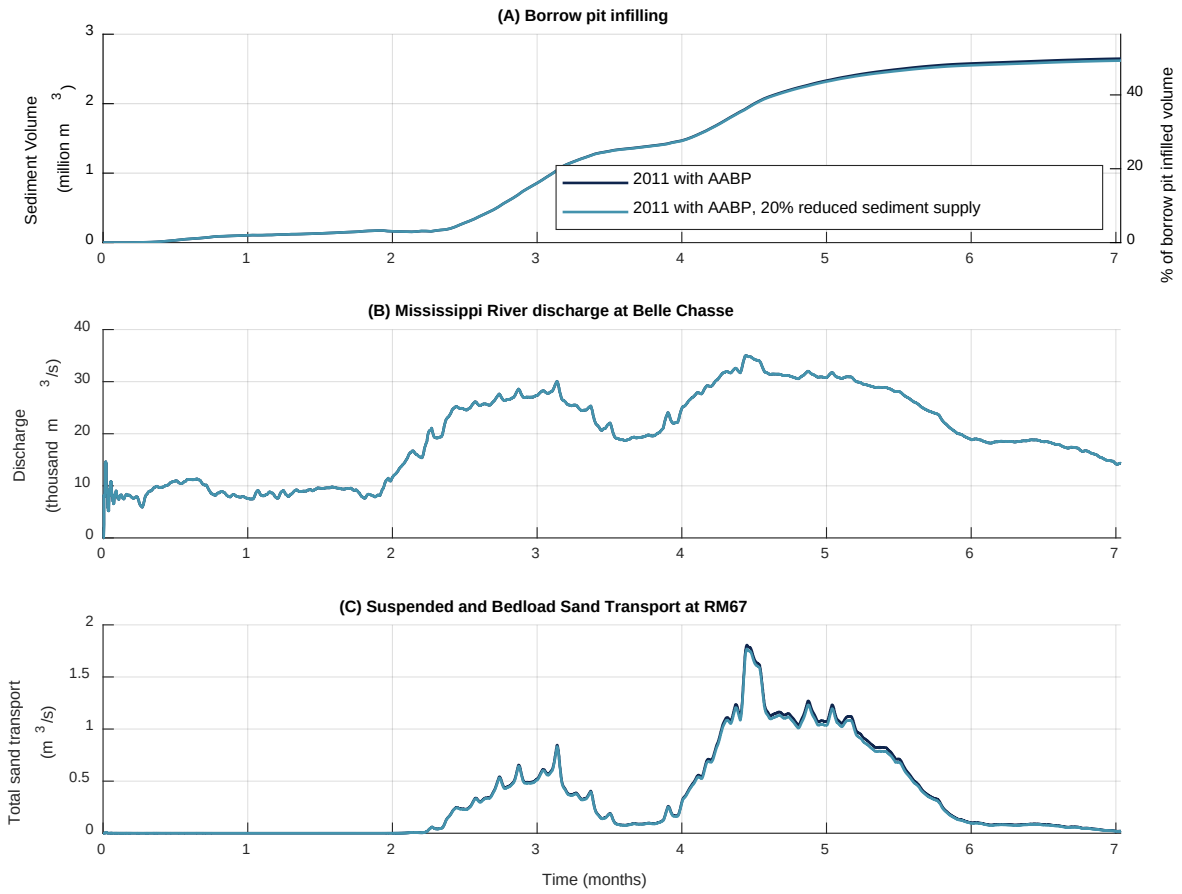

Figure B-13. AABP infilled volume of sediment and infilled percentage volume relative to the original pit volume (A), Mississippi River discharge at Belle Chasse (B), and total sand transport at RM 67 (i.e., just upstream of the pit) (C) modeled for the Alliance Model with default and 20% reduced upstream sediment supply scenarios (Table B-3).

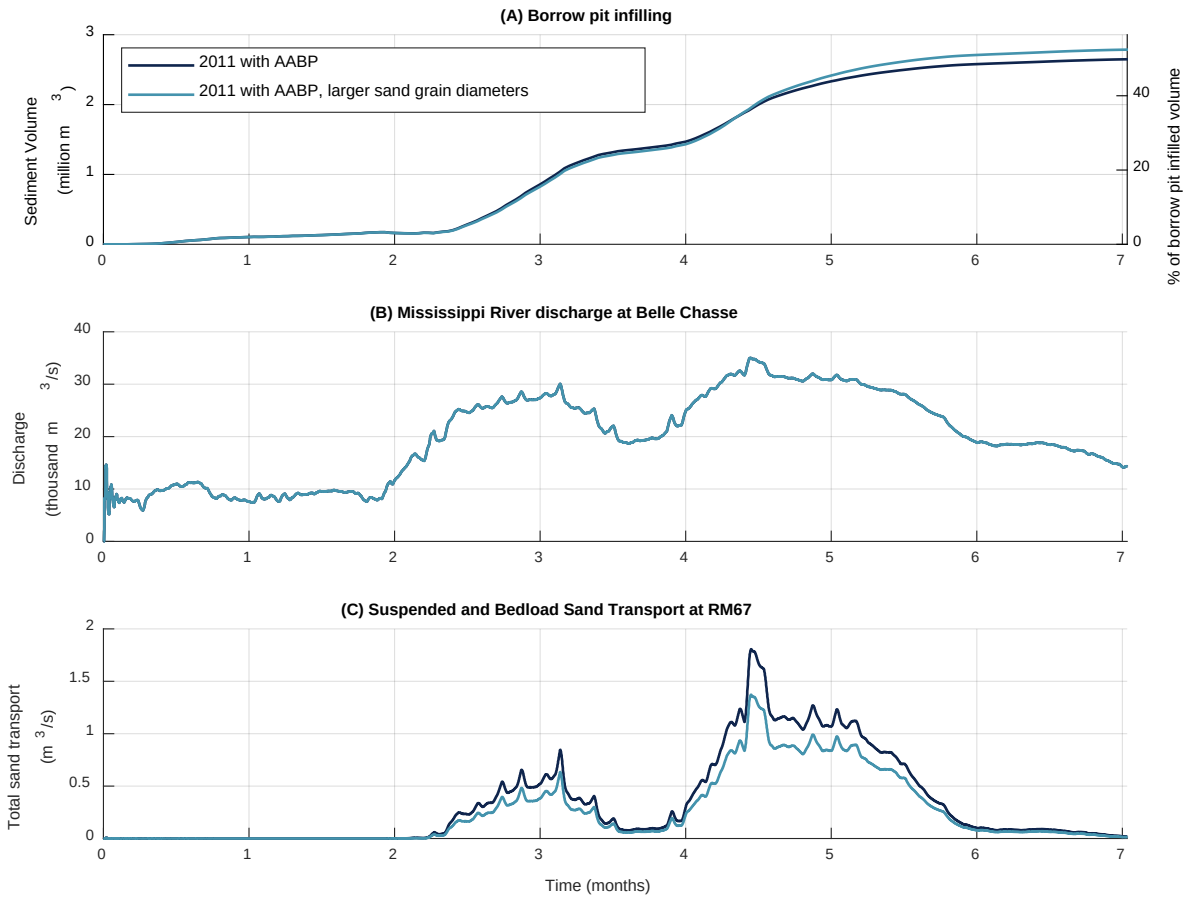

Figure B-14. AABP infilled volume of sediment and infilled percentage volume relative to the original pit volume (A), Mississippi River discharge at Belle Chasse (B), and total sand transport at RM 67 (i.e., just upstream of the pit) (C) modeled for the Alliance Model with the default and larger sediment grain diameters (Table B-3). The default scenarios has very fine, fine, and medium sand represented with fractions of 92, 183, and 367 microns, with an upstream supply split 20%/60%20% between the fractions, respectively. The scenario with adjusted sediment characteristics has very fine, fine, and medium sand represented with fractions of 150, 230, and 340 microns, with an upstream supply split 25%/50%25% between the fractions, respectively.

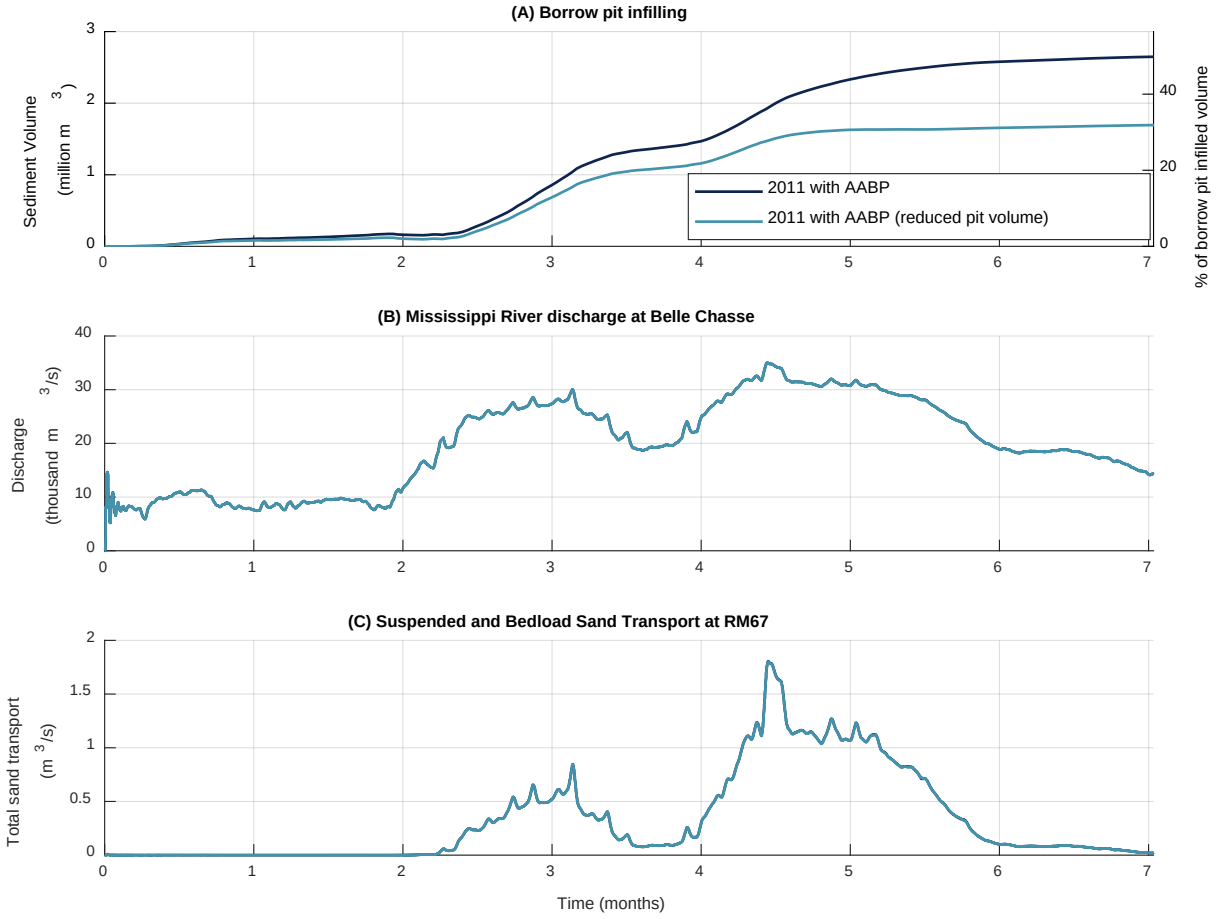

Figure B-15. AABP infilled volume of sediment and infilled percentage volume relative to the original pit volume (A), Mississippi River discharge at Belle Chasse (B), and total sand transport at RM 67 (i.e., just upstream of the pit) (C) modeled for the Alliance Model with the default and 36% reduced borrow pit volumes (Table B-3).

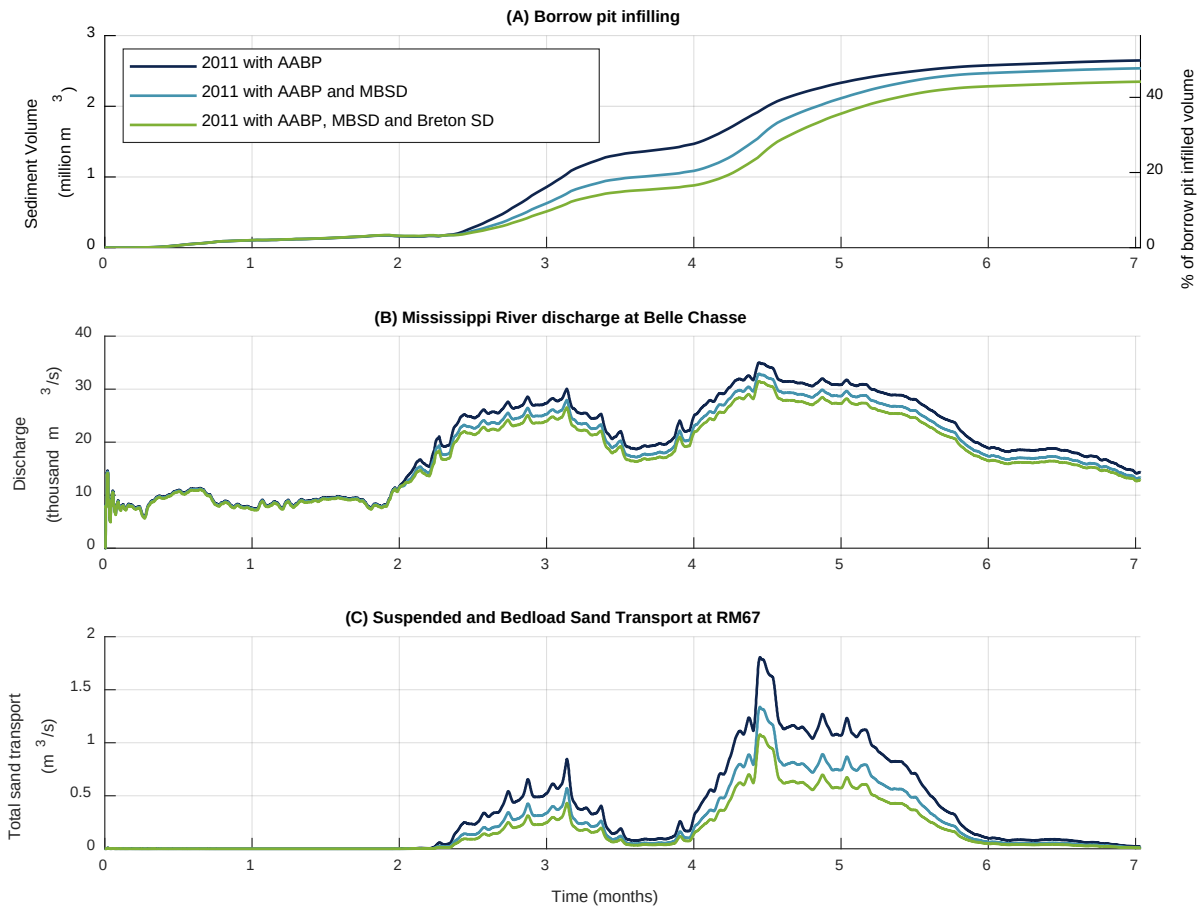

Figure B-16. AABP infilled volume of sediment and infilled percentage volume relative to the original pit volume (A), Mississippi River discharge at Belle Chasse (B), and total sand transport at RM 67 (i.e., just upstream of the pit) (C) modeled for the Alliance Model with and without presence of sediment diversions (Table B-3).

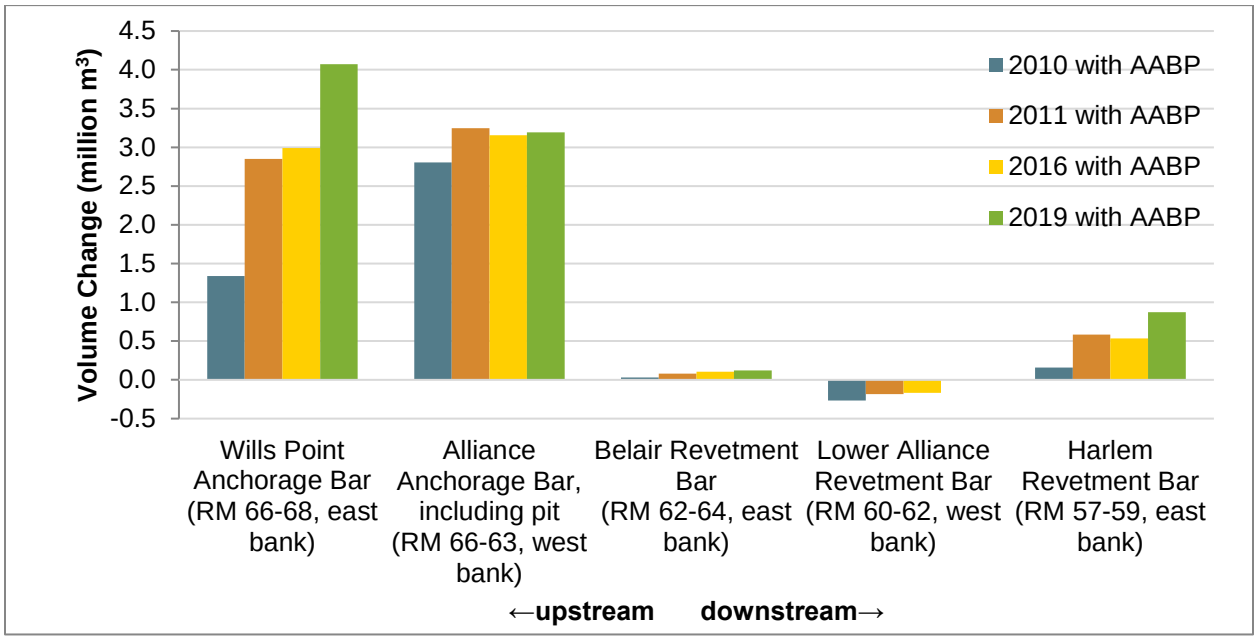

Figure B-17. Volume Changes at sand bars between Wills Point (RM 66) and Myrtle Grove (RM 58) for the first 7 months of different hydrographs with the AABP (RM 65). See Figure 2 for locations of polygons used to define bars for these calculations.

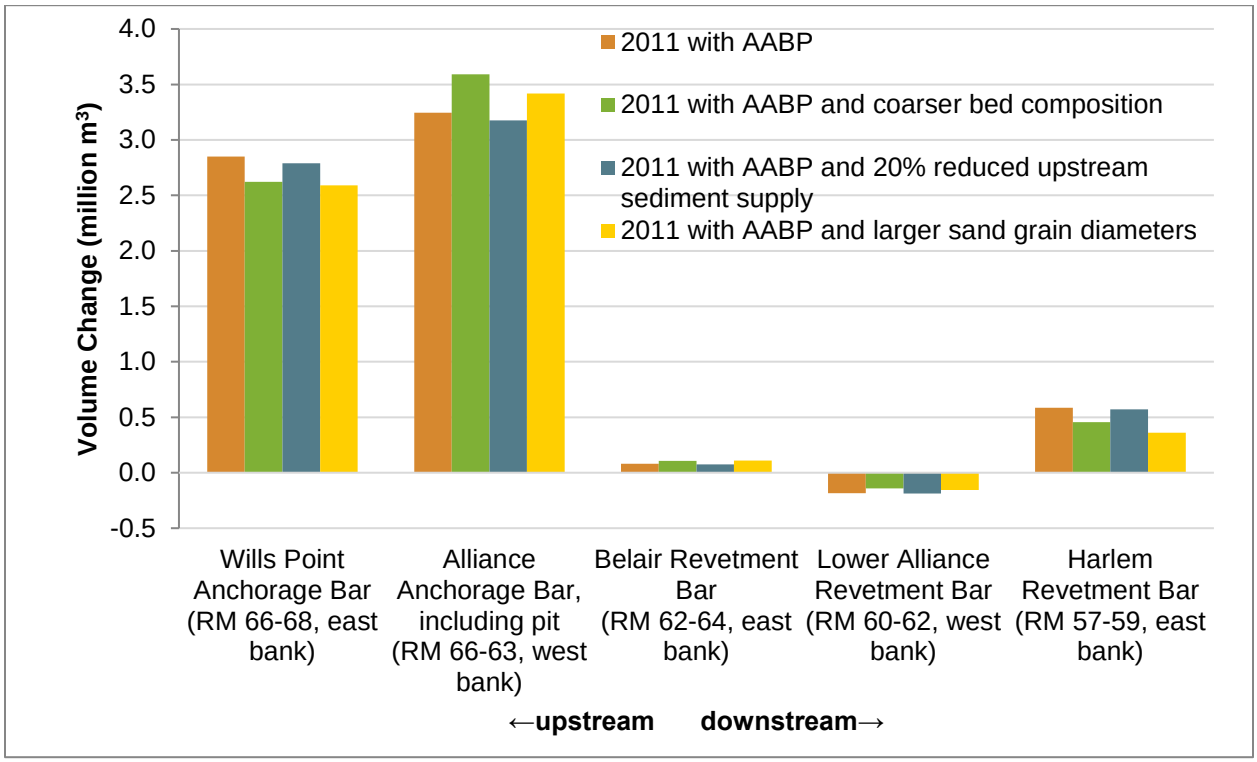

Figure B-18. Volume Changes at sand bars between Wills Point (RM 66) and Myrtle Grove (RM 58) for various sensitivity tests simulated for the first 7 months of hydrograph 2011 with the AABP , RM 65. See Figure 2 for locations of polygons used to define bars for these calculations.

B.8 PREVIOUS FIELD OBSERVATIONS

Figure B-19 shows the inter-survey infilling rates found for the borrow area dredged in 2010 from the Alliance Anchorage Bar as calculated by Yuill et al., (2015). The shown infilling rates are spatial averaged for the entire borrow pit. Bar-wide erosion led to net erosion in the borrow pit in the period between January 2011 and April 2011, while infilling occurred during the remainder of the spring 2011 flood peak (Yuill et al., 2015).

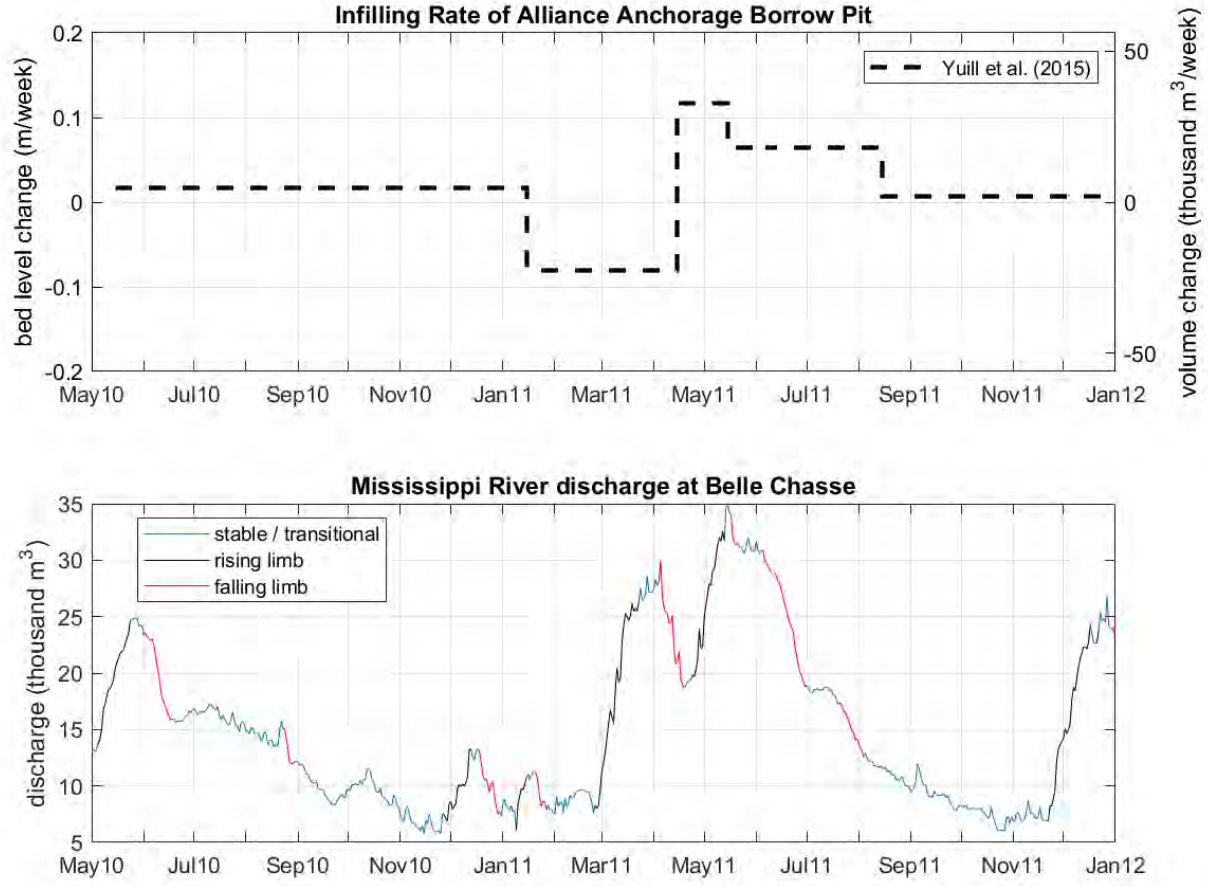

Figure B-19. Measured infilling rates of the Alliance Anchorage Borrow Area (280,000 m^2, 1,46 million m^3) after completion of dredging for the Bayou Dupont marsh creation project in March 2010 (Yuill et al., 2015) (upper panel). Mississippi River Discharge at Belle Chasse indicating periods with rising and falling limbs. Rising and falling limbs were calculated using a two-week window (lower panel).

APPENDIX C. LOWERMOST MISSISSIPPI RIVER MODEL

The LMR Model is a 3D hydro-morphodynamic Delft3D-4 model that represents the Mississippi River downstream of Empire, Louisiana, and includes the main Mississippi River delta distributaries. The model is an improvement of a previous regional model (Reins, 2018). This Appendix provides a detailed description of the model characteristics, improvements, the calibration process, and key results.

C.1 MODEL IMPROVEMENTS

The model domain was significantly modified from the original model (Reins, 2018) by expanding the model grid towards Breton Sound Basin around Neptune Pass and Fort St. Philip and by including all major distributaries. For this reason, most of the model input files (e.g., topography and bathymetry, boundary condition files) were recreated from the most recent available data and the model was re-calibrated.

C.2 MODEL DOMAIN AND GRID

The model domain covers the Mississippi River downstream of Empire, Louisiana (RM 33), and its distributaries. The borrow pit is located between RM 7 and 9. Additionally, the following crevasses, outflows, and distributaries are represented by the model domain (also shown in Figure C-1):

- Neptune Pass near Ostrica, Louisiana
- Multiple crevasses in the Fort St. Philip area
- Baptiste Collette
- Grand Pass and Tiger Pass
- West Bay Sediment Diversion
- Main Pass and Cubit's Gap (including Octave Pass)
- Pass a Loutre (including Dennis Pass and Southeast Pass)
- South Pass
- Southwest Pass

The structured curvilinear grid consists of 190 cells in lateral direction and 990 cells in streamwise direction. The main stem of the Mississippi River is composed of 38 grid cells across the width of the channel, resulting in an average cell width (i.e., size in lateral direction) of 25 m. Between Neptune Pass and Head of Passes, grid cells have a length (i.e., size on streamwise direction) of 50 meters, which gradually increases outside of this reach while maintaining sufficient resolution to adequately resolve the curvature and bathymetric variability of the river channel. Downstream of Head of Passes, the main stem within the model domain bifurcates into Southwest Pass (14 grid cells wide), South Pass (7 grid cells wide), and Pass a Loutre (13 grid cells wide). The vertical grid consists of 10 non-equidistant sigma-layers with thinner layers near the bed and thicker layers near the water surface. The layers thicknesses

are as follows, expressed as percentage of the water column from top to bottom: 25.25, 20.5, 16.25, 12.5, 9.25, 6.5, 4.25, 2.7, 1.8, and 1.0%.

C.3 BATHYMETRY

The model bathymetry is primarily derived from multiple rasters that were collected for NOAA's NOS Hydrographic Survey (Dasler, 2019b). The rasters (survey IDs H13195, H13196, H13212) are based on multibeam echo sounder data collected between October 2018 and April 2019. A combined 5-meter raster was created from the individual rasters. However, the spatial coverage of these rasters is limited to the Mississippi River channel and a section in Southwest Pass is missing. This missing section and areas outside of the Mississippi River were derived from the 2022 USGS CoNED Topobathymetric Model with a 1-meter resolution that was developed for CPRA (OCM Partners, 2022). The data was interpolated onto the model grid through triangular interpolation.

After model calibration, the VABP was implemented to perform the matrix of simulations presented in Appendix C.6. The footprint and depth of the borrow pit were derived according to the dredging design drawings shared by the engineering team (Baird and Associates) and the dredging footprint received by Weeks Marine.

C.4 HYDRODYNAMICS

C.4.1 Boundary Conditions

A discharge boundary condition is applied to the upstream model boundary which is located near Bayou Lamoque (RM 33). The USGS station at Belle Chasse (station number 07374525) is the closest location with continuous discharge records of the Mississippi River (located at RM 76). To approximate the river discharge at the model upstream boundary, a reduction was applied to the discharge volumes to account for losses through Mardi Gras Pass (RM 43) and leakage through smaller cuts and channels along the Bohemia Spillway and other sections of the Mississippi River's east bank where no federal levees are present only natural levees, based on loss rates obtained by (Georgiou & Trosclair, 2013). The total loss of discharge between Belle Chasse and Empire varied between 2.5% for discharges up to 17,000 m^3/s (600,000 cfs) up to 7-8% for discharges above 28,000 m^3/s (1 million cfs).

Separate water level boundary conditions are specified for each of the Mississippi River's major distributaries as listed in Table C-1 and depicted in Figure C-1. The hourly water level timeseries were obtained from the nearest Coastwide Reference Monitoring System (CRMS) station. Not all CRMS stations had continuous data available for the period of interest, in which case the closest neighboring stations was used as a replacement for missing data. In several instances, the nearest CRMS station was located significantly (i.e., 5 km or more) upstream or downstream from the model's boundary condition location, which often led to an overestimation or underestimation of conveyed discharge. In some other cases, such as CMRS0163, the station was located outside of the primary channel of the distributary, leading to an underestimation of the stage and consequently an overestimation of the distributary discharge. Adjustments to the water level timeseries were therefore made during the calibration process to obtain a more accurate discharge distribution across the distributaries. The magnitude of these adjustments was typically 10–20 cm which equates to a water surface slope in the order or $2 \cdot 10^{-5}$ (i.e., 2

cm per kilometer), which is of the same order of magnitude as slopes found in previous studies (Esposito, Georgiou, & Kolker, 2013) (Esposito, Georgiou, & Straub, 2020).

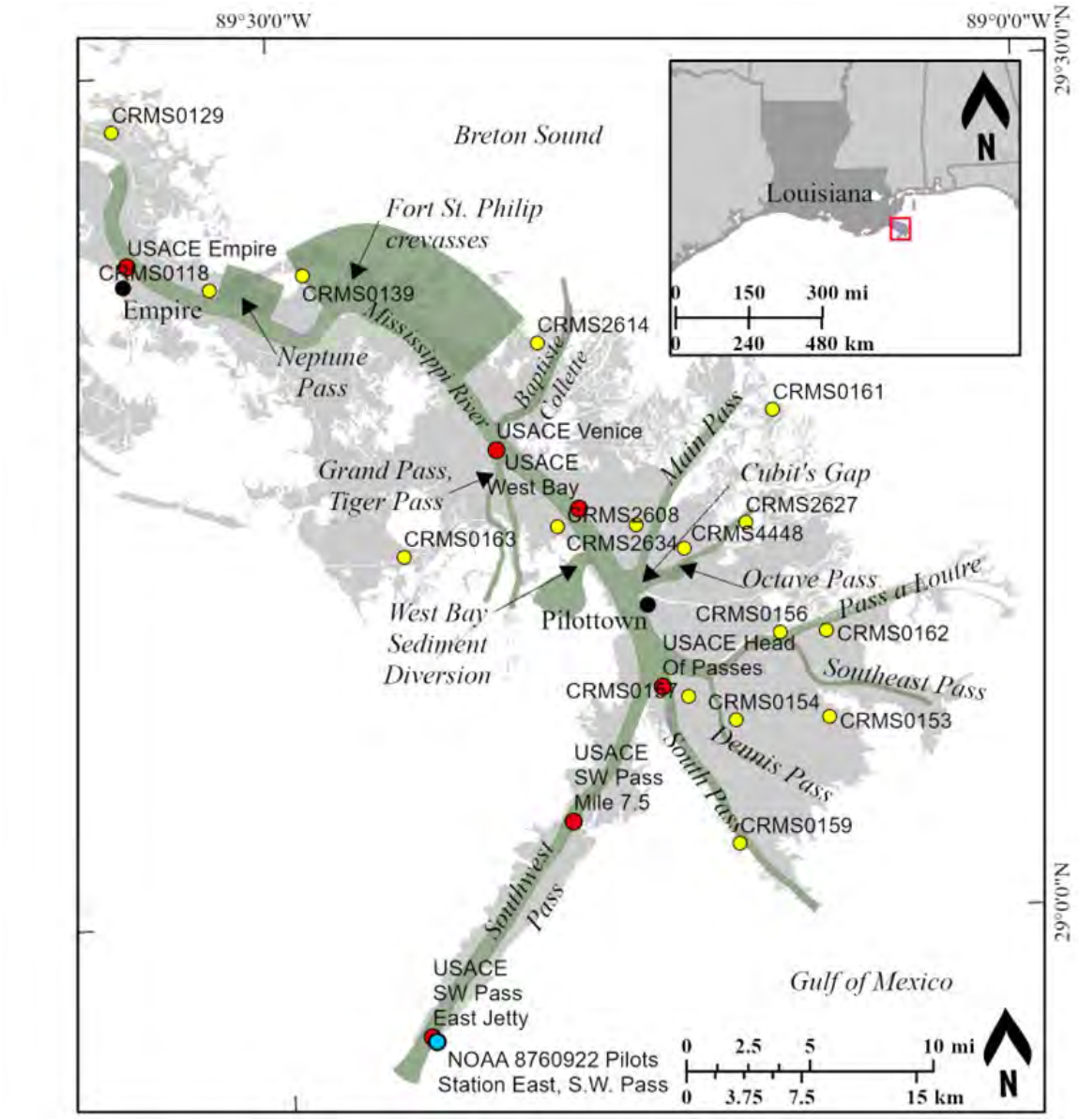

Figure C-1. Model domain of the LMR Model (in green) with the CRMS stations (yellow) and NOAA station (blue) that were used to define downstream model boundary conditions, and USACE stations (red) used for water level calibration.

Table C-1. Boundary condition data used for distributaries in the Lowermost Mississippi River that are resolved within the Delft3D-4 model.

Distributary name	Station used for water level boundary condition	Water level adjustment
Ostrica area (incl. Neptune Pass)	CRMS0118	NA
Fort St. Philip area	CRMS0139	NA
Baptiste Collette	CRMS2614	NA
Grand Pass	CRMS0163	+0.10 m
Tiger Pass	CRMS0163	+0.10 m
West Bay Sediment Diversion	CRMS2608	NA
Main Pass	CRMS4626	NA
Octave Pass	CMRS4448	-0.10 m
Pass a Loutre	CRMS0156	-0.20 m
Southeast Pass	CRMS0156	-0.20 m
Dennis Pass	CRMS0154	-0.08 m
South Pass	CMRS0159	-0.10 m
Southwest Pass	NOAA 8760922 Pilots Station East	NA

C.4.2 Calibration

The hydrodynamics model was calibrated for the years 2015, 2021, and the first half of 2022. Model results were compared to measurements of water levels along the Lowermost Mississippi River, and the distribution of discharge across the main distributaries. A spatially uniform Manning's roughness coefficient of 0.0165 yielded the closest agreement between modeled and measured water levels and discharges. A comparison between modeled and measured water levels is displayed in Figure C-2 for year 2015 and in Figure C-3 for January 2021 through June 2022.

An overview of the discharge calibration results is given by Figure C-4 for year 2015 and Figure C-5 for January 2021 through June 2022. The model calibration results were improved by adjusting downstream water levels as described in Appendix C.4.1 and by manually editing the bathymetry in some grid cells to ensure channel continuity and proper conveyance, which could have been lost when interpolating the original raster onto the model grid. These figures indicate a close agreement between diverted discharges in the model and measurements, for both high and low Mississippi River discharges. Additionally, adjustments were made to the bathymetry in Neptune Pass and to the Fort St. Philip crevasses to represent the changes in conveyance between 2015 and 2021. Discharges were calibrated to match measurement data of each period, as shown in Figure C-6 for Neptune Pass (referred to as Ostrica Reach) and Figure C-7 for Fort St. Philip for both the 2015 and 2021-2022 simulations

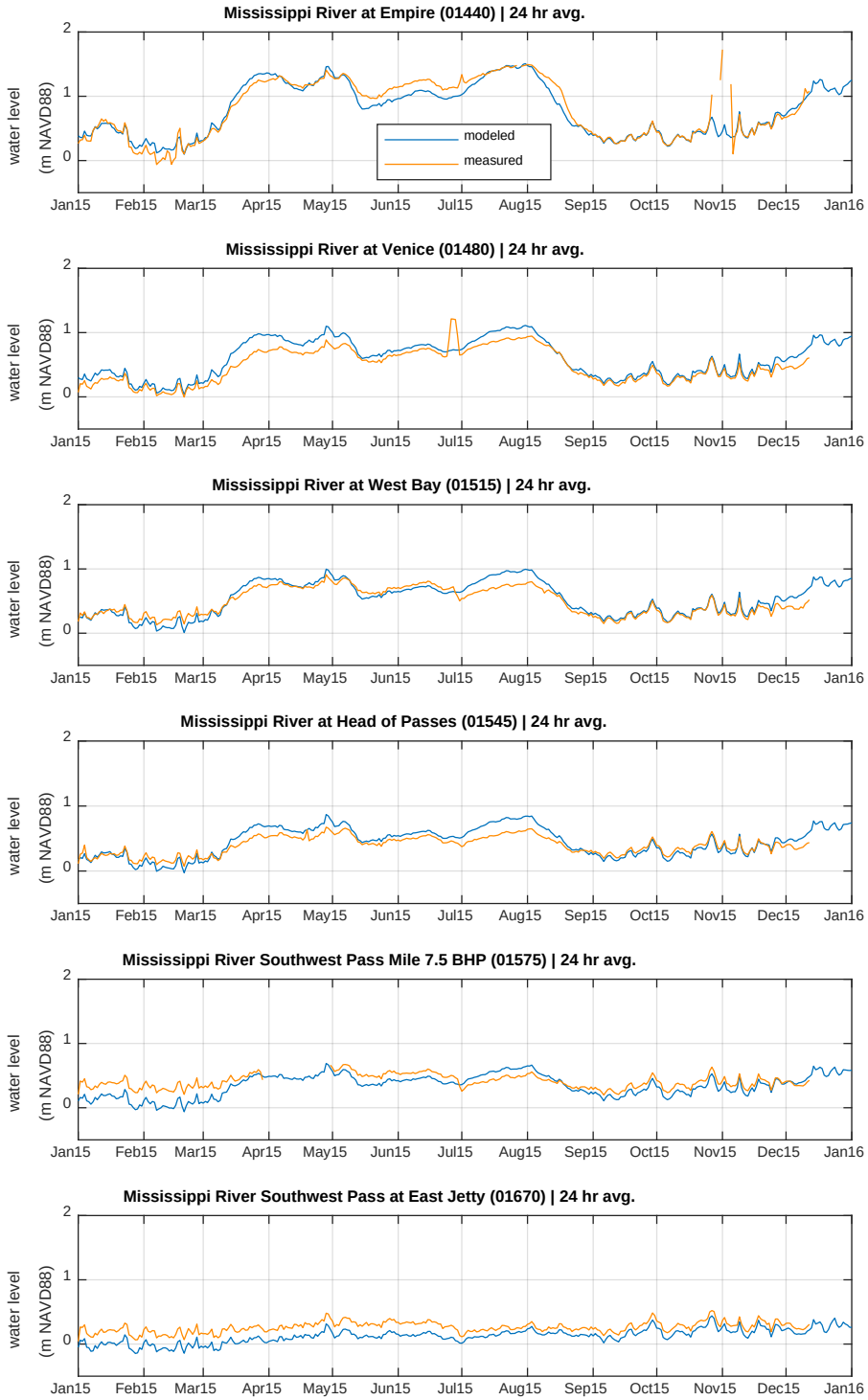

Figure C-2. Comparison of daily averaged water levels between model and observations at the USACE stations shown in Figure C-1 for year 2015.

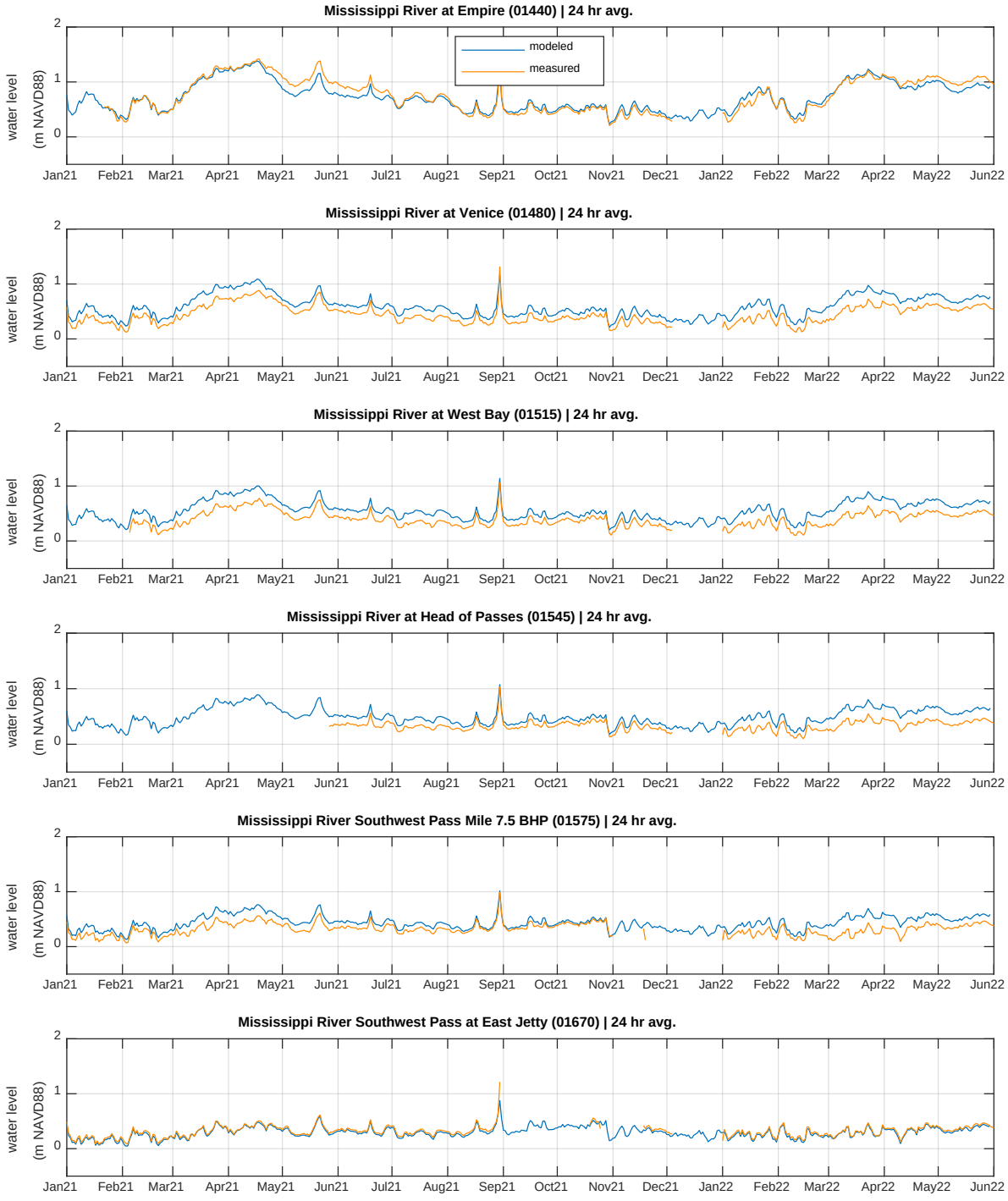

Figure C-3. Comparison of daily averaged water levels between model and observations at the USACE stations shown in Figure C-1 for between January 2021 and June 2022.

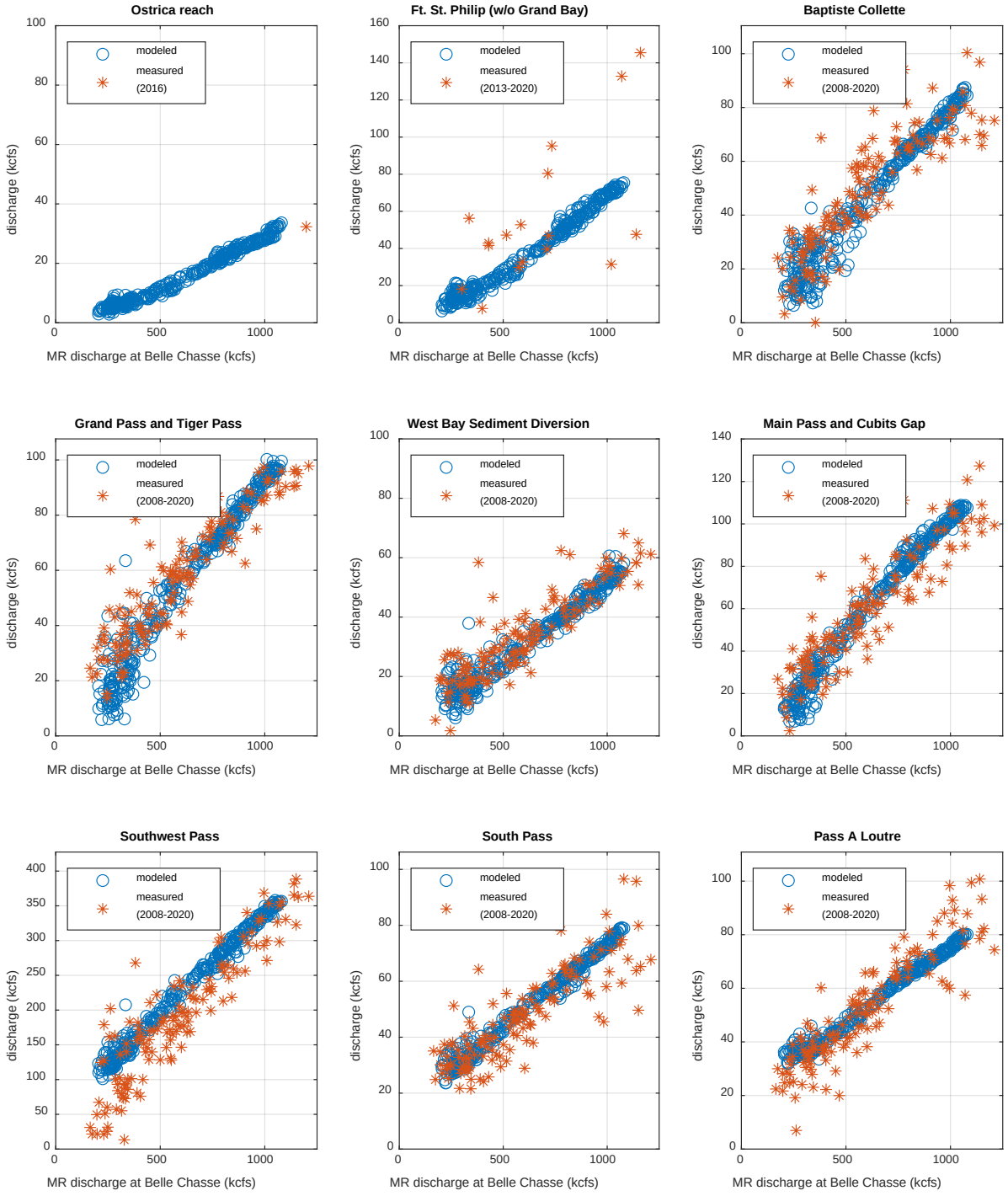

Figure C-4. Comparison of modeled and measured discharges diverted through distributaries in the Lowermost Mississippi River, displayed as function of the Mississippi River discharge at Belle Chasse. Modeled data is from the simulation that represents year 2015. Locations of the distributaries are indicated in Figure C-1. Data for the Fort St. Philip area is based on Olga Revetment discharge data provided by Dave Ramirez (USACE). Measured data in the Ostrica reach is derived from a survey between 18-29 January 2016 (Weathers, Allison, Ramatchandirane, & Yuill, 2016). Other discharges are obtained from synoptic ADCP surveys collected by the USACE New Orleans District.

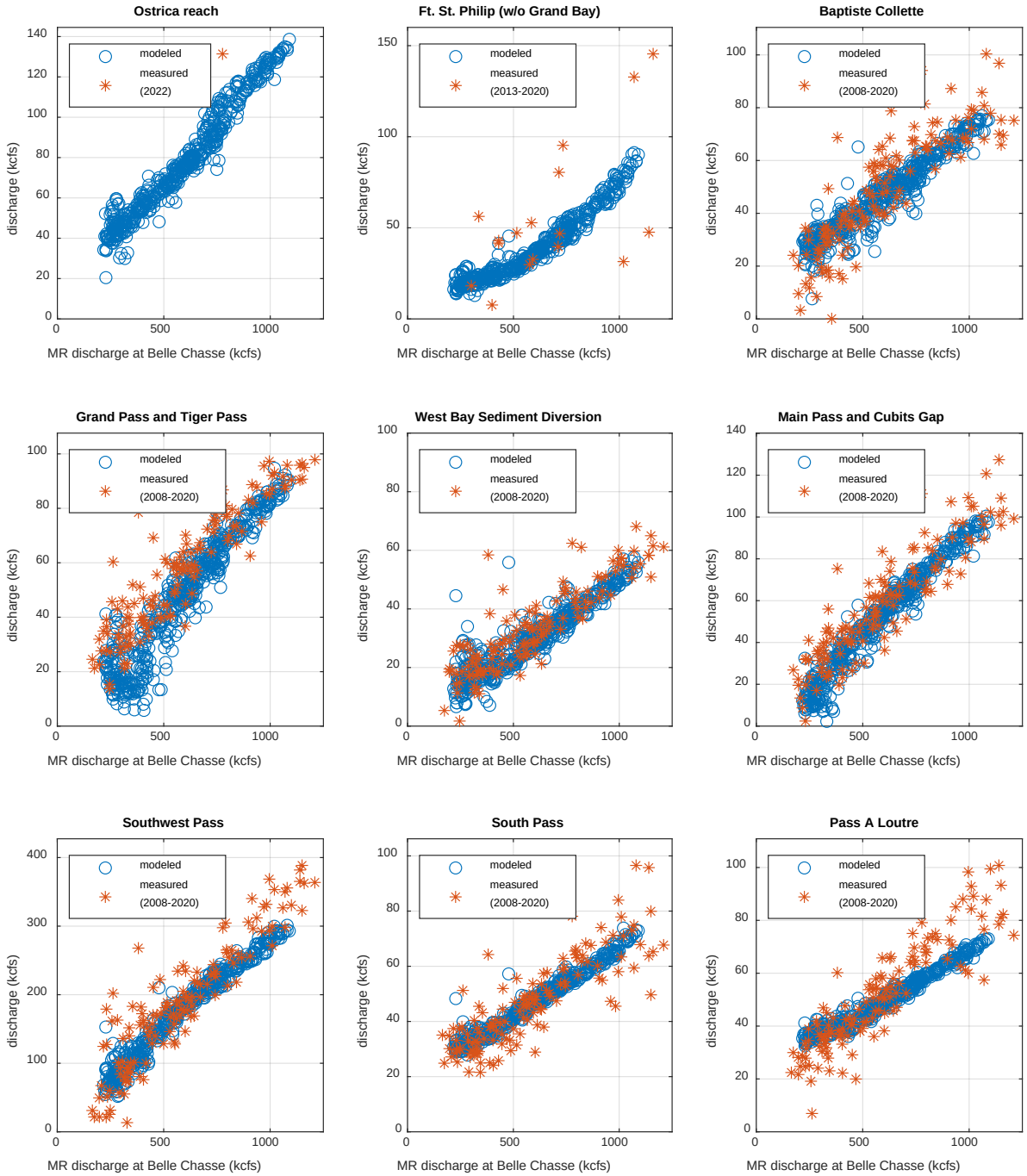

Figure C-5. Comparison of modeled and measured discharges diverted through distributaries in the Lowermost Mississippi River, displayed as function of the Mississippi River discharge at Belle Chasse. Modeled data is from the simulation that represents the period between January 2021 and June 2022. Locations of the distributaries are indicated in in Figure C-1. Data for the Fort St. Philip area is based on Olga Revetment discharge data provided by Dave Ramirez (USACE). Measured data in the Ostrica reach is derived from a survey on May 24, 2022 (Alexander S. Kolker & Weathers, 2022). Other discharges are obtained from synoptic ADCP surveys collected by the USACE New Orleans District.

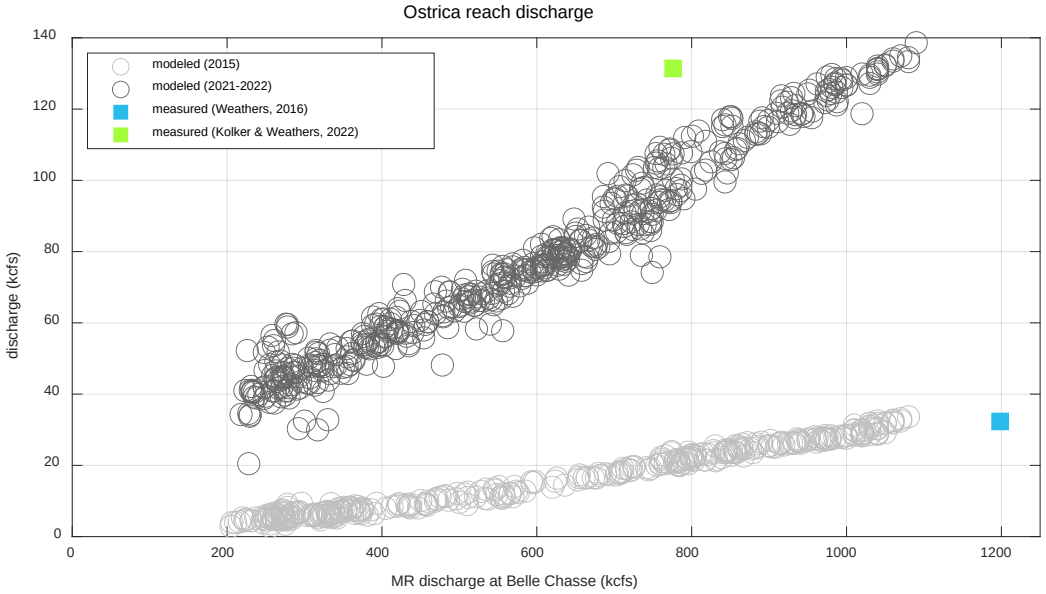

Figure C-6. Comparison of modeled and measured discharges diverted through Neptune Pass and other crevasses in the Ostrica area, displayed as function of the Mississippi River discharge at Belle Chasse. Modeled data is from the simulations that represent the year 2015 and the period between January 2021 and June 2022. Measured data is derived from a survey between 18-29 January 2016 (Weathers et al., 2016) and another survey on May 24, 2022 (Alexander S. Kolker & Weathers, 2022).

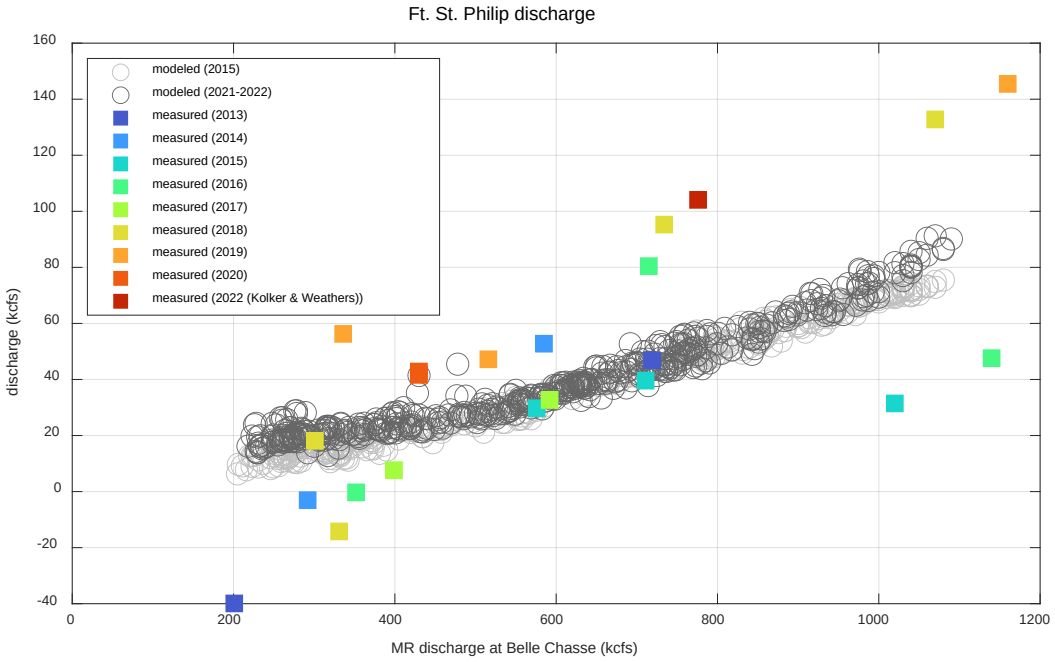

Figure C-7. Comparison of modeled and measured discharges diverted through the crevasses in the area near Fort St. Philip, displayed as function of the Mississippi River discharge at Belle Chasse. Modeled data is from the simulations that represent the year 2015 and the period between January 2021 and June 2022. Measured data is based on Olga Revetment discharge data provided by Dave Ramirez (USACE) and a survey on May 24, 2022 (Alexander S. Kolker & Weathers, 2022).

C.5 SEDIMENT TRANSPORT AND MORPHOLOGY

C.5.1 Boundary Conditions

The Van Rijn 2004 sediment transport formulae were used in the model to predict a base value for the sand fraction of sediment flux, including suspended sediment and bedload transport. Four sediment fractions were included in the model: silt (50 micron) and three classes of sand, consisting of very fine sand (92 micron), fine sand (183 micron), and medium sand (367 micron). These sediment classes were the same as in (Reins, 2018), which follows methodology that was developed and employed previously by McCorquodale et al. (2017). These sediment classes were further confirmed by using bore logs, grab samples and other available geotechnical information conducted by GeoEngineers Inc. in the Venice Anchorage area.

The upstream boundary of the river is located at RM 33, just upstream of Empire (Figure C-1), where no sediment concentration data is available. In order to approximate the sediment concentrations at RM 33, results from a regional 3D model of the Lower Mississippi River developed at the University of New Orleans (Reins, 2018), which covers the Mississippi River between Belle Chasse and Head of Passes, were used. The relationship between sand concentrations at the upstream boundary condition of the LMR Model (RM 33) and the discharge at Belle Chasse was determined for all three sand classes (Figure C-8 to Figure C-10). These relationships were applied to Belle Chasse discharge measurements taken at the USGS station 07374525 and used to calculate the model upstream boundary conditions. The relationship between silt concentrations at the upstream boundary condition of the LMR Model (RM 33) and at Belle Chasse was determined for silt (Figure C-11). This relationships was applied to silt load at Belle Chasse calculated with the hysteresis rating curve presented in Appendix B.5.1(Liang et al., 2016).

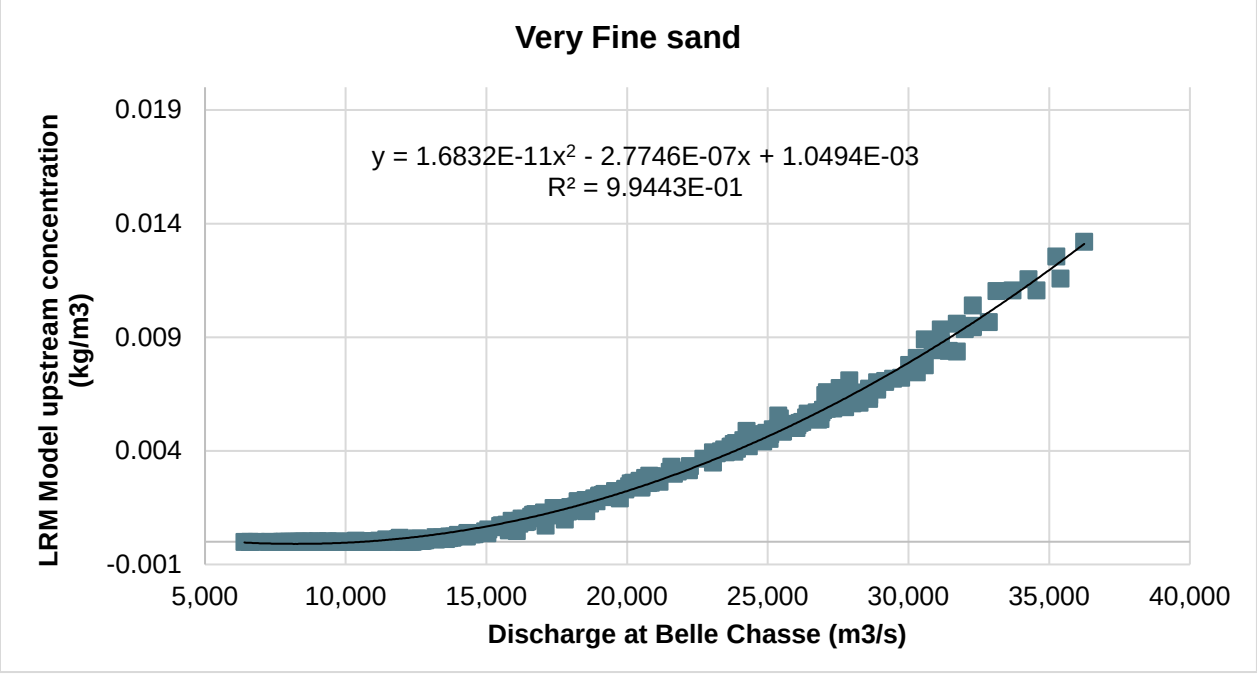

Figure C-8. Comparison between very fine sand concentrations at RM 33 (upstream location of the LMR Model) and discharge at Belle Chasse.

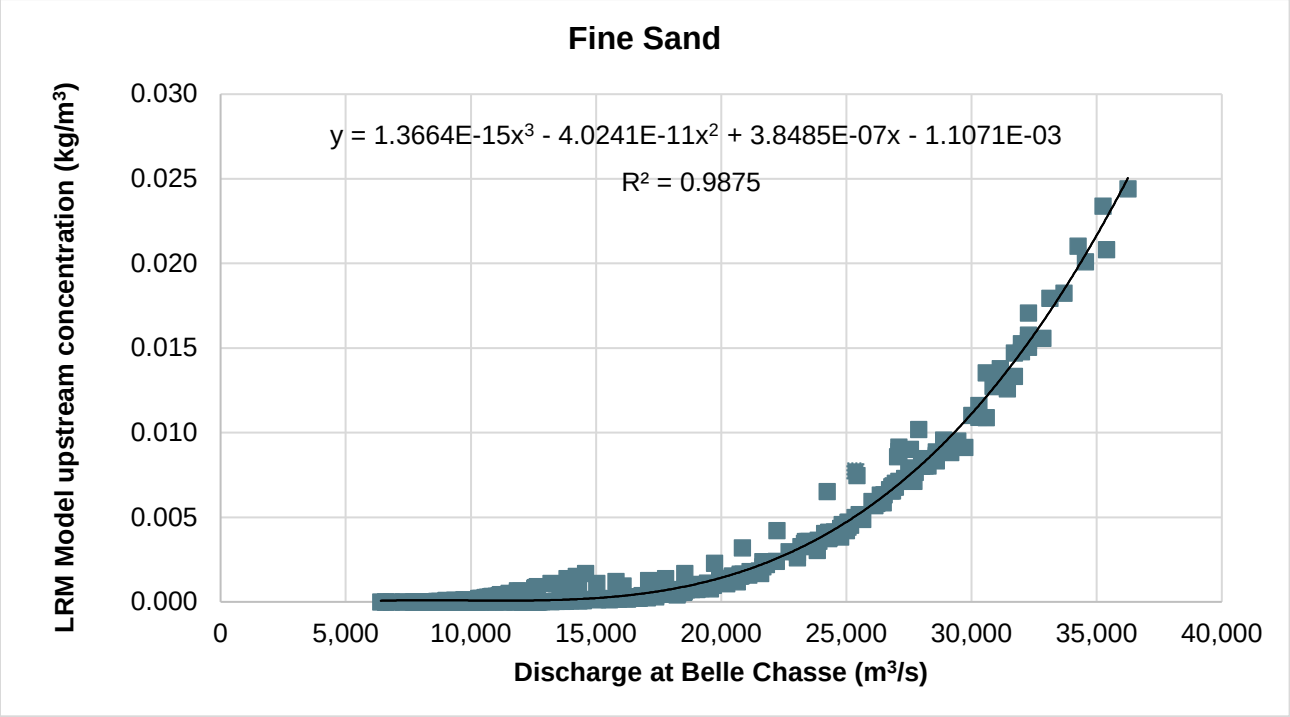

Figure C-9. Comparison between fine sand concentrations at RM 33 (upstream location of the LMR Model) and discharge at Belle Chasse.

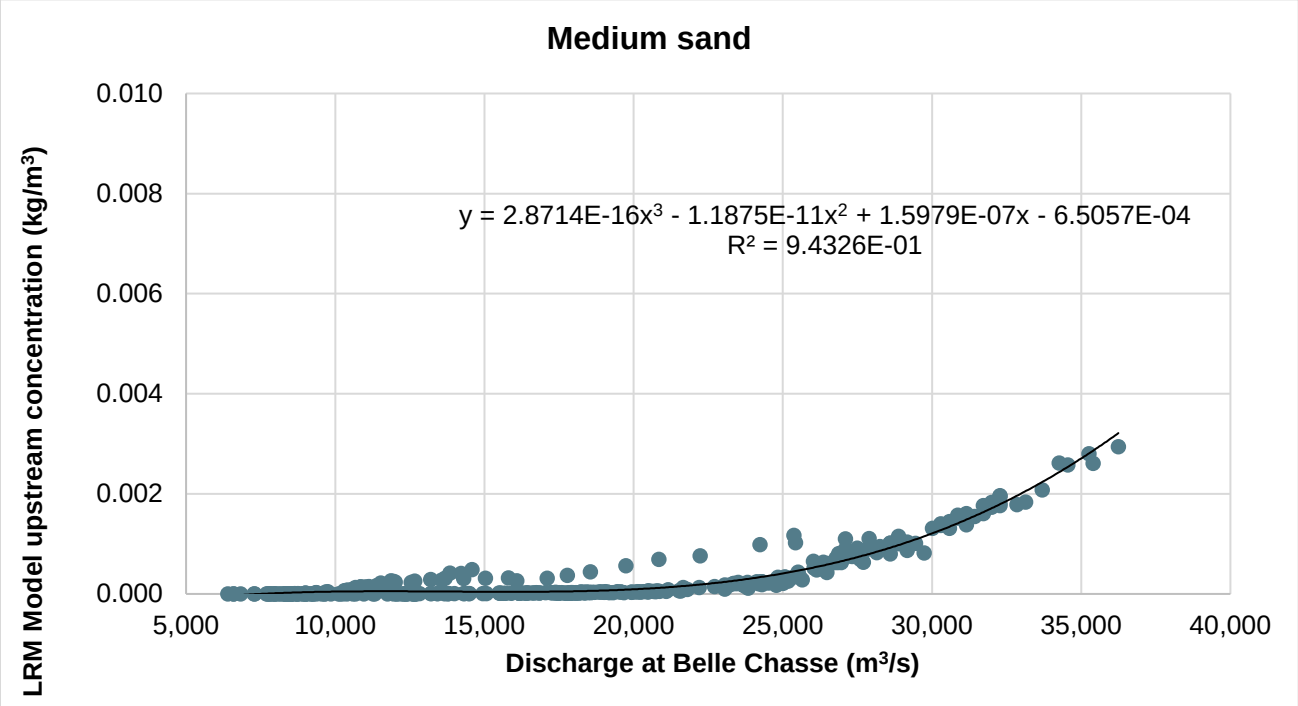

Figure C-10. Comparison between medium sand concentrations at RM 33 (upstream location of the LMR Model) and discharge at Belle Chasse.

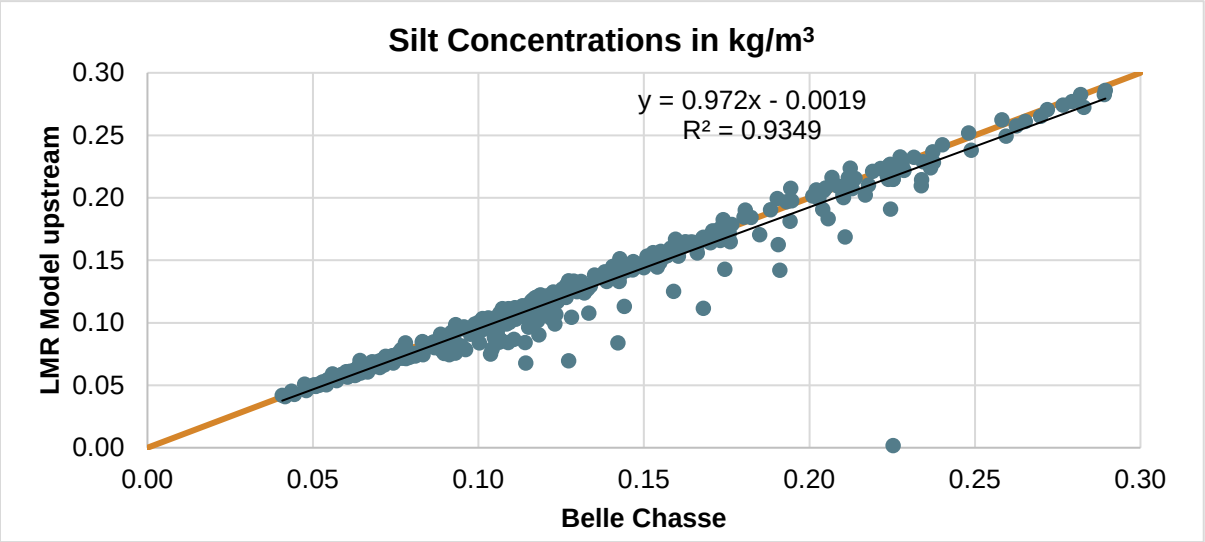

Figure C-11. Comparison between silt concentrations at RM 33 (upstream location of the LMR Model) and at Belle Chasse. The line of equality is displayed in orange.

C.5.2 Bed Stratigraphy

The morphology model employs the mobile bed capability of Delft3D-4 with a single mixed initial sediment layer that consists of 10% very fine sand, 80% fine sand, and 10% medium sand, which is based on sediment borings collected by GeoEngineers Inc. in the Venice Anchorage area in September 2019. Sensitivity simulations were performed with a finer bed composition of 20% very fine sand, 75% fine sand, and 5% medium sand (see Appendix C.6 Model Simulation Matrix). The thickness of the sediment layer is spatially varying and increases proportionally with bed elevation, ranging from a thickness of 0 m at bed elevations of -25 m NAVD88 to a thickness of 5 m at bed elevations of -20 m NAVD88 or higher. No erodible sediment is available in the initial sediment layer in areas with bed elevations below -25 m NAVD88. These areas represent the substrate that is exposed in deeper sections of the river, including the thalweg along the Tropical Bend and Buras revetments near Empire, and the Fort Jackson and Olga revetments near Fort St. Philip (Figure C-1). This designation is based on the river bathymetry and the sediment borings conducted by GeoEngineers Inc. in the Venice Anchorage area.

C.5.3 Calibration

The morphology model was calibrated in a similar fashion as described for the Alliance Model (Section B.5.3) and the same calibration factors were applied as shown in Table B-2. The model was calibrated by adjusting multiplication factors for suspended sediment reference concentrations to obtain agreement between measured and modeled sediment transport (sand, silt, and total) at six locations within several kilometers from the borrow pit. No sediment transport data were available for the years that were used for model calibration (i.e., 2015 and 2020), but some data were available for 2009, 2010, and 2011 at different river miles along the river. These datasets were collected by USACE (Sharp et al., 2013). To leverage these datasets, the model relationship between sediment transport fluxes and discharge was compared with the same relationships for the observations (Figure C-12 and Figure C-13).

The sensitivity of the model was tested for variations in parameters such as grain sizes, composition and thickness of the bed sediment layer, diffusivity, and viscosity. Some variations such as the adjustments in bed sediment grading or upstream sediment load were also assessed in the final simulation matrix described in Appendix C.6, due to lacking or inconclusive field data of sediment transport and morphology.

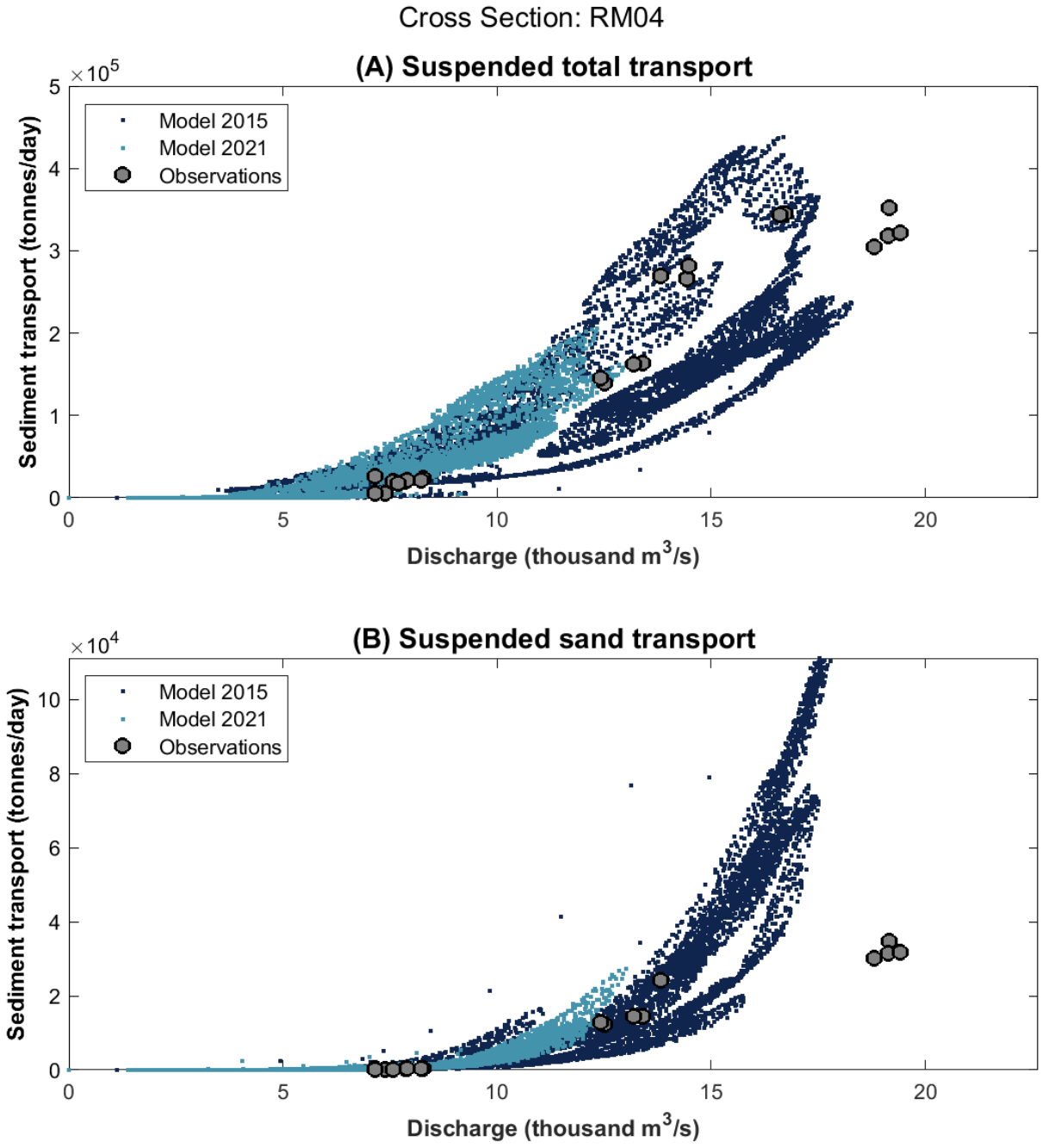

Figure C-12. Top panel: total sediment transport as a function of discharge at RM4, bottom panel: sand transport as a function of discharge at RM 4. Model results are in blue (for 2015 simulations) and light blue (for 2021 simulations), black circles are observations.

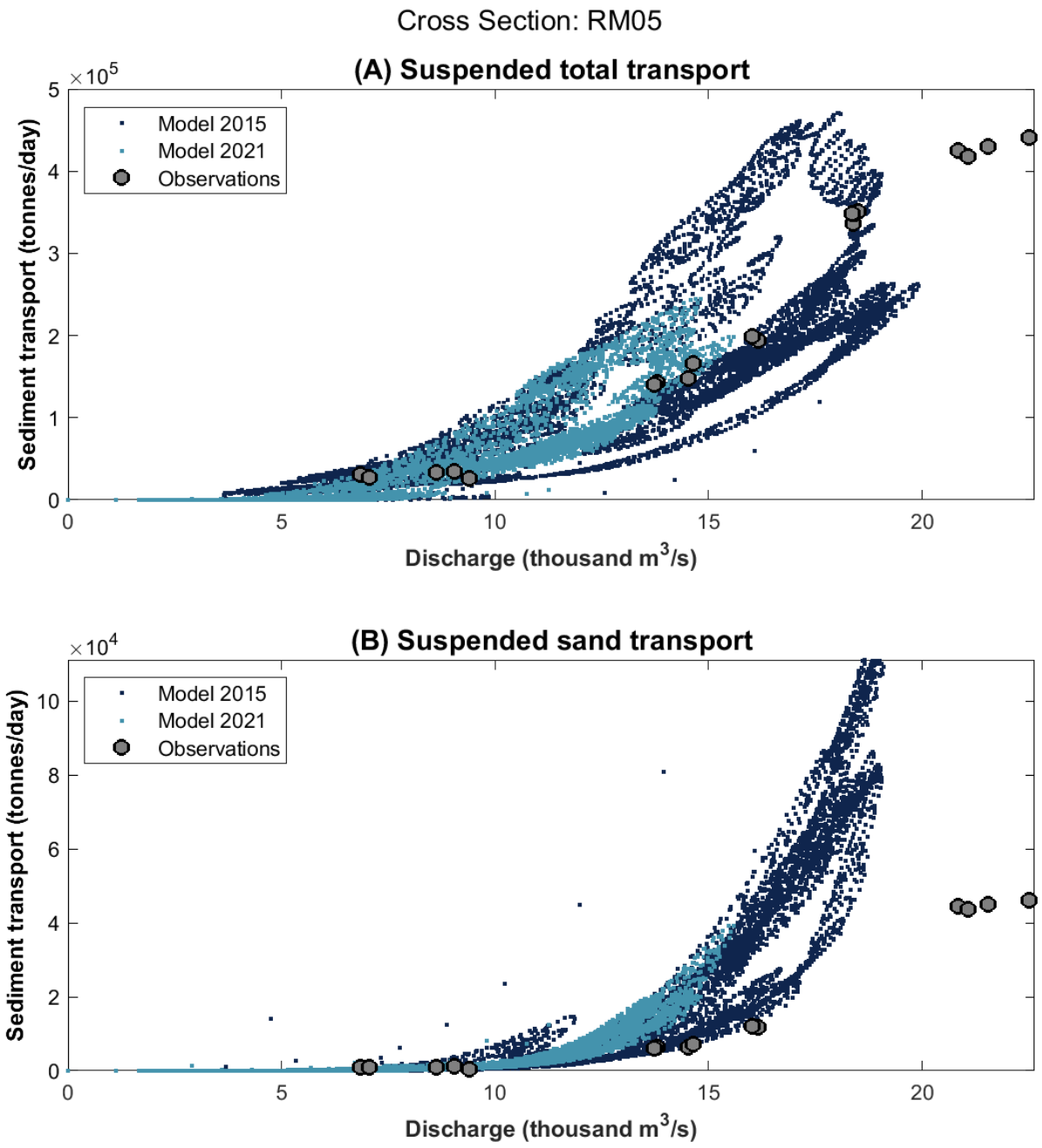

Figure C-13. Top panel: total sediment transport as a function of discharge at RM5, bottom panel: sand transport as a function of discharge at RM 5. Model results are in blue (for 2015 simulations) and light blue (for 2021 simulations), black circles are observations.

C.6 MODEL SIMULATION MATRIX

The results presented in the main report are the outcome of a wide matrix of simulations that were performed with the LMR Model. The baseline simulation included the sediment transport setting and boundary conditions presented in this appendix, 2021 hydrograph and the presence of a 4,500,000 m^3

borrow pit. Other simulations were performed considering: absence of borrow pit, borrow pit with smaller volume, different hydrographs, presence of sediment diversion, changes in upstream sediment concentration, changes in bed composition. Table C-2 presents the matrix of all simulations that were performed and highlight the parameter or model input that was investigated.

Table C-2. Matrix of all simulations performed with the LMR Model. VF=very fine, F=fine and M=medium sand. The box highlighted in light blue for each simulation represent the model input that was varied from the baseline simulation.

Simulation name	Hydrograph	Upstream sediment supply	Bed sediment grading	Presence of sediment diversion	Variation
2015 without VABP	2015		Bed composition: 10/80/10	None	Pit
2021 without VABP	2021		Bed composition: 10/80/10	None	Pit
2015 with VABP	2015		Bed composition: 10/80/10	None	BASELINE
2021 with VABP	2021		Bed composition: 10/80/10	None	BASELINE
2021 with VABP and 20% reduced sediment supply	2021	20% sand supply reduction	Bed composition: 10/80/10	None	Sediment concentration
2021 with VABP and 20% increased sediment supply	2021	20% sand supply increase	Bed composition: 10/80/10	None	Sediment concentration
2021 with VABP, finer bed composition	2021		Bed composition changed to 25/70/5 (VF/F/M)	None	Bed composition
2021 with VABP and MBSD	2021		Bed composition: 10/80/10	MBSD	Anthropogenic factors
2021 with VABP and MBSD and Breton SD	2021		Bed composition: 10/80/10	MBSD + Breton AS	Anthropogenic factors
2015 with VABP and MBSD	2015		Bed composition: 10/80/10	MBSD	Anthropogenic factors
2015 with VABP and MBSD and Breton SD	2015		Bed composition: 10/80/10	MBSD + Breton AS	Anthropogenic factors
2015 with VABP Reduced pit volume	2015		Bed composition: 10/80/10	None	Pit volume

C.7 MODEL RESULTS

Figure C-14 to Figure C-17 present the trend of infilled volume over time for all cases tested with the LMR Model. Figure C-18 to Figure C-20 show the volume changes at sand bars between Wills Point (RM 66) and Myrtle Grove (RM 58) for cases tested with the LMR Model.

Sensitivity tests evaluating the influence of bed composition on sediment entrainment and resulting changes in infilling rates showed that when the bed composition coarsens, total sand transport remains unchanged (Figure C-14C) regardless of flow (Figure C-14B) however, cumulative infilling shows a small increase in the volume within the pit of the order of 2–3% (Figure C-14A).

Change (increase and reduction) in upstream sediment supply, tested by modifying the upstream sediment concentration by ±20% showed no changes in infilling rates (Figure C-15A, although small deviations in the total sand transport were observed (Figure C-15C). Testing the influence of the borrow pit depth on infilling showed that while total sand transport is similar between compared to a simulation with a deeper pit, as expected (Figure C-16C), borrow pit infilling volumes were lower, proportional to the borrow pit depth (Figure C-16A), whereby simulations with a shallower borrow pit infilled at a slower rate and to half the volume by the of the year compared to their deeper borrow pit counterpart (Figure C-16A).

Finally, upstream extractions of water and sediment due to the implementation of sediment diversions, showed noticeable change in the total sand transport results (Figure C-17C) mostly proportional to the river hydrograph (Figure C-17B), with smaller deviations due to the presence of upstream sediment diversions (Figure C-17A). Proportionally, the decline is residual flow resulting from the removal of water due to the diversions diminishes stream power, and thus total sand transport (Figure C-17C). As a result, cumulative infilling rates vary proportional to the flow extraction magnitude, and deviation from the reference case can vary from 500,000 m^3 of sediment when MBSD is operating and up to 750,000 m^3, when both diversions are in operation, and by the end of the simulation period total percent infilling can be 5–12% lower (Figure C-17A).

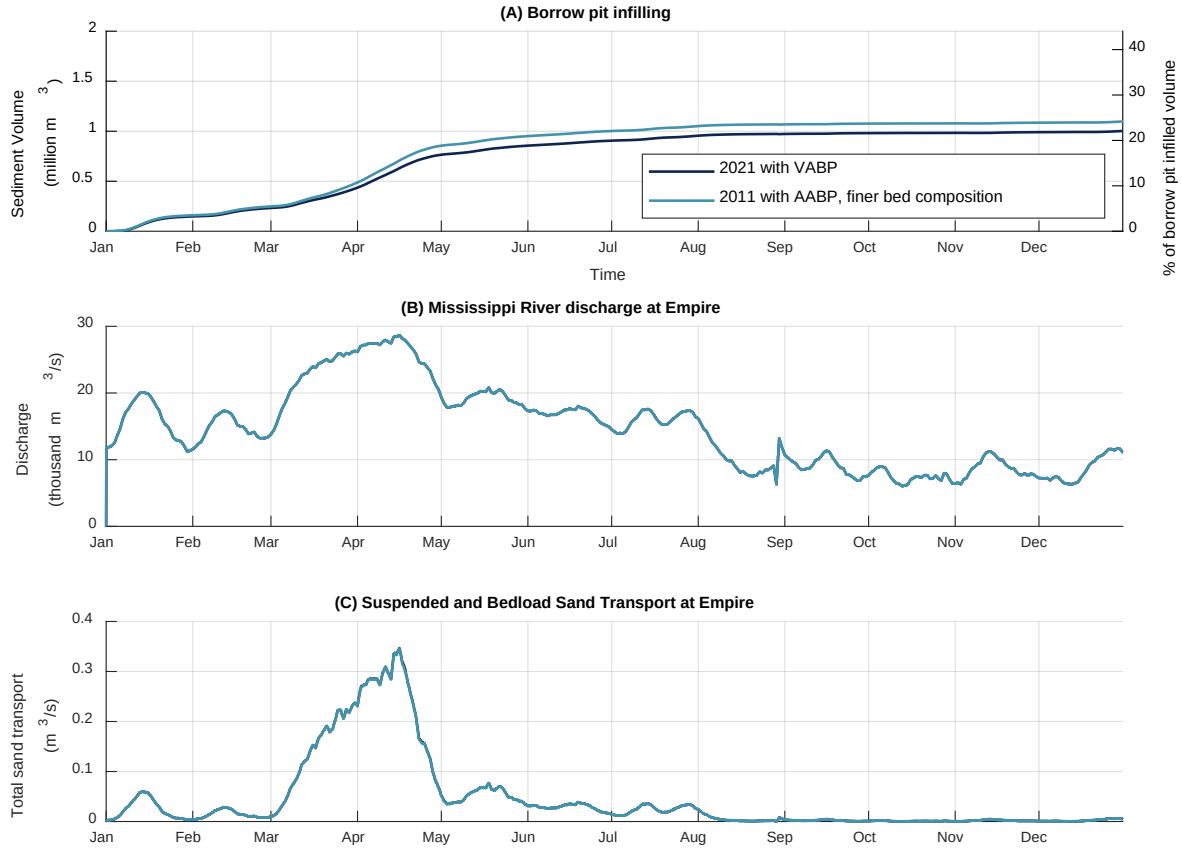

Figure C-14. VABP infilled volume of sediment and infilled percentage volume relative to the original pit volume (A), Mississippi River discharge at Empire (B), and total sand transport at Empire (C) modeled for the LMR Model with the default and a finer bed composition scenario (Table C-2). The default scenario has a bed composition consisting of 10% very fine sand, 80% fine sand and 10% medium sand. The variation has a finer bed composition with 25% very fine sand, 70% fine sand and 5% medium sand. Bed composition does not vary with depth in both scenarios.

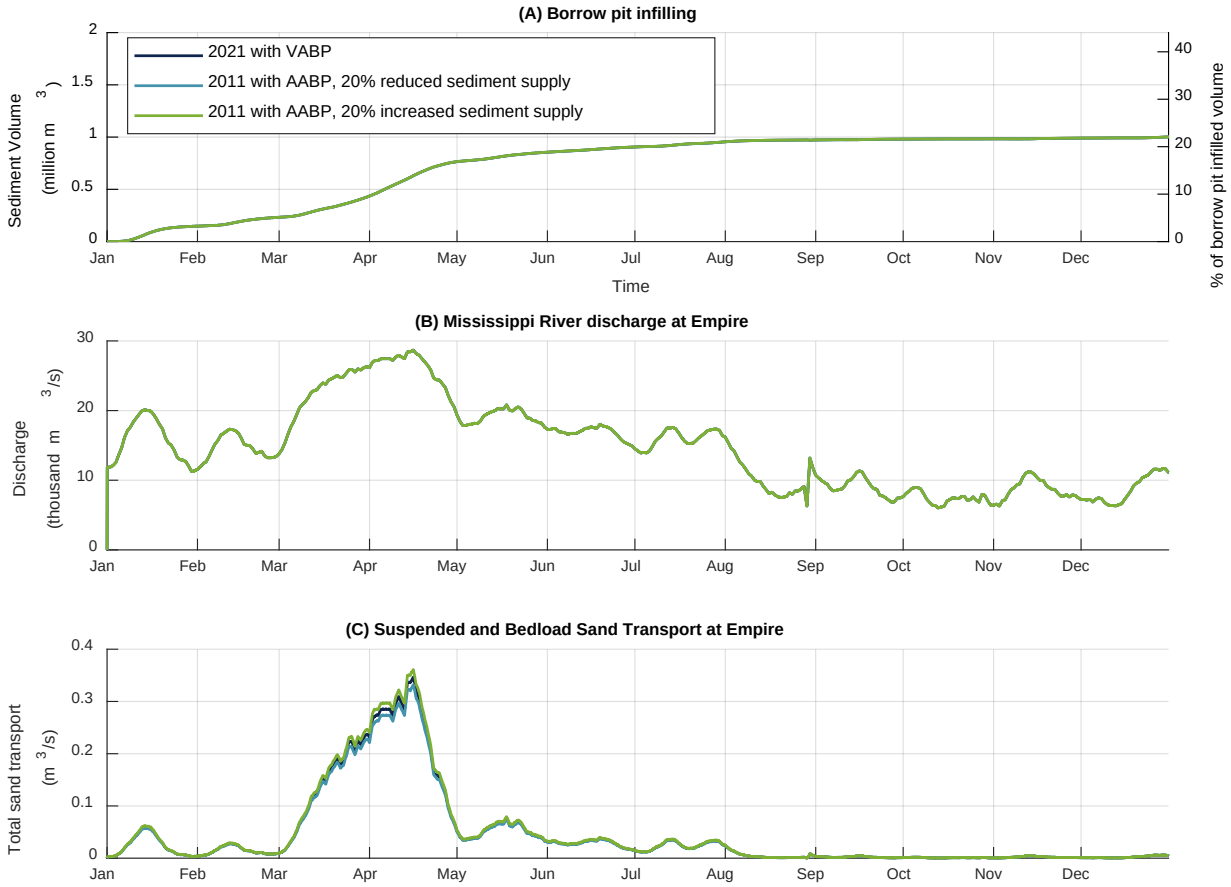

Figure C-15. VABP infilled volume of sediment and infilled percentage volume relative to the original pit volume (A), Mississippi River discharge at Empire (B), and total sand transport at Empire (C) modeled for the LMR Model with default, 20% increased, and 20% decreased sediment supply scenarios (Table C-2).

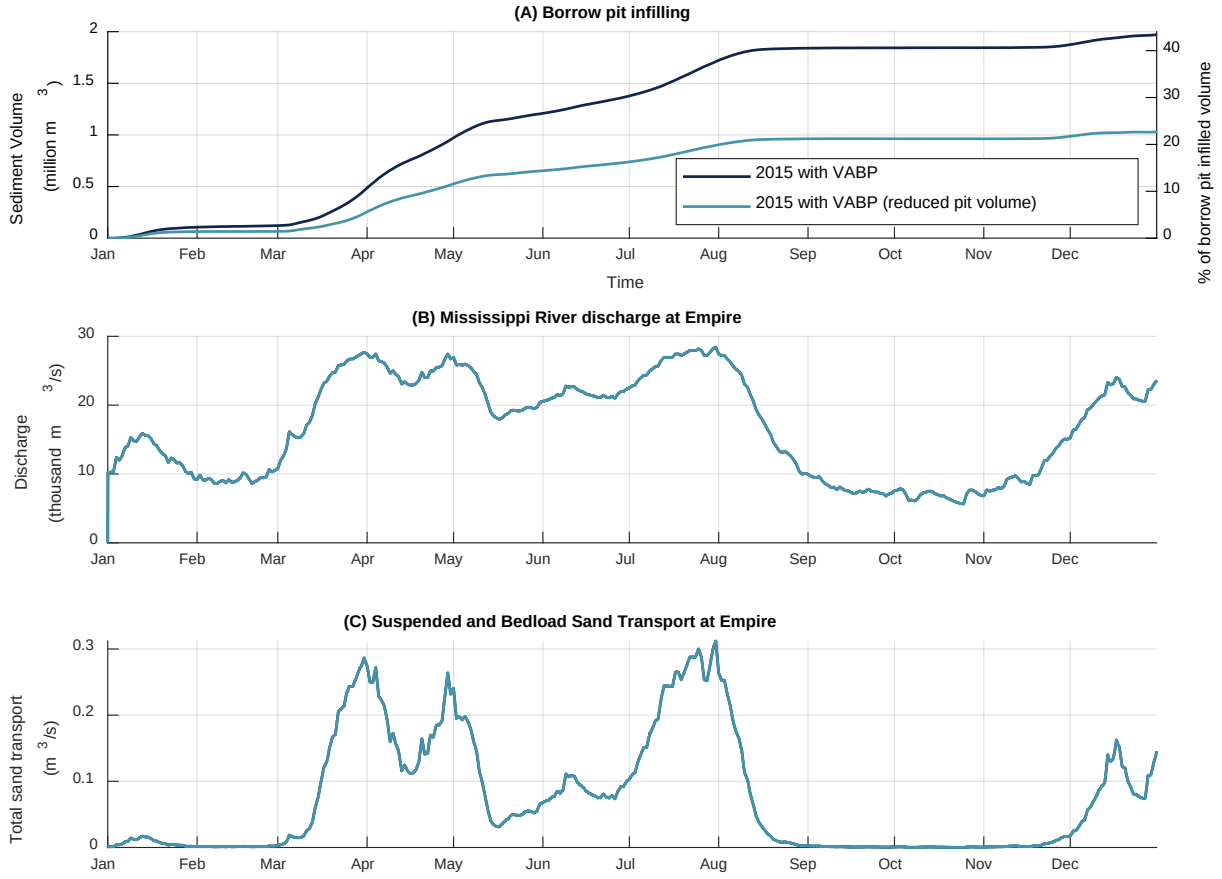

Figure C-16. VABP infilled volume of sediment and infilled percentage volume relative to the original pit volume (A), Mississippi River discharge at Empire (B), and total sand transport at Empire (C) modeled for the LMR Model with the default and 50% reduced borrow pit volumes (Table C-2).

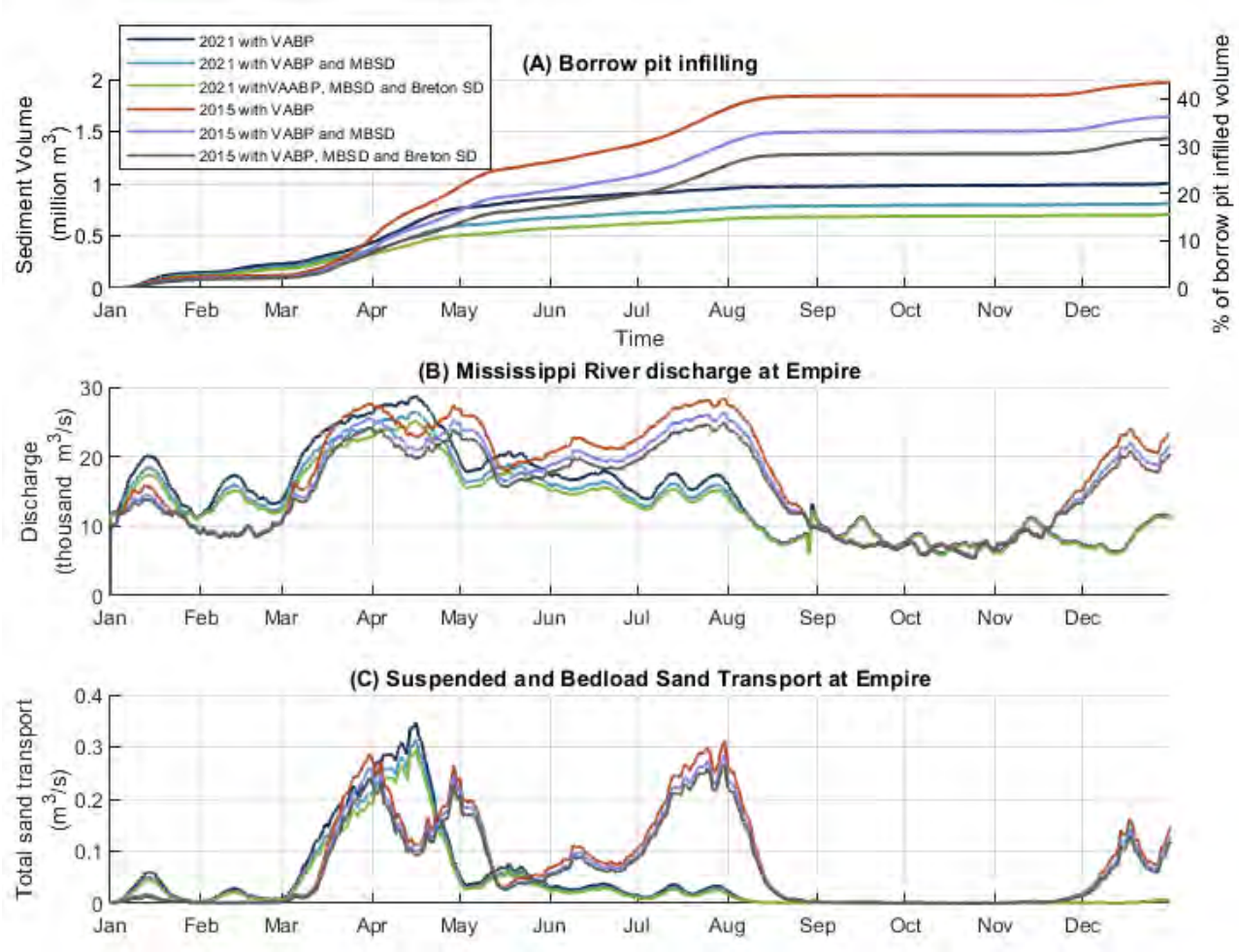

Figure C-17. VABP infilled volume of sediment and infilled percentage volume relative to the original pit volume (A), Mississippi River discharge at Empire (B), and total sand transport at Empire (C) modeled for the LMR Model with two different hydrographs (2015 and 2021) with and without presence of sediment diversions (Table C-2).

Model results for the 2015 hydrograph show that the Boothville Anchorage Bar exhibits small variance in aggradation trends proportional to the upstream extractions due to diversion (Figure C-18). The Venice Anchorage bar shows higher aggradation compared to the Boothville Bar, with aggradation declining proportional to the magnitude of flow extraction, and of the order of 400,000 m^3. Pilottown anchorage shows similar declining trends with lower volumes of aggradation however, the difference between with and without diversions is the same as the Venice Anchorage and approximately 500,000 m^3 (Figure C-18 and Figure C-19).

Downstream impacts of the VABP are not only limited to channel bar volumes but also affect navigation dredging in the MRSC between Venice and Head of Passes (Table 4). Model results suggest that the presence of the VABP reduces dredging volumes in the MRSC between Venice and Head of Passes by 9% and 3% for the 2015 and 2021 hydrographs, respectively. There are no noticeable changes in dredging volumes in the MRSC downstream of Head of Passes, which is in line with previously shown suspended sediment concentration maps (Figure 11) which show that borrow pit impacts are fully diminished at

Head of Passes. The presence of anthropogenic factors, such as sediment diversions, plays a role on navigation dredging activities. The presence of MBSD results in a 29% reduction of dredged volumes in the MRSD between Head of Passes and Venice and in a 18% reduction in Southwest Pass. The presence of both MBSD and Breton SD results in a 44% reduction of dredged volumes in the MRSC between Head of Passes and Venice and in a 26% reduction in Southwest Pass (Figure C-18).

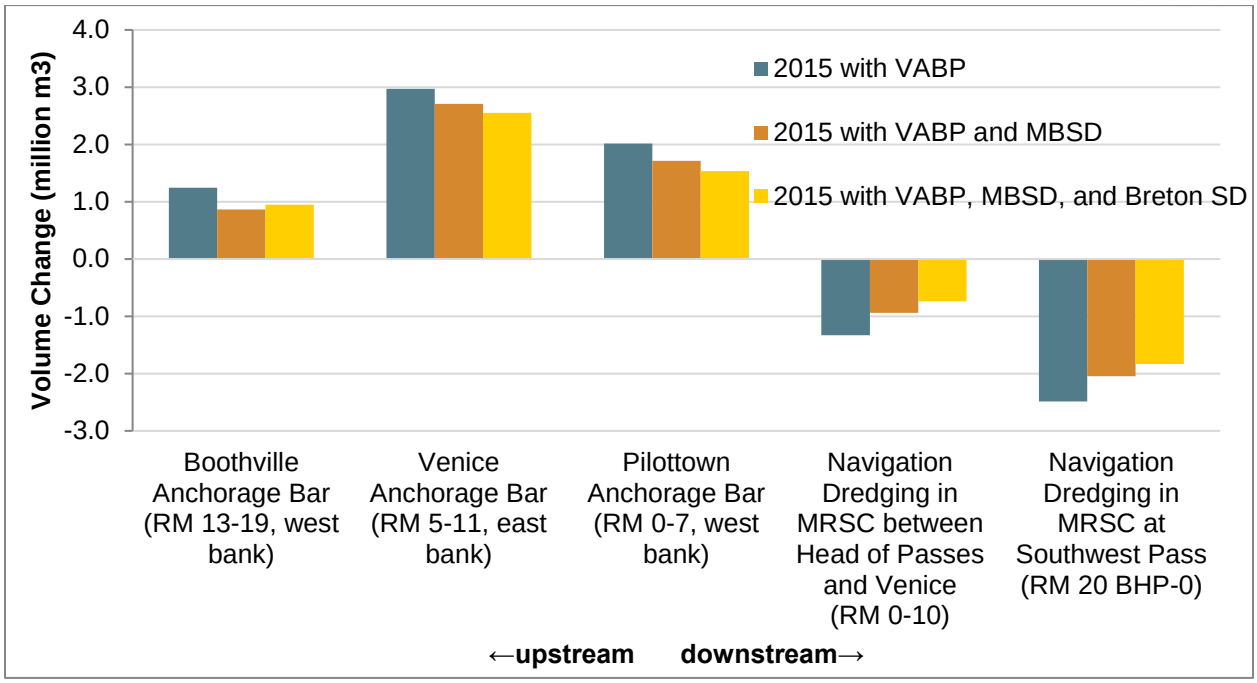

Figure C-18. Volume Changes at sand bars and dredged volumes from the Mississippi River Ship Channel (MRSC) between Venice (RM 13) and Southwest Pass (RM 20 BHP) for scenarios with the Venice Anchorage Borrow Pit (VABP, RM 8), and without and with the Mid-Barataria Sediment Diversion (MBSD) and Breton Sediment Diversion (Breton SD), for hydrographs 2021.

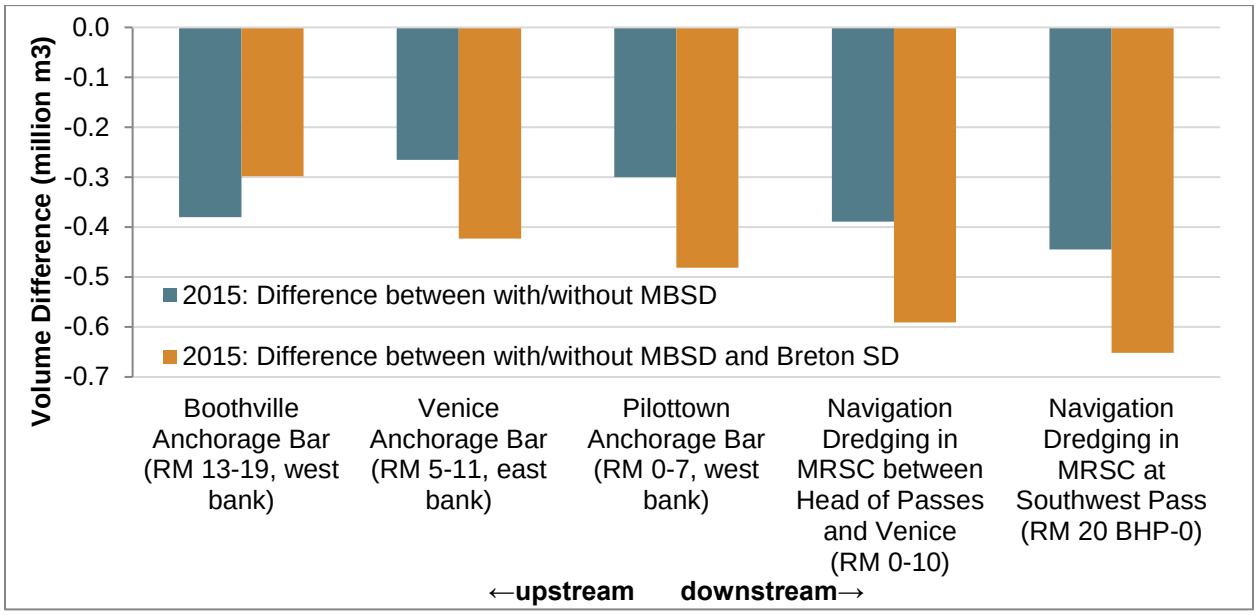

Figure C-19. Volume differences between scenarios with and without diversions showing the modeled impact of the MBSD individually and the MBSD and Breton SD combined on sand bars near the VABP and navigation dredging in the Mississippi River Ship Channel (MRSC). Negative volume difference indicates a decrease of aggradation (or increase of degradation) due to the presence of a borrow pit, or a decrease in navigation dredging.

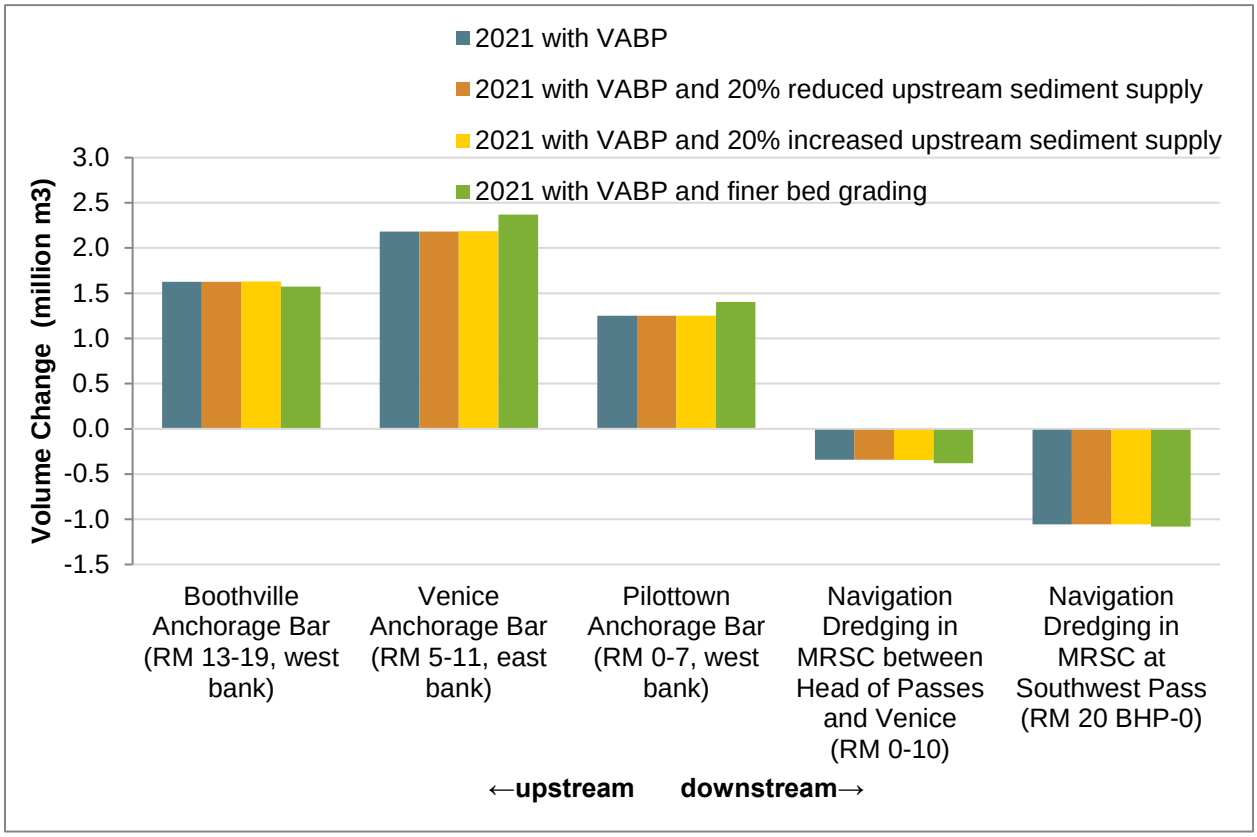

Figure C-20. Volume Changes at sand bars and dredged volumes from the Mississippi River Ship Channel (MRSC) between Venice (RM 13) and Southwest Pass (RM 20 BHP) for various sensitivity tests simulated for hydrograph 2021 with the Venice Anchorage Borrow Pit (VABP, RM 8).

APPENDIX D. MISSISSIPPI RIVER HYDROGRAPHS

Mississippi River hydrographs measured at the USGS Belle Chasse station were evaluated to select the hydrographs for the analysis presented in this report. The most recent decade from 2010 to 2021 was analyzed. For each year, the total annual discharge was calculated, as well as the discharge above specific thresholds: 11,000 m^3s, 23,000 m^3s, 25,000 m^3s, 28,000 m^3s, 31,000 m^3s (i.e., 400,000 cfs, 800,000 cfs, 900,000 cfs, 1,000,000 cfs and 1,100,000 cfs). Results are presented in Table D-1. The shape of the hydrographs, and specifically the number and duration of peaks, was also considered in the selection. The following years were selected for analysis in the Alliance Model:

- 2010 intermediate flow year with several peaks that do not exceed 28,000 m^3s (i.e., one million cfs).
- 2011 intermediate flow year with one single flood peak in spring
- 2016 intermediate flow year with two early peaks
- 2019 high flow year

Figure D-1 to Figure D-6 present the hydrographs for these four hydrographs and for the additional two hydrographs used for the LMR Model.

Table D-1. Summary table with total annual discharge and annual discharge above a specific threshold. Discharge data at USGS Belle Chasse gauge were used. The background-colored bars highlights the relative range of discharge: the longer the bar, the highest the discharge.

Year	Total Annual Discharge ($10^9 \cdot m^3$)	Total Annual Discharge ($10^9 \cdot m^3$) above specific threshold				
		Threshold of 11k m^3/s (400k cfs)	Threshold of 23k m^3/s (800k cfs)	Threshold of 25k m^3/s (900k cfs)	Threshold of 28k m^3/s (1.0 million cfs)	Threshold of 31k m^3/s (1.1 million cfs)
2010	503	423	154	68	23	3
2011	513	396	240	170	110	53
2012	323	199	18	0	0	0
2013	466	386	79	43	0	0
2014	436	347	16	0	0	0
2015	557	467	283	194	99	0
2016	543	469	199	156	105	61
2017	448	347	101	84	52	3
2018	575	510	262	187	105	49
2019	755	729	572	555	430	247
2020	639	566	424	406	338	212
2021	476	381	117	95	51	0

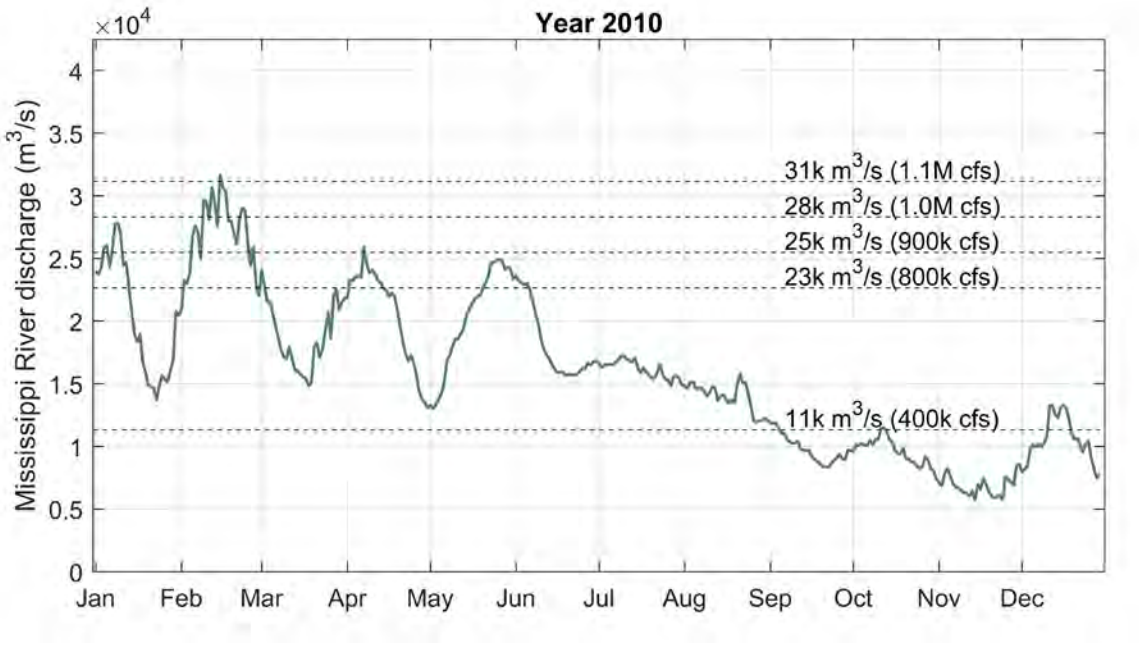

Figure D-1. Daily average discharge at Belle Chasse in 2010. Threshold of interest are also highlighted in the plot.

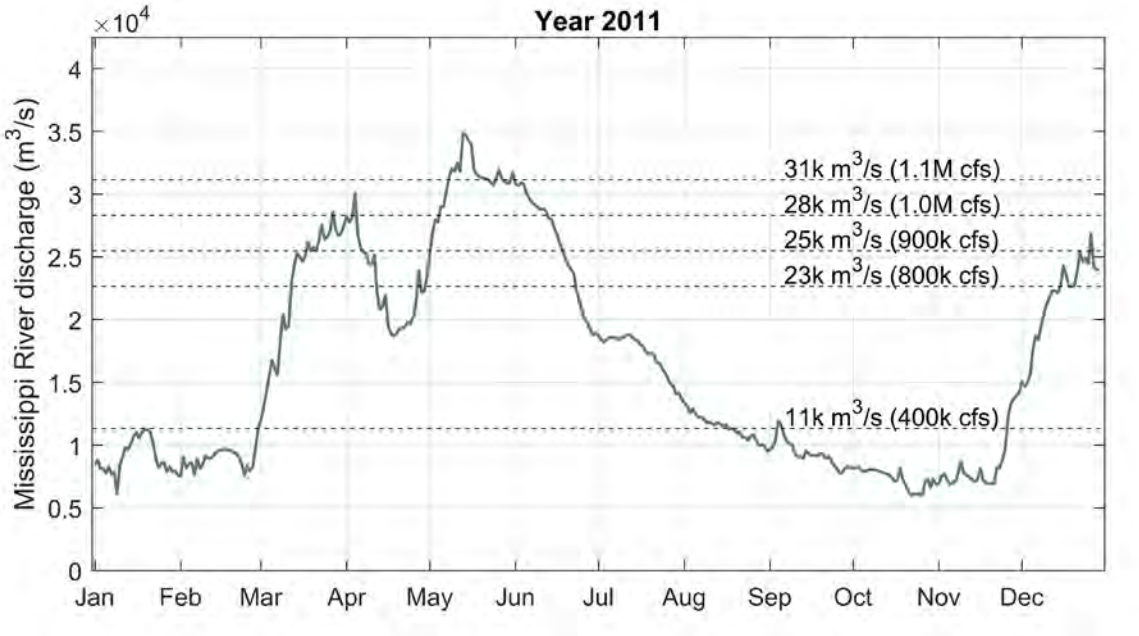

Figure D-2. Daily average discharge at Belle Chasse in 2011. Threshold of interest are also highlighted in the plot.

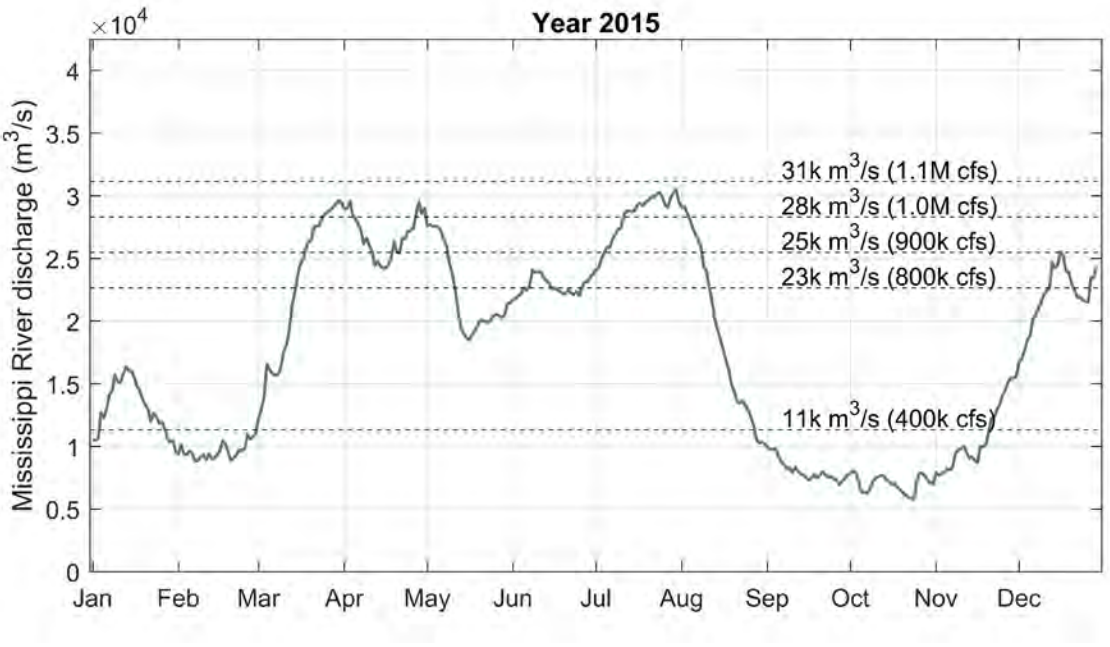

Figure D-3. Daily average discharge at Belle Chasse in 2015. Threshold of interest are also highlighted in the plot.

Figure D-4. Daily average discharge at Belle Chasse in 2016. Threshold of interest are also highlighted in the plot.

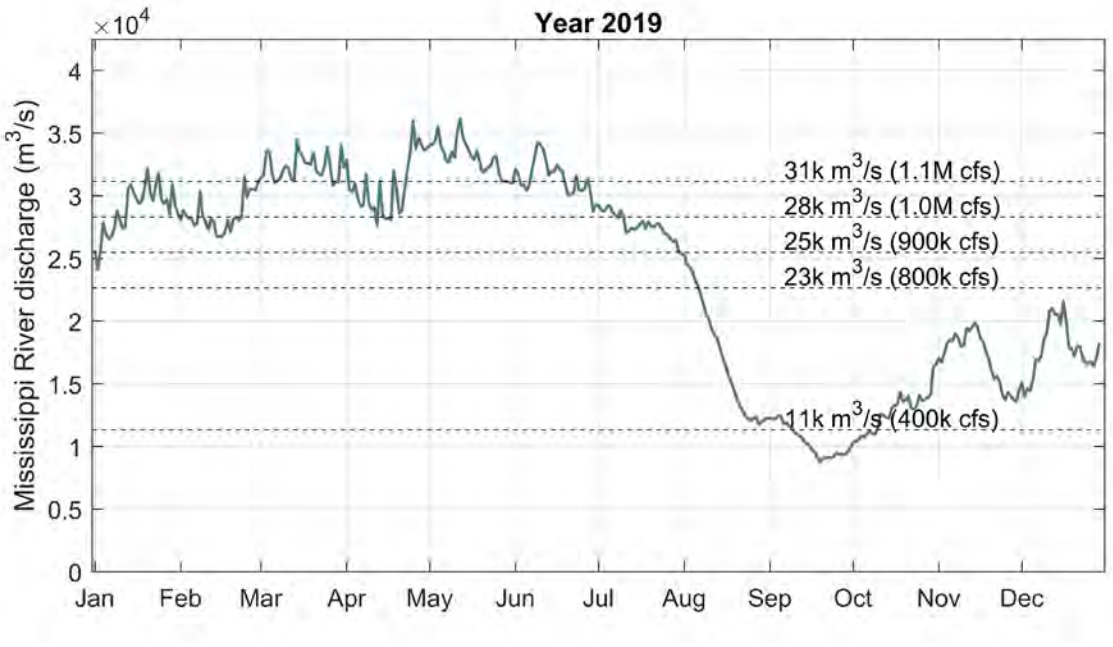

Figure D-5. Daily average discharge at Belle Chasse in 2019. Threshold of interest are also highlighted in the plot.

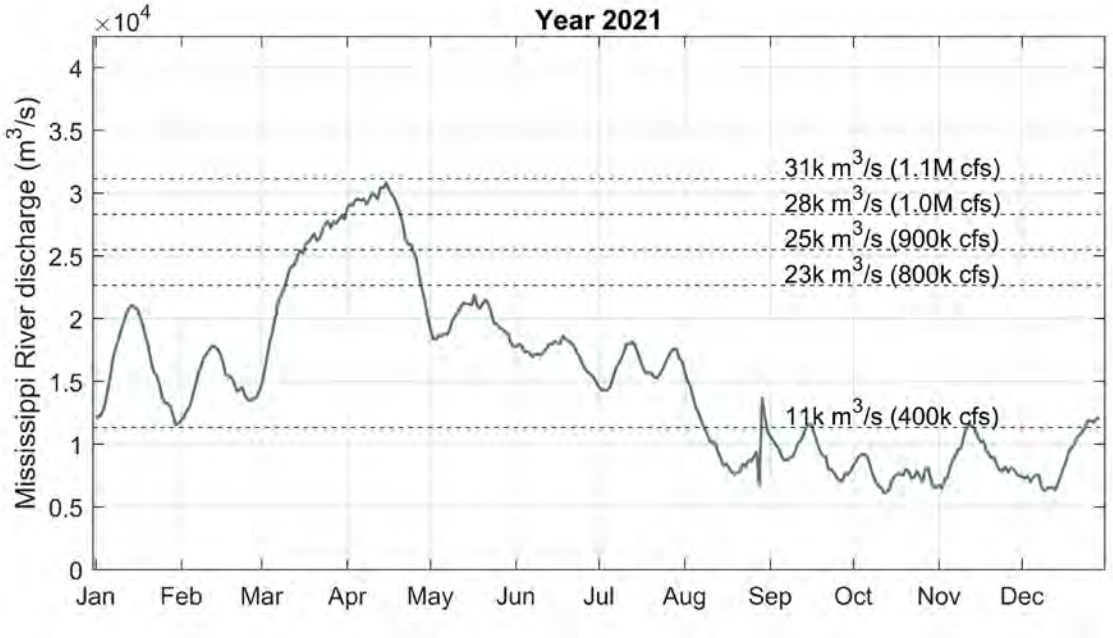

Figure D-6. Daily average discharge at Belle Chasse in 2021. Threshold of interest are also highlighted in the plot.

APPENDIX E. COMPUTATIONAL FLUID DYNAMICS SIMULATIONS

As a complement to the Delft3D-4 modeling study discussed in this report, a computational fluid dynamic (CFD) model, based on the CFD software FLOW-3D, was developed to evaluate the detailed flow structure and turbulence around a borrow pit.

E.1 SITE DESCRIPTION

High-resolution (i.e., 5 m) bathymetry survey data used for the Deflt3D model was also utilized to create the FLOW-3D model, as shown in Figure E-1 (Dasler, 2019b). A section of the river reach (about 4000 m) immediately downstream of Alliance, was identified as a potential borrow pit location (Figure 1), and thus was selected as the study region for this CFD analysis. As shown in Figure E-2, the upper panel shows the river bathymetry without dredging (existing condition) and the lower panel shows the bathymetry with a standard borrow pit near the right bank (looking downstream) of the river (with-pit condition). Note that the bathymetry data was rotated so that the main channel is aligned with the y-axis as requested for better modeling in FLOW-3D. The flow direction is from left to right. The borrowing region is about 2000 m long and 300 m wide. The pit bottom elevation is about -27.43 m (-90 ft) NAVD88 and the main channel elevation near the pit is about -18 m NAVD88 following information on the design cut, shared by the engineer on record for the project (Moffatt & Nichol, 2012).

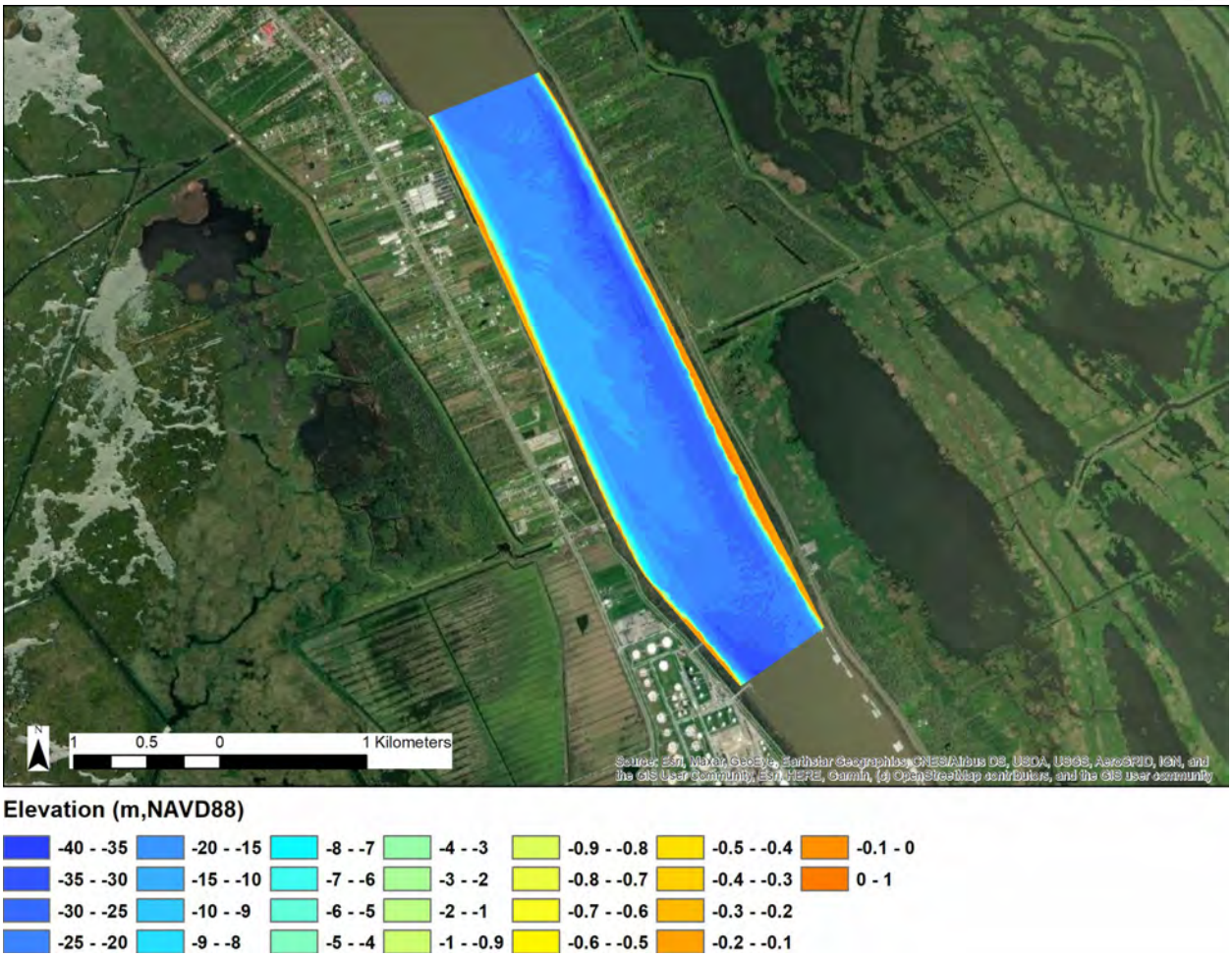

Figure E-1. Model domain and bathymetry of the FOLW-3D CFD model.

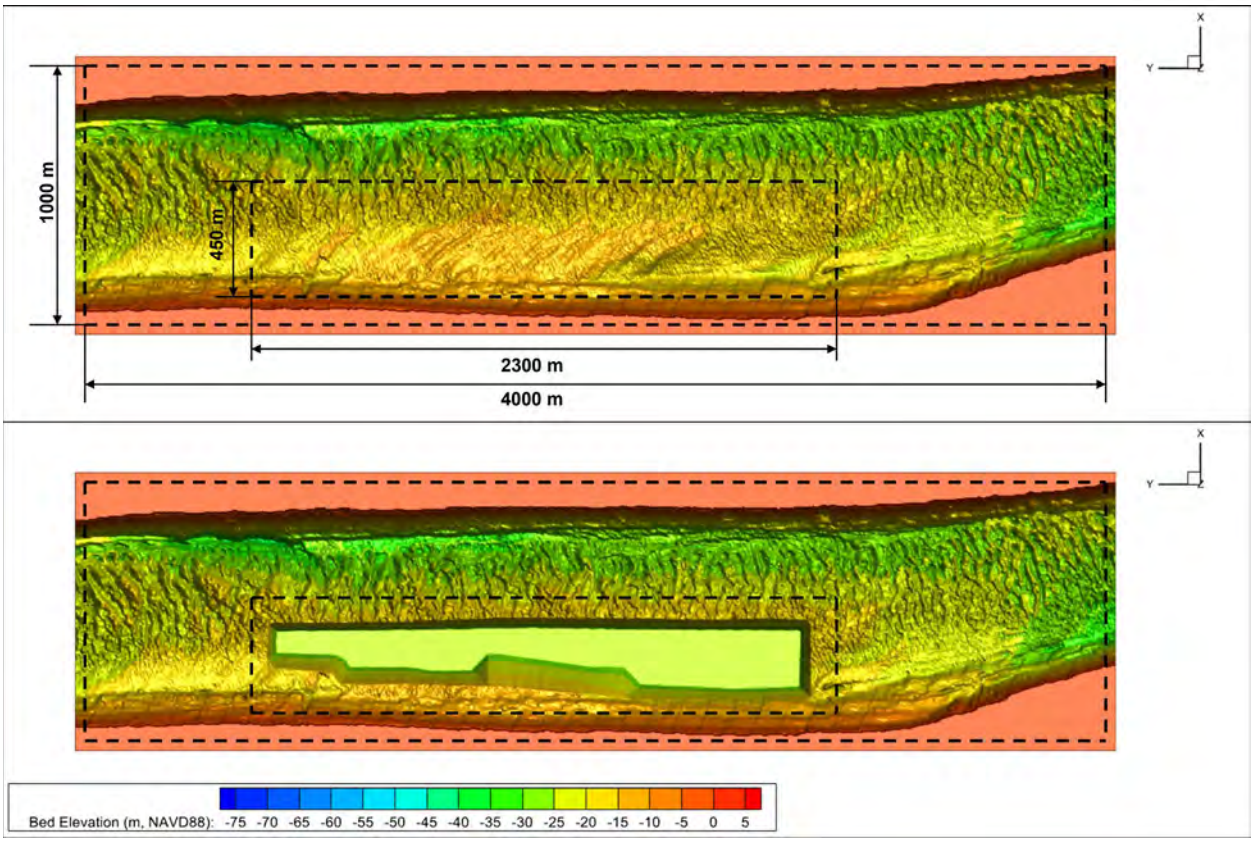

Figure E-2. Processed bathymetry for the FLOW-3D model: the upper panel represents the existing condition, and the lower panel represents the with-pit condition.

E.2 NUMERICAL MODEL

The commercial CFD software FLOW-3D was used to model flow and sediment transport with and without the borrow pit in this analysis. FLOW-3D is a three-dimensional model where fluid motion is described with non-linear transient, second-order differential Navier Stokes equations. The numerical algorithm used in FLOW-3D is based on both finite difference and finite volume methods applied to a structured computational grid. The river hydrodynamics is solved with the incompressible Reynolds-averaged Navier–Stokes (RANS) equations together with the Renormalized group (RNG) k-epsilon model (Yakhot & Orszag, 1986; Yakhot & Smith, 1992) for turbulence closure. The one-fluid volume of fluid (VOF) method was used to track the air/water interface, and the first order-accurate spatiotemporal discretization schemes were used in all modeled cases. The selected methods and approaches outlined above have been widely used to study similar open channel flow and sediment transport in the literature (ALDEN Research Laboratory, Inc, 2020).

The river channel shown in Figure E-2 was meshed with hexahedral elements for a 10 m in horizontal and 1.5 m resolution in the vertical direction. Near the borrow pit region, the mesh resolution was refined to 2.5 m horizontally and 0.75 m vertically to resolve the detailed flow field near the region of interest. A mesh sensitivity analysis was performed, and it was found that the model results are not sensitive to the mesh resolution.

A constant flow rate of 33,980 m^3/s (1,200,000 cfs) was selected to represent the high-flow condition and imposed at the upstream inflow boundary. The turbulent variables at the upstream inflow were assumed to be low. A sensitivity analysis was performed and confirmed that the model results are not sensitive to the inflow turbulent values. The water surface elevation at the downstream end of the model domain was set to be 2.82 m NAVD88. It was determined using the rating curve developed from observed discharge at the Belle Chasse (USGS 07374525 Mississippi River at Belle Chasse, LA) and observed stage at Alliance (USACE 01390 Mississippi River at Alliance). The roughness height of the riverbed was calibrated based on the predicted local surface slope from the Delft3D-4 study discussed in Appendix B. These simulation conditions were referred to as the 'Baseline condition' to evaluate the flow field with and without the borrow pit.

To evaluate the sediment transport with and without the borrow pit, the Sediment Transport module in FLOW-3D was activated which uses the Drift-flux model to predict sediment deposition. Since the focus of this analysis is mostly on the sand, three sand classes: $9.2e^{-5}$ m, $1.83e^{-4}$ m, and $3.67e^{-4}$ m, were selected, to represent the fine, medium, and coarse sand, respectively. The sand concentration at the upstream inflow was assumed to be 0.086 km/m^3 based on the rating curve used for the Delft3D-4 Alliance model (Section B.5.1), and composites of 20%, 60%, and 20% of the three sand classes, from fine to coarse.

Lastly, the impacts of inflow direction on the hydrodynamics and turbulent variables were evaluated by adjusting the inflow directions 15º and 30º toward the right bank.

E.3 MODEL RESULTS AND DISCUSSION

Cutting planes are created in both the streamwise and transverse directions to extract data for comparison. As shown in Figure E-3, cross-sections a and b are in the streamwise direction, along the main channel and cutting through the borrow pit, respectively. Cross-sections c, d, and e are in the transverse direction and located at the first half, second half, and downstream of the borrow pit.

Figure E-4through Figure E-7 show the velocity magnitudes at the pre-defined cutting planes. The upper panels for these figures show model results for the existing condition and the lower panels show model results for the with-pit condition. As illustrated in Figure E-4, the overall velocity is reduced at the borrow pit due to the increase in flow area. Velocity contours and vectors showing the flow direction on cutting planes a and b are shown in Figure E-5. Note that the velocity vectors show flow directions parallel to the cutting planes. As illustrated, the velocity reduction can be found in both the main channel (cross-section a) as well as along the borrow pit (cross-section b). No flow separation is found at the leading edge, due to the relatively low velocity in the river. An upward velocity is found at the tailing edge of the borrow pit and creates a small high-velocity region immediately downstream of the borrow pit. Sediment resuspension is reduced with a lower velocity at the borrow pit while the deeper bed elevation allows more time for sediment settling. Note that the up-lifting velocity at the tailing end of the borrow pit could increase sediment vertical mixing locally.

The velocity contours and vectors at the transverse cutting planes c, d, and e are shown in Figure E-6. Figure E-7 shows the same transverse cross-sections with only velocity magnitude in the transverse direction. It can be found that velocity in the transverse direction is relatively low when compared to the

streamwise direction. No significant secondary recirculation is found due to the relatively straight channel in the model domain.

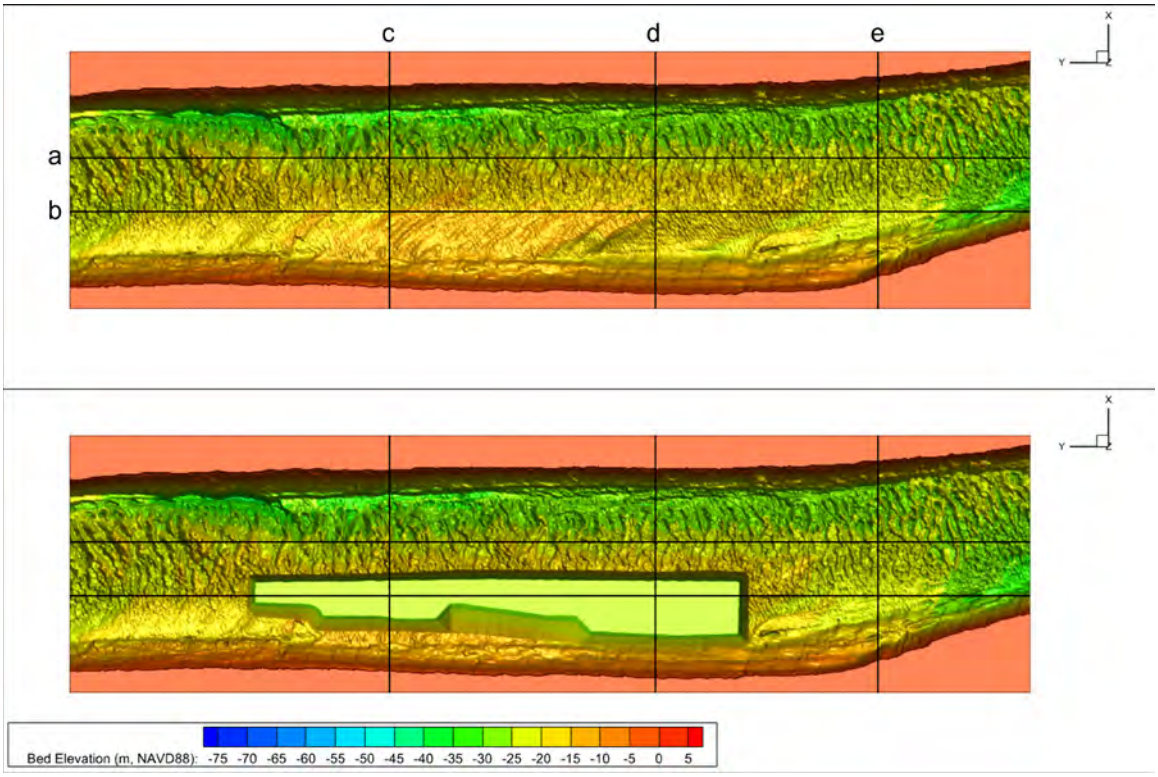

Figure E-3. Data extraction cross-sections: cross-sections a and b are in the streamwise direction; cross-sections c, d, and e are in the transverse direction. The upper panel represents the existing condition, and the lower panel represents the with-pit condition.

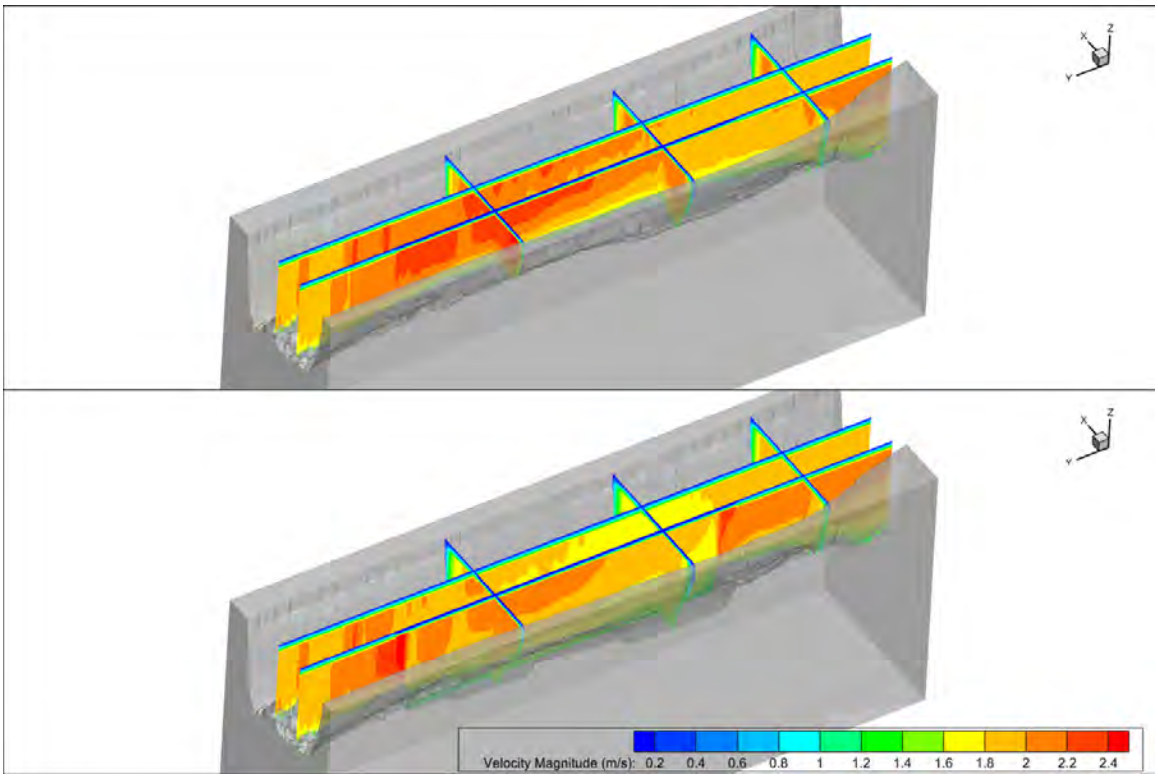

Figure E-4. Velocity magnitude contours at the selected cross-sections: the upper panel represents the existing condition, and the lower panel represents the with-pit condition.

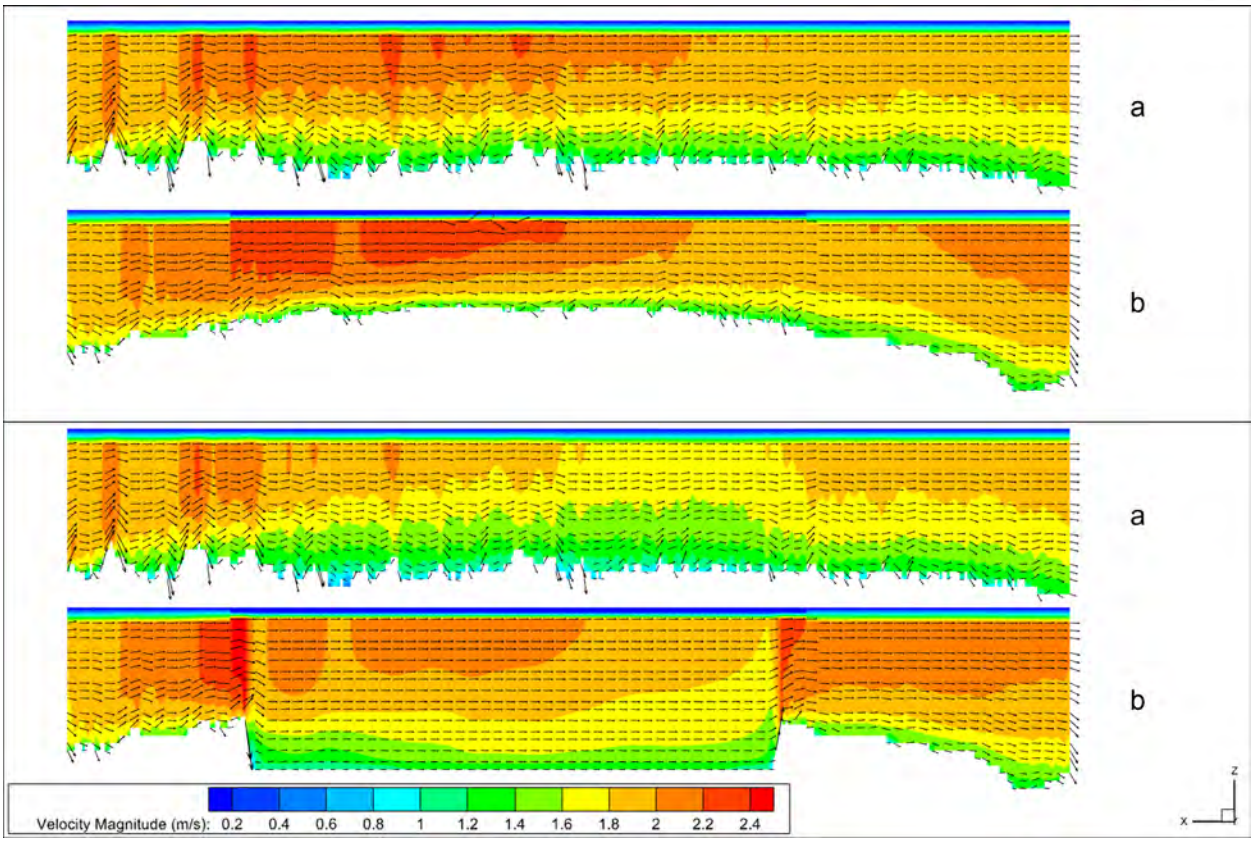

Figure E-5. Side view of velocity magnitude contours and velocity vectors at the selected streamwise cross-sections a and b: the upper panel represents the existing condition, and the lower panel represents the with-pit condition.

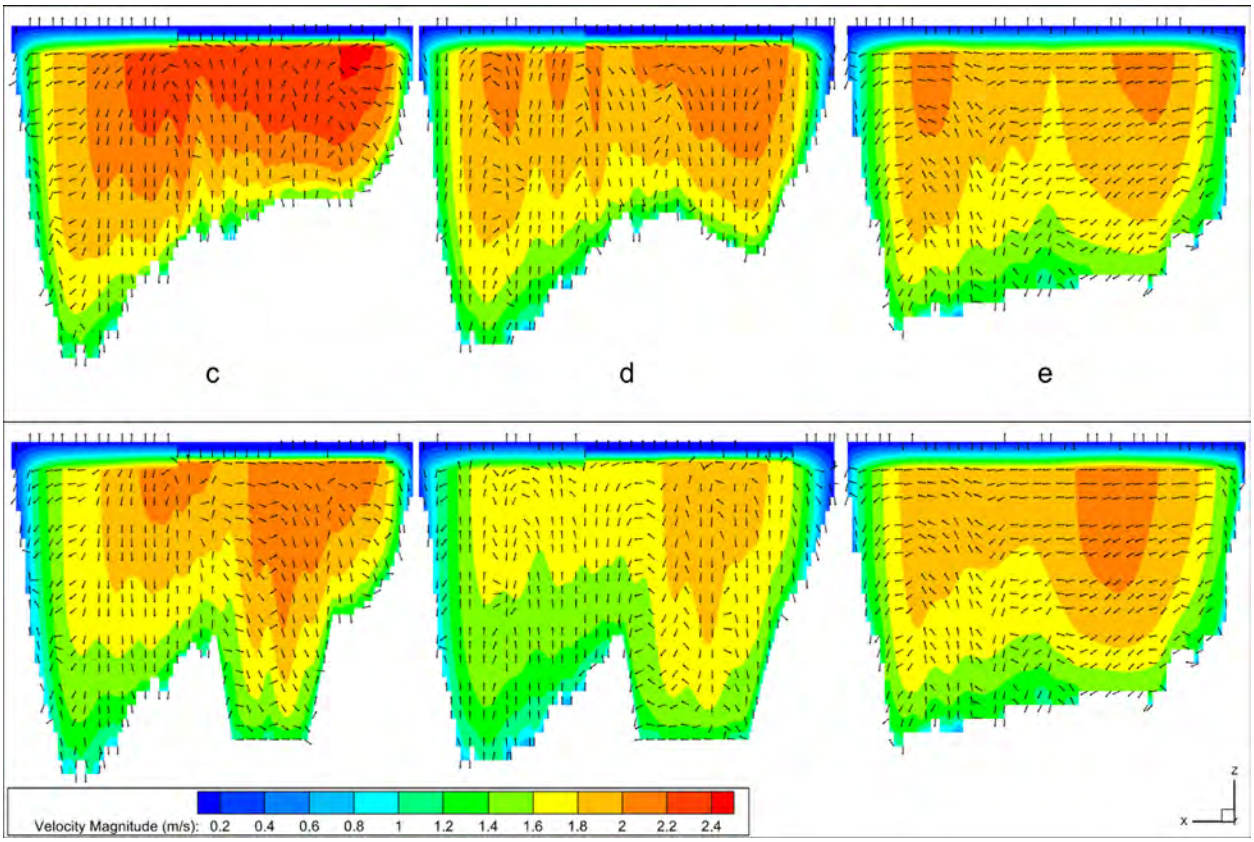

Figure E-6. Front view of velocity magnitude contours and projected velocity vectors at the selected transverse cross-sections c, d, and e : the upper panel represents the existing condition, and the lower panel represents the with-pit condition.

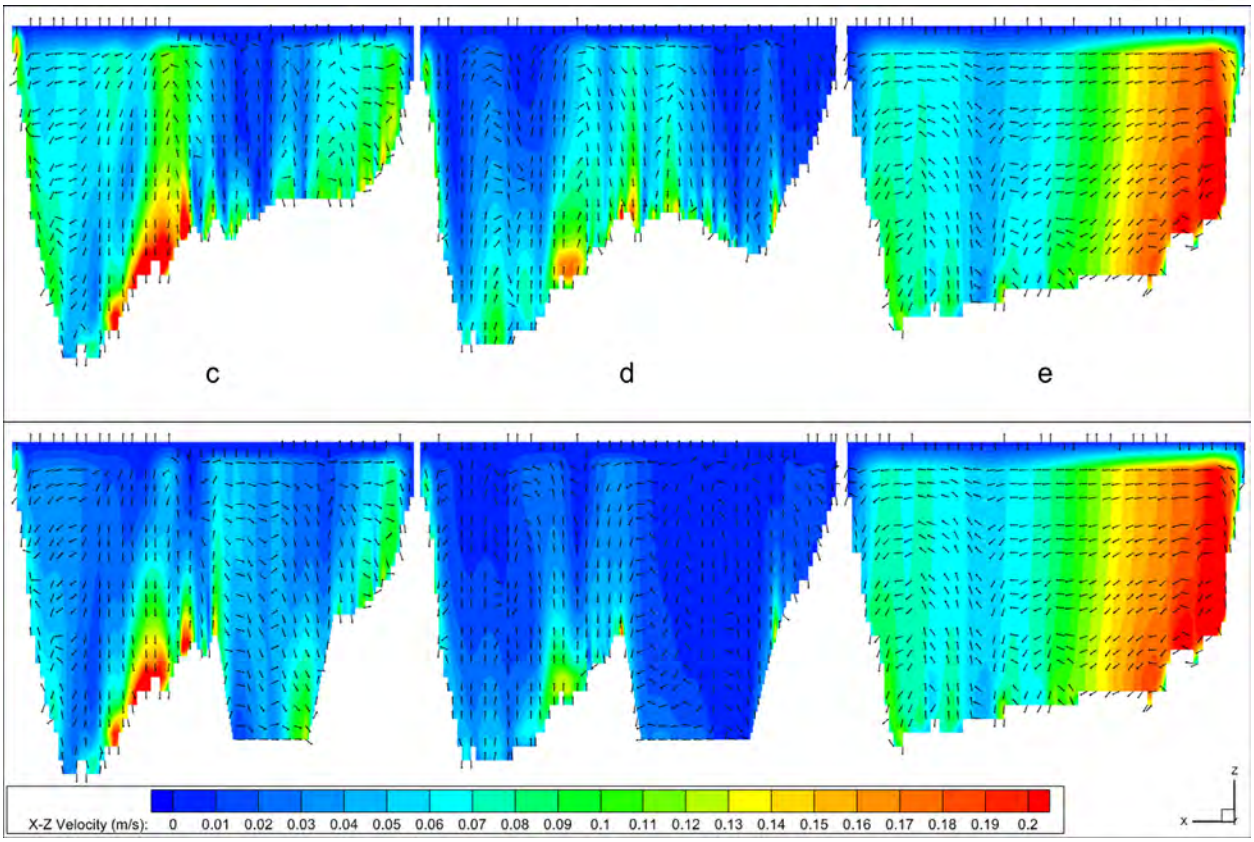

Figure E-7. Front view of transverse velocity magnitude contours and projected velocity vectors at the selected transverse cross-sections c, d, and e : the upper panel represents the existing condition, and the lower panel represents the with-pit condition.

The eddy viscosity (turbulent viscosity) is a variable in the CFD model to represent the mixing effects of the un-resolved eddies in the fluid. It enhances the turbulent mixing of suspended sediment in a water column. Figure E-8 through Figure E-11 show the eddy viscosity at the pre-defined cutting planes for the existing condition and the with-pit condition. It can be found that high eddy viscosities are predicted along the sides of the borrow pit, as shown in Figure E-11 at cross-sections c and d. A highly turbulent region is also created near the tailing end of the borrow pit as seen in Figure E-10 cross-section b. These are regions where sediments can be disturbed and mixed vertically. In contrast, a slight reduction in eddy viscosity is predicted downstream of the borrow pit.

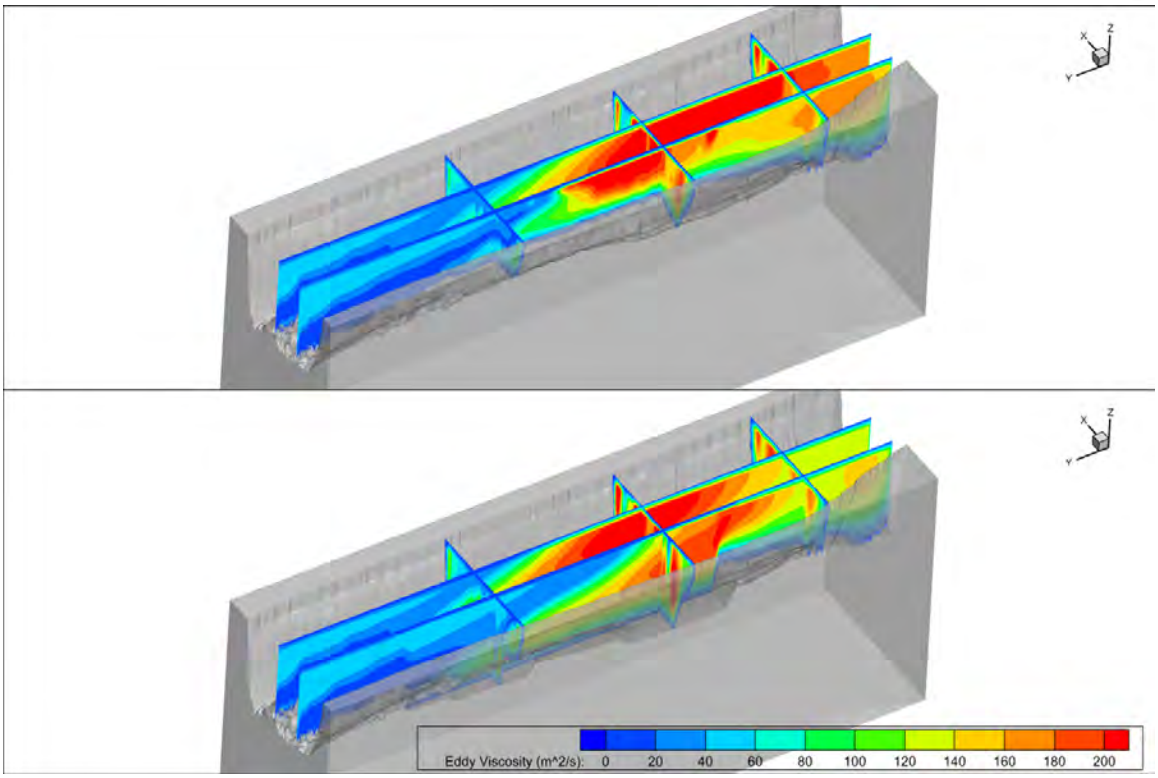

Figure E-8. Eddy viscosity contours at the selected cross-sections: the upper panel represents the existing condition, and the lower panel represents the with-pit condition.

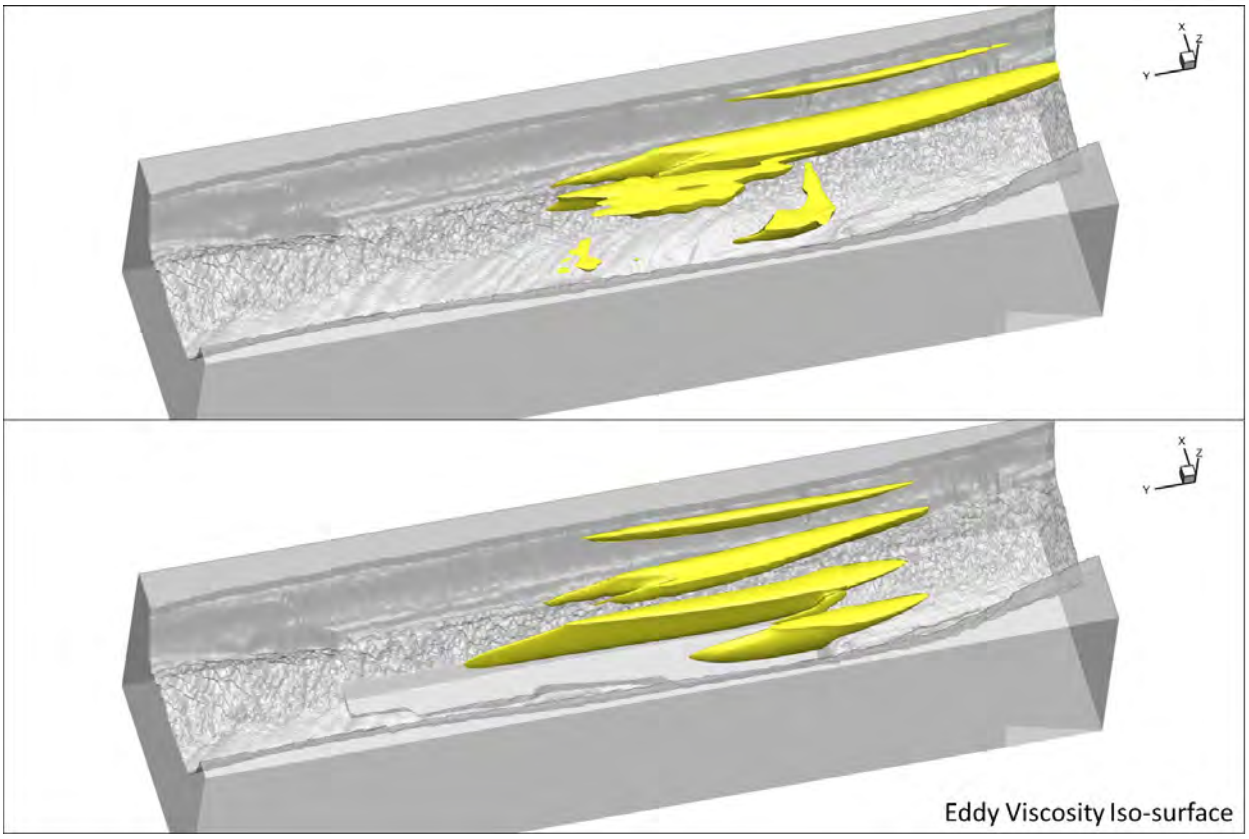

Figure E-9. Eddy viscosity iso-surface at 100 m^2/s showing sediment deposition regions. The upper panel represents the existing condition, and the lower panel represents the with-pit condition.

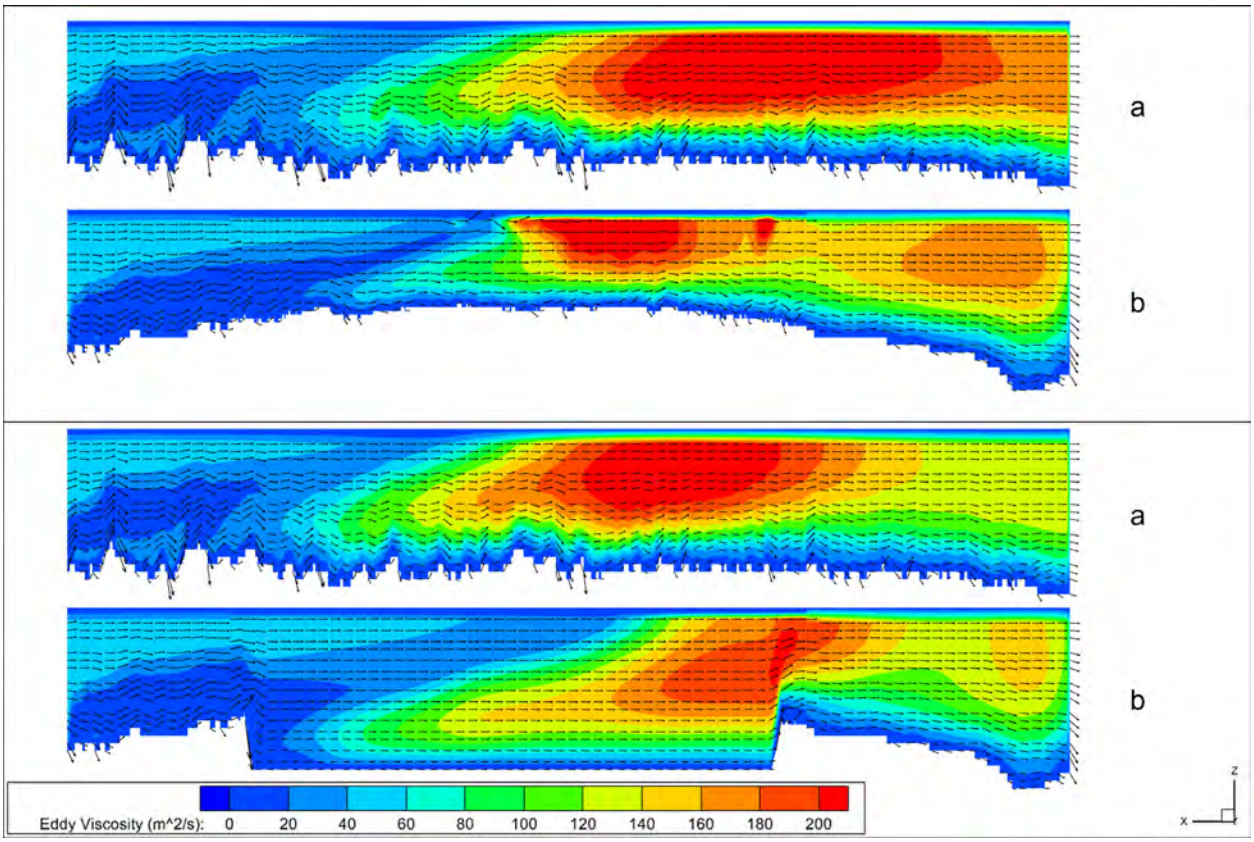

Figure E-10. Side view of eddy viscosity contours and velocity vectors at the selected streamwise cross-sections a and b: the upper panel represents the existing condition, and the lower panel represents the with-pit condition.

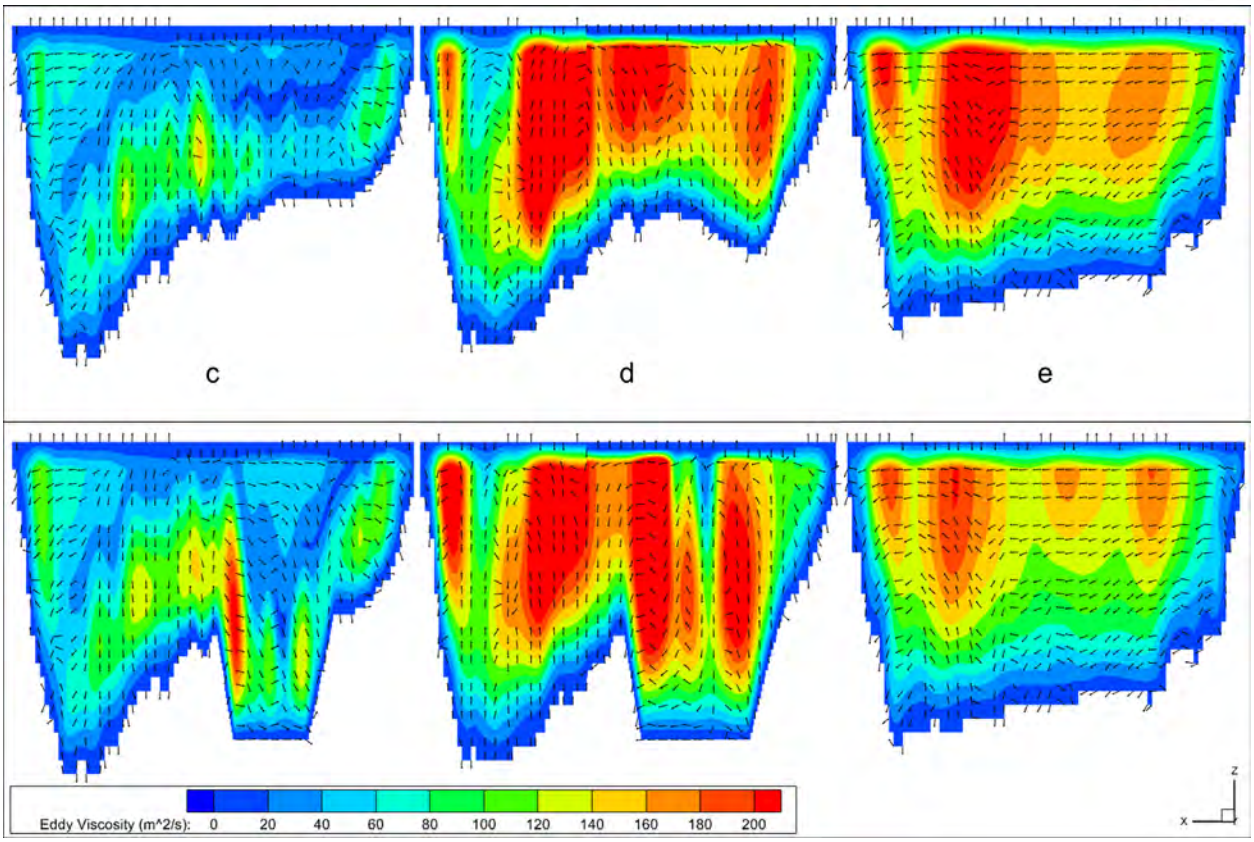

Figure E-11. Front view of eddy viscosity contours and projected velocity vectors at the selected transverse cross-sections c, d, and e : the upper panel represents the existing condition, and the lower panel represents the with-pit condition.

The suspended sediment concentrations on the pre-defined cross-sections are shown in Figure E-12 through Figure E-15. Because the sediments are assumed well-mixed at the model inflow, the analysis mostly focuses on modeling sediment settling along the river reach under different conditions. As can be seen in these figures, high sediment concentrations near the riverbed represent deposition. Under the existing condition, more sediment are depositing near the right bank due to the elevated sand bar, as shown in Figure E-13 upper panel. When compared between the existing condition and the with-pit condition, it is evident that more sediments are deposited on the riverbed for the existing conditions. This is attributed to the combined effects of dredged pit and relatively high turbulence discussed above.

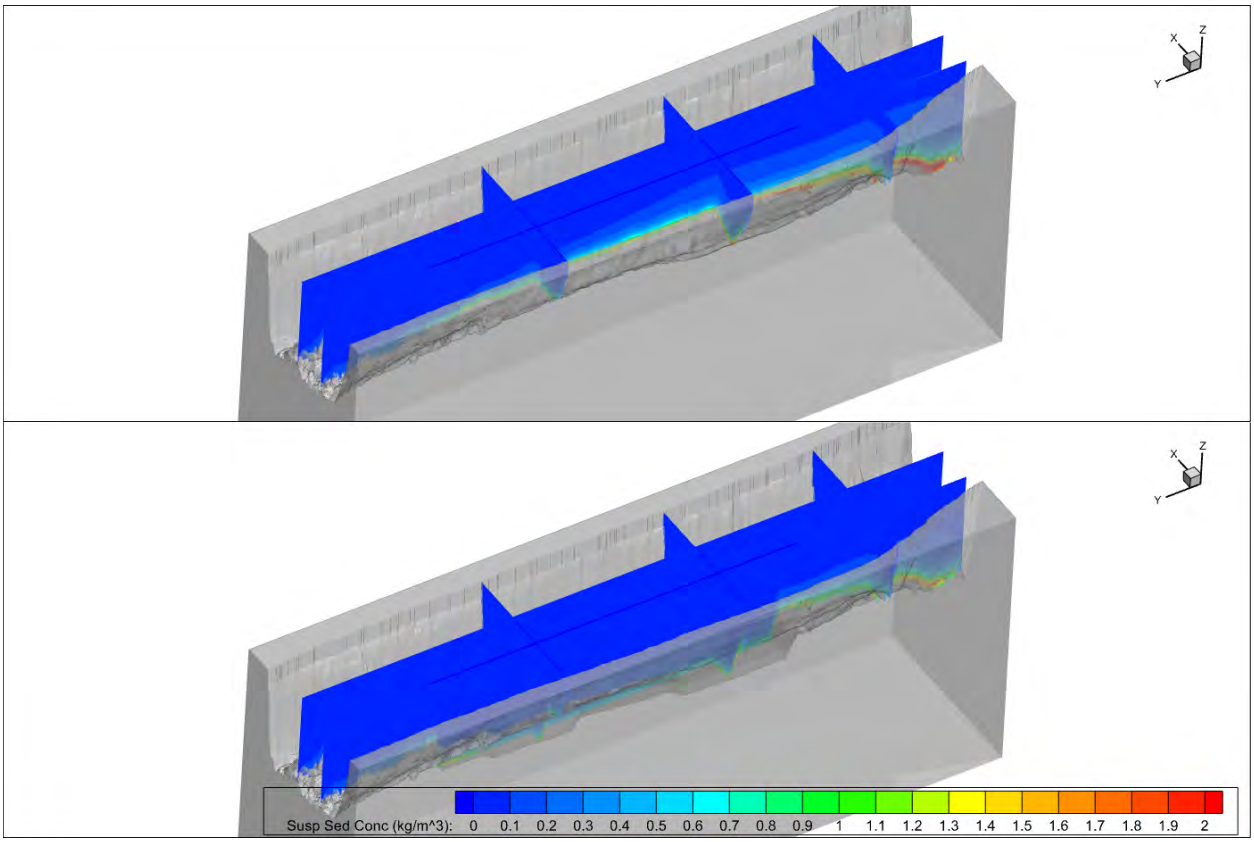

Figure E-12. Suspended sediment concentration contours at the selected cross-sections : the upper panel represents the existing condition, and the lower panel represents the with-pit condition.

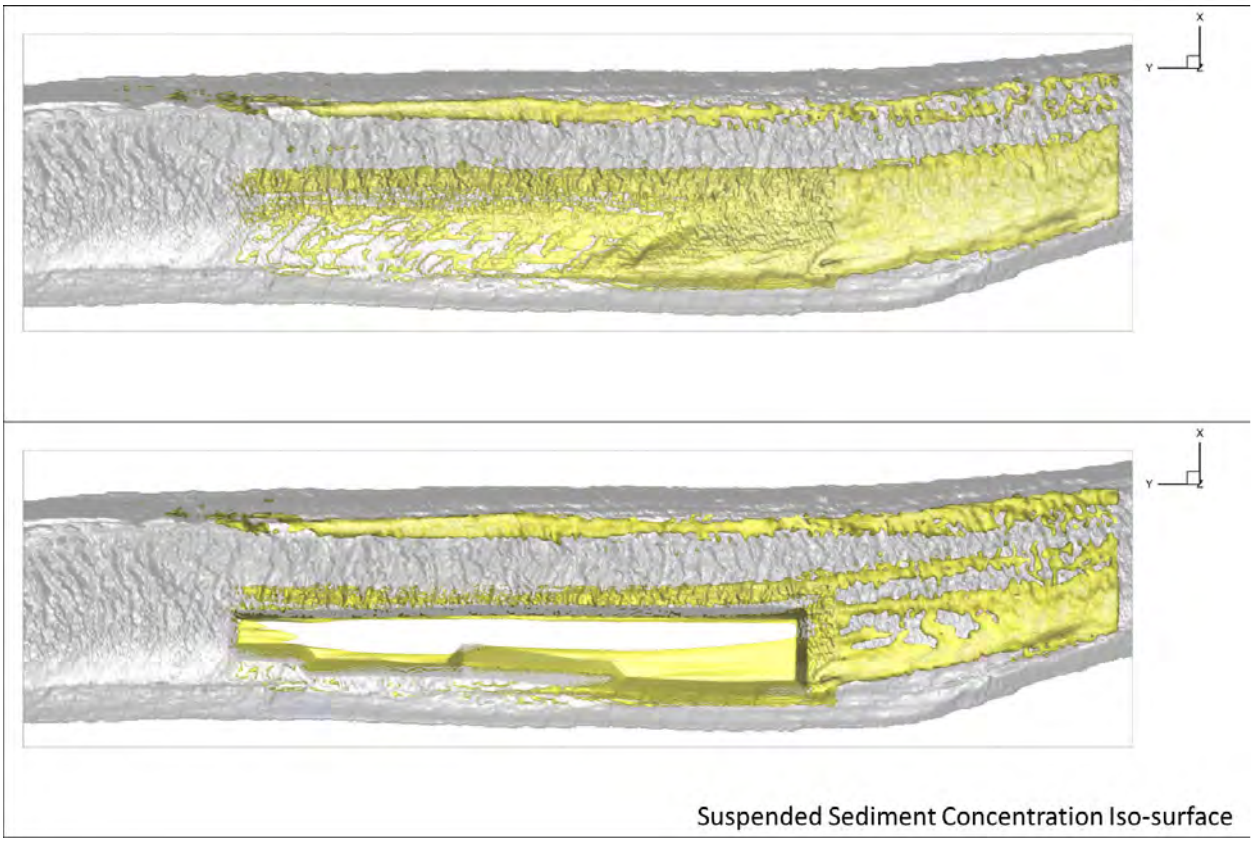

Figure E-13. Suspended sediment concentration iso-surface at 1 kg/m^3 showing sediment deposition regions. The upper panel represents the existing condition, and the lower panel represents the with-pit condition.

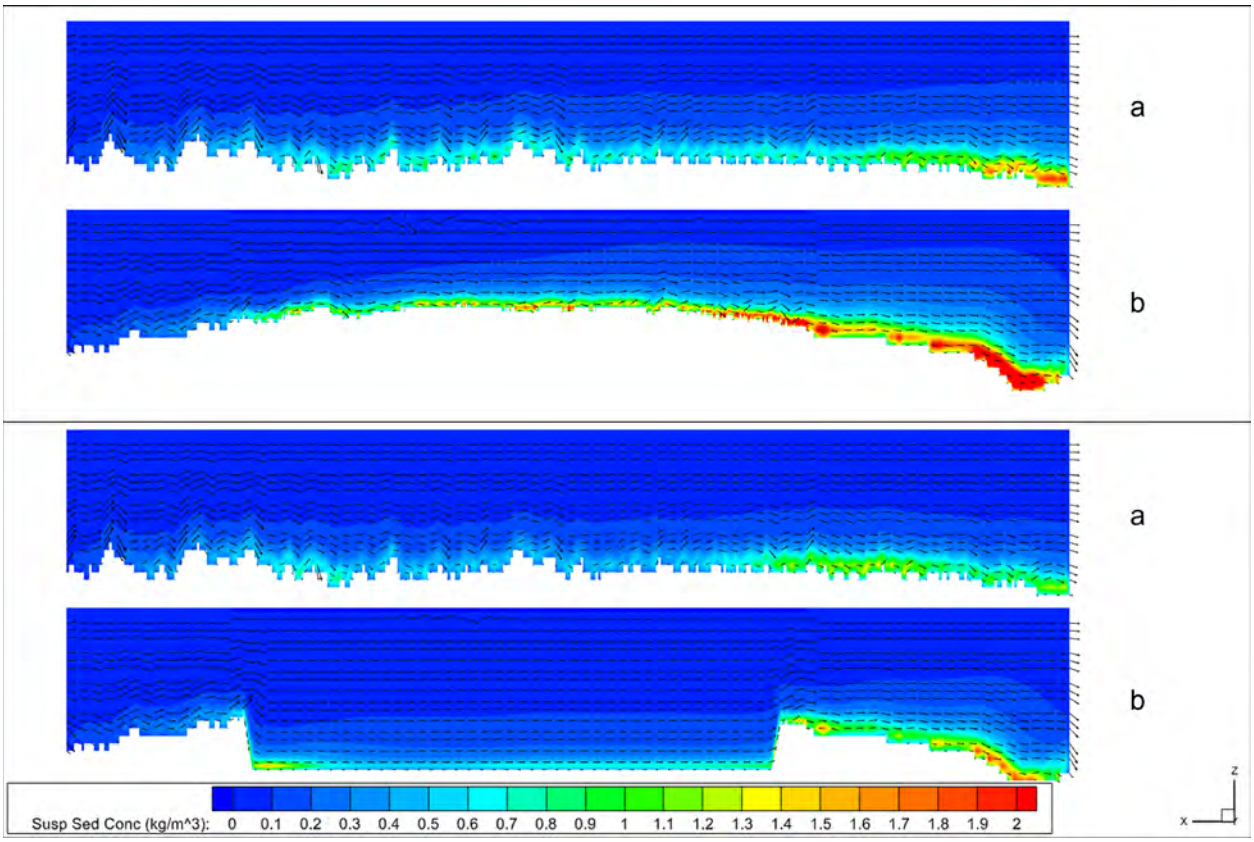

Figure E-14. Side view of suspended sediment concentration contours and velocity vectors at the selected streamwise cross-sections a and b: the upper panel represents the existing condition, and the lower panel represents the with-pit condition.

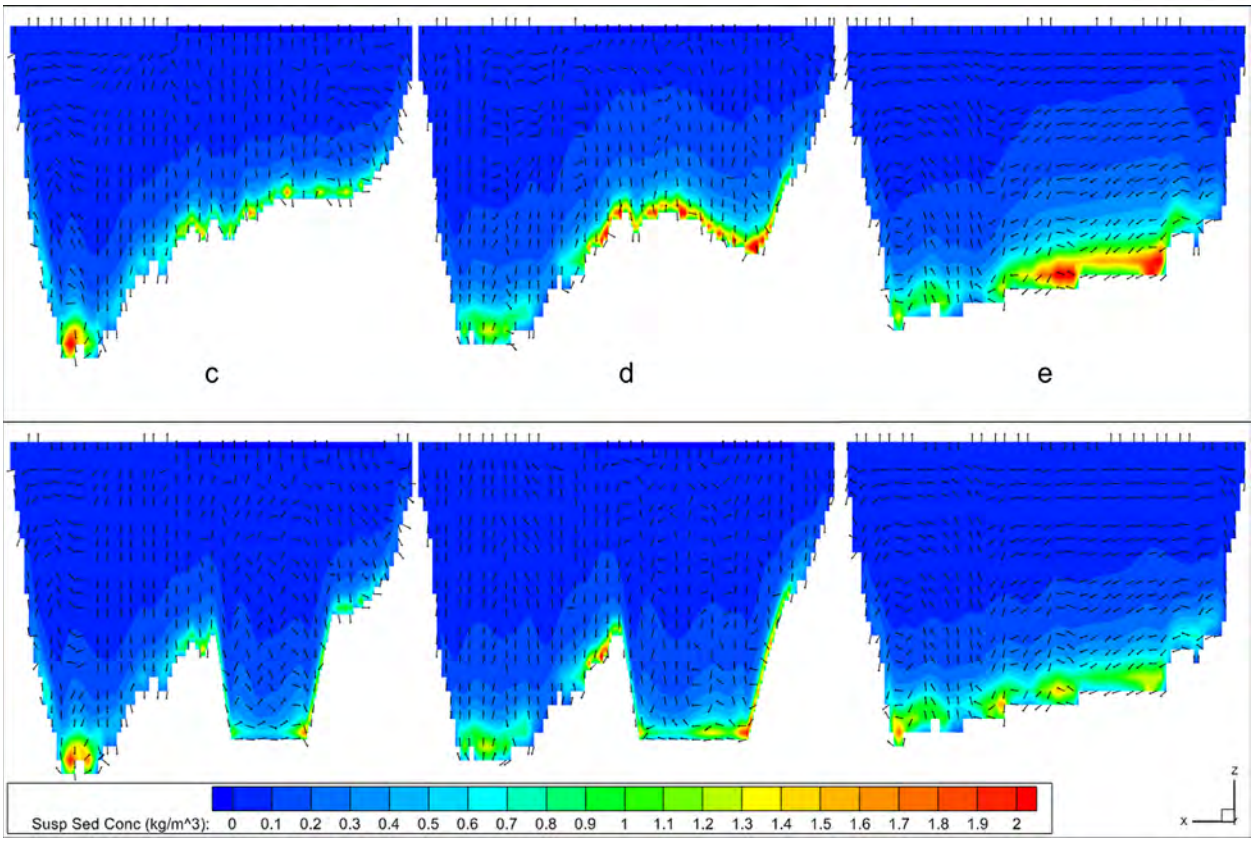

Figure E-15. Front view of suspended sediment concentration contours and projected velocity vectors at the selected transverse cross-sections c, d, and e: the upper panel represents the existing condition, and the lower panel represents the with-pit condition.

1110 RIVER ROAD S., SUITE 200
BATON ROUGE, LA 70802

(225) 448-2813
WWW.THEWATERINSTITUTE.ORG